Siderophore-Based Drug Repurposing of Platinum Anticancer Agents as Targeted Antibiotics and Investigation of Pt-Induced DNA Damage in Gram-Negative Bacteria

By
Chuchu Guo

Bachelor of Science
Fudan University, 2018

Submitted to the Department of Chemistry
in Partial Fulfillment of the Requirements for the Degree of
Doctor of Philosophy in Chemistry
at the
MASSACHUSETTS INSTITUTE OF TECHNOLOGY
September 2023

Authored by: _____
Chuchu Guo
Department of Chemistry
August 8, 2023

Certified by: _____
Elizabeth M. Nolan
Ivan R. Cottrell Professor of Immunology
Thesis Supervisor

Accepted by: _____
Adam P. Willard
Associate Professor of Chemistry
Graduate Officer

This doctoral thesis has been examined by a Committee of the

Department of Chemistry as follows:

Professor Ronald T. Raines _____

Thesis Committee Chair

Roger and Georges Firmenich Professor of Natural Products Chemistry

Professor Elizabeth M. Nolan _____

Thesis Supervisor

Ivan R. Cottrell Professor of Immunology

Professor Daniel L.M. Suess _____

Thesis Committee Member

Associate Professor of Chemistry

Siderophore-Based Drug Repurposing of Platinum Anticancer Agents as Targeted Antibiotics and Investigation of Pt-Induced DNA Damage in Gram-Negative Bacteria

by

Chuchu Guo

Submitted to the Department of Chemistry on August 8, 2023 in Partial Fulfillment of the Requirements for the Degree of Doctor of Philosophy in Chemistry

Abstract

Bacterial infections are a growing threat to human health. This crisis has been exacerbated by the overuse of broad-spectrum antibiotics, resulting in adverse consequences such as the rapid emergence and spread of antibiotic resistance. Additionally, the use of broad-spectrum antibiotics disrupts the human microbiota, potentially leading to the onset of diseases associated with microbial dysbiosis. Consequently, there is an urgent need for innovative strategies to develop narrow-spectrum antibiotics. One promising approach involves the development of siderophore–antibiotic conjugates (SACs), which aim to achieve targeted antibacterial activity by leveraging siderophores, secondary metabolites utilized by bacteria to acquire the essential transition metal nutrient iron (Fe). This SAC approach exploits the molecular recognition between siderophores and their cognate transport machinery, hijacking siderophore-based Fe acquisition pathways for selective and efficient drug delivery as a "Trojan-horse" strategy. This thesis explores the application of a SAC strategy based on enterobactin (Ent), a native triscatecholate siderophore, to repurpose platinum (Pt) anticancer agents as targeted antibiotics against Gram-negative bacteria, involving four Ent-based conjugates incorporating Pt(V) prodrugs (Ent–Pt(IV)).

Chapter 1 introduces the fundamental concepts and background relevant to this thesis. It includes a comprehensive discussion of siderophores and antibiotic development using synthetic SACs. This chapter also highlights previous studies conducted by the Nolan laboratory, specifically focusing on the utilization of Ent for SAC development and its broader applications. Furthermore, it explores the role of Pt anticancer agents within the context of this research.

Chapter 2 focuses on repurposing cisplatin, the first FDA-approved Pt anticancer drug, as a targeted antibiotic with enhanced potency. This study demonstrates that through the conjugation of Ent onto the axial ligand of a cisplatin-based Pt(IV) prodrug, the resulting conjugates selectively inhibit growth and induce filamentous morphology in *E. coli* via the Ent uptake machinery. Ent conjugation facilitates Pt accumulation in *E. coli* cells while reducing Pt uptake in the human cell line HEK293T. This proof-of-concept study represents the first example of using the SAC approach to repurpose Pt compounds as antibiotics.

Chapter 3 expands the scope of Ent–Pt(IV) conjugates by repurposing oxaliplatin, the third-generation Pt anticancer drug, as a targeted antibiotic against Gram-negative bacteria that express the Ent uptake machinery. This study further investigates the DNA damage induced by Ent–Pt(IV) conjugates based on cisplatin and oxaliplatin. These findings establish a correlation between the antibacterial activities and the levels of DNA damage caused by Pt complexes. Collectively, this study generalizes the Ent-based drug repurposing strategy and provides insights into the cellular consequences of Ent–Pt(IV) conjugates in bacterial cells.

Thesis supervisor: Elizabeth M. Nolan
Title: Ivan R. Cottrell Professor of Immunology

Acknowledgements

When I was about to begin my PhD journey, I often wondered whether five years would feel long or short and how it would shape me by the end. Looking back now, I can say that while some days felt long, the years passed quickly. The PhD experience has helped me grow both professionally and personally. I would like to take this opportunity to thank all the remarkable individuals I have met along this journey.

First and foremost, I would like to express my heartfelt gratitude to my supervisor, Professor Elizabeth Nolan. Liz offered unwavering support and dedicated a significant amount of time to guide me, particularly during my initial year. She exemplifies an exceptional scientist, imparting valuable lessons on scientific research that range from attention to small experimental details to critical thinking about the bigger picture. Liz offered me a perfect balance of mentorship and flexibility, allowing me to lead the project while providing guidance whenever I felt lost. Thanks to Liz's invaluable guidance, I am very proud to have translated our ideas into the results presented in this thesis. Moreover, Liz provided me with many opportunities to engage in collaborative projects, mentor other students, and present my work at conferences and events. Attending two GRCs was a highlight, where I found exciting research avenues for my future endeavors. I also express deep appreciation to Liz for her understanding and support for my personal life, particularly during the pandemic. I truly value Liz as both a scientist and a person. Moving forward, I aspire to become a researcher and individual like her, and I am committed to working towards this goal.

I am also very grateful to Professor Ronald Raines and Professor Daniel Suess for their support as my thesis committee. Their insightful discussions and constructive feedback have played a crucial role in shaping the trajectory of my PhD. Their perspectives have broadened my understanding and encouraged me to think creatively and approach my project from different angles.

The Nolan lab has been my home throughout these years, providing a nurturing environment where I have grown alongside remarkable lab members. I extend a special thank you to Dr. Artur Sargun, who has been an outstanding mentor to me. From setting up my fume hood to guiding me through the synthesis process, Artur offered important assistance during my early lab experiences. He not only taught me how to approach research challenges but also instilled in me the importance of critical thinking and independence as a researcher. I believe our mentorship and friendship will continue to benefit me in the future. Moreover, I would also like to thank former graduate students in the Nolan lab. I thank Dr. Emily Zygiel for helping me adapt to my PhD life, regularly checking in with me, and providing valuable career advice. I am grateful to Dr. Rose Hadley for mentoring me during my rotation, and to Dr. Lisa Cunden for her advice on time management and work-life balance. Additionally, I want to thank Dr. Jules Stephan for his career advice and assistance. Regarding the former and current members of the siderophore subgroup. I am grateful to Dr. Abraham Wang for engaging inspiring discussions and organizing team-building events. I also thank Dr. Timothy Johnstone and Dr. Wilma Neumann for their prompt responses to my questions. I appreciate Alvin Chan's assistance with my synthesis work. Working with Rachel Motz and Ghazal Kamyabi has been a pleasure, and I look forward to seeing their future accomplishments. I also acknowledge Janet Peet for the daily chats we shared, which brought a lot of joy and provided a great way to unwind from our hard work. Additionally, I am thankful to Wei Hao Lee and Dr. Mayukh Bhadra for listening to my complaints during difficult

times, and Wei Hao for sharing great food. I appreciate Joanne Baldini for her prompt assistance as our lab administrator.

I always felt a sense of joy and belonging whenever I visited the Department of Chemistry Instrumentation Facility (DCIF), which I consider my second home at MIT. I would like to express my sincere gratitude to Dr. Walt Massefski, Dr. Bruce Adams, and Dr. John Grimes for their training and assistance with NMR. I also thank Dr. Mohan Kumar for his training and assistance with mass spectrometry. Working as a student steward in the DCIF has been an incredible opportunity for me, allowing me to receive invaluable support and care from the DCIF team. Walt and Bruce have consistently shown care, checking in with me and being willing to listen when I was frustrated or lost. Mohan has shown great patience in training me and has provided support and comfort during times of stress and uncertainty. The joyful moments of sharing donuts and bagels while chatting with everyone after our Thursday maintenance sessions have been very delightful. I have also enjoyed working with other student stewards such as Sam Etkind, Victoria Marando, Molly Warndorf, and my labmate Rachel Motz.

I would also like to express my appreciation to our collaborators in the Raffatellu laboratory at UCSD, for offering bacterial mutants and sharing inspiring ideas. Furthermore, I would like to thank the Shoulders lab, our neighboring group, for creating a vibrant and enjoyable environment on the 5th floor of building 56. A special thank you goes to Jessica Patrick for assisting me with tissue culture. Dr. Fang Wang from the Lippard group has shared important knowledge of Pt compounds and provided invaluable guidance for my project.

I am deeply grateful to the Department of Chemistry for fostering an excellent scientific environment. I would like to thank Jennifer Weisman for answering my questions about the program. Dr. Gang Liu deserves thanks for his assistance in instrument repairs and for providing helpful advice on my life. I am particularly grateful for the support from the Stephen J. Lippard Fellowship and the Daniel S. Kemp Fellowship. Furthermore, I would like to express my gratitude to MIT for creating a welcoming and supportive atmosphere. In particular, during the pandemic, the institution took great care of international students who had to stay on campus. The supportive emails from the previous president, L. Rafael Reif, provided tremendous comfort and support during those difficult times.

Finally, I want to extend my heartfelt thanks to my friends and family who have been by my side throughout the ups and downs. Within MIT chemistry, I want to thank Jinyi Yang for being my best companion during coffee breaks. The hallway conversations with Xiyun Ye have been cherished moments. Gen Li and Mengshan Ye have provided me with important advice as senior PhD students. I have had many wonderful memories through dinners and trips with Xin Gu, Yongli Lu, and Qilin He. Outside of the chemistry department, I would like to thank my neighbor, Xiang Chen, for generously sharing his delicious homemade meals, which provided comfort during moments of homesickness and supported me during my thesis writing. I also want to thank my friends Fanghemei Zhang, Kungang Li, Shasha Shi, Fulang Chen, and Kwan Yee Koo for always being there for me and helping me navigate my emotions. Their generous care has meant a lot to me. Lastly, I would like to express my deepest appreciation to my family, especially my mom, aunt, uncle, and grandparents, for their unconditional love and support. They have taught me the values of kindness, understanding, and love. I dedicate this thesis to my family and friends.

To all of you, thank you for inspiring me to become a better person.

Table of Contents

List of Figures

Chapter 1

Chapter 2

List of Tables

List of Schemes

Chapter 1.

Introduction to Siderophore-Based Antibacterial Agents and Platinum-Based Anticancer Agents

Sections of this chapter are based on a manuscript in preparation (Guo, C., Nolan, E. M. Exploring the antibacterial activity and cellular fates of enterobactin–drug conjugates that selectively target Gram-negative bacterial pathogens. 2023).

1.1 Bacterial infections and broad-spectrum antibiotics

The human body is a complex ecosystem that harbors diverse microbial communities collectively known as the human microbiota.[1] These microorganisms have coevolved with the human host, giving rise to a multitude of human–microbe interactions and establishing a symbiotic relationship. The human body generally provides a nutritious and hospitable environment for microbes. In turn, the symbiotic microbial community plays a crucial role in maintaining human health by regulating various physiological processes, such as metabolism, immune homeostasis, immune responses, and colonization resistance, which is a mechanism crucial for protecting against pathogen colonization and preventing bacterial infections.[1-2]

Not all human–microbe interactions are beneficial. Bacterial infections have long posed a significant threat to human health, leading to a continuous battle between humans and bacterial pathogens. Since the discovery of penicillin in the 1940s,[3] antibiotics have contributed greatly to controlling and treating life-threatening bacterial infections. Broad-spectrum antibiotics are widely used in empiric therapy against infections; however, the overuse of broad-spectrum antibiotics has resulted in the rapid development of antibiotic resistance and the spread of resistance mechanisms among various bacterial species.[4-5] These consequences of broad-spectrum antibiotic use have further exacerbated the current dwindling arsenal of effective antibiotics. Furthermore, treatment with broad-spectrum antibiotics disrupts the composition of the microbiota, leading to reduced colonization resistance. This disruption creates an environment conducive to the overgrowth of pathobionts (indigenous bacteria which can promote disease under certain circumstances) and increases the risk of pathogen infections.[2] For example, a common side effect of broad-spectrum antibiotics is the overgrowth of difficult-to-treat bacteria such as *Clostridioides difficile* which can cause debilitating secondary infections.[6-9] These concerns highlight the urgent need to develop

narrow-spectrum antibiotics, aiming to mitigate the negative impacts on the host microbiota while effectively combatting bacterial infections.[10]

1.2 The need for narrow-spectrum antibiotics targeting Gram-negative pathogens

Gram-negative pathogens cause acute and chronic infections in both hospital and community settings, presenting a pressing global concern.[11] These bacteria possess an outer membrane (OM) that serves as a permeability barrier, rendering them resistant to many existing antibiotics.[11-12] Additional mechanisms of antibiotic resistance in Gram-negative bacteria that involve the OM include preventing entry or enhancing efflux of antibiotics, such as downregulating the expression of certain OM proteins like porins and upregulating the expression of bacterial efflux pumps, respectively.[12] The World Health Organization (WHO) has prioritized research and development efforts for new antibiotics to combat drug-resistant bacterial infections, particularly those caused by Gram-negative pathogens.[13] Notable pathogens in this category include *Pseudomonas aeruginosa*, *Acinetobacter baumannii*, and members of the Enterobacteriaceae such as *Escherichia coli* and *Klebsiella pneumoniae.* Given the vital role of the OM in conferring antibiotic resistance to Gram-negative bacteria and therefore rendering infections challenging to treat, understanding the function of the OM at the host–pathogen interface remains a critical area of research to identify novel therapeutic strategies.

1.3 Nutritional immunity, siderophores, and sideromycins

Nutritional immunity. Bacterial infection follows a progression in which non-indigenous bacterial strains enter the host, colonize, and cause disease.[1] Bacterial pathogens have evolved

diverse strategies to invade and colonize the host, including acquiring nutritional resources. Transition metal nutrients are essential for all forms of life; however, the availability of these metals is tightly regulated in the host environment to prevent the development of pathologies caused by metal deficiency or metal excess.[14] During infection, the hosts have developed strategies to further restrict metal availability in order to starve invading bacterial pathogens and prevent their proliferation. This process is a host-defense mechanism termed "nutritional immunity".[14-16] In response, bacteria have evolved adaptive mechanisms to acquire metals under metal-deficient conditions.[14]

Iron and siderophores at the host–pathogen interface. In this thesis, we focus on iron (Fe), a transition metal nutrient essential for many physiological processes, such as oxygen transport, energy metabolism, and DNA replication.[17] Fe also serves as a key cofactor in many enzymes and participates in redox reactions in primary metabolic pathways.[17-18] Thus, acquiring Fe from the host environment is crucial for the survival of bacterial pathogens.

Despite the abundance of Fe in the earth's crust, its bioavailability is low in aerobic environments due to the low solubility of $Fe(OH)_3$ (free [Fe(III)] $\approx 10^{-18}$ M).[19] Fe levels in the host environment must be tightly regulated (free [Fe(III)] $\approx 10^{-24}$ M in serum)[19] to avoid problems resulting from iron deficiency (*e.g.*, anemia) and Fe excess (*e.g.*, Fenton-mediated oxidative damage).[17, 20] The majority of vertebrate Fe is coordinated within the porphyrin ring of heme as a cofactor of hemoglobin or myoglobin.[21] Non-heme Fe is stored in association with ferritin or released into the plasma, where it is complexed with transferrin and gets distributed to target organs and cells.[17] During infection, Fe availability is further restricted by nutritional immunity to starve invading pathogens and prevent bacterial infections.[14-16]

In response, bacterial cells synthesize and secrete siderophores to sequester Fe(III) from the host environment. Siderophores are secondary metabolites with high affinities for Fe(III) (500–1500 daltons, $K_{a,Fe(III)} > 10^{30}$ M^{-1})[22]. Common functional groups for coordinating Fe(III) in siderophores include catecholates (as in enterobactin), phenolates (as in pyochelin), hydroxamates (as in desferrioxamine B), carboxylates (as in staphyloferrin A), and heterocycles (as in pyochelin) (**Figure 1.1**).[23] Since the resulting Fe(III)-siderophore complexes are too large to permeate porins, bacterial cells express cognate siderophore uptake machinery.[22] In Gram-negative bacteria, Fe(III)-siderophore complexes are captured and assimilated into the bacteria via active transport systems, including designated OM receptors.[24] While some bacteria express OM receptors that specifically recognize their own siderophores, others utilize siderophores produced by different strains as "xenosiderophores" to minimize the energy cost of siderophore biosynthesis.[25-26] In response to this "siderophore thievery" strategy, certain bacteria have evolved to produce siderophore-conjugated antibiotics or antimicrobial peptides that selectively deliver toxic agents to competing strains, such as sideromycins and class IIb microcins.[27-33]

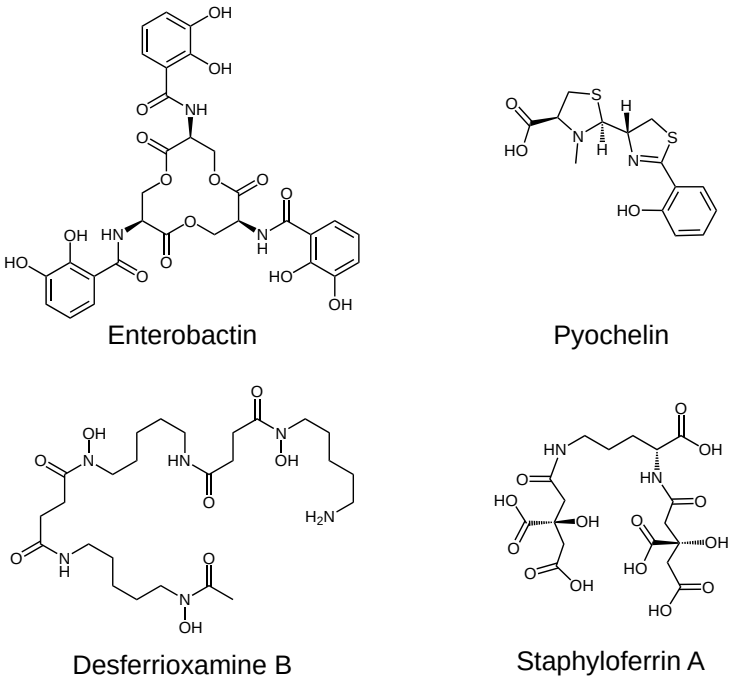

Figure 1.1. Chemical structures of siderophores with various Fe-binding moieties, including catecholates (enterobactin), phenolates (pyochelin), heterocycles (pyochelin), hydroxamates (desferrioxamine B), and carboxylates (staphyloferrin A).

Sideromycins and class IIb microcins. Sideromycins are naturally occurring siderophore–antibiotic conjugates.[27] The first reported sideromycins were the albomycins (previously reported as grisein), which were isolated from *Streptomyces griseus* in 1947.[34-37] Albomycins exhibit potent antibacterial activities against both Gram-negative and Gram-positive bacteria, and they were used in the former Soviet Union as antibiotics.[37] Their structures were fully characterized in 1982, consisting of a toxic thionucleoside antibiotic covalently attached to a trihydroxamate siderophore via a peptide linkage (**Figure 1.2**).[35] Albomycins are transported via the ferrichrome transporter and inhibit seryl-tRNA synthetases.[38-39] Enteric bacteria have shown a tendency to rapidly develop resistance to albomycins.[22]

Other examples of sideromycins include ferrimycin A_1 and the salmycins (**Figure 1.2**). Ferrimycin A_1, as isolated from *Streptomyces griseoflavus*,[40-41] consists of an iminoester-

substituted lactam antibiotic covalently linked to ferrioxamine B via a bridging aminohydroxybenzoic acid. Ferrimycin A_1 selectively targets Gram-positive bacteria through the ferrioxamine B transport system. Salmycins possess an aminodisaccharide attached to a ferrioxamine backbone. Similar to ferrimycin A_1, salmycins target Gram-positive bacteria through the ferrioxamine B transport system.[42-43]

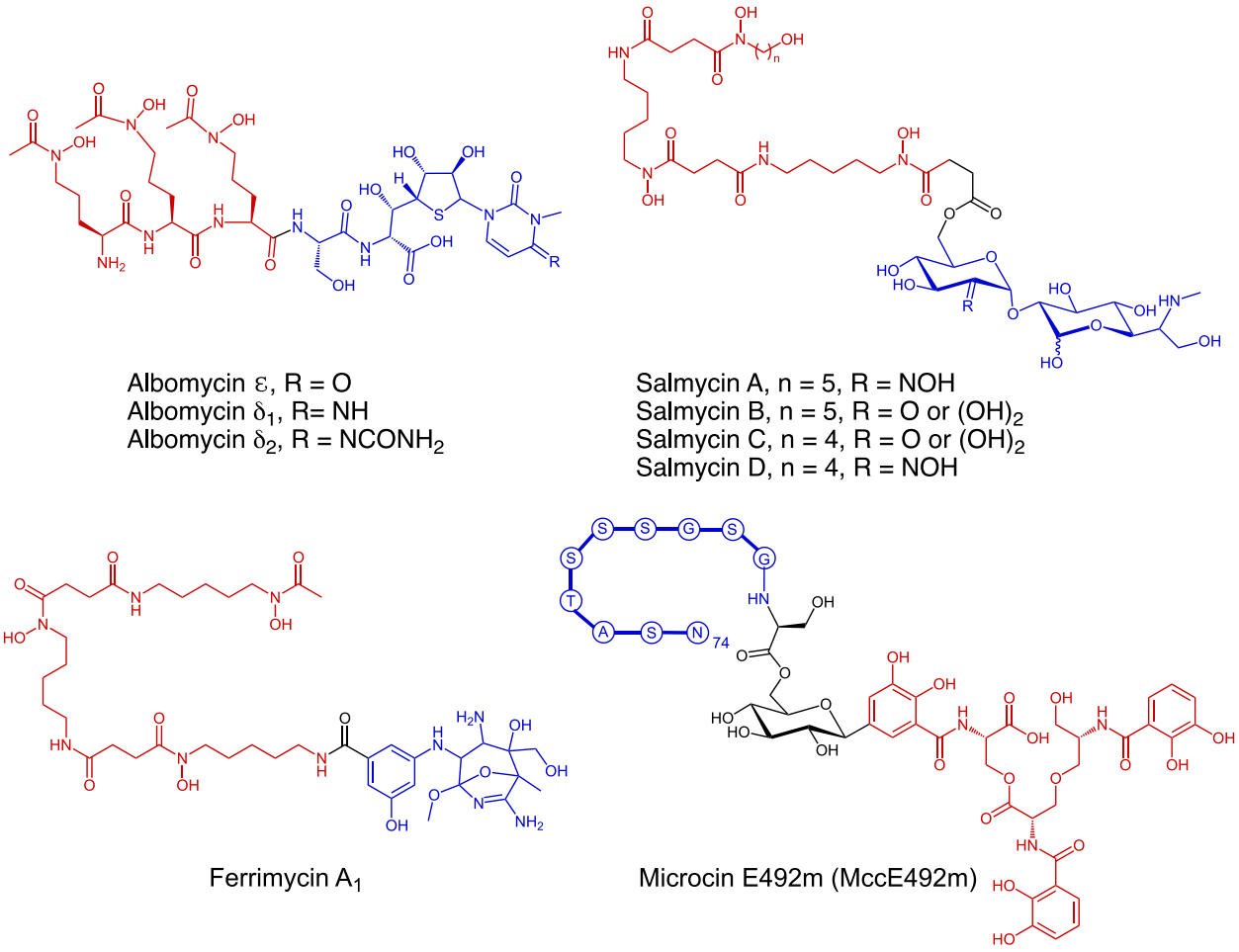

Figure 1.2. Chemical structures of natural sideromycins, including albomycins, salmycins, ferrimycin A_1, and microcin E492m. The siderophore moiety is shown in red, and the cargo moiety is shown in blue.

In general, sideromycins, characterized by a general structure comprising a siderophore moiety linked to an antibiotic via a linker, exhibit enhanced effectiveness compared to the attached

antibiotics alone due to active transport into bacteria mediated by siderophore transport pathways.[22, 44]

Class IIb microcins are antibacterial peptides with a conserved serine-rich C-terminal domain that is post-translationally modified with a glucosylated catecholate siderophore. This modification enables cellular uptake through catecholate siderophore receptors.[32, 45] The first characterized class IIb microcin was microcin E492m (MccE492m, **Figure 1.2**), produced by *K. pneumoniae* RYC492.[29] MccE492m exhibits potent antibacterial activity against a wide range of Enterobacteriaceae, including *Klebsiella, Enterobacter, E. coli,* and *Salmonella*.[46] Studies in *E. coli* have attributed the antibacterial activity to inner membrane damage and interaction with the mannose permease complex.[47] Other examples of class IIb microcins include MccH47 and MccM, which are produced by some *E. coli* strains including the uropathogenic *E. coli* CFT073 and probiotic *E. coli* Nissle 1917. MccH47 and MccM demonstrate antibacterial activity against *E. coli* and *Salmonella*.[28, 32]

1.4 Synthetic siderophore–antibiotic conjugates (SACs).

The natural occurrence of SACs highlights the potential of exploiting siderophore uptake pathways as an efficient approach for antibiotic delivery. The specific molecular recognition between various siderophores and their cognate receptors offers a strategy for selectively targeting different bacterial strains. In the 1970s, synthetic chemists initiated the development of synthetic SACs as novel antibiotics by mimicking the chemical structures of sideromycins, such as albomycins and salmycins.[22] The generalized structure of SACs consists of three components: a drug cargo agent connected to a siderophore via a linker.[48]

Examples of siderophore-β-lactam conjugates. The early efforts in synthetic SACs focused on identifying the minimal requirements for simplified Fe(III) chelators that could effectively mimic the function of natural siderophores (sideromimics). Conjugating β-lactam antibiotics onto sideromimics through an amide bond was widely explored.[44] β-Lactam antibiotics were chosen due to their availability, known mode of action, and relative high tolerance for side chain modifications. New derivatives of β-lactam antibiotics have been extensively studied to increase the antibacterial potency and overcome resistance. These antibiotics target penicillin-binding proteins (PBPs) and inhibit cell wall biosynthesis.[49-50] In the case of Gram-negative bacteria, PBPs are located in the periplasm, necessitating the transport of β-lactam antibiotics across the OM for effectively targeting these microorganisms.

In the 1980s, siderophore conjugates with β-lactam antibiotics including monobactams and cephalosporins were investigated, and some conjugates exhibited impressive in vitro activity;[51-56] however, these studies were not progressed beyond in vitro activity evaluation, primarily attributed to their limited activity against Gram-positive bacteria and the restricted market potential at a time when broad-spectrum antibiotics with simpler chemical structures were dominant.[57]

In the 2010s, interest in the SAC approach was rekindled in response to the growing crisis of antibiotic resistance, particularly in Gram-negative bacteria. Notable compounds from industry include BAL30072 at Basilea,[58] MC-1 and MB-1 at Pfizer,[57, 59-60] and cefiderocol at Shionogi[61] (**Figure 1.3**). BAL30072 is a sulfactam conjugated to a dihydropyridone Fe-chelator with potent activity against multidrug-resistant (MDR) *P. aeruginosa* and *Acinetobacter* spp., and many MDR Enterobacteriaceae isolates harboring a class A carbapenemase or a metallo-β-lactamase.[58] MC-1 and MB-1 were two hydroxypyridone-monocarbam conjugates with excellent in vitro activities against MDR Gram-negative pathogens including *P. aeruginosa*.[59-60] Although the reasons behind

the abandonment of MC-1 and BAL30072 as clinical candidates remain undescribed in the literature, concerns regarding adaptive resistance through antibiotic exclusion were mentioned.[62-63] MB-1 was abandoned due to its inconsistent in vivo efficacy in a neutropenic murine infection model, which could not be accurately predicted based on its in vitro activity. This variability was attributed to the inability of MB-1 to effectively compete with endogenous siderophores like pyochelin and pyoverdines.[59] This study highlighted the importance of designing SACs based on native siderophores with high affinities for Fe(III).

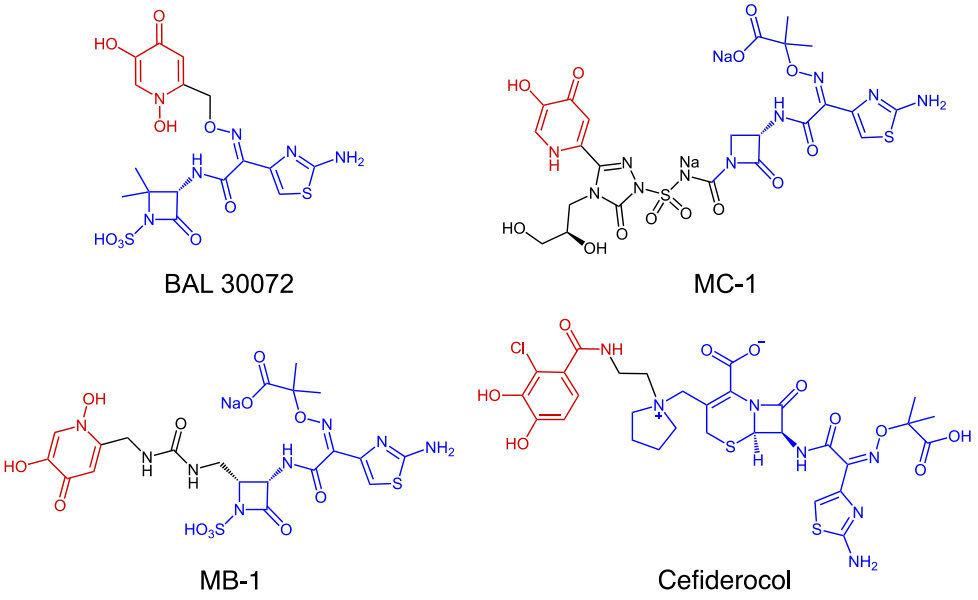

Figure 1.3. Chemical structures of siderophore-β-lactam conjugates, including BAL30072, MC-1, MB-1, and cefiderocol. The siderophore moiety is shown in red, and the cargo moiety is shown in blue.

Cefiderocol, a catecholate cephalosporin developed by Shionogi, became the first siderophore-based drug approved by the FDA in 2019 for the treatment of complicated urinary tract infections (UTIs).[61] Cefiderocol, which incorporates a chlorinated mono-catecholate moiety

as a simplified sideromimic, exhibited resistance to hydrolysis by both serine- and metallo-β-lactamases. It displayed antibacterial activity against problematic Gram-negative bacteria including *P. aeruginosa*, *K. pneumoniae*, *E. coli*, and *A. baumannii*.[61] Although cefiderocol represents a successful example of SACs in clinical use, further research is needed to further elucidate its uptake pathway(s) and its impact on the gut microbiota. Moreover, since cefiderocol incorporates a mono-catecholate as a sideromimic, it is reasonable to expect that the efficacy of the compound could be further improved by incorporating appropriate native siderophores in future design and optimization. Collectively, the "Trojan-horse" strategy has shown promise in delivering β-lactams into the periplasm of Gram-negative bacteria.

Early studies on siderophore–fluoroquinolone conjugates. Cargos with cytoplasmic targets were also investigated in SAC studies, which pose greater challenges as they need to cross both the outer and inner membranes. The existence of natural sideromycins with cytoplasmic targets highlights the feasibility of this approach but also underscores the potential higher requirements for drug release mechanisms. For instance, albomycins rely on enzymatic activation by a serine protease to release their toxin and reach their target, the seryl t-RNA synthetase (**Figure 1.4A)**. Similarly, the aminoglycoside warhead of salmycins is proposed to undergo intramolecular cyclization triggered by Fe reduction (**Figure 1.4B**).[64-65] Overall, linkers and drug release mechanisms are important considerations in SACs with cytoplasmic targets.

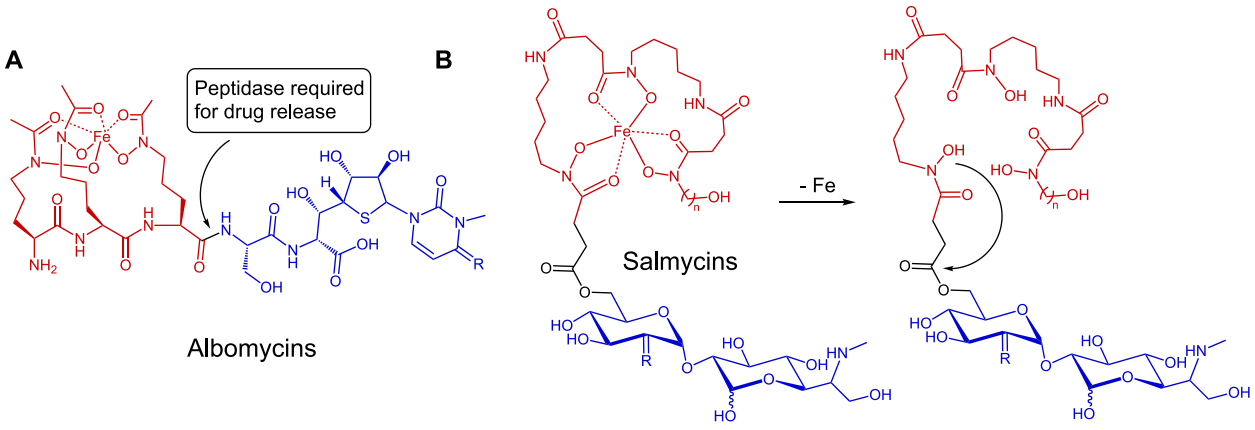

Figure 1.4. Drug release mechanisms of **(A)** albomycins and **(B)** salmycins.[66] The siderophore moiety is shown in red, and the cargo moiety is shown in blue.

Various linker options have been explored in the design of siderophore-antibiotic conjugates with cytoplasmic targets,[67] including but not limited to amino acids,[68] succinic acid,[69] alkyl chains,[70] poly(ethylene glycol) (PEG) chains,[70-71] triazoles,[72] acetal groups,[73] disulfide bonds,[74] thiol-maleimides,[75] citric acid,[76] esters,[77] "trimethyl lock",[78-79] and even β-lactam antibiotics.[66] Ciprofloxacin has been commonly selected as a cargo in these studies because it is a widely-used broad-spectrum antibiotic with low molecular weight and amenable to synthetic modification. The interaction between ciprofloxacin and its target is relatively stringent, with its carboxyl group stabilizing the drug–enzyme–DNA complex and its fluoroquinolone moiety intercalating into the DNA in this complex.[80] A significant body of research has focused on the design and synthesis of siderophore–ciprofloxacin conjugates with many attempts showing reduced antibacterial activity.[44, 67, 81] This thesis selects some representative examples to demonstrate that the reduced activity is generally attributed to inefficient cytoplasmic delivery, problematic linkers, and/or compromised drug–target interaction due to the bulky siderophore modification.[69, 78-79, 82-83]

The importance of linker cleavability in siderophore–drug conjugates can be demonstrated by two examples of pyochelin-ciprofloxacin conjugates (**Figure 1.5**). These conjugates employed either a stable succinic linker or a labile methylenedioxy linker.[82] The pyochelin moiety of the conjugates was functionalized at the N3'' position with a propyl-amine extension, which led to solubility issues and compromised recognition with the OM receptor for pyochelin. The conjugate with the succinic linker showed no activity against three *P. aeruginosa* strains (PAO1, PAD07 and PAD14), whereas the conjugate with the labile methylenedioxy linker showed reduced activity compared to the unmodified ciprofloxacin (a 15-fold increased MIC value relative to unmodified ciprofloxacin against *P. aeruginosa* PAO1). The observed activity against PAD14, a *P. aeruginosa* strain unable to acquire Fe(III) through the pyochelin uptake pathway, indicated that the readily hydrolyzable linker underwent hydrolysis in the medium. This hydrolysis led to premature drug release, and the released antibiotic was attributed to its antibacterial activity.[82]

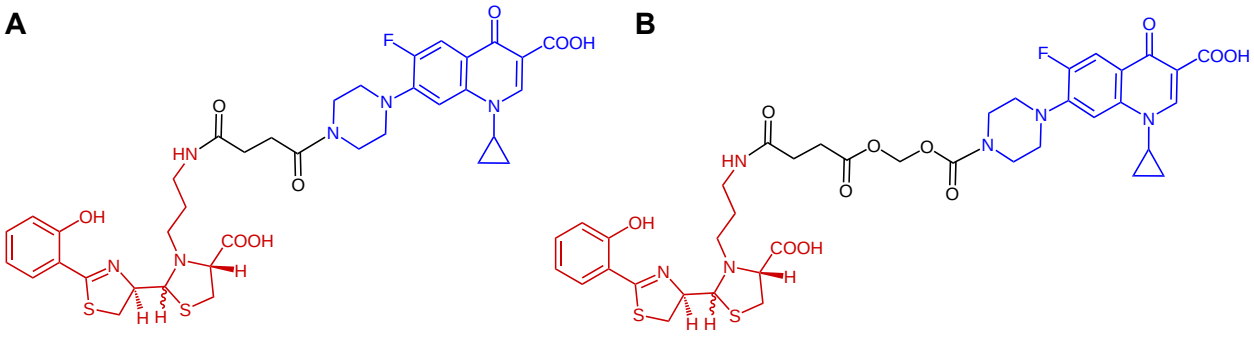

Figure 1.5. Chemical structures of pyochelin-ciproflxoacin conjugates. The siderophore moiety is shown in red, and the cargo moiety is shown in blue.

Another informative example is a series of desferrioxamine B (DFO B)-ciprofloxacin conjugates connected by "trimethyl lock" based linkers (**Figure 1.6A**).[78-79] This series explored

general chemical and biological mechanisms inside the target bacteria to induce drug release. The trimethyl lock is an *o*-hydroxydihydrocinnamic acid derivative with three pendant methyl groups. These methyl groups exhibit unfavorable steric interactions, promoting lactonization and resulting in the formation of a hydrocoumarin (**Figure 1.6B**).[84] Conjugates incorporating an acyl-masked or phosphoryl-masked trimethyl lock were designed and synthesized, aiming to release ciprofloxacin through hydrolysis mediated by bacterial endogenous esterase or phosphatase. This hydrolysis leads to the formation of a transient "trimethyl lock" structure, which is expected to undergo rapid lactonization with concomitant release of the unmodified drug. (**Figure 1.6B**).[78]

The phosphoryl-masked conjugate was inactive against all tested strains except for an *E. coli* penetration mutant, suggesting that the phosphoryl-masked conjugate could not be transported via the siderophore OM receptor. The acyl-masked conjugate displayed reduced activity against ferrioxamine-utilizing strains compared to the parent ciprofloxacin, likely due to the compromised interaction of the conjugate with bacterial esterases. Moreover, it exhibited moderate activity against the *E. coli* strain which was not able to use DFO B for Fe acquisition, indicating the possibility of premature drug release due to extracellular esterases.[79]

The subsequent design of conjugates with a quinone "trimethyl lock" proposed activation through the reduction of quinone to hydroquinone (**Figure 1.6B**).[78] Electrochemical and LC-MS studies confirmed that this reduction occurred smoothly using common biological reductants such as NAD(P)H; however, these conjugates exhibited lower activity relative to the parent drug, which was attributed to compromised recognition of the modified siderophore with the OM receptor and the low activation efficiency of the linker inside bacteria.

Recently, the quinone trimethyl lock was reevaluated in a study involving a range of conjugates with cytoplasmic cargos. These conjugates incorporated desferrioxamine (DFO) or DOTAM (1,4,7,10-tet-raazacyclododecane-1,4,7,10-tetraacetic acid amine) as the siderophore moiety, and ciprofloxacin or RNA polymerase inhibitors as the cargo.[83] The authors tested the antibacterial activity of a panel of conjugates and found that, in the case of ciprofloxacin, both DFO-Cipro (*vide supra*, **Figure 1.6B**) and DOTAM-Cipro exhibited antibacterial activity against MDR *E. coli*; however, their activity was still lower compared to unmodified ciprofloxacin. Additionally, the conjugates containing RNA polymerase inhibitors exhibited reduced activity when compared to the parent drug.

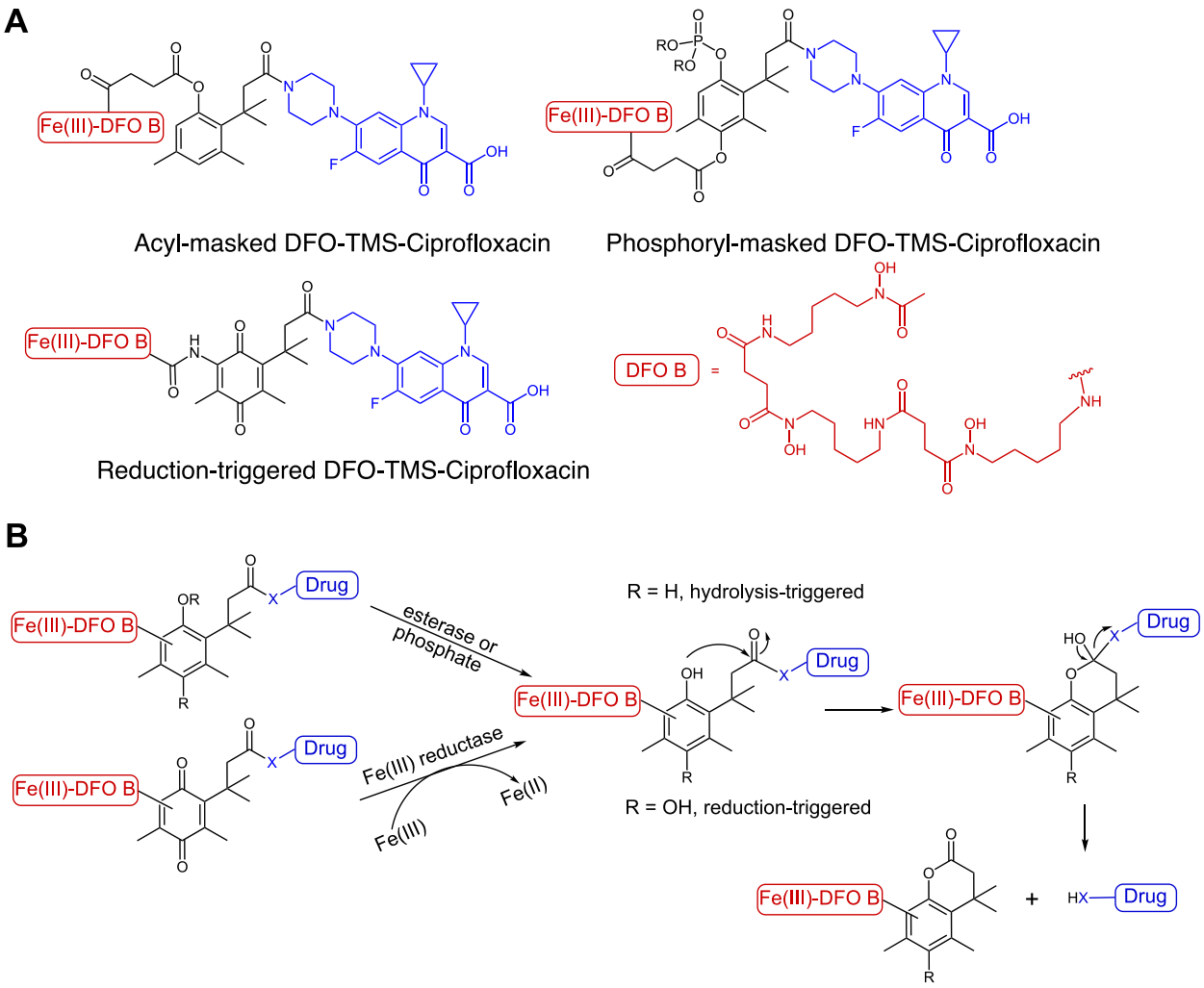

Figure 1.6. (A) Chemical structures of "trimethyl lock (TMS)" derived SACs. **(B)** Drug release mechanism of the trimethyl lock.[78-79] The siderophore moiety is shown in red, and the cargo moiety is shown in blue.

Collectively, by examining unsuccessful examples, it becomes evident that molecular design efforts aiming to develop potent SACs with cytoplasmic targets should focus on linker cleavability and drug release strategies. Proper selection of linkers and understanding their activation mechanisms can significantly impact the activity and efficacy of these conjugates.

Illustrative examples of improved antibacterial properties through rational design of SACs. The continued exploration of SAC studies has led to much progress and significant advancements in this field, as highlighted in recent comprehensive reviews.[44, 81] Two notable examples of well-designed SACs are discussed here, which illustrate the efficacy of rational structural design in achieving potent and selective activity against specific pathogens.[66, 85]

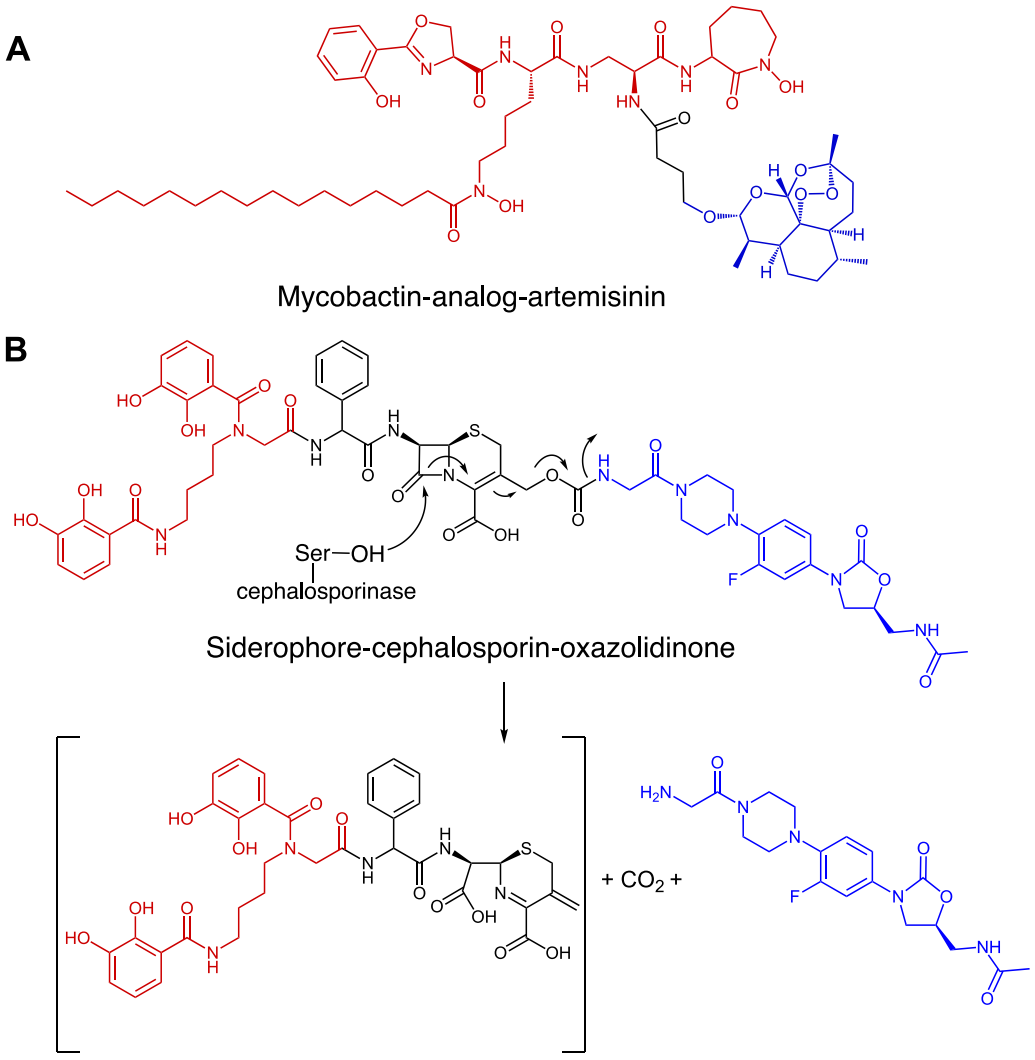

Figure 1.7. Chemical structures of **(A)** mycobactin analog-artemisinin and **(B)** siderophore-cephalosporin-oxazolidinone conjugates. The siderophore moiety is shown in red, and the cargo moiety is shown in blue.

In one study, artemisinin, an antimalarial agent, was conjugated to an analogue of mycobactin T, a mycobacterial siderophore (**Figure 1.7A**). The resulting mycobactin analog-artemisinin conjugate showed potent activity against multi- and extensively drug-resistant strains of *Mycobacterium tuberculosis*, while still retaining its antimalarial activity.[85]

Another investigation focused on the design and synthesis of a dual drug conjugate, siderophore-cephalosporin-oxazolidinone, for β-lactamase-triggered drug release (**Figure 1.7B**).[66] Oxazolidinone is an effective antibiotic against Gram-positive bacteria with a ribosomal target. It is inactive against Gram-negative bacteria due to impermeability or rapid efflux mechanisms.[86] In this study, oxazolidinone was attached to a bis-catecholate siderophore mimic via a cephalosporin linker. This linker could be hydrolyzed by periplasmic β-lactamases, leading to the intracellular release of oxazolidinone. The resulting siderophore-cephalosporin-oxazolidinone conjugate exhibited approximately 100-fold enhanced activity against clinical isolates of *A. baumannii*, particularly those strains which produce significant amounts of ADC-1 β-lactamase, compared to unmodified oxazolidinone. This study utilized the originally deleterious β-lactamase to trigger drug release, providing a new approach to exploit drug resistance mechanisms to induce self-destruction in resistant strains. Overall, these studies offer valuable strategies and insights into combating drug-resistant strains by SACs.

1.5 Enterobactin–drug conjugates that selectively target Gram-negative pathogens

Through a comprehensive analysis of both successful and unsuccessful examples in the field of synthetic SACs, our laboratory has acquired valuable insights and compiled a list of factors that have contributed to these unsuccessful outcomes, including (1) the use of non-native

siderophores with relatively low Fe(III) affinities and/or compromised receptor recognition; (2) modification of antibiotics that leads to a reduction or loss of antibacterial activity; (3) inadequate linker design, such as excessively labile or stable linkers resulting in premature release of insufficient drug release within the targeted cells, respectively.[87]

To address these issues, our laboratory proposed and tested refined principles for the structural design and biological evaluation of effective SACs.[87] The principles included (i) using native siderophores with high Fe(III) affinities; (ii) strategically modifying the siderophore moiety to preserve its Fe(III) binding affinity and the molecular recognition with cognate uptake machinery; (iii) installing the drug warhead such that drug–target interactions are retained; (iv) looking beyond minimum inhibitory concentration (MIC) determination to further inform the antibacterial activity and cellular fates of SACs.[71, 87] Along these lines, we have focused on SACs based on enterobactin (Ent **1**, **Figure 1.8A**), a well-studied native siderophore that is biosynthesized by many enteric Gram-negative pathogens.

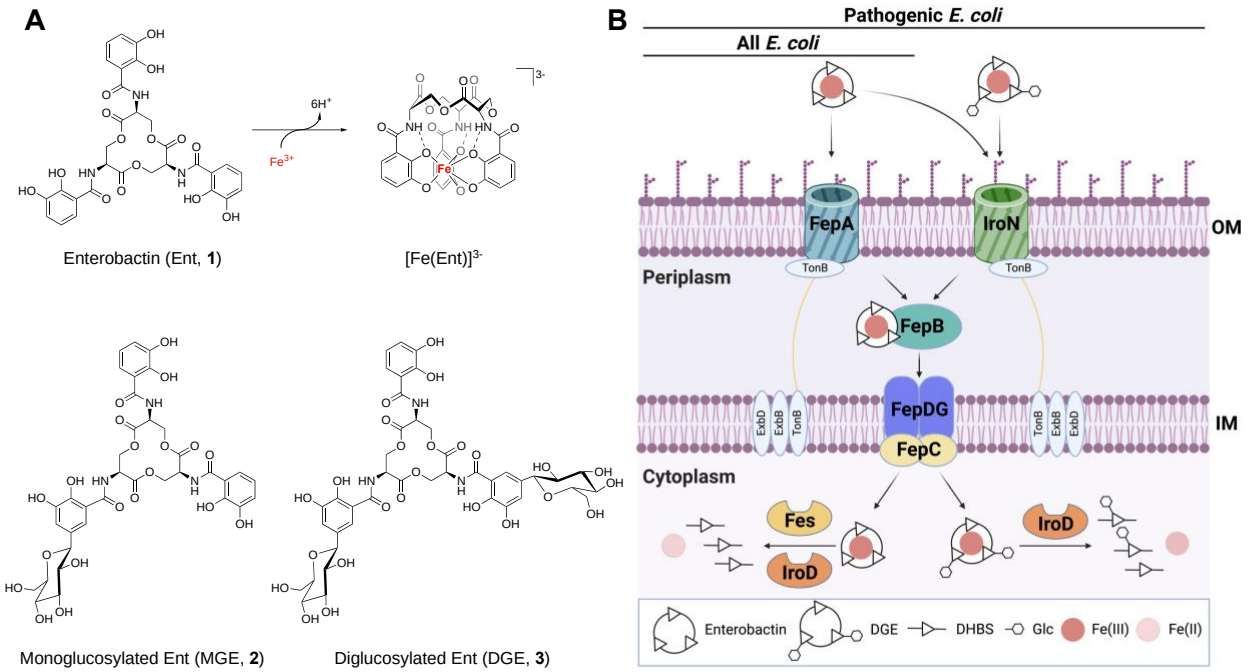

Figure 1.8. (A) Structures of enterobactin (Ent, **1**), mono- and di-glucosylated Ent (MGE, **2** and DGE, **3**). **(B)** Cartoon depiction of the Ent transport and processing machinery for Ent and DGE in *E. coli*. The periplasmic esterase IroE encoded by the *iroA* gene cluster and the Fe(III) reductase YqjH are not shown. DHBS, 2,3-dihydroxybenzoyl serine. Figure created with BioRender.com.

Enterobactin and salmochelins. Ent **1** is a triscatecholate siderophore produced and utilized by Gram-negative bacteria including *E. coli, Salmonella* spp., and *K. pneumoniae*.[88] It also serves as a xenosiderophore for select ESKAPE pathogens including *P. aeruginosa* and *A. baumannii*.[89-90] Ent affords the highest affinity for Fe(III) among all known siderophores (K_a ~ 10^{49} M^{-1}).[91] This exceptional binding affinity can be attributed to its structure, which is preorganized for Fe(III) binding with the three pendent catecholate ligands attached to the trilactone backbone (**Figure 1.8A**).[92] After Ent scavenges Fe(III) from the extracellular environment, the resulting Fe(III)-Ent complex is transported into the bacterial cytoplasm via the Ent uptake machinery FepABCDG (**Figure 1.8B**).[93] Specifically, the OM receptor FepA transports Fe(III)-Ent into bacterial periplasm with energy provided by the TonB-ExbB-ExbD system. The

periplasmic solute-binding protein FepB directs Fe(III)-Ent to the inner-membrane (IM) ATP-binding cassette (ABC) transporter FepCDG, which further imports the complex into the cytoplasm.[94-95] To release Fe from the complex, bacteria employ the Ent processing machinery, including the cytoplasmic esterase Fes for hydrolyzing the trilactone ring and a Fe(III) reductase (*e.g.*, YqjH in *E. coli*), to facilitate the release of the nutrient Fe for bacterial metabolic use.[96-98]

Certain Ent producers including *Salmonella* spp. and many pathogenic *E. coli* also biosynthesize and utilize salmochelins, C-glucosylated Ent derivatives including mono- and di-glucosylated Ent (MGE **2**, DGE **3**, **Figure 1.8A**). Salmochelin producers harbor the pathogen-associated *iroA* gene cluster (*iroBCDEN*) which encodes proteins for Ent tailoring (*e.g.*, the C-glucosyltransferase IroB), Fe(III)-salmochelin uptake (*e.g.*, the OM receptor IroN) and processing (*e.g.*, the cytoplasmic esterase IroD).[96, 99-100] Salmochelins contribute to pathogenicity by allowing bacteria to evade lipocalin-2, a host-defense protein that participates in nutritional immunity by sequestering Fe(III)-Ent.[99]

Design and syntheses of monofunctionalized Ent scaffolds and Ent–drug conjugates. The first total synthesis of Ent **1** was reported five decades ago,[92] but utilization of Ent for SACs was unexplored because of the lack of a suitable functional group on this highly symmetric molecule. In 2012, our laboratory reported the first monofunctionalized Ent scaffolds.[71] These molecules have an alkene, aldehyde or carboxylic acid attached to the C5 position of one catechol moiety. Modification at the C5 position was inspired by the chemical structures of salmochelins and MccE492m (a natural siderophore–peptide conjugate); we reasoned that attaching a linker at the C5 position would retain the Fe(III) binding affinity of Ent and its molecular recognition by the Ent transport machinery.[29, 71, 100] The carboxylic acid in Bn_6Ent-COOH **4** (**Figure 1.9**) has served as a good conjugation handle allowing for amide coupling reactions between the

monofunctionalized Ent moiety and an amine-functionalized linker.[70] These linkers can harbor a drug cargo or terminal functional groups that allow for subsequent cargo attachment. For example, L-Ent-PEG_3-N_3 **5** and L-Ent-PEG_3-COOH **7** are two Ent-linker molecules that have been routinely used for cargo conjugation by copper-catalyzed alkyne-azide cycloaddition (CuAAC)[87, 101-103] or standard peptide coupling chemistry, respectively.[70] Similar strategies were employed to synthesize monofunctionalized D-Ent, including D-Ent-PEG_3-N_3 **6**, because D-Ent is efficiently transported to the cytoplasm by FepABCDG but cannot provide Fe to bacterial cells because it is not a substrate for Ent esterases.[71, 87, 97] Moreover, our laboratory established a chemoenzymatic synthesis of monofunctionalized salmochelins (MGE/DGE-PEG_3-N_3 **8,9**) which employs C-glucosyltransferases IroB or MceC to install glucose moieties at the C5 position of one or both of unmodified catechol rings.[101]

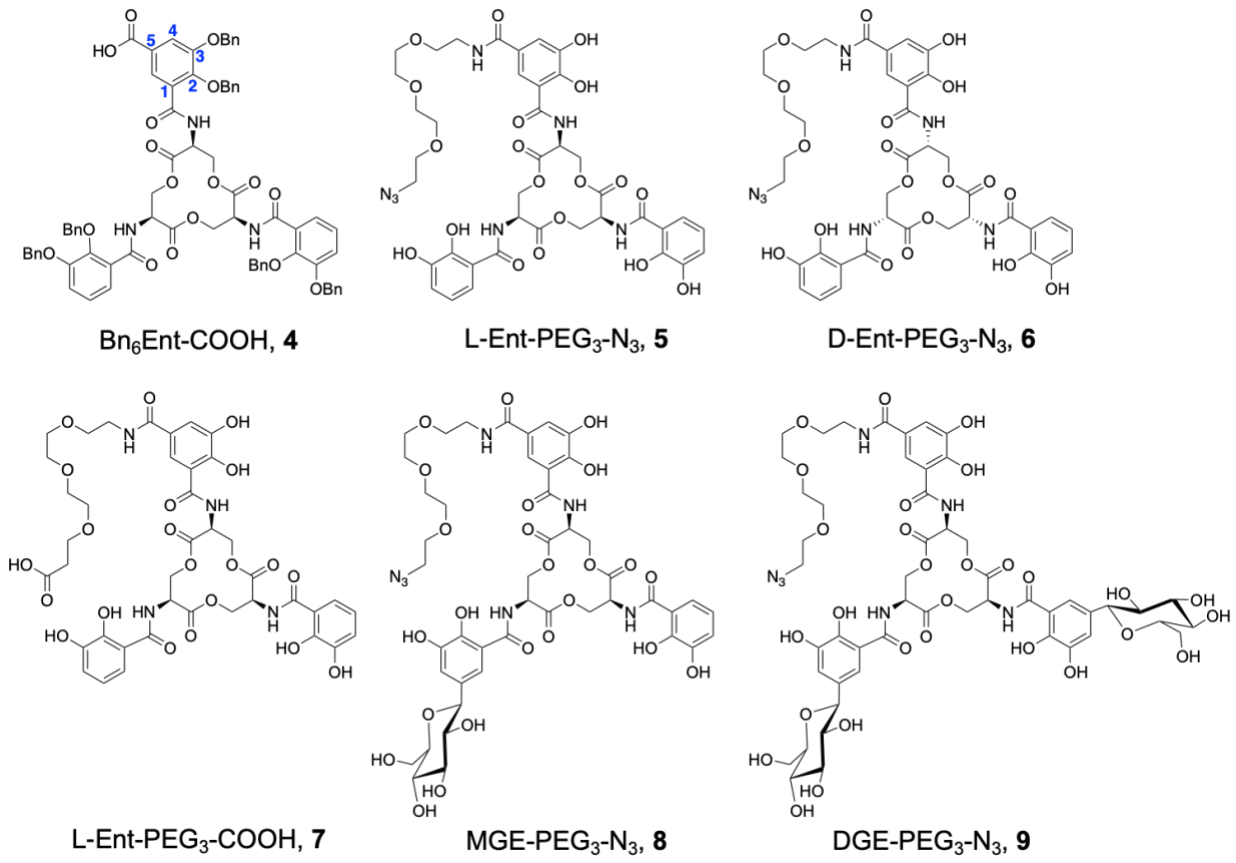

Figure 1.9. Chemical structures of key monofunctionalized Ent scaffolds used for the syntheses of Ent–drug conjugates. Numbering of the catechol carbon atoms is shown with the structure of Bn_6Ent-COOH **4**.

Our laboratory first assessed the ability of monofunctionalized Ent to transport cargos of different sizes into Gram-negative bacterial cells by synthesizing a variety of Ent–cargo conjugates.[71] We deciphered the potential of intracellular cargo delivery by testing how these conjugates affected the growth of an Ent-deficient strain of *E. coli* and a siderophore-deficient strain of *P. aeruginosa*. These assays revealed that Ent delivered relatively small cargos into both strains, including Boc, cyclohexyl, napthyl, and phenylmethylbenzyl cargos. By contrast, other cargos showed species-specific growth promotion (*e.g.*, coumarin 343) or negligible effect on bacterial growth (*e.g.*, vancomycin and ciprofloxacin). Although this work afforded questions

about the size limit for Ent-mediated cargo uptake, the positive outcomes motivated us to pursue SACs using Ent.

Our laboratory commenced with two β-lactam antibiotics, ampicillin and amoxicillin, which target penicillin-binding proteins (PBPs) in the Gram-negative periplasm.[87] These small-molecule antibiotics have a relatively high tolerance for synthetic modification and were used in previous SAC studies.[44] We conjugated alkyne-modified β-lactams to L-Ent-PEG_3-N_3 **5** by CuACC to afford Ent-Amp/Amx **10,11** (**Figure 1.10A**). The PEG_3 linker was selected because it is flexible, stable and water-compatible, and we reasoned that it would provide adequate separation between the β-lactam and the Ent moieties to preserve the function of each component. We found that Ent-Amp/Amx were delivered to the *E.* coli periplasm by FepA and displayed markedly decreased MICs and faster killing kinetics than the parent antibiotics.[87] These findings motivate us to synthesize and evaluate additional Ent-β-lactam conjugates including Ent-cephalexin (Ent-Lex **12**) and Ent-meropenem (Ent-Mem **13**).[102-103] We also prepared and evaluated DGE-Amp/Amx/Lex/Mem **14,15,16,17** as a strategy for targeting pathogenicity and evading lipocalin-2.[101-103]

To investigate Ent–drug conjugates with cytoplasmic targets, our laboratory selected the fluoroquinolone antibiotic ciprofloxacin which inhibits DNA gyrase. The interaction between ciprofloxacin and its target involves its carboxyl group stabilizing the drug–enzyme–DNA complex and its fluoroquinolone moiety intercalating into the DNA in this complex.[80] Many reported attempts to develop siderophore–fluoroquinolone conjugates failed due to poor antibacterial activity, which was attributed to problematic linkers, inefficient cytoplasmic delivery, and/or compromised drug–target interaction due to the bulky siderophore modification.[69, 78, 82] Consequently, our laboratory examined Ent-ciprofloxacin conjugates with four types of linkers

(**Figure 1.10B**).[70-71, 74, 77] Remarkably, we discovered that Ent-Cipro **18** with an alkyl linker displayed potent and targeted antibacterial activity against *E. coli* that possess the pathogen-associated *iroA* gene cluster. Further investigation uncovered an intracellular drug release mechanism mediated by the salmochelin esterase IroD, which contributes to its pathogen selectivity. This example represents the first siderophore–fluoroquinolone conjugate that exhibits comparable activity to unmodified ciprofloxacin against Gram-negative pathogens.

Collectively, through the design and utilization of monofunctionalized Ent scaffolds, our laboratory has achieved a family of Ent–drug conjugates using a modular synthesis approach. In what follows, we present the key outcomes from biological activity of these Ent-based Trojan-horse antibiotics (**Table 1.1**).

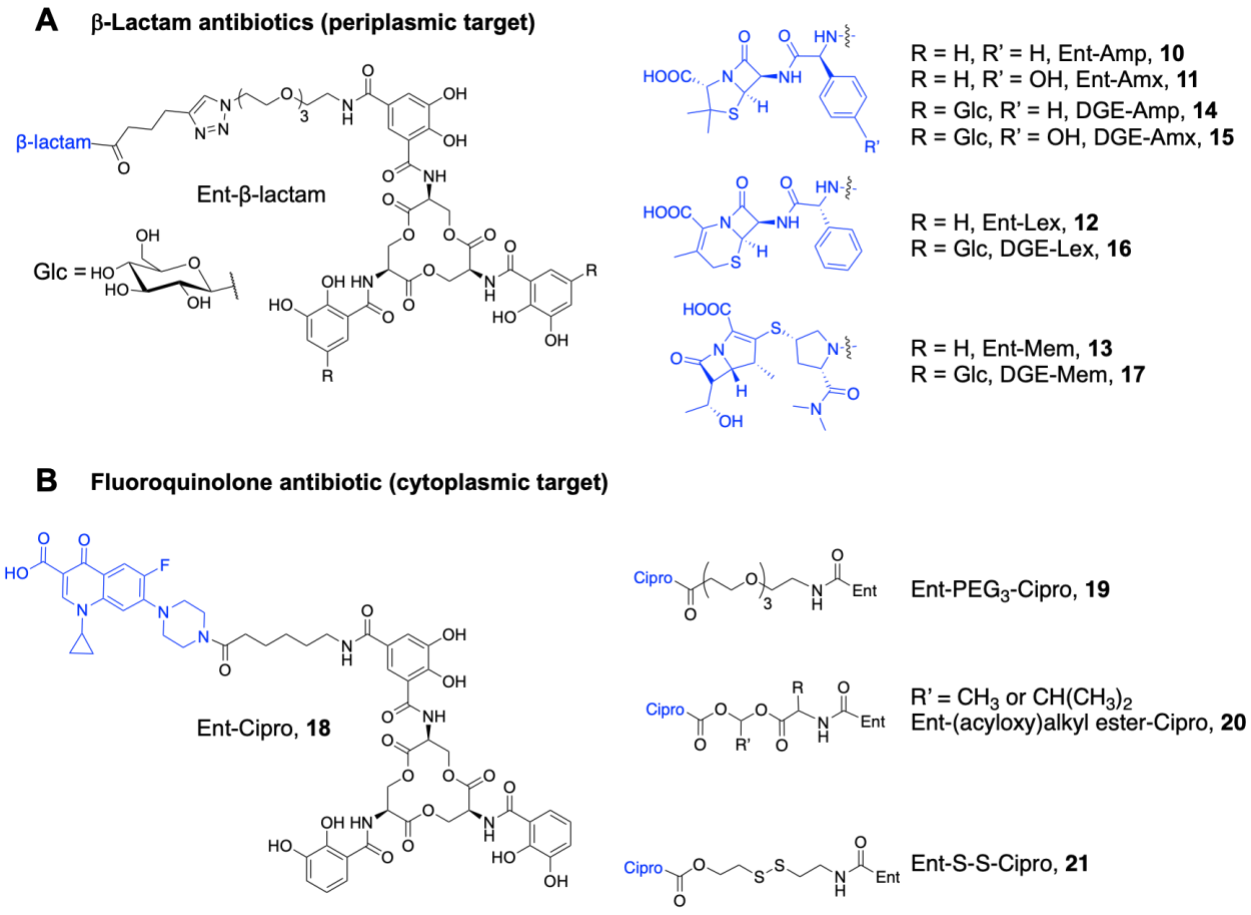

Figure 1.10. Chemical structures of **(A)** Ent-β-lactam conjugates and **(B)** Ent-ciprofloxacin conjugates.

Table 1.1. Summary of Ent–drug conjugates previously reported by the Nolan laboratory.

Conjugate (target)	**MIC** (VS. parent drug)[a]	**Antibacterial spectrum**		**Medium conditions**
		Activity greater than or comparable to the parent drug	No activity	
Ent-Amp/Amx[87, 101-103] (PBP3)	10^{-8} M (10^{-5} M)	*E. coli* K12, ATCC 25922, H9049, UTI89, CFT073, ATCC 35401, ATCC 43895[b] *P. aeruginosa* PAO1 *K. pneumoniae* ATCC 13883[c] *B. cereus* ATCC 14579[d] *Salmonella enterica*	*S. aureus* ATCC 25923[d] *E. coli* ATCC 35218[e] *A. baumannii* ATCC 17961[f] *L. rhamnosus* GG[g]	apo conjugates; (1) 50% MHB medium with 200 μM DP[h] in refs 87 and 101; (2) modified M9 with 16.5 μg/mL thiamine in refs 102 and 103; (3) 50% MHB for *S. aureus* and 1:1 MRS/MHB for *L. rhamnosus* GG
DGE-Amp/Amx[87, 101-103] (PBP3)	10^{-8} M (10^{-5} M)	*E. coli* CFT073, UTI89	*E. coli* K12, B, H9049 *S. aureus* ATCC 25923 *A. baumannii* ATCC 17961 *L. rhamnosus* GG	
D-Ent-Amp/Amx[87] (PBP3)	10^{-7} M (10^{-5} M)	*E. coli* K12, ATCC 25922, 43895 CFT073, ATCC 35401		apo conjugates; 50% MHB medium with 200 μM DP
Ent-Lex[102-103] (PBP3)	10^{-5} M (>10^{-5} M)	*E. coli* K12, CFT073, UTI89 *Salmonella enterica*	*E. coli* ATCC 35218 *S. aureus* ATCC 25923	apo conjugate; (1) modified M9 with 16.5 μg/mL thiamine; (2) 50% MHB medium with 100 μM DP for *S. aureus*
Ent-Mem[102-103] (PBP2)	10^{-8} M (10^{-6} M)	*E. coli* CFT073, UTI89, ATCC 35218 *Salmonella enterica*	*S. aureus* ATCC 25923	
DGE-Mem[102-103] (PBP2)	10^{-8} M (10^{-6} M)	*E. coli* CFT073, UTI89, ATCC 35218 *Salmonella enterica*	*E. coli* K12 *S. aureus* ATCC 25923	apo conjugate; (1) modified M9 with 16.5 μg/mL thiamine; (2) 50% MHB medium with 100 μM DP for *S. aureus*
DGE-Lex[102-103] (PBP3)	10^{-5} M (>10^{-5} M)	*E. coli* UTI89, CFT073 *Salmonella enterica*	*E. coli* K12, ATCC 35218 *S. aureus* ATCC 25923	

Ent-Cipro[70] (DNA gyrase)	10^{-6} M (10^{-7} M)	*E. coli* UTI89, CFT073	*E. coli* K12, B	apo & ferric conjugate; modified M9 with 16.5 μg/mL thiamine

[a] MIC values against *E. coli* CFT073
[b] *E. coli* ATCC 25922: a laboratory susceptibility test strain; H9049: a non-pathogenic clinical isolate; UTI89 and CFT073: uropathogenic strains harboring the *iroA* gene cluster; ATCC 35401: an enterotoxigenic strain; ATCC 43895: an enterohemorrhagic strain
[c] *K. pneumoniae* ATCC 13883 has a chromosomally encoded class A β-lactamase (SHV-1) and lacks sensitivity to Amp/Amx
[d] *B. cereus* ATCC 14579 and *S. aureus* ATCC 25923: Gram-positive strains with the ability to utilize Fe(III)-Ent
[e] *E. coli* ATCC 35218 expresses class A serine β-lactamase
[f] *A. baumannii* ATCC 17961 does not express FepA or IroN
[g] *L. rhamnosus* GG: a Gram-positive commensal that is susceptible to β-lactam antibiotics
[h] n.i. no inhibition.

Ent-β-lactam conjugates exhibit enhanced potency and accelerated cell killing against Gram-negative bacteria. Studies of SACs involve examining their antibacterial properties under Fe-deficient conditions, which induce the expression of siderophore transport and processing pathways. Our laboratory primarily focused on non-pathogenic and pathogenic *E. coli* strains but have also examined *Salmonella enterica*, a species that has been largely overlooked by the SAC field. Throughout, we have taken a genetic approach using a collection of bacterial mutants with defects in different components of the Ent transport and processing machinery, which has allowed us to investigate how these pathways affect the antibacterial properties of Ent-based conjugates.

Under Fe-deficient conditions, Ent-Amp/Amx **10,11** showed markedly enhanced antibacterial activity against all tested *E. coli* strains compared to the unmodified β-lactams. These conjugates provided MIC values of 100 nM for most *E. coli*, corresponding to a 100-fold decrease in MIC compared to the parent antibiotics. Remarkably, Ent-Amp/Amx were 1000-fold more potent against uropathogenic *E. coli* CFT073 (MIC = 10 nM). Moreover, time-kill kinetic studies showed that Ent-Amp/Amx **10,11** killed *E. coli* cells more rapidly compared to Amp/Amx, which was attributed to active transport by the Ent uptake machinery.[87]

These results motivated our laboratory to consider different classes of β-lactam antibiotics as cargos, including cephalosporins and carbapenems (**Figure 1.10A**). We selected cephalexin (Lex), which exhibits enhanced stability to acid hydrolysis, and meropenem (Mem), which exhibits resistance to serine β-lactamases.[102] Consistent with Ent-Amp/Amx, both Ent-Lex **12** and Ent-Mem **13** displayed enhanced antibacterial activity against *E. coli* compared to the unmodified antibiotics. Notably, Ent-Mem **13** retained its potency (MIC ~ 10 nM) against *E. coli* ATCC 35218

expressing a class A serine β-lactamase, whereas Ent-Amp/Amx/Lex **10,11,12** showed no activity against this strain.

Diglucosylated Ent (DGE)-β-lactam conjugates selectively target Gram-negative pathogens. Our laboratory also further this SAC strategy by investigating salmochelin-β-lactam conjugates, aiming to address two specific issues associated with Ent-β-lactams: the antibacterial activity against non-pathogenic *E. coli* and the attenuated potency in the presence of the Fe(III)-Ent-sequestering protein lipocalin-2.[87, 103] We expected that C-glucosylation of the Ent-β-lactam conjugates would require the pathogen-associated OM receptor IroN for uptake and prevent binding with lipocalin-2. MGE-Amp/Amx and DGE-Amp/Amx **14,15** exhibited similar antibacterial activity against pathogenic strains of *E. coli* as their Ent-based counterparts. MGE-Amp/Amx also inhibited the growth of the non-pathogenic *E. coli* K12, which was attributed to the ability of FepA to transport MGE. By contrast, DGE-Amp/Amx selectively targeted uropathogenic *E. coli* that express the salmochelin receptor IroN.[101] DGE-Lex/Mem **16,17** were subsequently investigated and shown to target IroN-expressing strains. Moreover, the DGE-β-lactams retained antibacterial activity in the presence of lipocalin-2 and, like the Ent-based congeners, showed accelerated cell killing compared to the parent antibiotics.[102-103]

To study the contributions of Ent transport and processing pathways on the antibacterial properties of Ent/DGE-β-lactams, our laboratory first probed the role of the FepABCDG system in *E. coli* K12 (**Figure 1.8B**) and later examined both the Fep system and IroN in *E. coli* CFT073. We evaluated antibacterial activity against the OM receptors using the Δ*fepA* and Δ*iroN* mutants, the IM transporter using the Δ*fepC* and Δ*fepDG* mutants, and the cytoplasmic esterase using the Δ*fes* mutant. In *E. coli* K12, the antibacterial activity of Ent-Amp/Amx **10,11** was attenuated

against the K12 Δ*fepA* mutant but retained against the K12 Δ*fepC* and Δ*fes* mutants, indicating that these conjugates were translocated across the OM by FepA and trapped in the periplasm, presumably due to covalent binding to PBPs.[87] Later studies in *E. coli* CFT073 allowed us to examine the contribution of IroN. Whereas single deletion of either Δ*fepA* or Δ*iroN* did not affect the antibacterial activity of the Ent-β-lactams, antibacterial activity was attenuated in the Δ*fepA* Δ*iroN* double mutant, indicating that both FepA and iroN transport Ent-β-lactams.[102] Regarding the pathogen selectivity of DGE-β-lactams, we observed abolished antibacterial activity against the CFT073 Δ*iroN* mutant and retained activity against the Δ*fepA* mutant, indicating the requirement of IroN for DGE-β-lactam uptake, which affords selectivity against *iroA*-harboring Gram-negative pathogens.

We further probed the selectivity of Ent/DGE-β-lactams in co-cultures. Our results revealed that these conjugates selectively killed two uropathogenic *E. coli* strains (CFT073 and UTI89) in co-culture with the Gram-positive strain *Staphylococcus aureus*.[87, 102] Ent/DGE-Amp/Amx selectively killed *E. coli* CFT073 in co-culture with the commensal microbe *Lactobacillus rhamnosus* GG.[101] Moreover, DGE-Amp/Amx selectively target *E. coli* CFT073 and UTI89 in the presence of the non-pathogenic K12. Furthermore, low cytotoxicity against human T84 intestinal cells was observed for Ent/DGE-Amp/Amx.[87]

Taken together, these investigations highlight the ability of Ent and salmochelins to facilitate the targeted delivery of β-lactam antibiotics into the periplasm of *E. coli*, converting broad-spectrum β-lactams to narrow-spectrum antibiotics against Gram-negative bacteria with improved potency. The DGE-based scaffold provides an effective strategy for selectively targeting *iroA*-harboring Gram-negative bacteria, which are predominantly pathogenic strains, and retaining

their potency in the presence of lipocalin-2. Notably, our laboratory extended these studies to *Salmonella enterica* serovars Typhimurium (*S*Tm) and Enteritidis (*S*Ed), Gram-negative gastrointestinal pathogens which produce and utilize Ent and salmochelins. Similar to observations in *E. coli* studies, Ent/DGE-β-lactam conjugates also showed enhanced antibacterial activity against *S*Tm and *S*Ed (MICs of Ent/DGE-Mem **13, 17** ~ 10 nM) and faster time-kill kinetics compared to the parent antibiotics, and the same OM receptor dependence.[103]

Ent-Cipro exhibits pathogen-targeted activity and unveils an intracellular drug release mechanism activated by the cytoplasmic salmochelin esterase IroD. Ent-Cipro **18** was serendipitously discovered as a strain-selective antibiotic five years after its initial report. In this early study, Ent-Cipro **18** was assayed against *E. coli* K12 and *P. aeruginosa* PAO1, and no antibacterial activity was observed.[71] During subsequent years, our laboratory synthesized additional Ent–ciprofloxacin conjugates with different linkers and investigated them using a larger panel of *E. coli* strains. During these studies, we reevaluated Ent-Cipro **18**. We reproduced our original data that demonstrated no antibacterial activity against K12 as well as the laboratory strain B, and we were astonished to find that it displayed antibacterial activity comparable to the unmodified antibiotic against uropathogenic *E. coli* (UTI89 and CFT073). Because UTI89 and CFT073 harbor the *iroA* gene cluster and K12 and B do not, we questioned whether a component of this gene cluster was responsible for the targeted Ent-Cipro activity.

We first hypothesized that IroN is required, speculating that FepA is unable to transport the ciprofloxacin cargo across the OM. An experiment with the Δ*fepA*, Δ*iroN* and Δ*fepA* Δ*iroN* mutants refuted this hypothesis. Ent-Cipro **18** retained full antibacterial activity against the single mutants and deletion of both *fepA* and *iroN* was required to abolish activity, indicating that Ent-Cipro enters CFT073 through both FepA and IroN. We also found that the FepCDG system was

essential for Ent-Cipro **18** activity: deletion of *fepC* or *fepDG* abolished its antibacterial activity, demonstrating the FepCDG-mediated cytoplasmic delivery.[70] This set of observations led us to consider the fate of Ent and salmochelins in the cytoplasm, which involves esterase-catalyzed hydrolysis of the trilactone ring. Following our hypothesis that the *iroA* cluster is important, we questioned if the salmochelin esterase IroD is necessary for Ent-Cipro **18** activity. A study of CFT073 Δ*fes* and Δ*iroD* mutants as well as complementation of K12 with *iroD*+ uncovered that IroD is required for the activity of Ent-Cipro **18**. Our current working model is that IroD hydrolyzes the Ent moiety, resulting in the formation of a less bulky conjugate, 2,3-dihydroxybenzoyl serine (DHBS)-Cipro **22** (**Figure 1.11**). This species inhibits DNA gyrase and confers the antibacterial activity or undergoes further intracellular processing to give the active species.[70] Given that IroD is primarily expressed by pathogens, this esterase-mediated prodrug activation mechanism confers pathogen-selective activity.[99, 104]

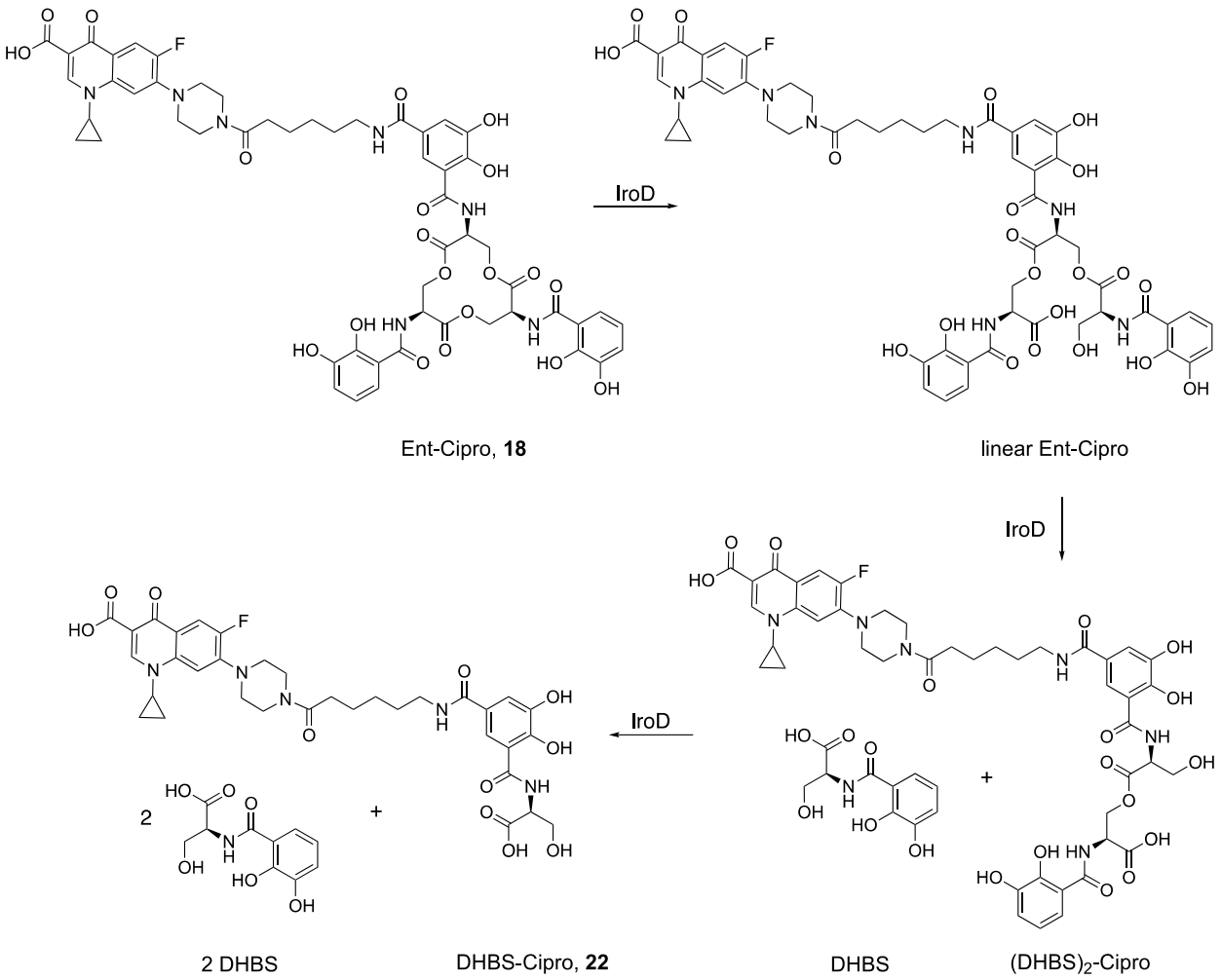

Figure 1.11. Intracellular activation of Ent-Cipro **18** by IroD-mediated hydrolysis of the trilactone ring.

Our explorations of alternative linkers for the Ent-ciprofloxacin conjugates included evaluatioan of (acyloxy)alkyl esters that are proposed to be hydrolyzed by intracellular esterases,[77] and a disulfide-based linker that is designed to be self-cleavable in the reducing cytoplasmic environment (**20,21, Figure 1.10B**).[74] However, all of these conjugates exhibited diminished antibacterial activity compared to unmodified ciprofloxacin. The relatively unstable (acyloxy)alkyl esters were found to cause premature release of ciprofloxacin,[77] and the disulfide

linker was found to be unsuitable within the complex intracellular environment, at least in this context.[74] Further exploration of this topic is crucial for advancing our understanding and optimizing SAC design.

Cellular consequences of Ent-based conjugates. Most reported studies on synthetic SACs primarily focused on assessing antibacterial activities and exploring the contributions of OM siderophore receptors to SAC uptake. Although it has been generally assumed that the antibacterial mechanisms of synthetic SACs mirror those of the unmodified drug warhead, this assumption often lacks experimental evidence. Moreover, the possibility of additional secondary mechanisms resulting from siderophore modification remains unexplored. Throughout our work, our laboratory sought to address the underlying mechanisms of cell death induced by Ent-based conjugates (**Figure 1.12**). In this section, we describe studies that informed the interactions of Ent/DGE-β-lactams with PBPs and the impact of Ent-Cipro **18** on the activity of DNA gyrase.

To further probe the antibacterial activity of Ent/DGE-β-lactams, our laboratory examined cell morphologies by phase-contrast microscopy. Cell morphologies can distinguish and identify specific classes of PBPs targeted by different β-lactam antibiotics. For example, Amp and Lex cause cell filamentation because they primarily inhibit PBP3 which is involved in cell division. Mem induces spheroplast formation because it targets PBP2 which is involved in cell elongation.[105] Consistent with the morphologies induced by sub-MIC concentrations of the parent antibiotics, cell elongation was observed in *E. coli* CFT073 after treatment with Ent/DGE-Amp/Lex **10,12,14,15**, and round or ovoid-shaped spheroplasts was observed after treatment with Ent/DGE-Mem **13,17**.[102] We also acquired time-lapse images to visually depict the progression of cell killing by Ent/DGE-Amp/Mem at MIC levels. This imaging revealed that CFT073 cells treated with Ent/DGE-Amp ceased to grow and divide, while those treated with Ent/DGE-Mem exhibited

explosive lysis. Together, these microscopic studies indicated that the antibacterial activity of Ent/DGE-β-lactams originates from the inhibition of specific PBPs by the β-lactam warheads. Similar results were obtained in studies using *Salmonella* strains.[103]

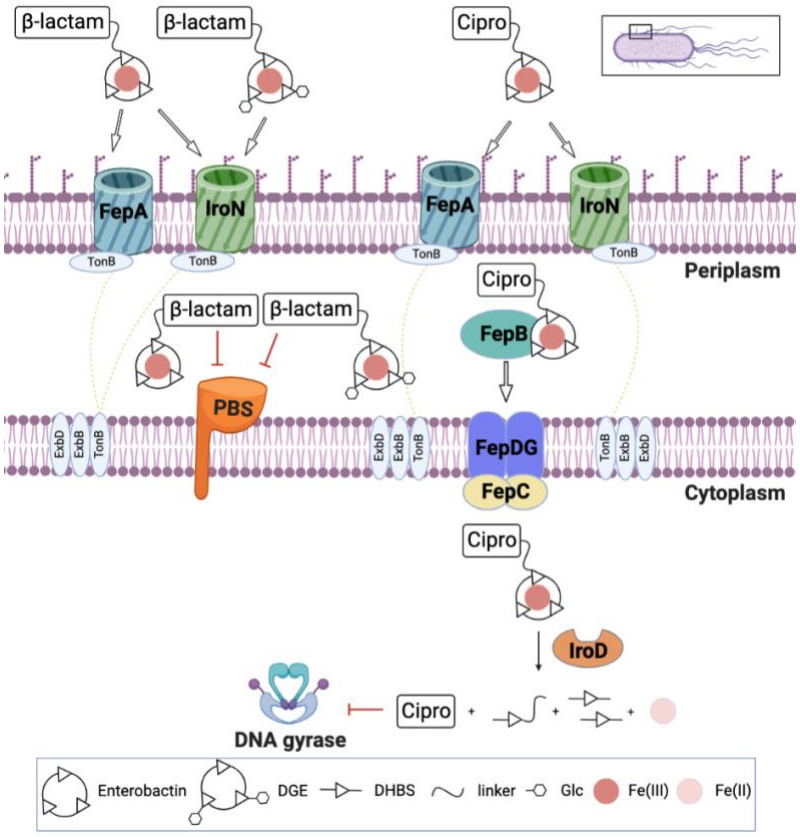

Figure 1.12. Working models of Ent–β-lactams and Ent-Cipro. Figure created with BioRender.com

To further examine the prodrug mechanism of Ent-Cipro **18**, our laboratory examined the ability of Ent-Cipro **18** and the hydrolytic product DHBS-Cipro **22** to inhibit *E. coli* DNA gyrase by monitoring the negative supercoiling of plasmid DNA using gel electrophoresis. This assay showed that both Ent-Cipro **18** and DHBS-Cipro **22** exhibited attenuated activity to inhibit DNA

gyrase, raising an inconsistency with the observed comparable potency of Ent-Cipro **18** to the parent antibiotic. Nevertheless, DHBS-Cipro **22** showed higher inhibitory activity against DNA gyrase compared to Ent-Cipro **18**, and one possible explanation is that Ent-mediated active transport increased the accumulation of DHBS-Cipro **22** in the cytoplasm, thereby compensating for its diminished DNA gyrase inhibitory activity when attached to DHBS.[70] Futher investigation is required to fully understand the activity and cellular fate of Ent-Cipro **18**, including ascertaining the identity of the active species and investigating the potential secondary mechanisms or other cellular targets that contribute to its antibacterial activity.

Other applications of the monofunctionalized Ent scaffolds. In addition to delivering toxic agents to Gram-negative bacterial cells, the monofunctionalized Ent scaffolds can be utilized for diverse applications by attaching cargos with different properties or functions (**Figure 1.13**). For instance, the fluorescent conjugate Ent-coumarin **23** was employed to visualize the periplasmic accumulation of Ent in an *E. coli* Δ*tolC* mutant, which lacks the OM component of tripartite efflux pumps.[106] The biotinylated conjugate Ent-biotin **24** was used to identify interacting proteins, furthering our understanding of the role of Ent in host–microbe and microbe–microbe interactions.[107-108] In future research, we envision the development of Ent-based conjugates for diagnostics and imaging as inspired by studies using other siderophores.[109]

Over the past decade, our laboratory has collaborated with the Raffatellu laboratory on developing Ent-based immunization as a strategy to prevent and ameliorate bacterial infections.[107, 110] We designed, synthesized, and evaluated conjugates of Ent and the mucosal adjuvant cholera toxin subunit B (Ent-CTB **25**, **Figure 1.13**). Our collaborative studies demonstrated that mice immunized with Ent-CTB **25** developed anti-Ent and anti-DGE antibodies in the gut mucosa. This immunization effectively reduced the colonization of *S*Tm or adherent invasive *E. coli* in murine

models of colitis, leading to reduced colitis severity.[107, 110] We also established a flow cytometry-based approach utilizing Ent-biotin **24** that allows for isolation and characterization of these siderophore-specific B cells.

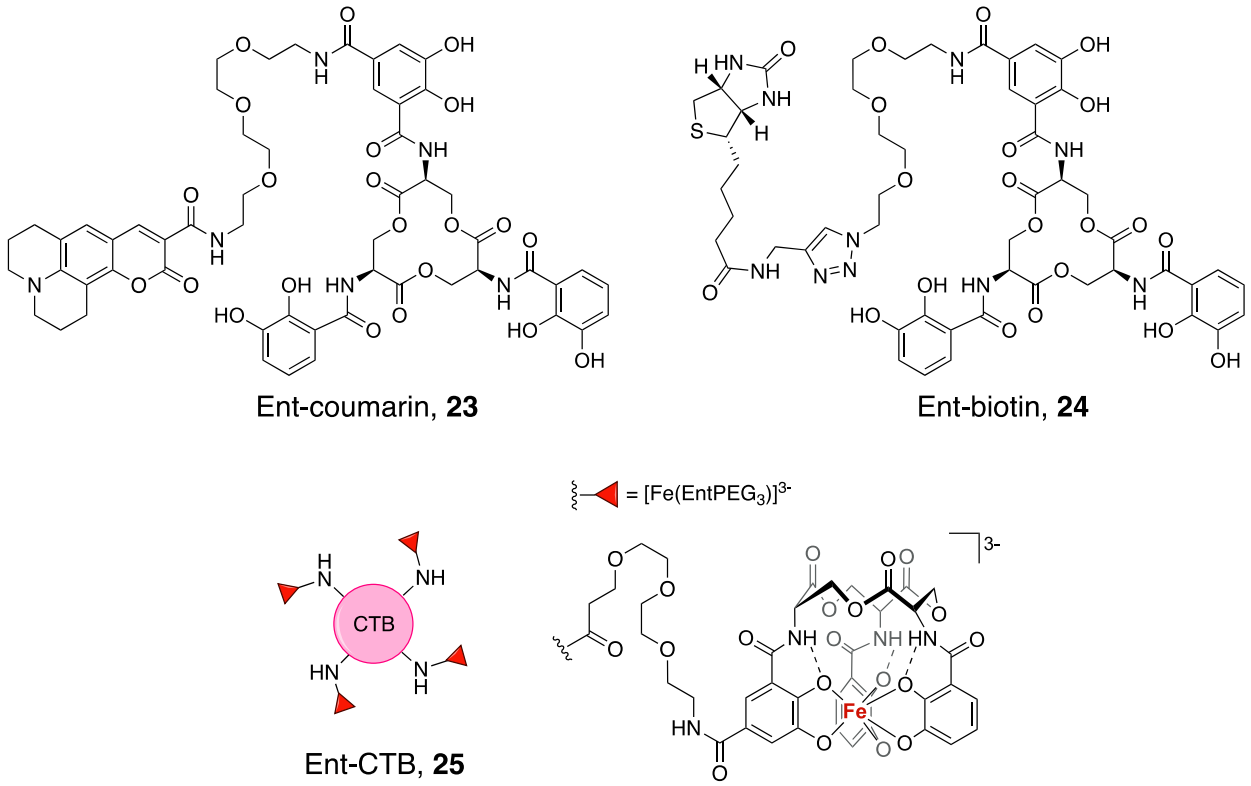

Figure 1.13. Chemical structures of Ent-coumarin **23**, Ent-biotin **24** and Ent-CTB **25**.

Summary and perspectives. Our laboratory has explored the potential of monofunctionalized Ent scaffolds, including L/D-Ent and salmochelins, in delivering classical antibiotics into bacterial cells. This strategy provides potent antibacterial activity and converts the broad-spectrum antibacterial cargos into narrow-spectrum antibiotics that target Gram-negative

bacteria, yielding promising candidates for future studies. In addition to antibacterial properties, we also elucidated the cellular consequences of Ent/DGE-drug conjugates. Such a thorough understanding is crucial for advancing SACs and guiding the future design of these antibacterial agents, an aspect lacking in many previous studies.

In recent years, progress has been made by others in developing new modifiable Ent scaffolds. Notably, Nodwell *et al* developed a solid-phase platform for rapid and combinatorial synthesis of Ent analogues.[111] Additionally, Zscherp *et al* established the synthesis of a novel monofunctionalized Ent derivative incorporating 3-hydroxy lysine on the macrocyclic trilactone, which holds promise as a new Ent-based scaffold.[112] Our pioneering work and these recent contributions will further explore the use of Ent as a tool to study the host–pathogen interactions.

With the long-term goal of furthering fundamental understanding and applying Ent–drug conjugates to the control and treatment of Gram-negative infections, our ongoing work involves evaluating their antibacterial activities against a broader range of pathogens, investigating the efficacies of promising candidates in animal models, furthering molecular design efforts, and developing other biological applications In closing, by leveraging the monofunctionalized Ent platform, we strive to make significant contributions to advancing our understanding of infectious disease and developing novel therapeutics to combat bacterial infections.

1.6 Platinum (Pt) anticancer agents.

Early studies on Pt anticancer agents and *E. coli.* Pt anticancer agents were serendipitously discovered by Rosenberg *et al.* during an investigation into the effects of an electric field on the growth of *E. coli*.[113] The application of the electric field resulted in the cessation of cell division and the formation of long filaments. Subsequently, upon the removal of the electric field, cell division gradually resumed along the entire length of the filament. This effect was attributed to the presence of 1–10 ppm of various group VIIIb transition metal ions in the culture medium, which inhibited cell division in *E. coli* without significantly interfering with growth.[113]

Subsequent research aimed to identify the active molecular species responsible for this growth effect on *E. coli*. It was observed that Pt chloride complexes formed during the electrolysis process, involving $(NH_4)_2[PtCl_6]$ which underwent a photochemical change. The doubly charged species $[PtCl_6]^{2-}$ that was produced rapidly converted to the singly negative species, $[PtCl_5(NH_3)]^-$, and finally to the neutral species $[PtCl_4(NH_3)_2]^0$, which was found to be the predominant species in the medium. Each species exhibited distinct effects on the growth of *E. coli*. The doubly negative species was bactericidal, while the singly negative species appeared to have minimal impact on the bacterial growth or cell division. The neutral species exhibited a limited effect on growth but significantly inhibited cell division processes, leading to filamentous growth.[114] It is noteworthy that Gram-negative bacilli were sensitive to cell division inhibition and filamentation induction caused by the neutral species, whereas Gram-positive bacilli only responded at near toxic levels. None of the tested cocci showed any apparent effect in this regard.[115]

The observation that Pt compounds inhibited cell division in Gram-negative bacteria sparked interest in testing Pt species for their antitumor activity. In this regard, cisplatin (*cis*-

$Pt(II)(NH_3)_2Cl_2$), was found to be the most effective compound, thus shifting the focus of Pt compounds as potential agents for anticancer therapies.[116] To investigate the mechanism of action and identify the cellular target of Pt, some studies examined the biological effects of cisplatin on bacterial cells, primarily *E. coli* as model systems.[117] Filamentation served as an indicator of Pt-induced DNA damage.[118] Further evidence of the interaction between Pt and DNA was achieved through the induction of lysis in lysogenic bacteria, which harbor the genetic information of a bacterial virus known as bacteriophage λ.[119-121] In lysogenic bacterial cells, viral gene expression is suppressed under normal conditions but induced in response to DNA damage, triggering the production of viral particles and ultimately resulting in cell lysis. The induction of lysis in lysogenic bacteria follows a mechanism similar to the initiation of the bacterial SOS response. Specifically, upon DNA damage, the major bacterial recombinase RecA binds to damaged DNA and subsequently activates SOS genes responsible for DNA repair during the SOS response as well as genes that are responsible for lytic transformation.[119, 121]

The ability of Pt agents to target DNA was further demonstrated by investigating the susceptibility of DNA repair-deficient mutants of *E. coli* to cisplatin.[122-125] Treatment of DNA repair-deficient mutants with cisplatin reduced cell viability to a significantly greater extent compared to the parent strain, indicating that the Pt-induced DNA damage is reversible, presumably through efficient mechanisms for DNA repair.[122-123] Direct evidence of Pt-DNA interaction was observed using closed circular DNA and analyzed through electron microscopy and electrophoresis, revealing the formation of intrastrand cross-links between adjacent guanine residues as a major effect of cisplatin on DNA.[126] Such DNA damage can be repaired by excision repair and recombination.[125, 127-128]

Early studies focused on investigating the biological effects of Pt compounds with the goal of establishing a correlation between their antitumor activities and their ability to inhibit bacterial cell division and induce lysis in lysogenic bacteria. The primary objective was to explore the potential use of bacterial cells as a screening tool for selecting novel Pt anticancer drugs based on the established correlation.[123] It is now recognized that there may not be a direct relationship between these two factors;[123] however, these studies provided valuable insights into the mode of action of Pt compounds in both mammalian cells and bacterial cells.

Commonly accepted mode of action of Pt compounds. The majority of studies on Pt agents focus on their fundamental understanding and translational application as anticancer agents in eukaryotic cells. Currently, three Pt anticancer drugs, namely cisplatin, carboplatin, and oxaliplatin, have been globally approved for clinical use in cancer treatment (**Figure 1.14A**). Through extensive investigations conducted by chemists, biologists, and physicians, a framework has been established to illustrate the underlying mechanisms of the anticancer activity of platinum drugs.[129] Taking cisplatin as an example, this complex is neutral and square-planar with two *cis*-ammine and two *cis*-chloro ligands. The ammine ligands, known as nonleaving groups, remain bound to the Pt center, while the chloro ligands, known as leaving groups, detach from the Pt(II) coordination sphere during intracellular transformation. The generalized mechanism of action involves four steps: cellular uptake, aquation/activation, DNA binding, and downstream effects induced by DNA lesions which results in cell death (**Figure 1.14B**).[129] The initial step in the generalized mechanism of action involves cellular uptake.[129] It is generally believed that Pt(II) anticancer agents like cisplatin and oxaliplatin primarily enter mammalian cells through passive diffusion, with active transport as a secondary pathway (*e.g.,* the organic cation transporter and the copper transporter 1).[130-131] Once inside the cell, cisplatin undergoes aquation, resulting in the loss

of one or both chloro ligands. The resulting Pt(II) aqua complexes are potent electrophiles, readily reacting with various biological nucleophiles with loss of the bound water molecules. The purine bases of nucleic acids, particularly at the N7 position, exhibit strong nucleophilicity. Consequently, cisplatin readily binds to DNA, predominantly forming bifunctional adducts with the loss of both chloro ligands. The primary DNA adduct is the intrastrand 1,2-d(GpG) crosslink, accounting for 60–65% of the bound platinum.[132] These DNA adducts distort and bend the DNA structure,[133-135] and such DNA lesions lead to downstream effects and ultimately cell death.[136]

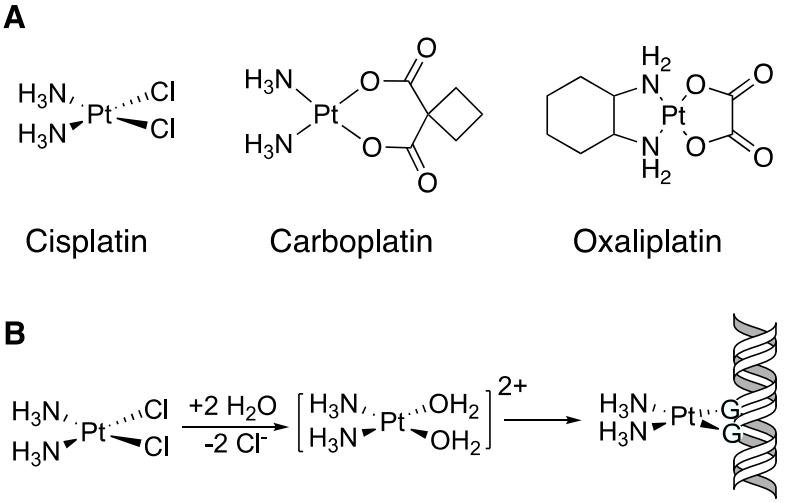

Figure 1.14. (A) Chemical structures of cisplatin, carboplatin, and oxaliplatin. **(B)** Generalized mechanism of action of cisplatin.

Pt(IV) prodrugs. Though cisplatin is one of the most effective chemotherapeutic agents used to treat 50% of all cancers, it is associated with significant dose-limiting toxicities including nephrotoxicity and neurotoxicity,[137-138] Consequently, extensive research has been dedicated to improving the efficacy and safety of Pt agents, and one prominent approach is the utilization of Pt(IV) prodrugs.

Unlike square-planar Pt(II) complexes, Pt(IV) complexes typically adopt octahedral geometries with six-coordinate structures. Due to their saturated d^6 electronic configuration, Pt(IV) complexes are more kinetically inert and therefore more resistant to ligand substitution compared to Pt(II) centers. This enhanced inertness minimizes unwanted side reactions with biomolecules prior to DNA binding. Upon entering cells, Pt(IV) prodrugs can be activated via reductive elimination in the reducing cytoplasmic environment, leading to the release of two axial ligands and the active Pt(II) species (**Figure 1.15A**).[129, 136]

Several Pt(IV) prodrugs have undergone clinical trials, though none have been approved for clinical use so far. For example, in the clinical trials, tetraplatin (or ormaplatin) exhibited excessive systemic toxicity,[139] whereas iproplatin showed low anticancer activity (**Figure 1.15B**).[140] The rapid reduction of the dichlorido complex (tetraplatin) and the slow reduction of the dihydroxido complex (iproplatin) in vivo hindered the optimal pharmacological activity of these compounds.

Efforts to optimize the carboxylation process of dihydroxido Pt(IV) compounds have led to the development of numerous dicarboxylato Pt(IV) complexes.[141] These complexes generally exhibit favorable stability in biological fluids and effective reductive activation upon cellular entry.[142-143] Notably, the diacetato prodrugs satraplatin (or JM216) and LA-12 have garnered attention through several clinical trials (**Figure 1.15B)**.[144-145] Despite promising in vitro and in vivo preclinical results, these prodrugs have not yet obtained full approval.

Pt(IV) complexes offer the opportunity to introduce different functionalities through the two additional axial ligands.[136] Various bioactive axial ligands have been incorporated, including specific tumor-targeting molecules, agents with additional pharmaceutical effects, or anticancer

drugs with different targets beyond DNA.[141] For example, mitaplatin incorporates two dichloroacetato units which inhibit pyruvate dehydrogenase kinase in cancer cells (**Figure 1.15B**). The cytotoxicity of mitaplatin toward various cancer cell lines has been demonstrated to be comparable to or greater than that of all known Pt(IV) compounds and is comparable to that of cisplatin.[146] Ethacraplatin possesses two axial units of ethacrynic acid, a clinical inhibitor of glutathione-S-transferase (GST) responsible for drug resistance in some cancers (**Figure 1.15B**). This compound has a fast-acting cytotoxicity with the capacity to inhibit GST activity, providing a strategy for using Pt(IV) to overcome resistance.[147]

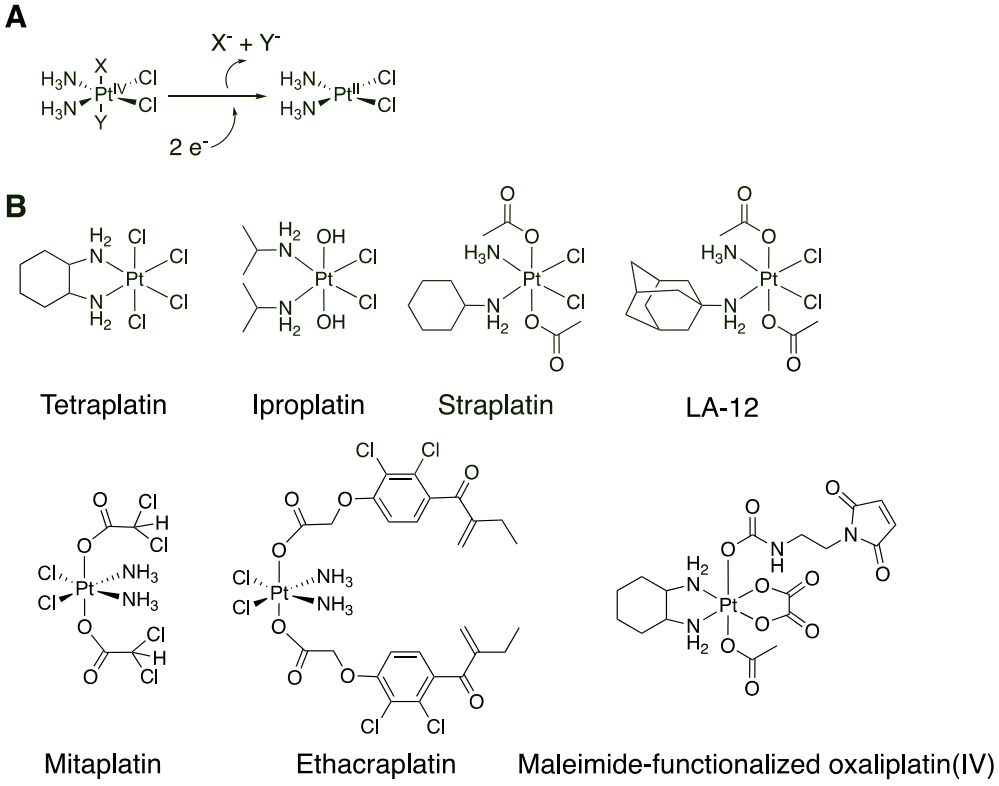

Figure 1.15. (A) Activation of Pt(IV) prodrugs by reductive elimination. **(B)** Chemical structures of Pt(IV) prodrugs.

Another example involves an oxaliplatin-based Pt(IV) complex with a maleimide moiety, enabling selective binding to serum albumin in the bloodstream (**Figure 1.15B**). This compound exhibits a prolonged plasma half-life, preferential accumulation in tumor tissue, and superior activity compared to the free drug, leading to successful treatment in mouse models.[148] The use of Pt(IV) prodrugs for targeting cancerous tissue has been extensively explored.[148-149] Overall, targeted delivery and controlled release of inactive Pt(IV) prodrugs hold promise for improving the efficacy and reducing side effects of Pt drugs.

Renewed interest in the antimicrobial properties of Pt compounds. In response to the rising crises of antibiotic resistance and the urgent need for novel antibacterial agents, there has been a renewed interest in exploring the antimicrobial properties of Pt agents. Joyce *et al.* investigated the antimicrobial spectrum of cisplatin by screening eight Gram-positive bacterial strains, seven Gram-negative bacterial strains, seven yeast strains, and seven mold strains, revealing that cisplatin effectively inhibited the growth of all tested microorganisms.[136, 150] Johnstone *et al.* revisited the ability of cisplatin to induce filamentous morphology in *E. coli* and initiate lysis in lysogenic bacteria. They also evaluated the effect of phenanthriplatin, a monofunctional Pt(II) agent, on non-lysogenic and lysogenic *E. coli*. Similar effects observed between phenanthriplatin and cisplatin suggested that phenanthriplatin also interacted with DNA.[119] Chowdhury *et al.* reported that cisplatin exhibited broad-spectrum activity against persister cells of *E. coli* K12 and several pathogens, including enterohemorrhagic *E. coli, S. aureus*, and *P. aeruginosa*. In particular, cisplatin was more effective than mitomycin C in eradicating *P. aeruginosa* persister cells.[151] The antibacterial activity of cisplatin against *P. aeruginosa* was also reported by Yuan *et al.* and Hummell *et al.*[152-153] Moreover, Yuan *et al.* demonstrated the effectiveness of cisplatin in eradicating in vitro biofilms and in vivo biofilms in

a murine keratitis model; however, this study noted that high doses of cisplatin were required, which could pose significant toxicity concerns in humans.[152]

1.7 Overview of thesis

Building upon the demonstrated effectiveness of Ent-based conjugates with traditional antibiotics, we reasoned that the Ent-based SAC approach can be further extended to drug repurposing for antibacterial purposes. Consequently, we expanded our exploration beyond traditional antibiotics to include Pt-based anticancer agents as cargos. Motivated by early studies on the antibacterial activity and mode of action of cisplatin in *E. coli*, as well as the renewed interest in the antibacterial effects of Pt compounds, our primary objective was to repurpose these anticancer agents as targeted antibiotics against Gram-negative bacteria (**Figure 1.16**). In this thesis, we describe the design and synthesis of four Ent-based conjugates incorporating Pt(IV) prodrugs. We evaluate the antibacterial properties of these conjugates and investigate the contributions of different components of the Ent uptake and processing machinery to their antibacterial features. Moreover, we decipher the underlying mechanisms behind their antibacterial activities, with a particular focus on the induction of DNA damage in bacterial cells. Furthermore, we conduct a comparative study to elucidate differing antibacterial activities and DNA damage profiles caused by these Ent–Pt(IV) conjugates.

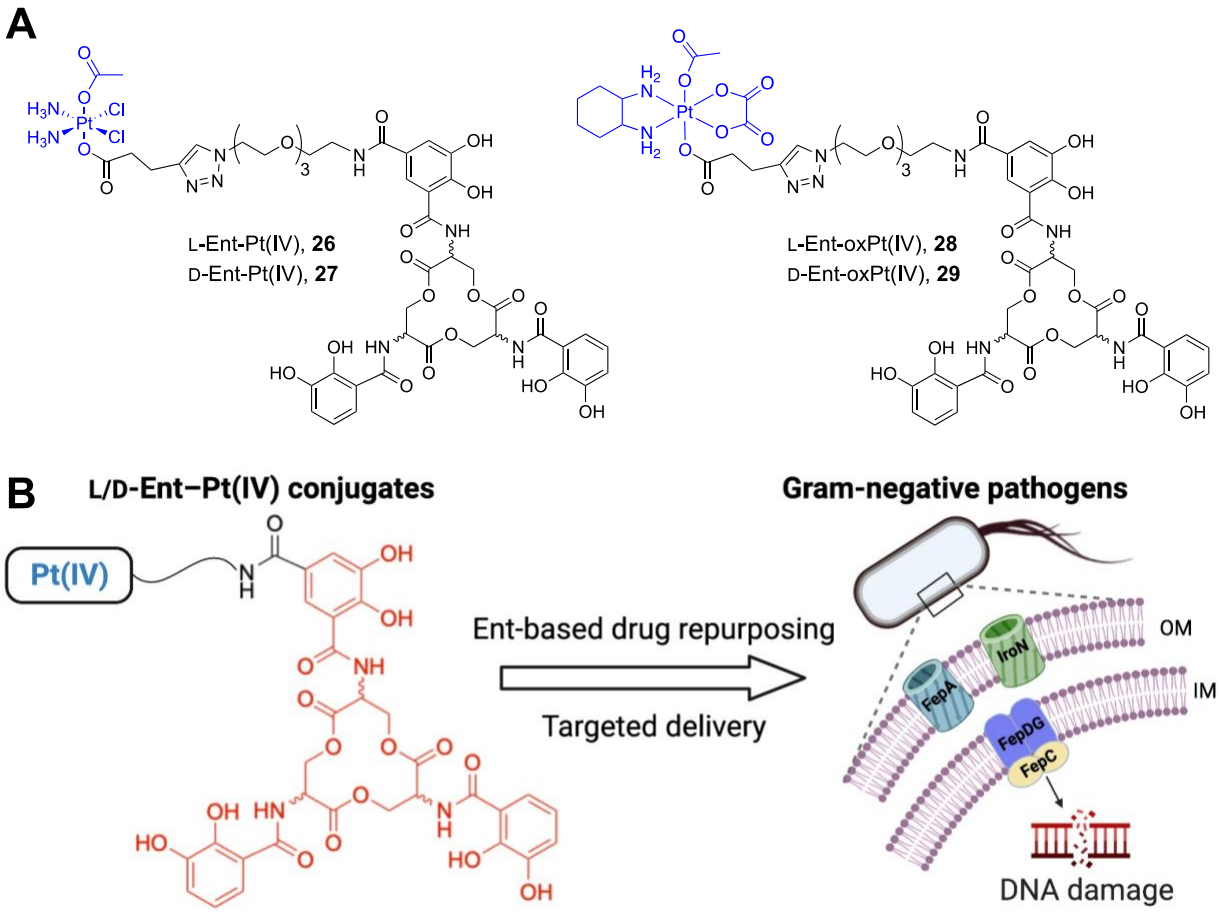

Figure 1.16. Overview of thesis. **(A)** Chemical structures of L/D-Ent-Pt(IV) (**26,27,** Chapter 2) and L/D-Ent-oxPt(IV) (**28,29,** Chapter 3). **(**B**)** Ent-based drug repurposing Pt anticancer agents as targeted antibiotics against Gram-negative bacteria. Figure created with BioRender.com

In Chapter 2, we present our work on repurposing cisplatin, the first FDA-approved Pt agent, as a Gram-negative antibiotic. We commenced with cisplatin because of its small size and known effects on Gram-negative bacteria. Cisplatin exhibits modest antibacterial activity and high cytotoxicity toward human cells. To conjugate Ent and mask the toxicity of Pt(II) prior to entering targeted bacterial cells, we employ a cisplatin-based Pt(IV) prodrug approach and install Ent to one of the axial ligands for targeted delivery into Gram-negative bacteria (L-Ent-Pt(IV) **26, Figure 1.16**). We demonstrate that L-Ent-Pt(IV) **26** is selectively imported into the *E. coli* cytoplasm by

the Ent uptake machinery (FepABCDG), where the Pt(IV) prodrug is activated by intracellular reduction, releasing cisplatin that causes growth inhibition and filamentation in *E. coli*. Based on our results of L-Ent-Pt(IV) **26**, we further design the D-enantiomer conjugate D-Ent-Pt(IV) (**27**, **Figure 1.16**), which shows enhanced antibacterial activity compared to L-Ent-Pt(IV) and cisplatin. This improved potency is attributed to the stability of the D-trilactone moiety toward hydrolysis catalyzed by the L-Ent esterase Fes, thereby preventing Fe release for bacterial metabolic use. We also demonstrate that Ent conjugation enhances Pt uptake in *E. coli* but markedly reduces Pt uptake in the human cell line HEK293T. Overall, this study demonstrates that Ent conjugation to a Pt(IV) prodrug repurposes cisplatin as an antibiotic that selectively targets Gram-negative bacteria via Ent transport machinery, indicating the potential of using siderophore-based drug delivery for drug repurposing.[154]

In Chapter 3, we expand the application of Ent-based drug repurposing to oxaliplatin. We chose oxaliplatin due to its global approval as a Pt anticancer agent and its unique features, including a distinct spectrum of antitumor activity and no reported cross-resistance with cisplatin and carboplatin. We examine the conjugates L/D-Ent-oxPt(IV) (**28,29, Figure 1.16**), demonstrating that L/D-Ent-oxPt(IV) **28,29** show similar trends compared to L/D-Ent-Pt(IV) **26,27** with D-Ent-oxPt(IV) **29** exhibiting enhanced antibacterial activity; however, L/D-Ent-oxPt(IV) **28,29** exhibits lower potency in growth inhibition and filamentation induction compared to L/D-Ent-Pt(IV). This observation aligns with the reduced potency of oxaliplatin in inducing filamentation in *E. coli* compared to cisplatin. We further investigate the varying antibacterial activities of L/D-Ent-Pt(IV) **26,27** and L/D-Ent-oxPt(IV) **28,29** by examining the extent of DNA damage induced by these Pt complexes. Our data indicate that in comparison to oxaliplatin and L/D-Ent-oxPt(IV) **28,29**, cisplatin and L/D-Ent-Pt(IV) **26,27** induce markedly higher levels of DNA

damage. These findings establish a correlation between the antibacterial activity of Ent–Pt(IV) conjugates and their capacity to cause DNA damage in *E. coli*. This fundamental understanding provides crucial insights for further development and investigation of other siderophore-based Pt antibacterials.[155]

1.8 References

1. Libertucci, J.; Young, V. B., The role of the microbiota in infectious diseases. *Nat. Microbiol.* **2019,** *4*, 35-45.

2. Pickard, J. M.; Zeng, M. Y.; Caruso, R.; Núñez, G., Gut microbiota: role in pathogen colonization, immune responses, and inflammatory disease. *Immunol. Rev.* **2017,** *279*, 70-89.

3. Fleming, A., On the antibacterial action of cultures of a penicillium, with special reference to their use in the isolation of B. influenzae. *Br. J. Exp. Pathol.* **1929,** *10*, 226-236.

4. Wencewicz, T. A., New antibiotics from Nature's chemical inventory. *Bioorg. Med. Chem.* **2016,** *24*, 6227-6252.

5. Wencewicz, T. A.; Miller, M. J., Sideromycins as pathogen-targeted antibiotics. In *Antibacterials: Volume II*, Fisher, J. F.; Mobashery, S.; Miller, M. J., Eds. Springer International Publishing: Cham, 2018; pp 151-183.

6. Clatworthy, A. E.; Pierson, E.; Hung, D. T., Targeting virulence: a new paradigm for antimicrobial therapy. *Nat. Chem. Biol.* **2007,** *3*, 541-548.

7. Barczak, A. K.; Hung, D. T., Productive steps toward an antimicrobial targeting virulence. *Curr. Opin. Microbiol.* **2009,** *12*, 490-496.

8. Theriot, C. M.; Koenigsknecht, M. J.; Carlson Jr, P. E.; Hatton, G. E.; Nelson, A. M.; Li, B.; Huffnagle, G. B.; Z. Li, J.; Young, V. B., Antibiotic-induced shifts in the mouse gut microbiome and metabolome increase susceptibility to *Clostridium difficile* infection. *Nat. Commun.* **2014,** *5*, 3114.

9. Theriot, C. M.; Bowman, A. A.; Young, V. B., Antibiotic-induced alterations of the gut microbiota alter secondary bile acid production and allow for *Clostridium difficile* spore germination and outgrowth in the large intestine. *mSphere* **2016,** *1*, e00045-15.

10. Melander, R. J.; Zurawski, D. V.; Melander, C., Narrow-spectrum antibacterial agents. *Med. Chem. Commun.* **2018,** *9*, 12-21.

11. Antibiotic resistance threats in the United States, 2019. U.S. Centers for Disease Control and Prevention: 2019.

12. Walsh, C.; Wencewicz, T., *Antibiotics: challenges, mechanisms, opportunities*. John Wiley & Sons: 2020.

13. Prioritization of pathogens to guide discovery, research and development of new antibiotics for drug-resistant bacterial infections, including tuberculosis. World Health Organization: 2017.

14. Murdoch, C. C.; Skaar, E. P., Nutritional immunity: the battle for nutrient metals at the host–pathogen interface. *Nat. Rev. Microbiol.* **2022,** *20*, 657-670.

15. Weinberg, E. D., Nutritional immunity. Host's attempt to withold iron from microbial invaders. *J. Am. Med. Assoc.* **1975,** *231*, 39-41.

16. Hood, M. I.; Skaar, E. P., Nutritional immunity: transition metals at the pathogen-host interface. *Nat. Rev. Microbiol.* **2012,** *10*, 525-537.

17. Gerner, R. R.; Nuccio, S. P.; Raffatellu, M., Iron at the host-microbe interface. *Mol. Aspects. Med.* **2020,** *75*, 100895.

18. Obisesan, A. O.; Zygiel, E. M.; Nolan, E. M., Bacterial responses to iron withholding by calprotectin. *Biochemistry* **2021,** *60*, 3337-3346.

19. Raymond, K. N.; Dertz, E. A.; Kim, S. S., Enterobactin: an archetype for microbial iron transport. *Proc. Natl. Acad. Sci. U.S.A.* **2003,** *100*, 3584-3588.

20. Cornelis, P.; Wei, Q.; Andrews, S. C.; Vinckx, T., Iron homeostasis and management of oxidative stress response in bacteria. *Metallomics* **2011,** *3*, 540-549.

21. Skaar, E. P., The battle for iron between bacterial pathogens and their vertebrate hosts. *PLoS Pathog.* **2010,** *6*, e1000949.

22. Hider, R. C.; Kong, X., Chemistry and biology of siderophores. *Nat. Prod. Rep.* **2010,** *27*, 637-657.

23. Kramer, J.; Özkaya, Ö.; Kümmerli, R., Bacterial siderophores in community and host interactions. *Nat. Rev. Microbiol.* **2020,** *18*, 152-163.

24. Miethke, M.; Marahiel, M. A., Siderophore-based iron acquisition and pathogen control. *Microbiol. Mol. Biol. Rev.* **2007,** *71*, 413-51.

25. Cuív, P. Ó.; Clarke, P.; apos; Connell, M., Identification and characterization of an iron-regulated gene, chtA, required for the utilization of the xenosiderophores aerobactin, rhizobactin 1021 and schizokinen by *Pseudomonas aeruginosa*. *Microbiology* **2006,** *152*, 945-954.

26. Poole, K.; McKay, G. A., Iron acquisition and its control in *Pseudomonas aeruginosa*: many roads lead to Rome. *Front. Biosci.* **2003,** *8*, 661-686.

27. Braun, V.; Pramanik, A.; Gwinner, T.; Köberle, M.; Bohn, E., Sideromycins: tools and antibiotics. *Biometals* **2009,** *22*, 3-13.

28. Vassiliadis, G.; Destoumieux-Garzón, D.; Lombard, C.; Rebuffat, S.; Peduzzi, J., Isolation and characterization of two members of the siderophore-microcin family, microcins M and H47. *Antimicrob. Agents Chemother.* **2010,** *54*, 288-297.

29. Thomas, X.; Destoumieux-Garzón, D.; Peduzzi, J.; Afonso, C.; Blond, A.; Birlirakis, N.; Goulard, C.; Dubost, L.; Thai, R.; Tabet, J.-C.; Rebuffat, S., Siderophore peptide, a new type of post-translationally modified antibacterial peptide with potent activity. *J. Biol. Chem.* **2004,** *279*, 28233-28242.

30. Nolan, E. M.; Fischbach, M. A.; Koglin, A.; Walsh, C. T., Biosynthetic tailoring of microcin E492m: post-translational modification affords an antibacterial siderophore−peptide conjugate. *J. Am. Chem. Soc.* **2007,** *129*, 14336-14347.

31. Sassone-Corsi, M.; Nuccio, S.-P.; Liu, H.; Hernandez, D.; Vu, C. T.; Takahashi, A. A.; Edwards, R. A.; Raffatellu, M., Microcins mediate competition among Enterobacteriaceae in the inflamed gut. *Nature* **2016,** *540*, 280-283.

32. Palmer, J. D.; Mortzfeld, B. M.; Piattelli, E.; Silby, M. W.; McCormick, B. A.; Bucci, V., Microcin H47: a class IIb microcin with potent activity against multidrug resistant *Enterobacteriaceae*. *ACS Infect. Dis.* **2020,** *6*, 672-679.

33. Vassiliadis, G.; Destoumieux-Garzón, D.; Peduzzi, J., Class II microcins. In *Prokaryotic antimicrobial peptides: from genes to applications*, Drider, D.; Rebuffat, S., Eds. Springer New York: New York, NY, 2011; pp 309-332.

34. Reynolds, D. M.; Schatz, A.; Waksman, S. A., Grisein, a new antibiotic produced by a strain of *Streptomyces griseus*. *Proc. Soc. Exp. Biol. Med.* **1947,** *64*, 50-54.

35. Benz, G.; Schröder, T. D.; Kurz, J.; Wünsche, C.; Karl, W.; Steffens, G.; Pfitzner, J. D.; Schmidt, D., Constitution of the deferriform of the albomycins δ_1, δ_2, and ε. *Angew. Chem. Int. Ed. Engl.* **1982,** *21*, 527-528.

36. Sigel, A.; Sigel, H., Metal ions in biological systems. In *Enzyme Chemistry: Impact and applications*, Suckling, C. J., Ed. Springer Netherlands: Dordrecht, 1998; pp 162-195.

37. Al Shaer, D.; Al Musaimi, O.; de la Torre, B. G.; Albericio, F., Hydroxamate siderophores: natural occurrence, chemical synthesis, iron binding affinity and use as Trojan horses against pathogens. *Eur. J. Med. Chem.* **2020,** *208*, 112791.

38. Stefanska, A. L.; Fulston, M.; Houge-Frydrych, C. S.; Jones, J. J.; Warr, S. R., A potent seryl tRNA synthetase inhibitor SB-217452 isolated from a *Streptomyces* species. *J. Antibiot.* **2000,** *53*, 1346-1353.

39. Ferguson, A. D.; Braun, V.; Fiedler, H.-P.; Coulton, J. W.; Diederichs, K.; Welte, W., Crystal structure of the antibiotic albomycin in complex with the outer membrane transporter FhuA. *Protein Sci.* **2000,** *9*, 956-963.

40. Bickel, H.; Mertens, P.; Prelog, V.; Seibl, J.; Walser, A., Stoffwechselprodukte von mikroorganismen—53: Ueber die konstitution von ferrimycin A_1. *Tetrahedron* **1966,** *22*, 171-179.

41. Sackmann, W.; Reusser, P.; Neipp, L.; Kradolfer, F.; Gross, F., Ferrimycin A, a new iron-containing antibiotic. *Antibiot. Chemother.* **1962,** *12*, 34-45.

42. Vértesy, L.; Aretz, W.; Fehlhaber, H.-W.; Kogler, H., Salmycin A–D, antibiotika aus *Streptomyces violaceus*, DSM 8286, mit siderophor-aminoglycosid-struktur. *Helv. Chim. Acta.* **1995,** *78*, 46-60.

43. Bunet, R.; Brock, A.; Rexer, H.-U.; Takano, E., Identification of genes involved in siderophore transport in *Streptomyces coelicolor* A3(2). *FEMS Microbiol. Lett.* **2006,** *262*, 57-64.

44. Lin, Y. M.; Ghosh, M.; Miller, P. A.; Möllmann, U.; Miller, M. J., Synthetic sideromycins (skepticism and optimism): selective generation of either broad or narrow spectrum Gram-negative antibiotics. *Biometals* **2019,** *32*, 425-451.

45. Sargun, A.; Gerner, R. R.; Raffatellu, M.; Nolan, E. M., Harnessing iron acquisition machinery to target *Enterobacteriaceae*. *J. Infect. Dis.* **2020,** *223* (Supplement_3), S307-S313.

46. Baquero, F.; Moreno, F., The microcins. *FEMS Microbiol. Lett.* **1984,** *23*, 117-124.

47. Bieler, S.; Silva, F.; Soto, C.; Belin, D., Bactericidal activity of both secreted and nonsecreted microcin E492 requires the mannose permease. *J. Bacteriol.* **2006,** *188*, 7049-7061.

48. Miller, M. J.; Malouin, F., Microbial iron chelators as drug delivery agents: the rational design and synthesis of siderophore-drug conjugates. *Acc. Chem. Res.* **1993,** *26*, 241-249.

49. Kong, K. F.; Schneper, L.; Mathee, K., Beta-lactam antibiotics: from antibiosis to resistance and bacteriology. *APMIS* **2010,** *118*, 1-36.

50. Zhao, H.; Patel, V.; Helmann, J. D.; Dörr, T., Don't let sleeping dogmas lie: new views of peptidoglycan synthesis and its regulation. *Mol. Microbiol.* **2017,** *106*, 847-860.

51. Katsu, K.; Kitoh, K.; Inoue, M.; Mitsuhashi, S., In vitro antibacterial activity of E-0702, a new semisynthetic cephalosporin. *Antimicrob. Agents Chemother.* **1982,** *22*, 181-185.

52. Ohi, N.; Aoki, B.; Shinozaki, T.; Moro, K.; Noto, T.; Nehashi, T.; Okazaki, H.; Matsunaga, I., Semisynthetic beta-lactam antibiotics. I. synthesis and antibacterial activity of new ureidopenicillin derivatives having catechol moieties. *J. Antibiot.* **1986,** *39*, 230-241.

53. Sykes, R. B.; Koster, W. H.; Bonner, D. P., The new monobactams: chemistry and biology. *J. Clin. Pharmacol.* **1988,** *28*, 113-119.

54. Barbachyn, M. R.; Tuominen, T. C., Synthesis and structure-activity relationships of monocarbams leading to U-78608. *J. Antibiot.* **1990,** *43*, 1199-1203.

55. Ogino, H.; Iwamatsu, K.; Katano, K.; Nakabayashi, S.; Yoshida, T.; Shibahara, S.; Tsuruoka, T.; Inouye, S.; Kondo, S., New aminothiazolylglycylcephalosporins with a 1,5-dihydroxy-4-pyridone-2-carbonyl group. II. Synthesis and antibacterial activity of MT0703 and its diastereomers. *J Antibiot.* **1990,** *43*, 189-198.

56. Dolence, E. K.; Minnick, A. A.; Lin, C. E.; Miller, M. J.; Payne, S. M., Synthesis and siderophore and antibacterial activity of N^5-acetyl-N^5-hydroxyl-L-ornithine derived siderophore-β-lactam conjugates: iron transport mediated drug delivery. *J. Med. Chem.* **1991,** *34*, 968-978.

57. Flanagan, M. E.; Brickner, S. J.; Lall, M.; Casavant, J.; Deschenes, L.; Finegan, S. M.; George, D. M.; Granskog, K.; Hardink, J. R.; Huband, M. D.; Hoang, T.; Lamb, L.; Marra, A.;

Mitton-Fry, M.; Mueller, J. P.; Mullins, L. M.; Noe, M. C.; O'Donnell, J. P.; Pattavina, D.; Penzien, J. B.; Schuff, B. P.; Sun, J.; Whipple, D. A.; Young, J.; Gootz, T. D., Preparation, Gram-negative antibacterial activity, and hydrolytic stability of novel siderophore-conjugated monocarbam diols. *ACS. Med. Chem. Lett.* **2011,** *2*, 385-390.

58. Page, M. G.; Dantier, C.; Desarbre, E., In vitro properties of BAL30072, a novel siderophore sulfactam with activity against multiresistant Gram-negative bacilli. *Antimicrob. Agents Chemother.* **2010,** *54*, 2291-2302.

59. Tomaras, A. P.; Crandon, J. L.; McPherson, C. J.; Nicolau, D. P., Potentiation of antibacterial activity of the MB-1 siderophore-monobactam conjugate using an efflux pump inhibitor. *Antimicrob. Agents Chemother.* **2015,** *59*, 2439-2442.

60. McPherson, C. J.; Aschenbrenner, L. M.; Lacey, B. M.; Fahnoe, K. C.; Lemmon, M. M.; Finegan, S. M.; Tadakamalla, B.; O'Donnell, J. P.; Mueller, J. P.; Tomaras, A. P., Clinically relevant Gram-negative resistance mechanisms have no effect on the efficacy of MC-1, a novel siderophore-conjugated monocarbam. *Antimicrob. Agents. Chemother.* **2012,** *56*, 6334-6342.

61. Sato, T.; Yamawaki, K., Cefiderocol: discovery, chemistry, and in vivo profiles of a novel siderophore cephalosporin. *Clin. Infect. Dis.* **2019,** *69*, S538-S543.

62. Tillotson, G. S., Trojan horse antibiotics–a novel way to circumvent Gram-negative bacterial resistance? *Infect. Dis.* **2016,** *9*, 45-52.

63. Tomaras, A. P.; Crandon, J. L.; McPherson, C. J.; Banevicius, M. A.; Finegan, S. M.; Irvine, R. L.; Brown, M. F.; O'Donnell, J. P.; Nicolau, D. P., Adaptation-based resistance to siderophore-conjugated antibacterial agents by *Pseudomonas aeruginosa*. *Antimicrob. Agents Chemother.* **2013,** *57*, 4197-4207.

64. Miller, M. J.; Zhu, H.; Xu, Y.; Wu, C.; Walz, A. J.; Vergne, A.; Roosenberg, J. M.; Moraski, G.; Minnick, A. A.; McKee-Dolence, J.; Hu, J.; Fennell, K.; Kurt Dolence, E.; Dong, L.; Franzblau, S.; Malouin, F.; Möllmann, U., Utilization of microbial iron assimilation processes for the development of new antibiotics and inspiration for the design of new anticancer agents. *Biometals* **2009,** *22*, 61-75.

65. Wencewicz, T. A.; Möllmann, U.; Long, T. E.; Miller, M. J., Is drug release necessary for antimicrobial activity of siderophore-drug conjugates? Syntheses and biological studies of the naturally occurring salmycin "Trojan Horse" antibiotics and synthetic desferridanoxamine-antibiotic conjugates. *Biometals* **2009,** *22*, 633-648.

66. Liu, R.; Miller, P. A.; Vakulenko, S. B.; Stewart, N. K.; Boggess, W. C.; Miller, M. J., A synthetic dual drug sideromycin induces Gram-negative bacteria to commit suicide with a Gram-positive antibiotic. *J. Med. Chem.* **2018,** *61*, 3845-3854.

67. Negash, K. H.; Norris, J. K. S.; Hodgkinson, J. T., Siderophore-antibiotic conjugate design: new drugs for bad bugs? *Molecules (Basel, Switzerland)* **2019,** *24*, 3314.

68. Dolence, E. K.; Lin, C. E.; Miller, M. J.; Payne, S. M., Synthesis and siderophore activity of albomycin-like peptides derived from N^5-acetyl-N^5-hydroxy-L-ornithine. *J. Med. Chem.* **1991,** *34*, 956-968.

69. Milner, S. J.; Seve, A.; Snelling, A. M.; Thomas, G. H.; Kerr, K. G.; Routledge, A.; Duhme-Klair, A.-K., Staphyloferrin A as siderophore-component in fluoroquinolone-based Trojan horse antibiotics. *Org. Biomol. Chem.* **2013,** *11*, 3461-3468.

70. Neumann, W.; Sassone-Corsi, M.; Raffatellu, M.; Nolan, E. M., Esterase-catalyzed siderophore hydrolysis activates an enterobactin-ciprofloxacin conjugate and confers targeted antibacterial activity. *J. Am. Chem. Soc.* **2018,** *140*, 5193-5201.

71. Zheng, T.; Bullock, J. L.; Nolan, E. M., Siderophore-mediated cargo delivery to the cytoplasm of *Escherichia coli* and *Pseudomonas aeruginosa*: syntheses of monofunctionalized enterobactin scaffolds and evaluation of enterobactin–cargo conjugate uptake. *J. Am. Chem. Soc.* **2012,** *134*, 18388-18400.

72. Paulen, A.; Gasser, V.; Hoegy, F.; Perraud, Q.; Pesset, B.; Schalk, I. J.; Mislin, G. L., Synthesis and antibiotic activity of oxazolidinone-catechol conjugates against *Pseudomonas aeruginosa*. *Org. Biomol. Chem.* **2015,** *13*, 11567-11579.

73. Rivault, F.; Liébert, C.; Burger, A.; Hoegy, F.; Abdallah, M. A.; Schalk, I. J.; Mislin, G. L. A., Synthesis of pyochelin–norfloxacin conjugates. *Bioorganic Med. Chem. Lett.* **2007,** *17*, 640-644.

74. Neumann, W.; Nolan, E. M., Evaluation of a reducible disulfide linker for siderophore-mediated delivery of antibiotics. *J. Biol. Inorg. Chem.* **2018,** *23*, 1025-1036.

75. Juárez-Hernández, R. E.; Miller, P. A.; Miller, M. J., Syntheses of siderophore–drug conjugates using a convergent thiol–maleimide system. *ACS Med. Chem. Lett.* **2012,** *3*, 799-803.

76. Milner, S. J.; Snelling, A. M.; Kerr, K. G.; Abd-El-Aziz, A.; Thomas, G. H.; Hubbard, R. E.; Routledge, A.; Duhme-Klair, A. K., Probing linker design in citric acid-ciprofloxacin conjugates. *Bioorg. Med. Chem.* **2014,** *22*, 4499-4505.

77. Zheng, T.; Nolan, E. M., Evaluation of (acyloxy)alkyl ester linkers for antibiotic release from siderophore-antibiotic conjugates. *Bioorg. Med. Chem. Lett.* **2015,** *25*, 4987-4991.

78. Ji, C.; Miller, M. J., Siderophore–fluoroquinolone conjugates containing potential reduction-triggered linkers for drug release: synthesis and antibacterial activity. *BioMetals* **2015,** *28*, 541-551.

79. Ji, C.; Miller, M. J., Chemical syntheses and in vitro antibacterial activity of two desferrioxamine B-ciprofloxacin conjugates with potential esterase and phosphatase triggered drug release linkers. *Bioorg. Med. Chem.* **2012,** *20*, 3828-3836.

80. Mustaev, A.; Malik, M.; Zhao, X.; Kurepina, N.; Luan, G.; Oppegard, L. M.; Hiasa, H.; Marks, K. R.; Kerns, R. J.; Berger, J. M., Fluoroquinolone-gyrase-DNA complexes: two modes of drug binding. *J. Biol. Chem.* **2014,** *289*, 12300-12312.

81. Rayner, B.; Verderosa, A. D.; Ferro, V.; Blaskovich, M. A. T., Siderophore conjugates to combat antibiotic-resistant bacteria. *RSC Med. Chem.* **2023,** *14*, 800-822.

82. Noël, S.; Gasser, V.; Pesset, B.; Hoegy, F.; Rognan, D.; Schalk, I. J.; Mislin, G. L., Synthesis and biological properties of conjugates between fluoroquinolones and a N3′′-functionalized pyochelin. *Org. Biomol. Chem.* **2011,** *9*, 8288-8300.

83. Peukert, C.; Vetter, A. C.; Fuchs, H. L. S.; Harmrolfs, K.; Karge, B.; Stadler, M.; Brönstrup, M., Siderophore conjugation with cleavable linkers boosts the potency of RNA polymerase inhibitors against multidrug-resistant *E. coli*. *Chem. Sci.* **2023,** *14*, 5490-5502.

84. Levine, M. N.; Raines, R. T., Trimethyl lock: a trigger for molecular release in chemistry, biology, and pharmacology. *Chem. Sci.* **2012,** *3*, 2412-2420.

85. Miller, M. J.; Walz, A. J.; Zhu, H.; Wu, C.; Moraski, G.; Möllmann, U.; Tristani, E. M.; Crumbliss, A. L.; Ferdig, M. T.; Checkley, L.; Edwards, R. L.; Boshoff, H. I., Design, synthesis, and study of a mycobactin−artemisinin conjugate that has selective and potent activity against tuberculosis and malaria. *J. Am. Chem. Soc.* **2011,** *133*, 2076-2079.

86. Barbachyn, M. R., The Oxazolidinones. In *Antibacterials: Volume II*, Fisher, J. F.; Mobashery, S.; Miller, M. J., Eds. Springer International Publishing: Cham, 2018; pp 97-121.

87. Zheng, T.; Nolan, E. M., Enterobactin-mediated delivery of β-lactam antibiotics enhances antibacterial activity against pathogenic *Escherichia coli*. *J. Am. Chem. Soc.* **2014,** *136*, 9677-9691.

88. Thulasiraman, P.; Newton, S. M.; Xu, J.; Raymond, K. N.; Mai, C.; Hall, A.; Montague, M. A.; Klebba, P. E., Selectivity of ferric enterobactin binding and cooperativity of transport in Gram-negative bacteria. *J. Bacteriol.* **1998,** *180*, 6689-6696.

89. Poole, K.; Young, L.; Neshat, S., *Enterobactin-mediated iron transport in* Pseudomonas aeruginosa. *J. Bacteriol.* **1990,** *172*, 6991-6.

90. Subashchandrabose, S.; Smith, S.; DeOrnellas, V.; Crepin, S.; Kole, M.; Zahdeh, C.; Mobley, H. L. T., *Acinetobacter baumannii* genes required for bacterial survival during bloodstream infection. *mSphere* **2016,** *1*, 10.1128/msphere.00013-15.

91. Loomis, L. D.; Raymond, K. N., Solution equilibria of enterobactin and metal-enterobactin complexes. *Inorg. Chem.* **1991,** *30*, 906-911.

92. Corey, E. J.; Bhattacharyya, S., Total synthesis of enterobactin, a macrocyclic iron transporting agent of bacteria. *Tetrahedron Lett.* **1977,** *18*, 3919-3922.

93. Krewulak, K. D.; Vogel, H. J., Structural biology of bacterial iron uptake. *Biochim Biophys Acta* **2008,** *1778*, 1781-1804.

94. Shea, C.; McIntosh, M., Nucleotide sequence and genetic organization of the ferric enterobactin transport system: homology to other peripiasmic binding protein-dependent systems in *Escherichia coli*. *Mol. Microbiol.* **1991,** *5*, 1415-1428.

95. Chakraborty, R.; Storey, E.; van der Helm, D., Molecular mechanism of ferricsiderophore passage through the outer membrane receptor proteins of *Escherichia coli*. *BioMetals* **2007,** *20*, 263-274.

96. Lin, H.; Fischbach, M. A.; Liu, D. R.; Walsh, C. T., In vitro characterization of salmochelin and enterobactin trilactone hydrolases IroD, IroE, and Fes. *J. Am. Chem. Soc.* **2005,** *127*, 11075-11084.

97. Abergel, R. J.; Zawadzka, A. M.; Hoette, T. M.; Raymond, K. N., Enzymatic hydrolysis of trilactone siderophores: where chiral recognition occurs in enterobactin and bacillibactin iron transport. *J. Am. Chem. Soc.* **2009,** *131*, 12682-12692.

98. Miethke, M.; Hou, J.; Marahiel, M. A., The siderophore-interacting protein YqjH acts as a ferric reductase in different iron assimilation pathways of *Escherichia coli*. *Biochemistry* **2011,** *50*, 10951-10964.

99. Fischbach, M. A.; Lin, H.; Zhou, L.; Yu, Y.; Abergel, R. J.; Liu, D. R.; Raymond, K. N.; Wanner, B. L.; Strong, R. K.; Walsh, C. T., The pathogen-associated *iroA* gene cluster mediates bacterial evasion of lipocalin 2. *Proc. Natl. Acad. Sci. U.S.A.* **2006,** *103*, 16502-16507.

100. Hantke, K.; Nicholson, G.; Rabsch, W.; Winkelmann, G., Salmochelins, siderophores of *Salmonella enterica* and uropathogenic *Escherichia coli* strains, are recognized by the outer membrane receptor IroN. *Proc. Natl. Acad. Sci. U.S.A.* **2003,** *100*, 3677-3682.

101. Chairatana, P.; Zheng, T.; Nolan, E. M., Targeting virulence: salmochelin modification tunes the antibacterial activity spectrum of β-lactams for pathogen-selective killing of *Escherichia coli*. *Chem. Sci.* **2015,** *6*, 4458-4471.

102. Sargun, A.; Johnstone, T. C.; Zhi, H.; Raffatellu, M.; Nolan, E. M., Enterobactin- and salmochelin-β-lactam conjugates induce cell morphologies consistent with inhibition of penicillin-binding proteins in uropathogenic *Escherichia coli* CFT073. *Chem. Sci.* **2021,** *12*, 4041-4056.

103. Sargun, A.; Sassone-Corsi, M.; Zheng, T.; Raffatellu, M.; Nolan, E. M., Conjugation to enterobactin and salmochelin S4 enhances the antimicrobial activity and selectivity of *β*-lactam antibiotics against nontyphoidal *Salmonella*. *ACS Infect. Dis.* **2021,** *7*, 1248-1259.

104. Raffatellu, M.; George, M. D.; Akiyama, Y.; Hornsby, M. J.; Nuccio, S.-P.; Paixao, T. A.; Butler, B. P.; Chu, H.; Santos, R. L.; Berger, T.; Mak, T. W.; Tsolis, R. M.; Bevins, C. L.; Solnick, J. V.; Dandekar, S.; Bäumler, A. J., Lipocalin-2 resistance confers an advantage to *Salmonella enterica* serotype Typhimurium for growth and survival in the inflamed intestine. *Cell. Host. Microbe.* **2009,** *5*, 476-486.

105. Godinez, W. J.; Chan, H.; Hossain, I.; Li, C.; Ranjitkar, S.; Rasper, D.; Simmons, R. L.; Zhang, X.; Feng, B. Y., Morphological deconvolution of beta-lactam polyspecificity in *E. coli*. *ACS Chem. Biol.* **2019,** *14*, 1217-1226.

106. Vega, D. E.; Young, K. D., Accumulation of periplasmic enterobactin impairs the growth and morphology of *Escherichia coli tolC* mutants. *Mol. Microbiol.* **2014,** *91*, 508-521.

107. Sassone-Corsi, M.; Chairatana, P.; Zheng, T.; Perez-Lopez, A.; Edwards, R. A.; George, M. D.; Nolan, E. M.; Raffatellu, M., Siderophore-based immunization strategy to inhibit growth of enteric pathogens. *Proc. Natl. Acad. Sci. U. S. A.* **2016,** *113*, 13462-13467.

108. Qi, B.; Han, M., Microbial siderophore enterobactin promotes mitochondrial iron uptake and development of the host via interaction with ATP synthase. *Cell* **2018,** *175*, 571-582. e11.

109. Almeida, M. C.; da Costa, P. M.; Sousa, E.; Resende, D. I. S. P., Emerging target-directed approaches for the treatment and diagnosis of microbial infections. *J. Med. Chem.* **2023,** *66*, 32-70.

110. Gerner, R. R.; Hossain, S.; Sargun, A.; Siada, K.; Norton, G. J.; Zheng, T.; Neumann, W.; Nuccio, S. P.; Nolan, E. M.; Raffatellu, M., Siderophore immunization restricted colonization of adherent-invasive *Escherichia coli* and ameliorated experimental colitis. *mBio* **2022,** *13*, e0218422.

111. Nodwell, M. B.; Britton, R., Enterobactin on a bead: parallel, solid phase siderophore synthesis reveals structure–activity relationships for iron uptake in bacteria. *ACS Infect. Dis.* **2021,** *7*, 153-161.

112. Zscherp, R.; Coetzee, J.; Vornweg, J.; Grunenberg, J.; Herrmann, J.; Müller, R.; Klahn, P., Biomimetic enterobactin analogue mediates iron-uptake and cargo transport into *E. coli* and *P. aeruginosa*. *Chem. Sci.* **2021,** *12*, 10179-10190.

113. Rosenberg, B.; Van Camp, L.; Krigas, T., Inhibition of cell division in *Escherichia coli* by electrolysis products from a platinum electrode. *Nature* **1965,** *205*, 698-699.

114. Rosenberg, B.; Van Camp, L.; Grimley, E. B.; Thomson, A. J., The inhibition of growth or cell division in *Escherichia coli* by different ionic species of platinum(IV) complexes. *J. Biol. Chem.* **1967,** *242*, 1347-1352.

115. Rosenberg, B.; Renshaw, E.; Vancamp, L.; Hartwick, J.; Drobnik, J., Platinum-induced filamentous growth in *Escherichia coli*. *J. Bacteriol.* **1967,** *93*, 716-721.

116. Rosenberg, B.; Vancamp, L.; Trosko, J. E.; Mansour, V. H., Platinum compounds: a new class of potent antitumour agents. *Nature* **1969,** *222*, 385-386.

117. Rosenberg, B., Some biological effects of platinum compounds. *Platin. Met. Rev.* **1971,** *15*, 42-51.

118. Jamieson, E. R.; Lippard, S. J., Structure, recognition, and processing of cisplatin−DNA adducts. *Chem. Rev.* **1999,** *99*, 2467-2498.

119. Johnstone, T. C.; Alexander, S. M.; Lin, W.; Lippard, S. J., Effects of monofunctional platinum agents on bacterial growth: a retrospective study. *J. Am. Chem. Soc.* **2014,** *136*, 116-118.

120. Lippert, B., *Cisplatin: chemistry and biochemistry of a leading anticancer drug*. John Wiley & Sons: 1999.

121. Reslova, S., The induction of lysogenic strains of *Escherichia coli* by *cis*-dichlorodiammineplatinum (II). *Chem.-Biol. Interact.* **1971,** *4*, 66-70.

122. Beck, D. J.; Brubaker, R. R., Effect of cis-platinum(II)diamminodichloride on wild type and deoxyribonucleic acid repair deficient mutants of *Escherichia coli*. *J. Bacteriol.* **1973,** *116*, 1247-52.

123. Markham, B. E.; Brubaker, R. R., Influence of chromosome integrity on *Escherichia coli* cell division. *J. Bacteriol.* **1980,** *143*, 455-462.

124. Gibson, J. F.; Poole, R. K.; Hughes, M. N.; Rees, J. F., Filamentous growth of *Escherichia coli* K12 elicited by dimeric, mixed-valence complexes of ruthenium. *Arch. Microbiol.* **1984,** *139*, 265-271.

125. Zdraveski, Z. Z.; Mello, J. A.; Marinus, M. G.; Essigmann, J. M., Multiple pathways of recombination define cellular responses to cisplatin. *Chem. Biol.* **2000,** *7*, 39-50.

126. Cohen, G. L.; Bauer, W. R.; Barton, J. K.; Lippard, S. J., Binding of *cis*- and *trans*-dichlorodiammineplatinum(II) to DNA: evidence for unwinding and shortening of the double helix. *Science* **1979,** *203*, 1014-1016.

127. Cole, R. S., Repair of DNA containing interstrand crosslinks in *Escherichia coli*: sequential excision and recombination. *Proc. Natl. Acad. Sci. U.S.A.* **1973,** *70*, 1064-1068.

128. Friedberg, E. C.; Walker, G. C.; Siede, W.; Wood, R. D., *DNA repair and mutagenesis*. American Society for Microbiology Press: 2005.

129. Johnstone, T. C.; Suntharalingam, K.; Lippard, S. J., The next generation of platinum drugs: targeted Pt(II) agents, nanoparticle delivery, and Pt(IV) prodrugs. *Chem. Rev.* **2016,** *116*, 3436-3486.

130. Hall, M. D.; Okabe, M.; Shen, D.-W.; Liang, X.-J.; Gottesman, M. M., The role of cellular accumulation in determining sensitivity to platinum-based chemotherapy. *Annu. Rev. Pharmacol. Toxicol.* **2008,** *48*, 495-535.

131. Buß, I.; Hamacher, A.; Sarin, N.; Kassack, M.; Kalayda, G., Relevance of copper transporter 1 and organic cation transporters 1–3 for oxaliplatin uptake and drug resistance in colorectal cancer cells. *Metallomics* **2018,** *10*, 414-425.

132. Fichtinger-Schepman, A. M. J.; Van der Veer, J. L.; Den Hartog, J. H.; Lohman, P. H.; Reedijk, J., Adducts of the antitumor drug *cis*-diamminedichloroplatinum (II) with DNA: formation, identification, and quantitation. *Biochemistry* **1985,** *24*, 707-713.

133. Takahara, P. M.; Rosenzweig, A. C.; Frederick, C. A.; Lippard, S. J., Crystal structure of double-stranded DNA containing the major adduct of the anticancer drug cisplatin. *Nature* **1995,** *377*, 649-652.

134. Takahara, P. M.; Frederick, C. A.; Lippard, S. J., Crystal structure of the anticancer drug cisplatin bound to duplex DNA. *J. Am. Chem. Soc.* **1996,** *118*, 12309-12321.

135. Todd, R. C.; Lippard, S. J., Structure of duplex DNA containing the cisplatin 1, 2-{Pt $(NH_3)_2\}^{2+}$-d(GpG) cross-link at 1.77 Å resolution. *J. Inorg. Biochem.* **2010,** *104*, 902-908.

136. Wilson, J. J.; Lippard, S. J., Synthetic methods for the preparation of platinum anticancer complexes. *Chem. Rev.* **2014,** *114*, 4470-4495.

137. Galanski, M. S.; Jakupec, M. A.; Keppler, B. K., Update of the preclinical situation of anticancer platinum complexes: novel design strategies and innovative analytical approaches. *Curr. Med. Chem.* **2005,** *12*, 2075-2094.

138. Alberts, D. S.; Noel, J. K., Cisplatin-associated neurotoxicity: can it be prevented? *Anti-Cancer Drugs* **1995,** *6*, 369-383.

139. Schilder, R. J.; LaCreta, F. P.; Perez, R. P.; Johnson, S. W.; Brennan, J. M.; Rogatko, A.; Nash, S.; McAleer, C.; Hamilton, T. C.; Roby, D.; Young, R. C.; Ozols, R. F.; O'Dwyer, P. J., Phase I and pharmacokinetic study of ormaplatin (tetraplatin, NSC 363812) administered on a day 1 and day 8 schedule. *Cancer. Res.* **1994,** *54*, 709-717.

140. Friedman, H. S.; Krischer, J. P.; Burger, P.; Oakes, W. J.; Hockenberger, B.; Weiner, M. D.; Falletta, J. M.; Norris, D.; Ragab, A. H.; Mahoney Jr, D. H., Treatment of children with progressive or recurrent brain tumors with carboplatin or iproplatin: a pediatric oncology group randomized phase II study. *J. Clin. Oncol.* **1992,** *10*, 249-256.

141. Ravera, M.; Gabano, E.; McGlinchey, M. J.; Osella, D., Pt (IV) antitumor prodrugs: dogmas, paradigms, and realities. *Dalton Trans.* **2022,** *51*, 2121-2134.

142. Chen, S.; Yao, H.; Zhou, Q.; Tse, M. K.; Gunawan, Y. F.; Zhu, G., Stability, reduction, and cytotoxicity of platinum(IV) anticancer prodrugs bearing carbamate axial ligands: comparison with their carboxylate analogues. *Inorg. Chem.* **2020,** *59*, 11676-11687.

143. Ong, J. X.; Yap, S. Q.; Wong, D. Y. Q.; Chin, C. F.; Ang, W. H., Platinum(IV) carboxylate prodrug complexes as versatile platforms for targeted chemotherapy. *Chimia* **2015,** *69*, 100-103.

144. Choy, H.; Park, C.; Yao, M., Current status and future prospects for satraplatin, an oral platinum analogue. *Clin. Cancer Res.* **2008,** *14*, 1633-1638.

145. Sova, P.; Mistr, A.; Kroutil, A.; Zak, F.; Pouckova, P.; Zadinova, M., Preclinical anti-tumor activity of a new oral platinum (IV) drug LA-12. *Anti-Cancer Drugs* **2005,** *16*, 653-657.

146. Dhar, S.; Lippard, S. J., Mitaplatin, a potent fusion of cisplatin and the orphan drug dichloroacetate. *Proc. Natl. Acad. Sci. U.S.A.* **2009,** *106*, 22199-22204.

147. Ang, W. H.; Khalaila, I.; Allardyce, C. S.; Juillerat-Jeanneret, L.; Dyson, P. J., Rational design of platinum(IV) compounds to overcome glutathione-S-transferase mediated drug resistance. *J. Am. Chem. Soc.* **2005,** *127*, 1382-1383.

148. Mayr, J.; Heffeter, P.; Groza, D.; Galvez, L.; Koellensperger, G.; Roller, A.; Alte, B.; Haider, M.; Berger, W.; Kowol, C. R.; Keppler, B. K., An albumin-based tumor-targeted oxaliplatin prodrug with distinctly improved anticancer activity in vivo. *Chem. Sci.* **2017,** *8*, 2241-2250.

149. Barnes, K. R.; Kutikov, A.; Lippard, S. J., Synthesis, characterization, and cytotoxicity of a series of estrogen-tethered platinum(IV) complexes. *Chem. Biol.* **2004,** *11*, 557-564.

150. Joyce, K.; Saxena, S.; Williams, A.; Damurjian, C.; Auricchio, N.; Aluotto, S.; Tynan, H.; Demain, A. L., Antimicrobial spectrum of the antitumor agent, cisplatin. *J. Antibiot.* **2010,** *63*, 530-532.

151. Chowdhury, N.; Wood, T. L.; Martínez-Vázquez, M.; García-Contreras, R.; Wood, T. K., DNA-crosslinker cisplatin eradicates bacterial persister cells. *Biotechnol. Bioeng.* **2016,** *113*, 1984-1992.

152. Yuan, M.; Chua, S. L.; Liu, Y.; Drautz-Moses, D. I.; Yam, J. K. H.; Aung, T. T.; Beuerman, R. W.; Salido, M. M. S.; Schuster, S. C.; Tan, C.-H., Repurposing the anticancer drug cisplatin with the aim of developing novel *Pseudomonas aeruginosa* infection control agents. *Beilstein J. Org. Chem.* **2018,** *14*, 3059-3069.

153. Hummell, N. A.; Kirienko, N. V., Repurposing bioactive compounds for treating multidrug-resistant pathogens. *J. Med. Microbiol.* **2020,** *69*, 881-894.

154. Guo, C.; Nolan, E. M., Heavy-metal Trojan horse: enterobactin-directed delivery of platinum(IV) prodrugs to *Escherichia coli*. *J. Am. Chem. Soc.* **2022,** *144*, 12756-12768.

155. Guo, C.; Wang, K.-K. A.; Nolan, E. M., Investigation of siderophore–platinum(IV) conjugates reveals differing antibacterial activity and DNA damage depending on the platinum cargo. *submitted for publication* **2023**.

Chapter 2.

Heavy-Metal Trojan Horse: Enterobactin-Directed Delivery of Platinum(IV) Prodrugs to *Escherichia coli*

This chapter is reprinted with permission from Guo, C., Nolan, E. M. Heavy-metal Trojan horse: enterobactin-directed delivery of platinum(IV) prodrugs to *Escherichia coli*. *Journal of the American Chemical Society*, 2022, *144*(28), 12756-12768.

https://pubs.acs.org/doi/10.1021/jacs.2c03324

2.1 Contributions: E.M.N. and C.G. conceived of the presented idea. C.G. conducted the experiments and performed data analysis. C.G. wrote the manuscript with the support from E.M.N.

2.2 Abstract

The global crisis of untreatable microbial infections necessitates the design of new antibiotics. Drug repurposing is a promising strategy for expanding the antibiotic repertoire. In this study, we repurpose the clinically-approved anticancer agent cisplatin into a targeted antibiotic by conjugating its Pt(IV) prodrug to enterobactin (Ent), a triscatecholate siderophore employed by Enterobacteriaceae for iron (Fe) acquisition. The L-Ent-Pt(IV) conjugate (L-EP) exhibits antibacterial activity against *Escherichia coli* K12 and the uropathogenic isolate *E. coli* CFT073. Similar to cisplatin, L-EP causes filamentous morphology in *E. coli* and initiates lysis in lysogenic bacteria. Studies with *E. coli* mutants defective in Ent transport proteins show that Ent mediates the delivery of L-EP into the *E. coli* cytoplasm, where reduction of the Pt(IV) prodrug releases the cisplatin warhead, causing growth inhibition and filamentation of *E. coli*. Substitution of Ent with its enantiomer affords the D-Ent-Pt(IV) conjugate (D-EP), which displays enhanced antibacterial activity, presumably because D-Ent cannot be hydrolyzed by Ent esterases and thus Fe cannot be released from this conjugate. *E. coli* treated with L/D-EP accumulate ≥10-fold more Pt as compared to cisplatin treatment. By contrast, human embryonic kidney cells (HEK293T) accumulate cisplatin but show negligible Pt uptake after treatment with either conjugate. Overall, this work demonstrates that attachment of a siderophore repurposes a Pt anticancer agent into a targeted antibiotic that is recognized and transported by siderophore uptake machinery, providing a design strategy for drug repurposing by siderophore modification and heavy-metal "Trojan-horse" antibiotics.

2.3 Introduction

Antibiotics are invaluable for treating bacterial infections; however, the extensive use of broad-spectrum antibiotics has resulted in widespread antibiotic resistance and negative effects on the human microbiota.[1-3] The need for new classes of antibacterials is urgent. In addition to *de novo* antibiotic development, drug repurposing holds promise as a cost-effective strategy for identifying new clinical applications for approved drugs.[4] Nevertheless, potential toxicity is one major concern in repurposing existing drugs for treating bacterial infections because antibiotics are typically dosed at levels considerably higher than non-antibacterial drugs.[4] Accordingly, targeted delivery and controlled release strategies may address this challenge by enhancing therapeutic efficacy towards the target while minimizing off-target effects.[5] Herein, we report the repurposing of cisplatin, a Pt anticancer agent, as an antibiotic using the strategy of siderophore-mediated delivery.

Siderophores are secondary metabolites produced and utilized by bacteria for iron (Fe) acquisition in the vertebrate host.[6] Siderophore-mediated Fe acquisition is important for bacterial growth because Fe is an essential nutrient for almost all bacterial species, and its availability is tightly regulated in the host environment.[7-8] Moreover, during bacterial infection, Fe availability is further limited by the host to starve the pathogen in a host-defense strategy termed "nutritional immunity".[9-10] By scavenging Fe from the host environment, siderophores enable bacterial colonization and contribute to bacterial pathogenesis. To import Fe(III)-siderophore complexes, bacterial pathogens express siderophore uptake systems, and these transport systems can be hijacked for efficient and targeted antibiotic delivery.[11] This strategy is exemplified by naturally occurring siderophore–antibiotic conjugates (SACs), such as sideromycins and class IIb microcins, which are deployed by some microbes to target their microbial competitors.[12-16] These natural

products inspire the "Trojan-horse" strategy by which a toxic agent can be disguised in a synthetic SAC and actively transported into bacteria expressing the cognate siderophore uptake machinery.[17-18]

Many examples of synthetic SACs have been reported over the past decades. The vast majority of these reports describe SACs where the antibacterial cargo is a clinically-approved antibiotic.[18] For instance, we have designed and evaluated SACs based on the siderophore enterobactin (Ent, **1**) that have β-lactam or fluoroquinolone cargos (**Figures 2.1A** and **2.1B**).[19-22] Ent **1** is a major siderophore produced by Enterobacteriaceae including *Escherichia coli, Salmonella,* and *Klebsiella pneumoniae*.[23] Our studies of Ent-β-lactam and Ent-fluoroquinolone conjugates including Ent-Amp **2** and Ent-Cipro **3** (**Figure 2.1B**) demonstrated that the Ent transport machinery effectively recognizes and transports SACs, thereby delivering antibiotic cargos into the periplasm and cytoplasm of *E. coli*.[19-22] Thus far, we have found that the antibacterial activity of these SACs is generally equal to or greater than that of the corresponding unmodified antibiotics. In particular, conjugation of Ent to β-lactam antibiotics accelerates the rate of bacterial killing relative to the unmodified β-lactams, presumably because Ent conjugation changes the uptake pathway of β-lactams from passive diffusion to active transport.[19, 21-22] Moreover, the Ent modification narrows the antibacterial activity spectrum of these broad-spectrum antibiotics, which is one way to limit the spread of resistance across non-targeted bacteria and prevent secondary infections by preserving the host microbiota.[1, 24]

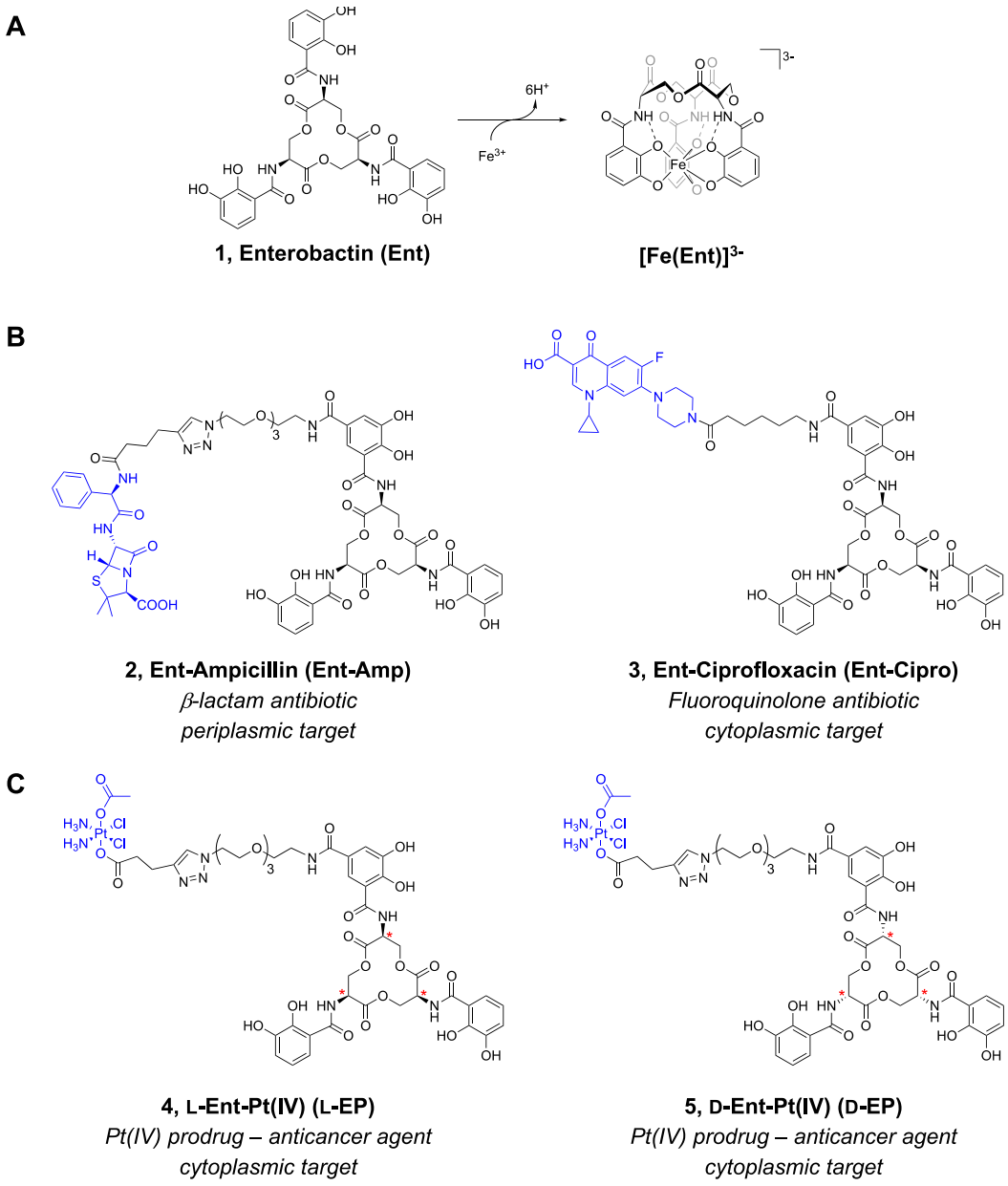

Figure 2.1. Overview of Ent and Ent-based SACs. **(A)** Chemical structure of L-Ent **1**. Deprotonation and binding of Fe(III) by Ent to give ferric Ent $[Fe(Ent)]^{3-}$. **(B)** Chemical structures of previously reported Ent-β-lactam **2** and Ent-fluoroquinolone **3** conjugates. **(C)** Chemical structures of the L- and D-Ent-Pt(IV) conjugates **4** and **5** described in this work. Stereocenters are designated with red asterisks. The antibiotic and Pt(IV) cargos are shown in blue.

During the course of these studies, we reasoned that SACs provide a framework for repurposing a broad range of toxic agents as antibiotics. Consequently, we looked beyond traditional antibiotics for new possibilities of expanding the cargo scope and hence the current

antibiotic arsenal. Taking inspiration from medicinal inorganic chemistry, we focused on metallodrugs and selected the FDA-approved anticancer drug cisplatin as a case study. Cisplatin was discovered serendipitously by its ability to inhibit cell division and induce filamentous growth in *E. coli*.[25] However, cisplatin exhibits low antibacterial activity and high toxicity towards human cells, which hinder its use as an antibiotic.[26-27] To improve anticancer treatment, strategies for safer and more effective Pt-based anticancer agents are under exploration, including investigations of targeted Pt(IV) prodrugs.[28] Guided by these studies, we reasoned that we could use Ent as a drug carrier to direct a Pt(IV) warhead to bacterial species expressing Ent receptors and thereby repurpose cisplatin into an antibiotic that targets Gram-negative bacteria via the Ent transport machinery.

Herein, we report the design and synthesis of two Ent-based Pt(IV) conjugates that combine targeted delivery by Ent and controlled release of Pt(IV) prodrugs (**Figure 2.1C**). We report that L-Ent-Pt(IV) (L-EP) **4** inhibits bacterial growth, causes filamentation in *E. coli*, and induces lysis in lysogenic bacteria. We demonstrate that L-EP is recognized and transported into the *E. coli* cytoplasm by the Ent uptake machinery FepABCDG. Moreover, we show that the enantiomer D-Ent-Pt(IV) (D-EP) **5** has improved potency against *E. coli* attributable to the D-Ent scaffold which is resistant to esterase-mediated cleavage, a key step in cytoplasmic Ent processing for Fe release. Both conjugates enhance Pt uptake in *E. coli* CFT073 cells and reduce Pt uptake in HEK293T cells. Overall, our results show that Ent conjugation repurposes a Pt anticancer agent as an antibacterial against *E. coli*, which provides a design strategy for a new family of heavy-metal "Trojan-horse" antibiotics.

2.4 Results and Discussion

Design and synthesis of L-Ent-Pt(IV). Guided by our prior research on Ent–antibiotic conjugates as well as work by others on Pt(IV) prodrugs,[19-22, 27, 29-30] we designed L-EP **4**, a conjugate that contains an Ent moiety for targeted delivery, a poly(ethylene glycol) $(PEG)_3$ linker, and a cisplatin-derived Pt(IV) prodrug cargo (**Figure 2.1C** and **Scheme 2.1**). We note that the Pt(IV) prodrug strategy has been widely explored in Pt-based anticancer agents to mask the activity of Pt(II) species before entering target cells.[27, 30] Unlike cisplatin and other square-planar Pt(II) species, Pt(IV) complexes are six-coordinate with octahedral geometries.[27] The saturated coordination spheres of low-spin d^6 Pt(IV) centers are substantially more kinetically inert than Pt(II), making Pt(IV) species more resistant to ligand substitution.[27] Moreover, the two axial ligands are important for controlling the physiochemical properties of Pt(IV) complexes like reduction potential.[30-35] In our design, we selected carboxylates as axial ligands because they have been shown to afford relatively good stability for Pt(IV) complexes in biological fluids and effective reductive activation upon cell entry.[36-37] In the proposed working model (**Figure 2.2**), L-EP is actively imported into bacteria by the Ent transport system, including the outer membrane receptor FepA, the periplasmic binding protein FepB, and the inner membrane ATP-binding cassette transporter FepCDG. Upon entry into the reducing environment of the cytoplasm, the Pt(IV) prodrug is activated, leading to the release of the Pt(II) species and two axial ligands.[38] The liberated active Pt(II) species targets bacterial DNA and causes cross-links, inhibiting cell division and ultimately resulting in cell death.[30]

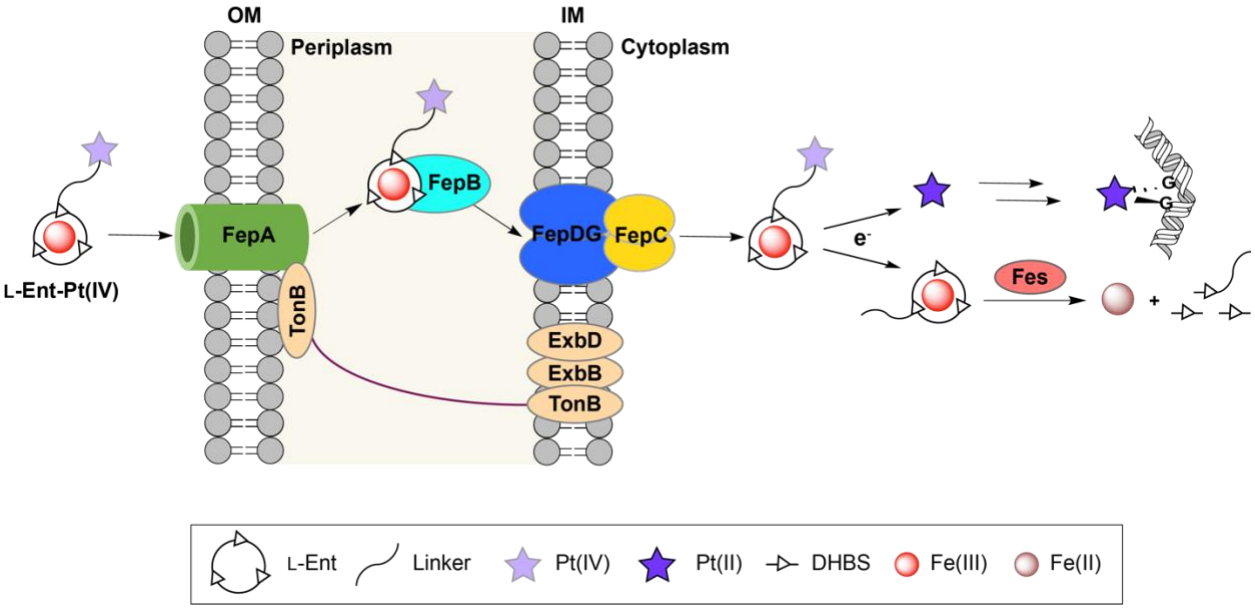

Figure 2.2. Cartoon depiction of working model for repurposing cisplatin as antibiotics that selectively target Gram-negative bacteria via Ent transport machinery. Ent transport and processing machinery is shown for *E. coli* K12. The TonB-ExbB-ExbD complex provides energy transduction for transport of ferric siderophores across the outer membrane. Fes is an esterase that hydrolyzes the trilactone ring of Fe-Ent. Reduction of Fe(III) to Fe(II) that occurs during release of the metal ion is not catalyzed by the Ent esterases. DHBS, 2,3-dihydroxybenzoyl serine; G, a guanine base. The intrastrand 1,2-d(GpG) crosslink shown is found as the major cisplatin-DNA adduct based on studies with salmon sperm DNA.[30]

We conjugated the Ent and Pt(IV) prodrug moieties by copper-catalyzed alkyne-azide cycloaddition (CuAAC) using alkyne-functionalized Pt(IV) **6** and L-Ent-N_3 **7** (**Scheme 2.1**).[39] In our prior syntheses of Ent-β-lactam conjugates, we performed CuAAC by using the Cu(II) salt $CuSO_4$ and sodium ascorbate (NaAsc) for *in situ* reduction, *tris*[(1-benzyl-1*H*-1,2,3-triazol-4-yl)methyl]amine (TBTA) as the Cu chelator, and a mixture of DMSO and water as the solvent.[19, 40] In the current work, we modified these conditions based on the properties of Pt(IV)-alkyne **6**. We employed the Cu(I) salt $Cu(MeCN)_4PF_6$[41] as the catalyst to avoid potential Pt(IV) reduction caused by NaAsc, and we substituted DMF for DMSO in the solvent mixture to avoid potential ligand replacement of the chloro ligands of Pt(IV)-alkyne **6** by the nucleophilic sulfur atom of DMSO.[42] We continued to use TBTA as a stabilizing ligand to protect Cu(I) from oxidation,

disproportionation, and potential interactions with the two reactants.[43] Using these conditions, the CuAAC reaction and subsequent purification by HPLC afforded L-EP **4** in high purity on a milligram scale sufficient for microbiological assays (**Figure 2.3**).

Scheme 2.1. Synthesis of L-EP via click chemistry.

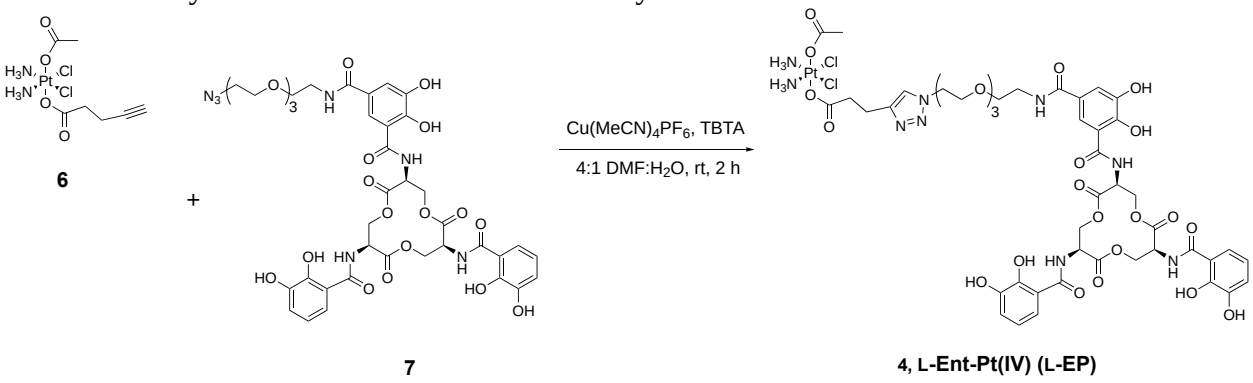

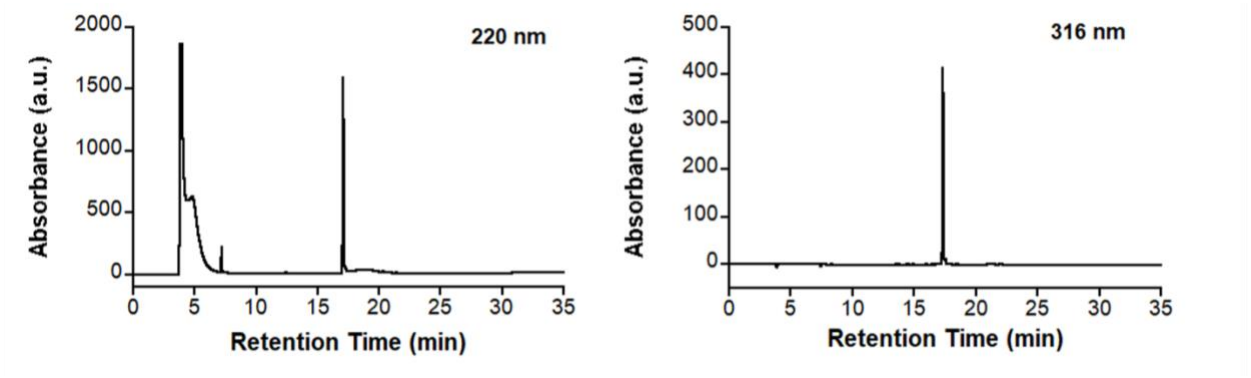

Figure 2.3. Analytical HPLC traces of purified L-EP. The peak at ca. 5 min in the 220 nm trace of L-EP is DMSO.

L-EP causes growth inhibition and induces filamentation in *E. coli*. In prior investigations of Ent-antibiotic conjugates, we employed a modified M9 growth medium which has low Fe content (600–700 nM by ICP-MS) and therefore induces expression of siderophore biosynthesis and transport machineries, including the Ent gene cluster that is responsible for Ent biosynthesis and transport.[20, 29, 44] In this work, we modified this medium by decreasing its

thiamine content for microbiology studies of conjugates **4** and **5** harboring the Pt(IV) prodrug (See section **2.7**, **Supporting Discussion**).

We first investigated the antibacterial activity of L-EP against two strains of *E. coli*, the laboratory strain K12 (BW25113) and the uropathogenic strain CFT073. Both strains biosynthesize Ent and express FepABCDG for the transport of Fe-Ent into the cytoplasm as well as the cytoplasmic esterase Fes that hydrolyzes the trilactone ring of Fe-Ent for Fe release (**Figure 2.2**). *E. coli* CFT073 also harbors the pathogen-associated *iroA* gene cluster, which is expressed under conditions of Fe limitation and includes genes for the biosynthesis, transport, and hydrolysis of salmochelins, C-glucosylated derivatives of Ent.[45-48] Consequently, CFT073 expresses the outer membrane receptor IroN, which binds and transports Fe-Ent and Fe-bound salmochelins,[47] and the corresponding cytoplasmic esterase IroD that hydrolyzes these Fe-siderophore complexes.[48] In addition, CFT073 expresses the outer membrane receptor IhA which also binds and transports Fe-Ent.[49]

Because the modified M9 medium contains less than 1 μM Fe, we treated *E. coli* with Fe(III)-bound L-EP, which was prepared by pre-incubating L-EP with 0.9 equiv of $Fe(acac)_3$. We first evaluated *E. coli* growth in the absence and presence of L-EP by monitoring culture turbidity and observed modest growth inhibition for *E. coli* treated with the conjugate. Treatment of *E. coli* K12 with 7.5 or 15 μM L-EP resulted in a ~20% reduction in OD_{600} value compared to the untreated control, and the relative OD_{600} was further reduced by ~30% with 30 and 60 μM L-EP (**Figure 2.4A**). L-EP showed a slightly larger growth inhibitory effect on *E. coli* CFT073, with the relative OD_{600} reduced by 37% with 60 μM L-EP (**Figure 2.4B)**. In comparison, cisplatin was somewhat more potent against both *E. coli* strains. Treatment of K12 with 30 or 60 μM cisplatin reduced the relative OD_{600} by 41% or 68%, respectively (**Figure 2.4A**). For *E. coli* CFT073,

treatment with 30 or 60 μM cisplatin reduced the OD_{600} value by 51 or 58% compared to the untreated control, respectively (**Figure 2.4B**).

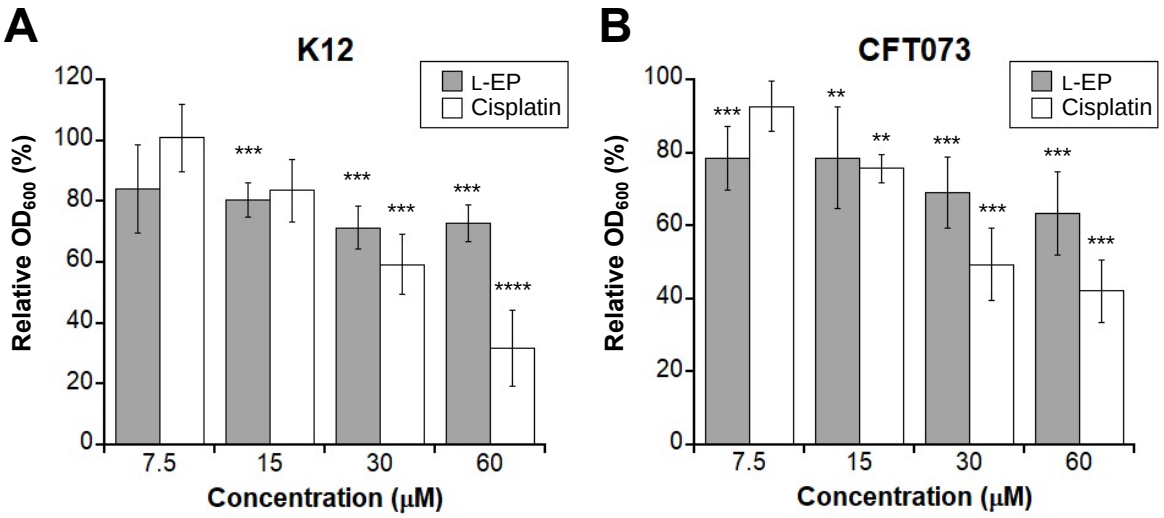

Figure 2.4. Antibacterial activity of L-EP and cisplatin against **(A)** *E. coli* K12 and **(B)** CFT073 based on OD_{600}. Relative OD_{600} refers to the OD_{600} value of the treated sample divided by that of the untreated control (mean ± standard deviation, n = 6 for K12 experiments, n = 7 for CFT073 and L-EP, n = 4 for CFT073 and cisplatin). Statistical differences compared to untreated controls were calculated using two-tailed student *t* test assuming unequal variances; ****$P < 0.0001$, ***$P < 0.001$, **$P < 0.01$.

Filamentous morphology is a hallmark of *E. coli* treated with cisplatin and other Pt compounds.[25, 50] Thus, we evaluated cellular morphology induced by L-EP using phase-contrast microscopy. Following treatment with L-EP, both K12 and CFT073 exhibited filamentous morphology similar to that observed for cisplatin-treated *E. coli* (**Figure 2.5**). Moreover, filamentation occurred at the lowest L-EP concentration tested (7.5 μM, **Figure 2.5**), and both the number of filaments and length of the filaments tended to increase with increasing L-EP concentration. Together, these initial experiments demonstrated that growth effects of L-EP on *E. coli* are similar to those observed for cisplatin, including growth inhibition and filamentation.

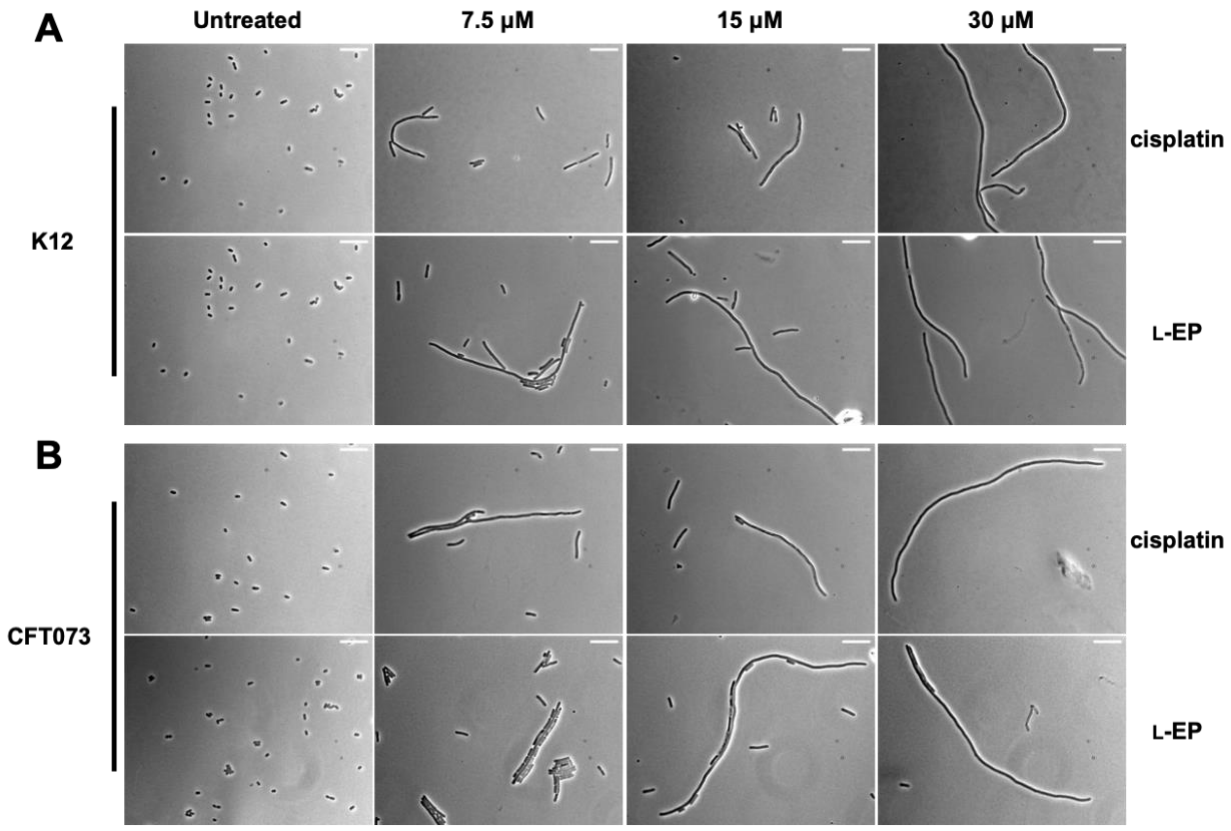

Figure 2.5. Representative phase-contrast micrographs of *E. coli* **(A)** K12 and **(B)** CFT073 treated with cisplatin and L-EP. Scale bar: 10 μm. All assays were performed in modified M9 medium at 30 °C for 11 h.

L-EP induces lysis in lysogenic bacteria. In early investigations, bacterial cell filamentation was a clue that cisplatin targets DNA because filamentation can also be a consequence of DNA damage caused by UV radiation, ionizing radiation and hydroxyurea.[51-54] In prior studies, another clue for the interaction between cisplatin and DNA was the ability of cisplatin to initiate lysis of *E. coli* cells containing bacteriophage λ.[50, 55-56] To compare L-EP to other reported Pt complexes and probe the origin of its activity, we examined its ability to induce a lytic transformation in *E. coli* W3104, a lysogenic strain infected with bacteriophage λ. Under normal conditions, this bacteriophage grows in a lysogenic mode in which viral genes are silently duplicated along with bacterial genes. When *E. coli* W3104 senses DNA damage, signals

generated by the SOS response initiate the lytic phase of bacteriophage λ, and the resulting production of viral particles leads to *E. coli* cell lysis. When a suspension of *E. coli* W3104 treated with cisplatin or other Pt compounds is spotted on a lawn of non-lysogenic *E. coli*, viral particles released from lysed *E. coli* W3104 can lead to plaque formation, which serves as an indicator of DNA damage triggered in *E. coli* W3104 by the Pt warheads.[50, 55-56]

Guided by these literature reports, we first treated aliquots of an exponentially growing *E. coli* W3104 culture with cisplatin (0–30 μM), diluted the resulting suspensions and spotted a 10 μL drop of each diluted suspension on a lawn of non-lysogenic *E. coli* CFT073.[50] Consistent with prior work,[50] we observed plaques on *E. coli* CFT073 when spotted with *E. coli* W3104 that was treated with 15 μM cisplatin at 1000-fold dilution. We then incubated *E. coli* W3104 with 15 μM L-EP, 15 μM L-Ent, or 1% DMSO. We observed plaque formation on *E. coli* CFT073 when *E. coli* W3104 was treated with 15 μM L-EP at 1000-fold dilution but not when the bacteria were treated with L-Ent, 1% DMSO, or the untreated control (**Table 2.1** and **Figure 2.6**). Moreover, no plaques formed where the lawn was spotted with solutions of the compounds only, indicating that the plaque formation was caused by viral particles released from lysed lysogenic bacteria rather than the compound alone. Collectively, the ability of L-EP to induce bacterial filamentation (**Figure 2.5**) and initiate lysis in lysogenic bacteria (**Table 2.1** and **Figure 2.6**) is congruent with previously reported Pt complexes, indicating induction of the SOS response and suggesting that the antibacterial activity of this conjugate may be attributed to Pt-induced DNA damage.

Table 2.1. Effect of L-EP on lysogenic *E. coli*[a]

	Cisplatin	L-EP	L-Ent	1% DMSO	Untreated
***E. coli* W3104 suspension**	+	+	–	–	–
Compound solution	–	–	–	–	–

[a] The development of plaques in a lawn of non-lysogenic *E. coli* CFT073 following spotting 1000-fold diluted suspensions of *E. coli* W3104 treated with 15 μM of each compound or solutions containing only the corresponding compound. +, plaque formation; –, no plaque observed. Representative images of agar plates are shown in **Figure 2.6**.

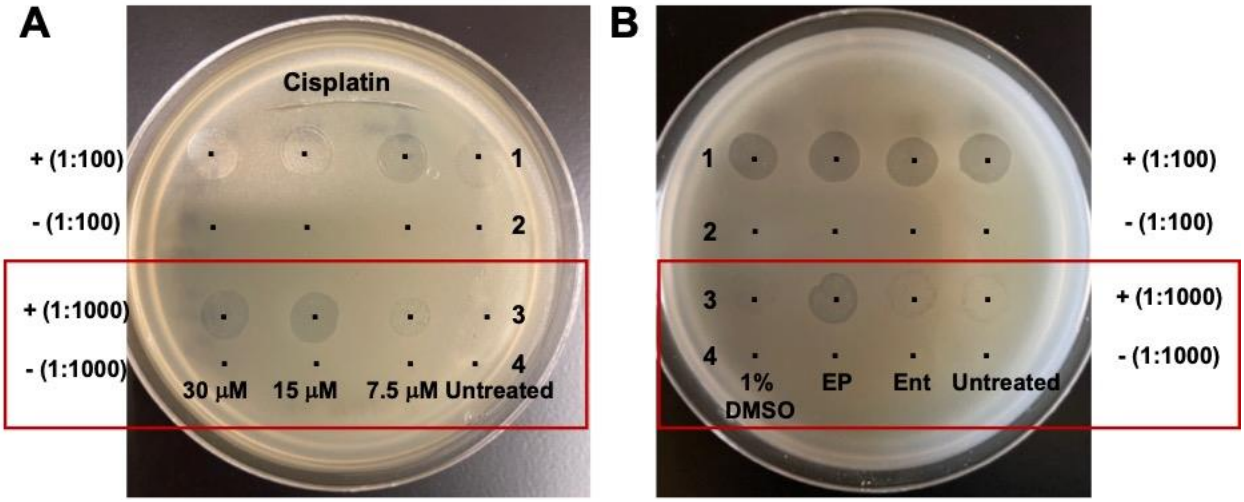

Figure 2.6. Effect of L-EP on lysogenic *E. coli*. Representative images of the development of plaques in a lawn of non-lysogenic *E. coli* CFT073 following application of 10 μL drops of 100-fold (row **1** and **2**) and 1000-fold (row **3** and **4**, in the red frame) diluted suspensions of treated *E. coli* W3104 (+) and solutions containing only the corresponding compound (-). **(A)** *E. coli* W3104 treated with cisplatin (0–30 μM). **(B)** *E. coli* W3104 treated with 15 μM L-EP, 15 μM Ent, 1% DMSO and the untreated control. We note that plaque formation was observed in all 100-fold diluted suspensions, including the untreated sample, which was presumably due to a small portion of lysogenic bacteria that enter the lytic cycle under normal growth conditions.

The outer membrane receptor FepA is involved in the uptake of L-EP. Next, we evaluated whether the outer membrane receptor FepA is important for L-EP activity against *E. coli.* We treated K12 and the Δ*fepA* mutant (obtained from the Keio Collection)[57] with 0–60 μM L-EP and then measured the culture turbidity and examined cellular morphology by microscopy. In contrast to the parent strain which exhibited growth inhibition and showed filamentous

morphology, growth of the Δ*fepA* mutant was not inhibited, and most of the Δ*fepA* mutant cells were normal-sized and rod-shaped following L-EP treatment (**Figures 2.7** and **2.8A**), indicating that FepA is required for the uptake of L-EP by *E. coli* K12. We note that the K12 Δ*fepA* mutant exhibits a growth defect in the modified M9 medium and appears to be very sensitive to any slight change in Fe content. Consequently, we speculate that the growth promotion observed for K12 Δ*fepA* treated with L-EP results from partial decomposition of L-EP which releases Fe into the growth medium providing this nutrient to the bacteria.

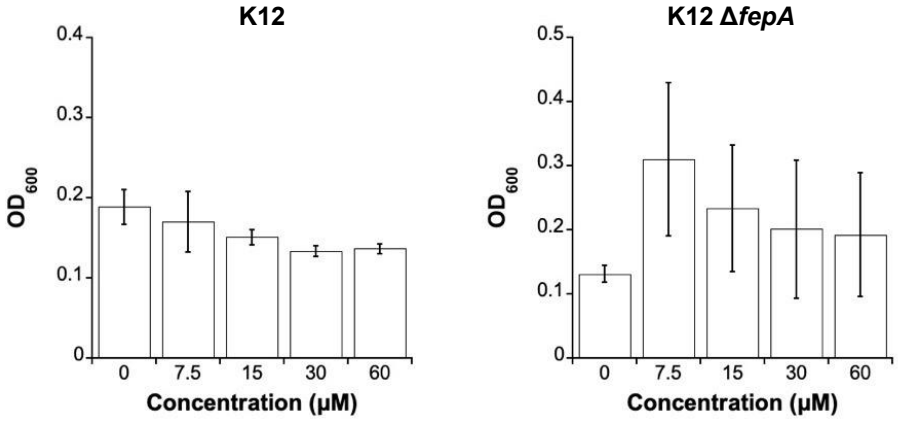

Figure 2.7. Antibacterial activity of L-EP against *E. coli* K12 and its Δ*fepA* mutant based on OD_{600} (data shown in **Table A.3**). All assays were performed in modified M9 medium (11 h, 30 °C, 500 rpm; mean ± standard deviation; n ≥ 4). The same data for K12 were also presented as relative OD_{600} (%) in **Figure 2.4A**.

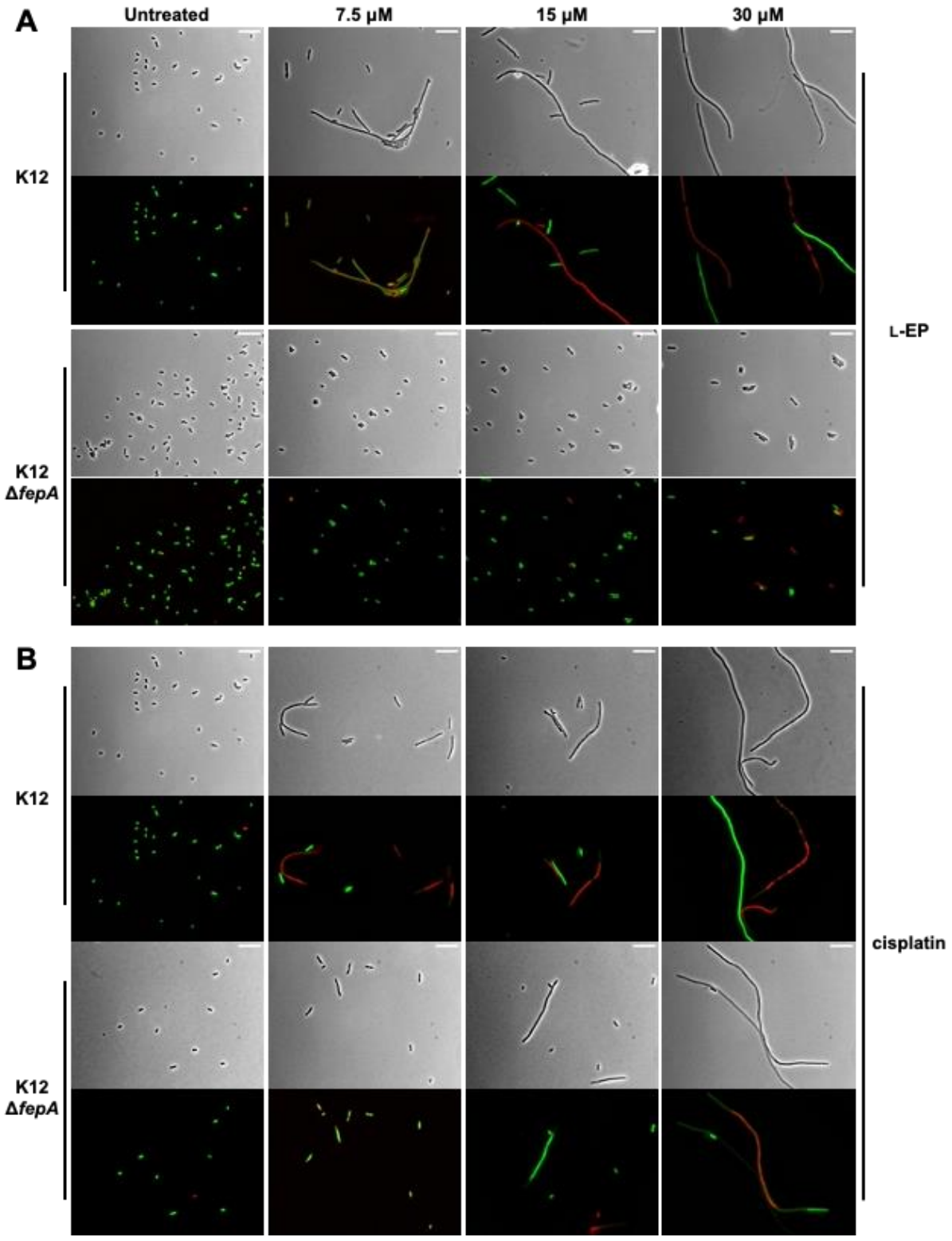

Figure 2.8. Representative phase-contrast and fluorescence micrographs of *E. coli* K12 and its Δ*fepA* mutant treated with **(A)** L-EP and **(B)** cisplatin in modified M9 medium for 11 h at 30 °C. Scale bar: 10 µm.

We also performed quantitative analysis on the cellular morphology in K12 and the Δ*fepA* mutant by measuring the perimeter of each bacterial cell in the phase-contrast images and determining the relative percentage of filamented cells at each L-EP concentration evaluated (**Figure 2.9A**). Because the size of a normal *E. coli* cell is ~2 μm in length and ~0.6 μm in diameter,[58] we grouped cells into four categories based on perimeter measurements: normal size (0–10 μm), elongation (10–20 μm), filamentation (20–50 μm), and extreme filamentation (>50 μm). With increasing concentration of L-EP, the percentage of normal-sized K12 cells decreased and more cells exhibited abnormal morphology, especially those showing extreme filamentation (10% at 7.5 μM and 66% at 60 μM) (**Figure 2.9A left**). By contrast, more than 90% of the Δ*fepA* mutant cells treated with ≤15 μM L-EP were normal-sized (**Figure 2.9A right**). Though we observed some Δ*fepA* cells with abnormal morphologies in the presence of 60 μM L-EP (49%), most of them were elongated (38%), and only 0.7% of the cells exhibited extreme filamentation. We reason that the abnormal morphologies observed for the Δ*fepA* mutant treated with high L-EP concentrations occurred because of some decomposition of L-EP in the growth medium, resulting in the release of Pt(II) species that can enter bacterial cells by passive diffusion. We note that cisplatin caused comparable filamentation in both K12 and the Δ*fepA* mutant (**Figure 2.8B**).

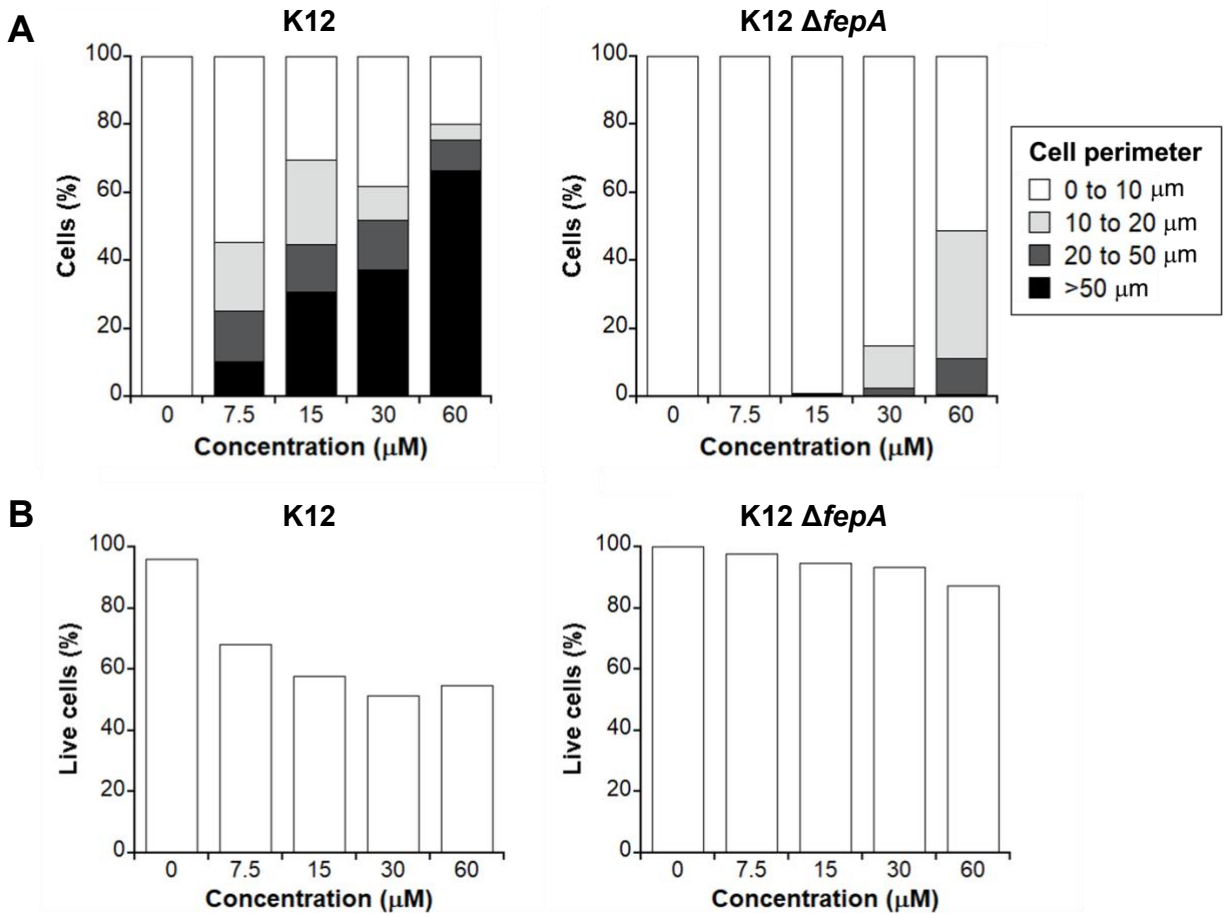

Figure 2.9. Activity of L-EP against *E. coli* K12 and its Δ*fepA* mutant based on microscopy. **(A)** Quantification of the L-EP-induced bacterial morphologies in *E. coli*. **(B)** Viability of *E. coli* determined by LIVE/DEAD staining. For morphology and viability quantification, 500–1000 cells were manually counted for each condition from micrographs. For morphology quantification, cell size was measured and grouped by perimeter (data shown in **Table A.2**).

We also examined the viability of K12 and the Δ*fepA* mutant using the LIVE/DEAD viability assay. This assay distinguishes cells with intact and compromised outer membranes by using the fluorescent dyes SYTO 9 (green) and propidium iodide (red), respectively.[59] Quantification was performed by counting the number of green (live) and red (dead) cells, respectively (**Figure 2.9B**). This analysis indicated that K12 was much more susceptible to L-EP than the Δ*fepA* mutant. For instance, ~50% of the K12 cells were stained red following treatment with ≥15 μM L-EP whereas 13% of the Δ*fepA* cells were stained red following treatment with 60

μM L-EP (**Figure 2.9B**). Moreover, compared to the initial turbidity measurements (**Figure 2.4**), examination of viability based on LIVE/DEAD staining and cell counting indicated more profound growth inhibition for K12. These microscopic results also indicated that turbidity measurements are insufficient to describe growth effects caused by Pt agents because the cultures include live cells with different morphologies, cells with compromised membranes, cell debris, *etc.*

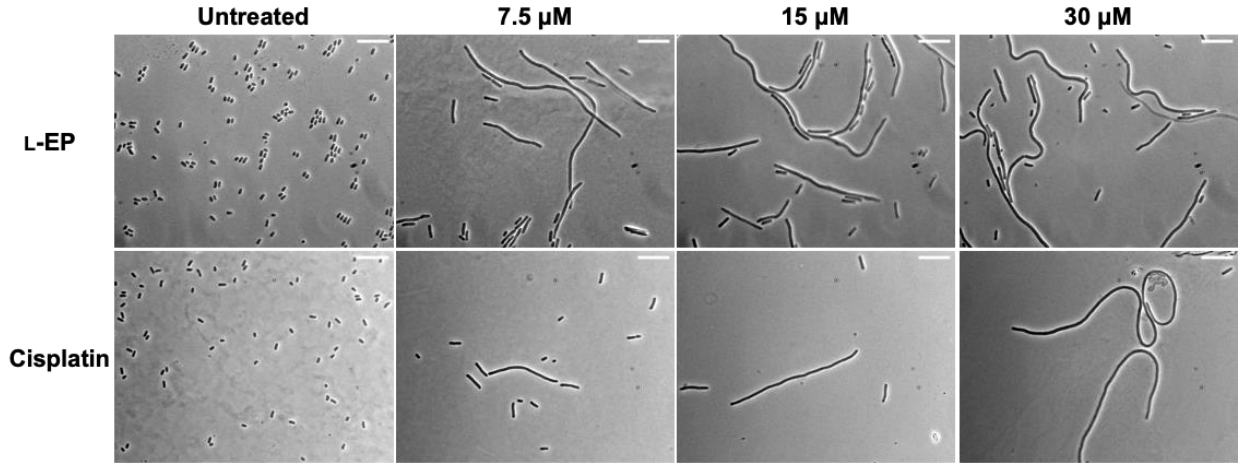

Figure 2.10. Representative phase-contrast micrographs of *E. coli* CFT073 Δ*fepA* Δ*iroN* mutant treated with L-EP (top) and cisplatin (bottom) (scale bar = 10 μm).

We extended these outer membrane receptor studies to CFT073, which presents a more complicated case because in addition to FepA, CFT073 expresses two other outer membrane receptors, IroN and IhA, that transport Fe-Ent.[47, 49, 60] We observed that treatment of CFT073 with L-EP resulted in filamentation of both the parent strain and the Δ*fepA* Δ*iroN* double mutant (**Figure 2.10**). This result is consistent with our prior studies of Ent-β-lactam conjugate uptake by CFT073; we found that Ent-β-lactam conjugates retained some antibacterial activity against the Δ*fepA* Δ*iroN* double mutant.[21] We note that deletion of *ihA* had negligible effect on cell killing by the Ent-β-lactams. One possible explanation is that L-EP or a hydrolysis product is recognized and

transported by another as-yet undetermined outer membrane receptor expressed by CFT073. Further studies are warranted to investigation the origin of activity observed for the Ent-β-lactam and L-EP conjugates against the Δ*fepA* Δ*iroN* double mutant.

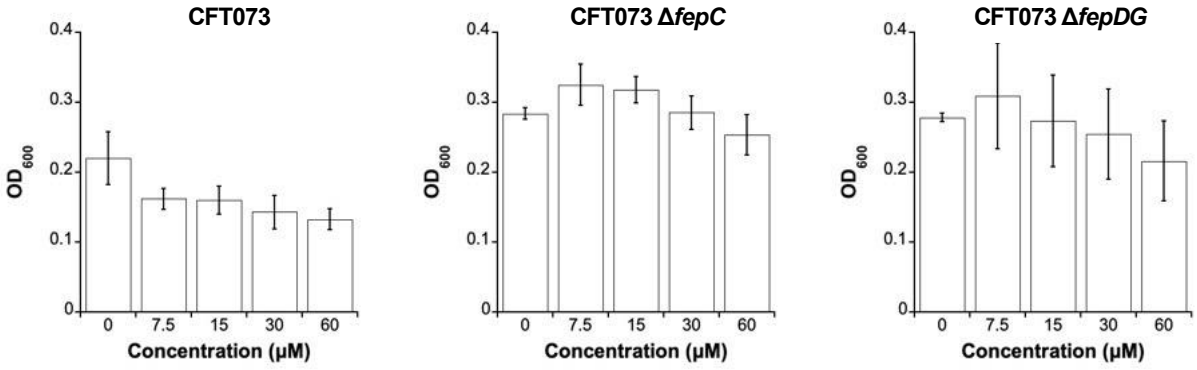

Figure 2.11. Antibacterial activity of L-EP against *E. coli* CFT073 and its Δ*fepC* and Δ*fepDG* mutants based on OD_{600} (data shown in **Table A.3**). All assays were performed in modified M9 medium (11 h, 30 °C, 500 rpm; mean ± standard deviation, $n \geq 6$). The same data for CFT073 were also presented as relative OD_{600} (%) in **Figures 2.4, 2.16,** and **2.20A**.

The inner membrane transporter FepCDG is involved in the uptake of L-EP. Next, we examined whether FepCDG, the inner membrane ABC transporter that delivers Fe-Ent to the cytoplasm, is necessary for L-EP antibacterial activity. We focused these studies on the CFT073 Δ*fepC* and Δ*fepDG* mutants because the *E. coli* K12 Δ*fepC,* Δ*fepD and* Δ*fepG* mutants obtained from the Keio Collection showed severe growth defects in the modified M9 medium. In contrast to the parent strain which was inhibited by L-EP, the growth of the Δ*fepC* and Δ*fepDG* mutants was not inhibited (**Figure 2.11)**. Microscopic studies showed that the parent strain exhibited abnormal morphologies with a mixture of live and dead cells in the presence of L-EP, and that most of the Δ*fepC* and Δ*fepDG* mutant cells remained normal-sized and viable (**Figure 2.12**). For instance, following treatment with 30 μM L-EP, 61% of the CFT073 cells were normal-sized

compared to 94% of the Δ*fepC* cells (**Figure 2.13A**). When 60 μM L-EP was employed, the percentage of normal-sized Δ*fepC* mutant cells slightly decreased to 79%, presumably due to some decomposition of the conjugate (*vide supra*). LIVE/DEAD staining and cell counting indicated that following treatment with 60 μM L-EP, only 53% of the parent strain cells remained viable, whereas 97% of the Δ*fepC* cells remained viable (**Figure 2.13B**). Morphology and cell viability analyses of the Δ*fepDG* mutant provided similar trends (**Figure 2.13**). Cisplatin, by contrast, induced comparable filamentation in all three strains (**Figure 2.14**), and Pt(IV)-alkyne **6** did not cause abnormal morphologies or cell death (**Figure 2.15**). Taken together, these results show that the inner membrane transporter FepCDG transports L-EP into the cytoplasm.

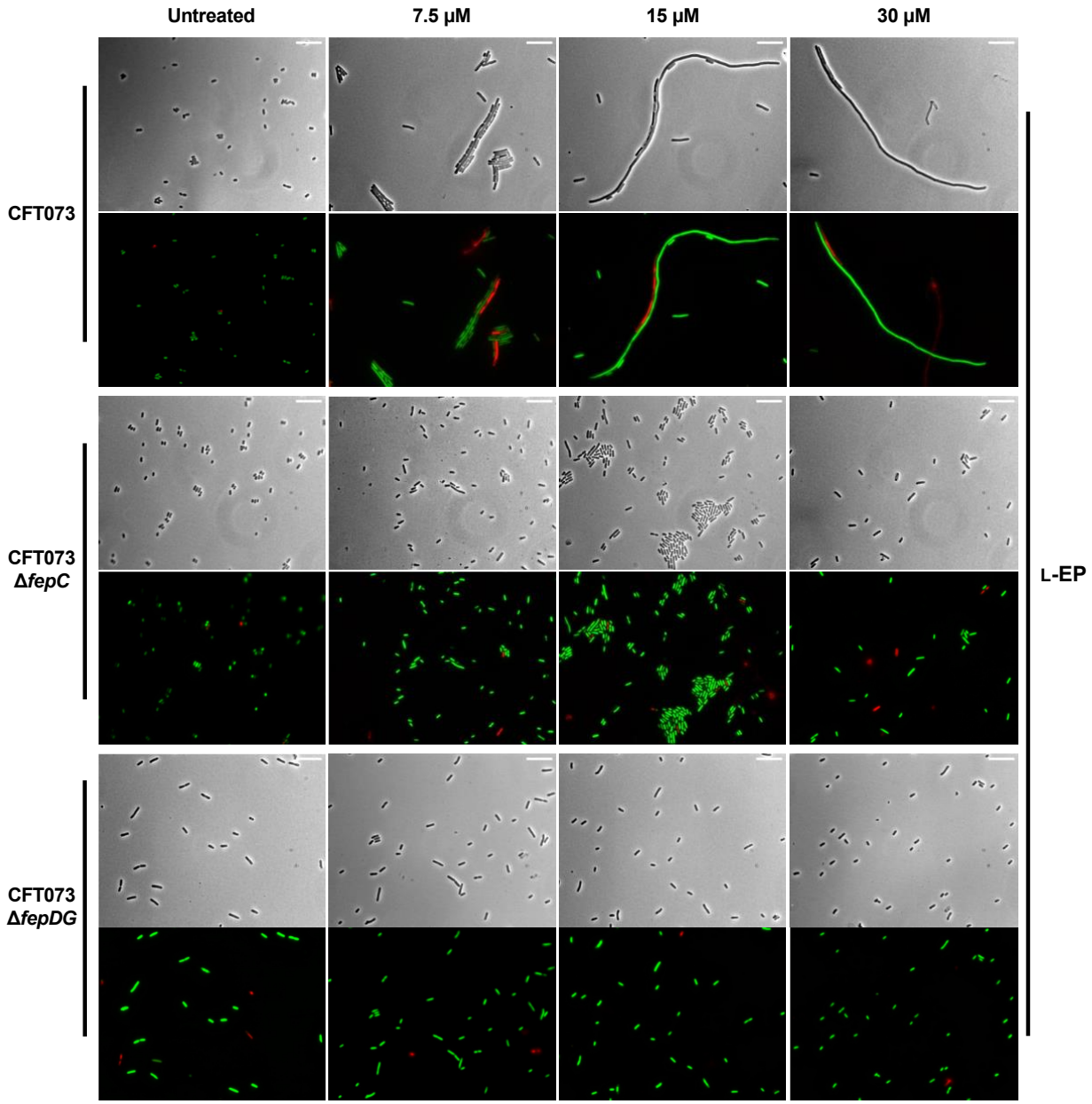

Figure 2.12. Representative phase-contrast and fluorescence micrographs of *E. coli* CFT073 and its Δ*fepC* and Δ*fepDG* mutants treated with L-EP in modified M9 medium for 11 h at 30 °C. Scale bar: 10 µm.

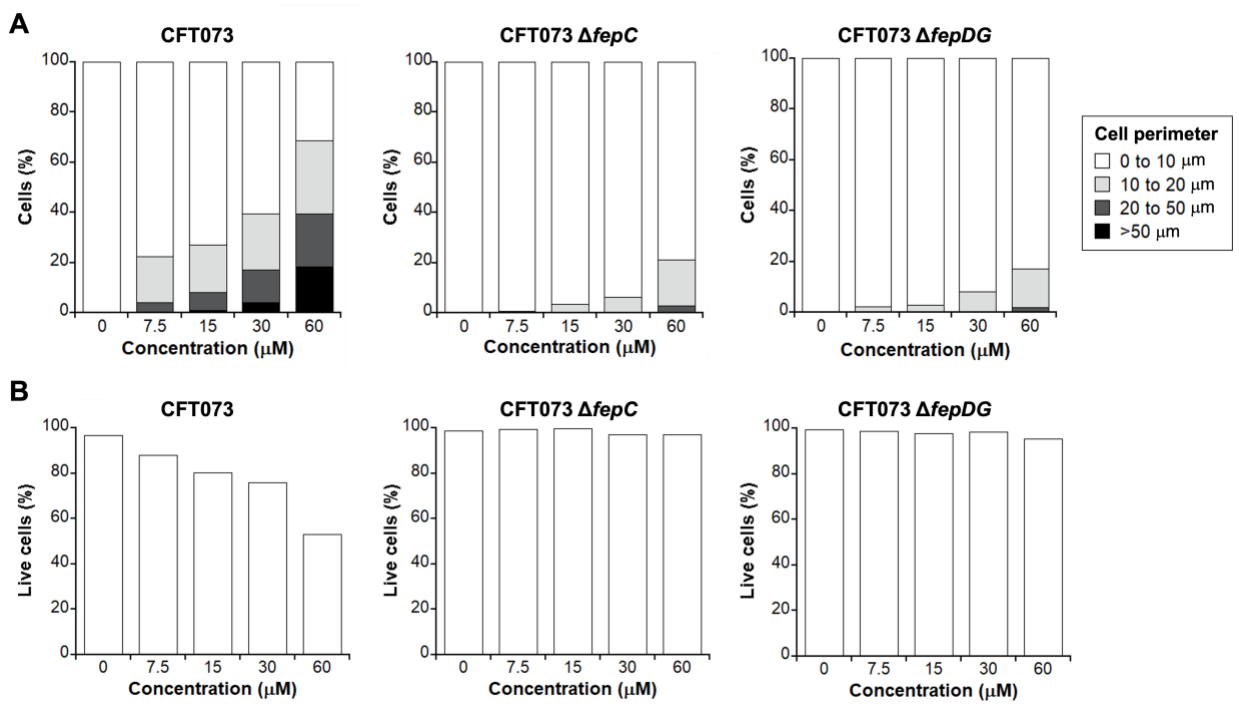

Figure 2.13. Activity of L-EP against *E. coli* CFT073 and its Δ*fepC* and Δ*fepDG* mutants based on microscopy. **(A)** Quantification of the L-EP-induced bacterial morphologies in *E. coli*. **(B)** Viability of *E. coli* determined by LIVE/DEAD staining. For morphology and viability quantification, 500–1000 cells were manually counted for each condition from micrographs. For morphology quantification, cell size was measured and grouped by perimeter (data shown in **Table A.3**).

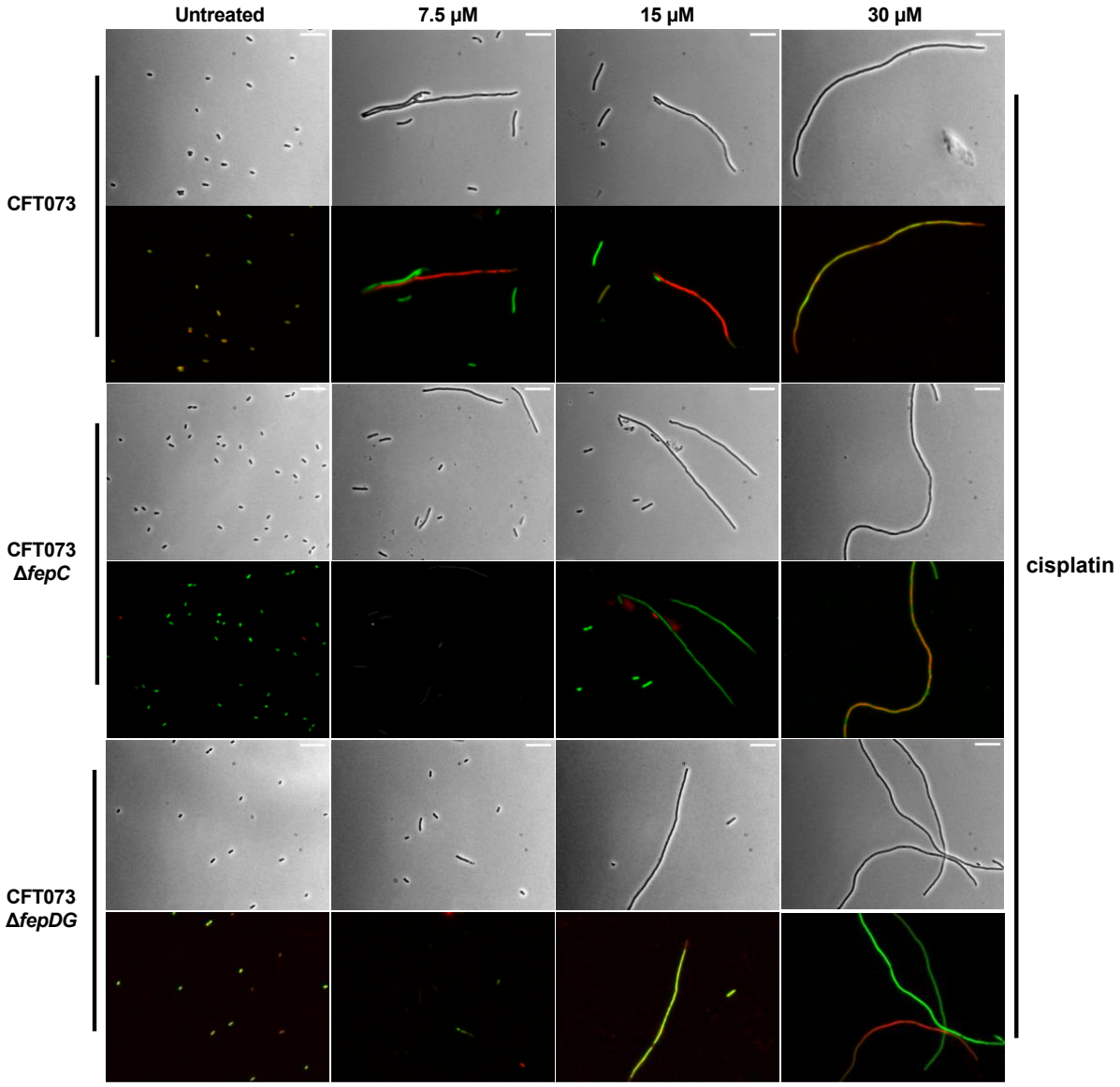

Figure 2.14. Representative phase-contrast and fluorescence micrographs of *E. coli* CFT073 and its Δ*fepC* and Δ*fepDG* mutants treated with cisplatin in modified M9 medium for 11 h at 30 °C. Scale bar: 10 µm.

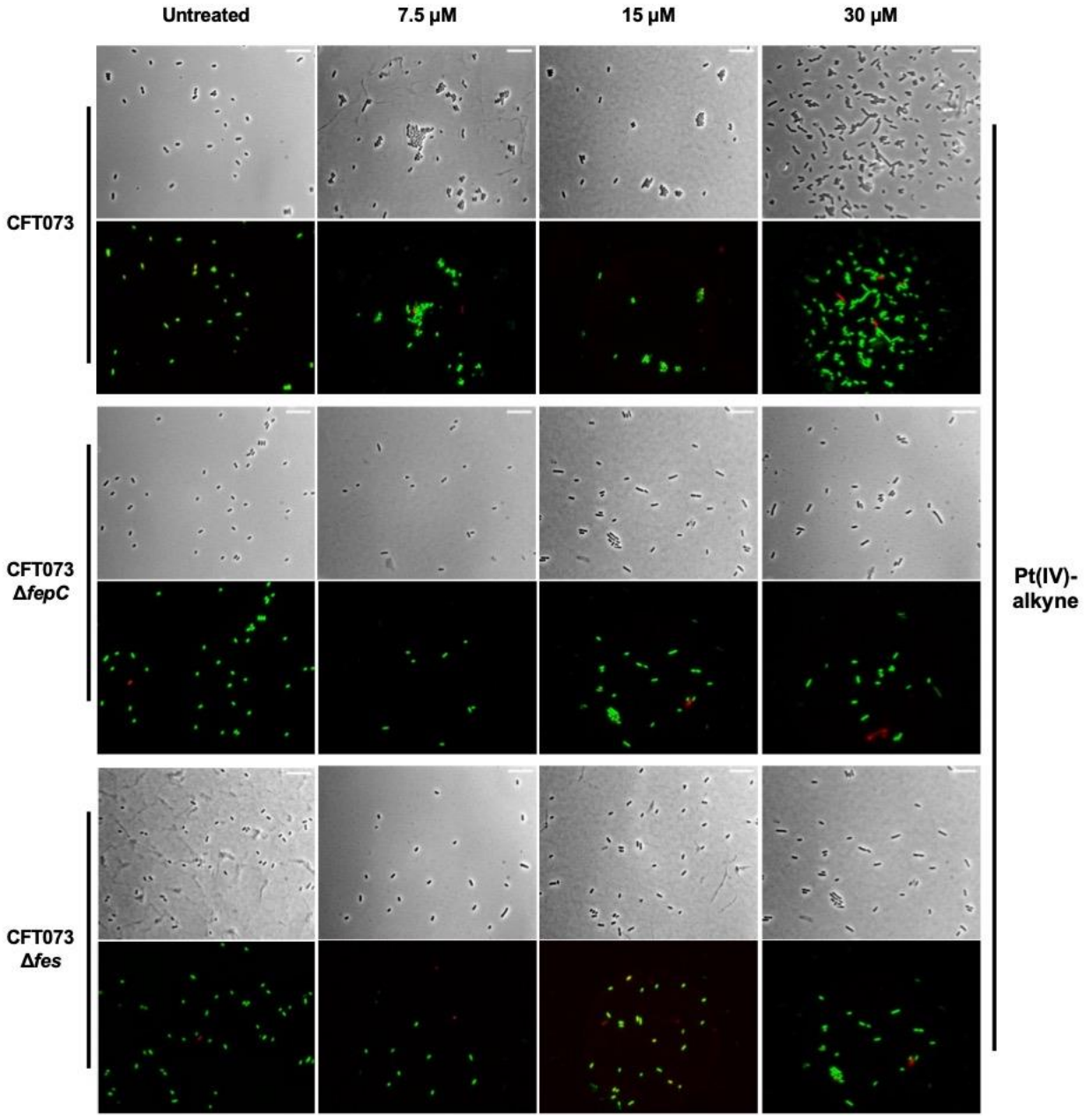

Figure 2.15. Representative phase-contrast and fluorescence micrographs of *E. coli* CFT073 and its Δ*fepC* and Δ*fepDG* mutants treated with Pt(IV)-alkyne in modified M9 medium for 11 h at 30 °C. Scale bar: 10 μm.

Loss of the Ent esterase Fes enhances the susceptibility of *E. coli* to L-EP. By evaluating the antibacterial activity and cellular morphology data we obtained for L-EP against *E. coli*, we demonstrated that Ent conjugation mediates the delivery of the Pt(IV) prodrug into bacterial

cytoplasm via the Ent transport machinery. We next considered the fate of L-EP in the cytoplasm and questioned whether co-delivery of the toxic Pt(IV) payload with nutrient Fe bound by the siderophore compromised antibacterial activity, which would provide a potential explanation for why L-EP was less effective in reducing culture turbidity than cisplatin (**Figure 2.4**). In addition to being an essential nutrient that contributes to overall fitness, Fe plays important roles in DNA metabolism, including DNA repair in *E. coli*. For instance, multiple DNA repair enzymes (helicases, nucleases, glycosylases, demethylases) use Fe as an indispensable cofactor.[61] In considering the fate of L-EP in the cytoplasm, we reasoned that Fe(III)-bound L-EP is a substrate for Fes and other Ent esterases like IroD and that its hydrolysis would provide *E. coli* with Fe that can be used metabolically and increase bacterial fitness. Thus, we examined the consequences of *fes* deletion on the antibacterial activity of L-EP against CFT073. Turbidity measurements showed that the Δ*fes* mutant is markedly more susceptible than the parent strain to L-EP treatment (**Figure 2.16**). In the Δ*fes* mutant, treatment with 15 μM L-EP reduced culture turbidity by 56% and further reduction was seen following the treatment with 30 and 60 μM L-EP (70% and 77%, respectively). In contrast, only 37% reduction in turbidity occurred at 60 μM L-EP for the parent strain.

Imaging of the Δ*fes* mutant further supported its enhanced susceptibility to L-EP compared to the parent strain (**Figures 2.17** and **2.18)**. Quantitative analysis of bacterial morphology demonstrated that the Δ*fes* mutant exhibited more extremely long filaments in the presence of L-EP than the parent strain at all tested concentrations, especially at 15 and 30 μM (≥15% in the *fes* mutant compared to <5% in the parent strain, **Figure 2.18A**). Moreover, LIVE/DEAD staining indicated that cell viability decreased by 10–15% for the Δ*fes* mutant compared to the parent strain in the presence of ≥15 μM L-EP (**Figure 2.18B**). These results suggest that Fes-catalyzed Ent hydrolysis with the release of Fe compromises the ability of the Pt cargo to inhibit cell division to

some degree, likely by increasing the fitness of *E. coli*. We tested Δ*iroD* mutant in parallel, which also showed increased susceptibility to L-EP treatment compared to the parent strain (**Figures 2.16, 2.17,** and **2.18**).

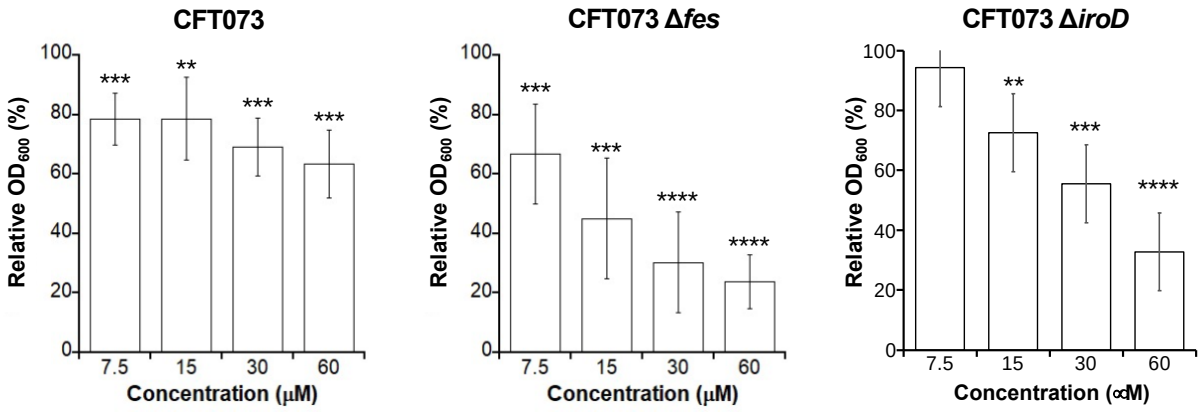

Figure 2.16. Antibacterial activity of L-EP against *E. coli* CFT073 and its Δ*fes* and Δ*iroD* mutants based on OD_{600}. Relative OD_{600} refers to the OD_{600} value of the treated sample divided by that of the untreated control (mean ± standard deviation, n = 7 for CFT073, n = 8 for the Δ*fes* mutant); statistical differences compared to untreated controls were calculated using two-tailed student *t* test assuming unequal variances; ****$P < 0.0001$, ***$P < 0.001$, **$P < 0.01$. All assays were performed in modified M9 medium at 30 °C for 11 h.

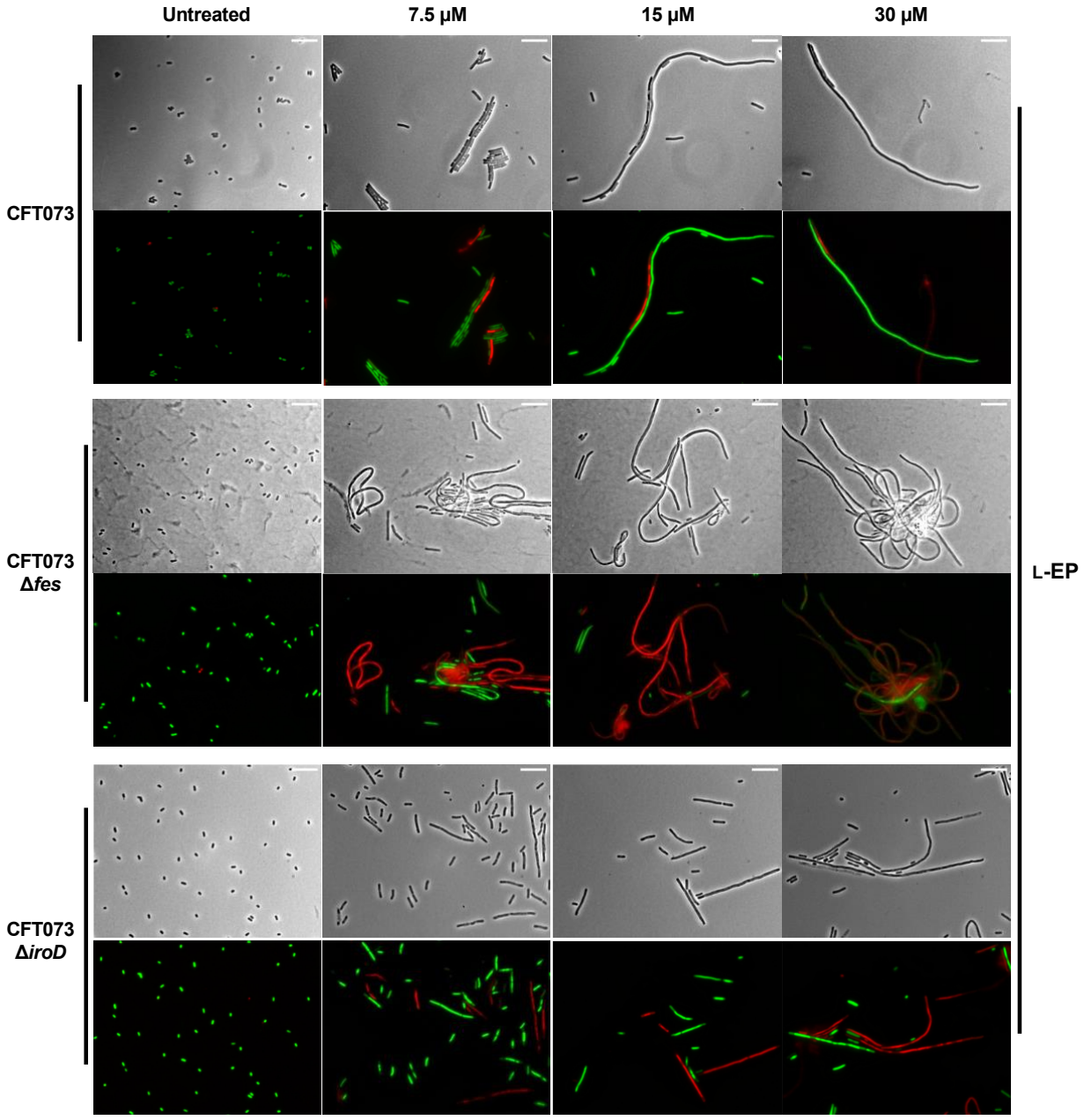

Figure 2.17. Representative phase-contrast and fluorescence micrographs of *E. coli* CFT073 and its Δ*fes* and Δ*iroD* mutants treated with L-EP in modified M9 medium for 11 h at 30 °C. Scale bar: 10 µm.

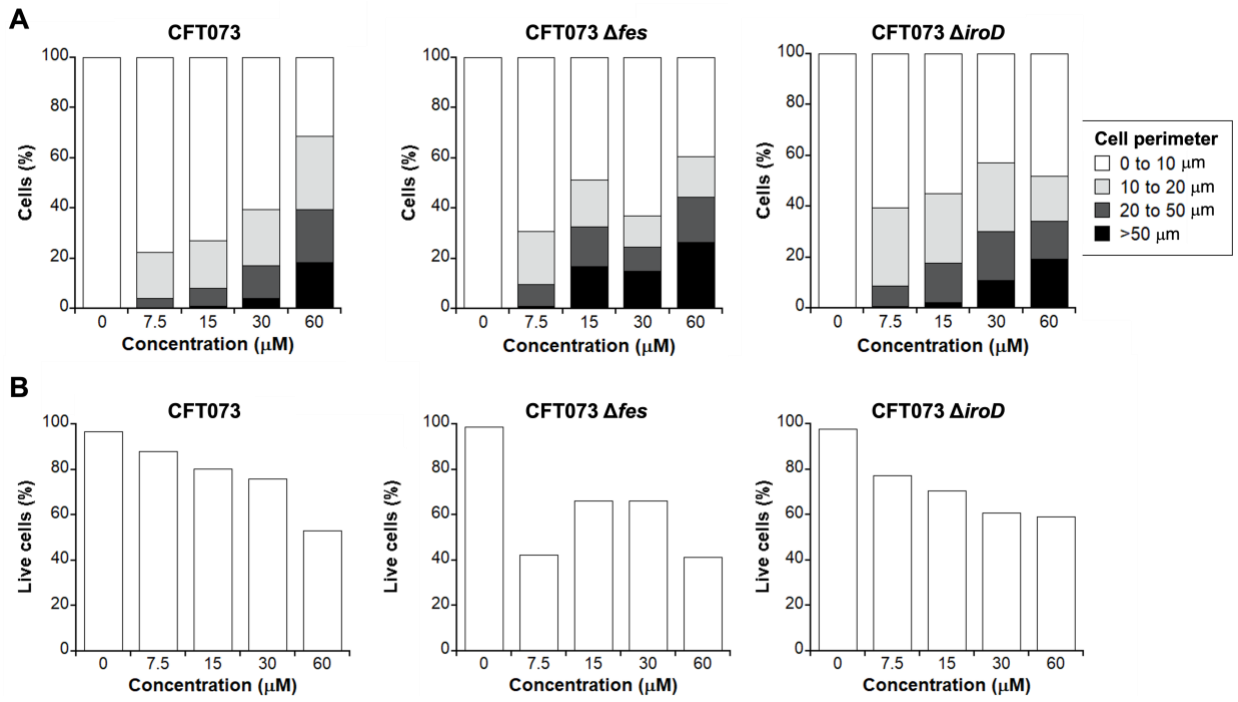

Figure 2.18. Activity of L-EP against *E. coli* CFT073 and its Δ*fes* and Δ*iroD* mutants based on microscopy. **(A)** Quantification of the L-EP-induced bacterial morphologies in *E. coli*. **(B)** Viability of *E. coli* determined by LIVE/DEAD staining. For morphology and viability quantification, 500–1000 cells were manually counted for each condition from micrographs. For morphology quantification, cell size was measured and grouped by perimeter (data shown in **Table A.3**).

Substitution of L-Ent with its enantiomer affords D-EP with enhanced antibacterial activity. Prior studies demonstrated that the Fe(III)-bound D-enantiomer of Ent (D-Ent) is actively transported into the cytoplasm of *E. coli* at levels similar to that of the Fe(III)-bound L-form;[62] however, D-Ent does not recover the growth of *E. coli* under Fe limitation because Fes does not accept D-Ent as a substrate and thus bound Fe(III) cannot be released.[40, 62] As IroD shares sequence similarity with Fes,[62] we speculated that IroD is also stereospecific and cannot hydrolyze D-Ent. Based on these studies and our observation that loss of *fes* or *iroD* enhanced the susceptibility of CFT073 to L-EP, we hypothesized that the enantiomer D-Ent-Pt(IV) (D-EP) **5** would display enhanced antibacterial activity compared to L-EP. We therefore synthesized D-EP from D-Ent-N_3

and Pt(IV)-alkyne **6** as described for L-EP (**Scheme 2.2**, **Figure 2.19**) and evaluated its antibacterial activity.

Scheme 2.2. Synthesis of D-EP via click chemistry.

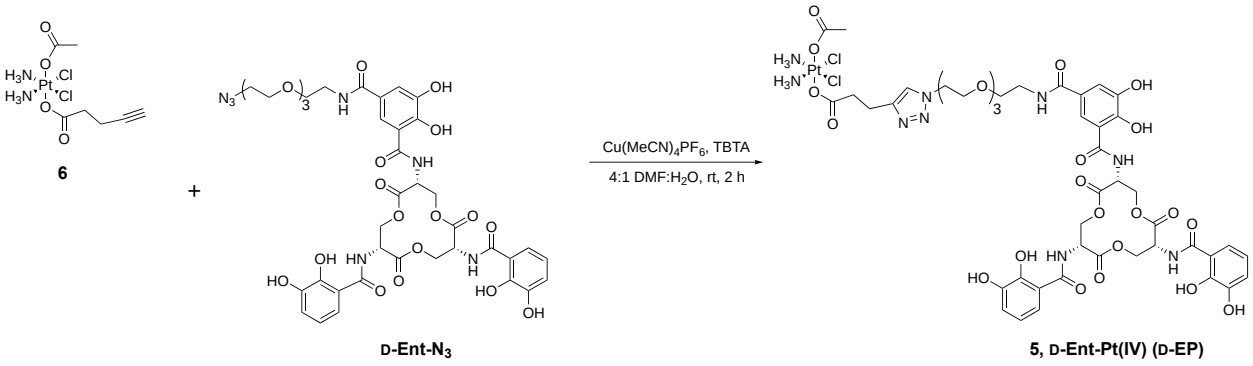

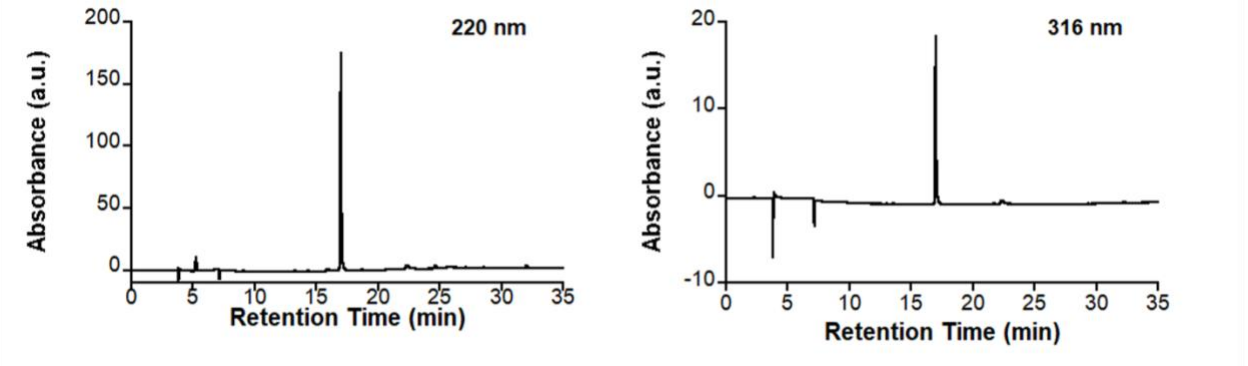

Figure 2.19. Analytical HPLC traces of purified D-EP.

In an initial antibacterial activity assay using a dilution series spanning 0–60 μM, we found that treatment of CFT073 with 7.5 μM D-EP resulted in a greater reduction in culture turbidity compared to treatment with 60 μM L-EP, indicating that D-EP is more potent than either L-EP or cisplatin (**Figure 2.20A**). We then examined the antibacterial activity of D-EP over a concentration range of 0–10 μM and found that the turbidity of CFT073 cultures decreased markedly in the presence of 1 μM D-EP (**Figure 2.20B**). This concentration of L-EP, cisplatin and Pt(IV)-alkyne

had negligible effect on culture turbidity **(Figure 2.20B)**. We also found that 10 μM D-EP almost fully reduced the OD_{600} value of *E. coli* CFT073 cultures to the baseline (OD_{600} = 0.05 compared to 0.2 for the untreated control, **Figures 2.20B** and **2.20D**). In the case of K12, the culture turbidity was reduced by 72% in the presence of 0.1 μM D-EP and was fully reduced to the baseline when treated with 1 and 10 μM D-EP (**Figure 2.20C**). We also evaluated whether the outer membrane receptor FepA and the inner membrane transporter FepCDG are important for D-EP activity against *E. coli* (**Figures 2.20C** and **2.20D**). The results were consistent with our findings for L-EP. In particular, 10 μM D-EP had negligible effect on the growth of the K12 Δ*fepA* mutant and the CFT073 inner membrane transporter mutants Δ*fepC and* Δ*fepDG*, indicating that the Ent transport machinery is required for D-EP to enter the *E. coli* cytoplasm and exert antibacterial activity.

We also examined the morphologies of *E. coli* CFT073 treated with D-EP, L-EP, cisplatin and Pt(IV)-alkyne **6** in this low concentration range (**Figure 2.21**). Both D-EP and L-EP induced filamentation at 1 and 10 μM, and bacteria treated with L-EP and D-EP displayed different morphologies (**Figure 2.21**). The cells treated with L-EP were mostly very long filaments, but those treated with D-EP were comparatively sparse and exhibited various morphologies, including filaments (relatively shorter than those caused by L-EP), elongated cells, and normal cells. By contrast, only slight elongation was induced by 10 μM cisplatin. Almost all bacterial cells treated with Pt(IV)-alkyne were normal-sized and rod-shaped, presumably a consequence of poor penetration of the molecule across cell membrane. Thus, by synthesizing the D-enantiomer of Ent-Pt(IV), we leveraged fundamental understanding of chiral recognition by Fes to achieve enhanced antibacterial activity against *E. coli* compared to L-EP and cisplatin.

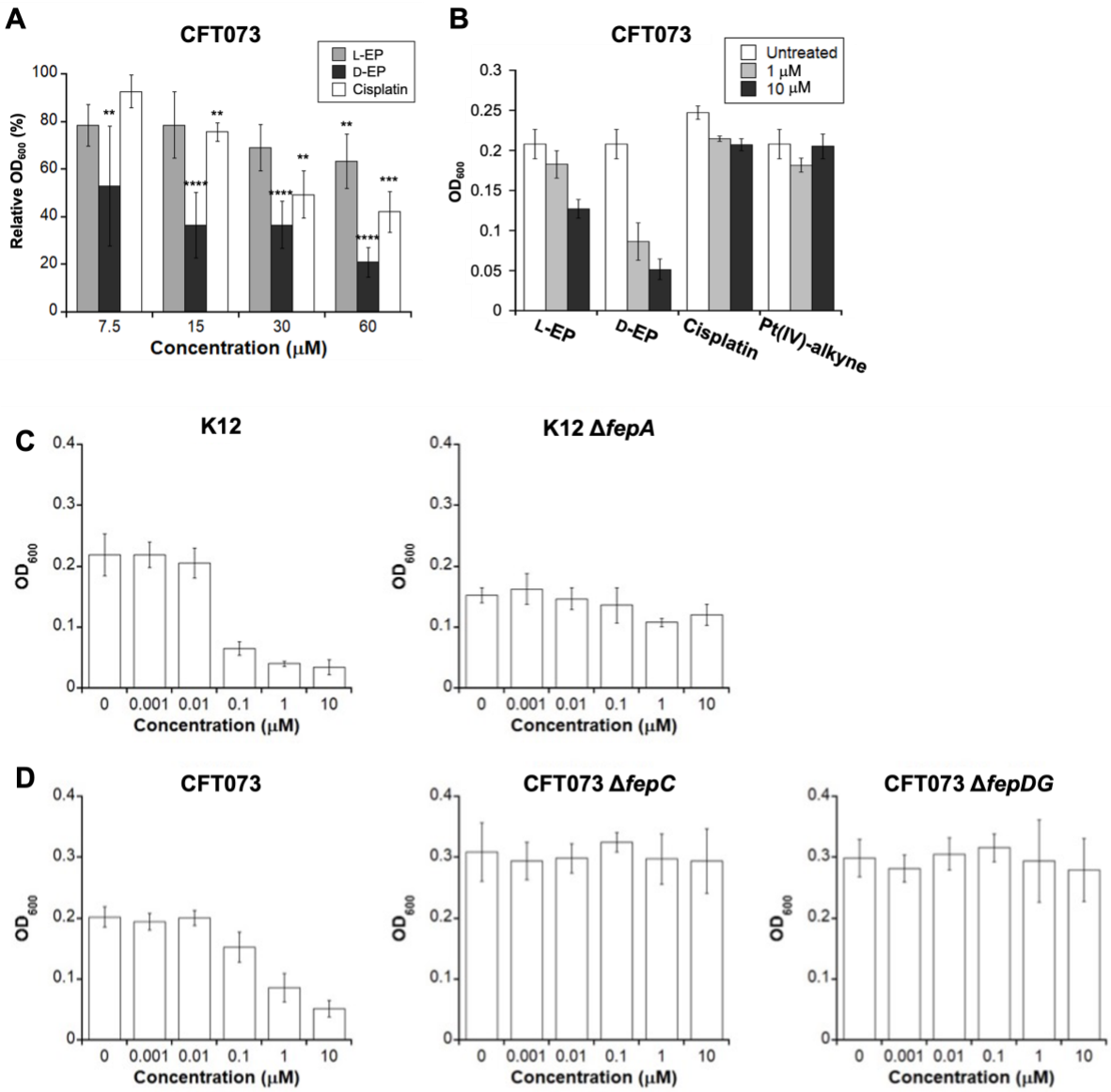

Figure 2.20. Comparison of activity of L-EP, D-EP and other Pt species. **(A)** Antibacterial activity of L-EP, D-EP and cisplatin against *E. coli* CFT073 (0–60 μM). Relative OD_{600} refers to the OD_{600} value of the treated sample divided by that of the untreated control (mean ± standard deviation, n ≥ 6). Statistical differences compared to untreated controls were calculated using two-tailed student *t* test assuming unequal variances; ****P < 0.0001, ***P < 0.001, **P < 0.01. **(B)** Comparison of the antibacterial activity of L-EP, D-EP, cisplatin and Pt(IV)-alkyne at 1 μM and 10 μM, respectively (mean ± standard deviation, n=3; the untreated control in L-EP, D-EP and Pt(IV)-alkyne refers to treating bacteria with 1% DMSO in modified M9 medium; the untreated control in cisplatin refers to incubating bacteria in modified M9 medium). **(C)** Antibacterial activity of D-EP against *E. coli* K12 and its Δ*fepA* mutant and **(D)** *E. coli* CFT073 and its Δ*fepC*, Δ*fepDG* mutants based on OD_{600} (data shown in **Table A.3**). All assays were performed in modified M9 medium (11 h, 30 °C, 500 rpm; mean ± standard deviation, n ≥ 4).

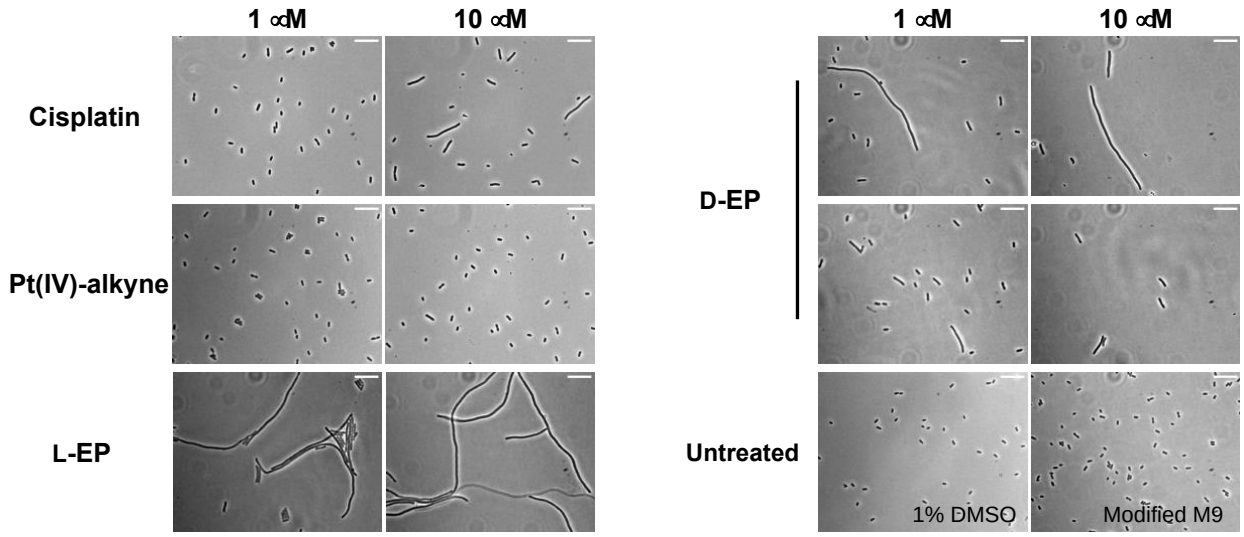

Figure 2.21. Representative phase-contrast micrographs of *E. coli* CFT073 treated with cisplatin, Pt(IV)-alkyne, L-EP and D-EP (Scale bar: 10 μm). All assays were performed in modified M9 medium at 30 °C for 11 h. Untreated controls with 1% DMSO and no DMSO in the modified M9 medium were included.

Ent conjugation affords enhanced Pt uptake by bacterial cells. To examine whether Ent conjugation affects Pt uptake by bacterial cells**,** we treated *E. coli* CFT073 with 1 μM of L/D-EP, cisplatin, or Pt(IV)-alkyne in modified M9 medium at 30 °C for 30 min, and then quantified cell-associated Pt levels by ICP-MS. We found that Pt uptake was markedly enhanced for the Ent conjugates compared to cisplatin and Pt(IV)-alkyne. In particular, Pt uptake was ≥10-fold greater for *E. coli* CFT073 treated with L-EP or D-EP (8-10%) compared to cells treated with cisplatin or Pt(IV)-alkyne (**Figure 2.22A**), which showed negligible Pt uptake (<1%). This result indicates that Ent conjugation facilitates Pt uptake, which presumably results from the active transport of L/D-EP by the Ent transport system compared to passive diffusion of cisplatin and Pt(IV)-alkyne.

Ent conjugation reduces Pt uptake by human cells. Lastly, we examined whether Ent conjugation affects Pt uptake by human cells. To our knowledge, human cells do not have an Ent

receptor. We reasoned that the L/D-EP conjugates are too large (1369 Da) to enter human cells by passive diffusion. We performed a Pt uptake assay with HEK293T cells, which were treated with 1 μM of L/D-EP, cisplatin, or Pt(IV)-alkyne in DMEM supplemented with 1% penicillin/streptomycin at 37 °C for 6 h. The cell-associated Pt levels were then quantified by ICP-MS.[63] Under these conditions, the HEK293T cells showed ~9-fold greater Pt uptake for cisplatin (~0.09%) than for L/D-EP or Pt(IV) alkyne (~0.01%) (**Figure 2.22B**). The negligible uptake of Pt(IV) alkyne is presumably attributed to its poor lipophilicity due to its short carbon chain axial ligands.[64-65] Because higher cellular Pt accumulation is accompanied by greater DNA platination and therefore cell growth inhibition,[66-67] our Pt uptake assay suggests that Ent modification affords decreased cytotoxicity towards human cells compared to cisplatin.

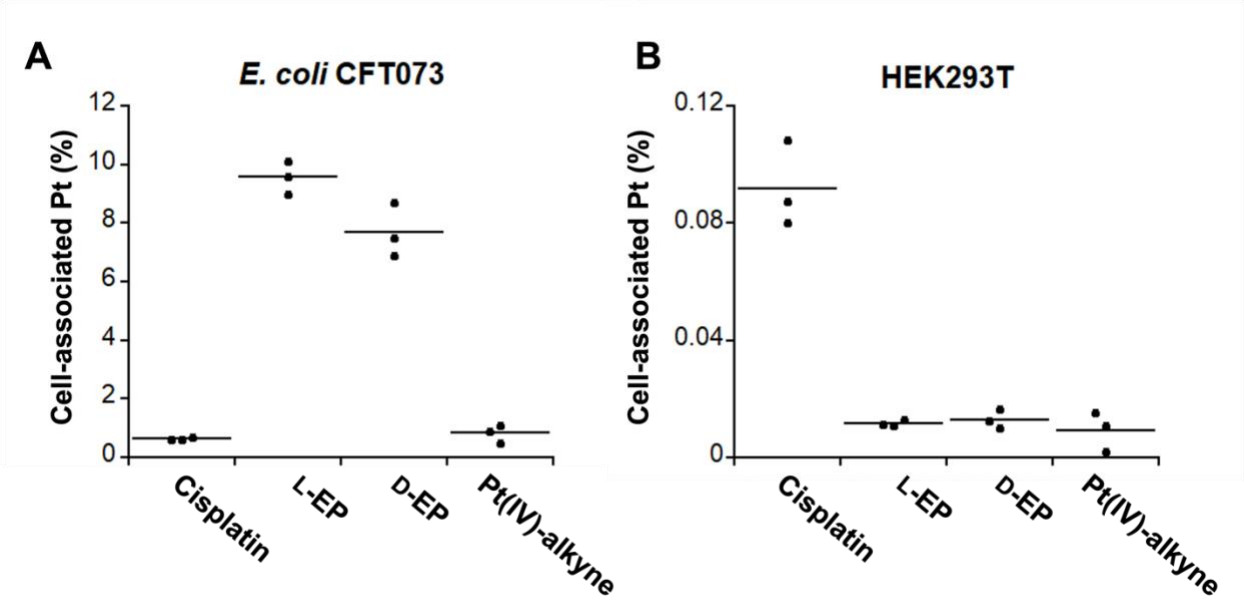

Figure 2.22. Pt uptake of **(A)** *E. coli* CFT073 and **(B)** HEK293T cells treated with 1 μM cisplatin, L-EP **4**, D-EP **5**, or Pt(IV)-alkyne **6**, respectively. *E. coli* CFT073 cells were treated for 30 min in modified M9 medium at 30 °C, and HEK293T cells were treated for 6 h in DMEM+1% penicillin/streptomycin at 37 °C, 5% CO_2 (n = 3).

2.5 Conclusion

In this work, we used L-EP as a proof-of-concept to show that Ent conjugation repurposes cisplatin as an antibiotic and mediates its delivery to the cytoplasm of *E. coli*. Then, guided by fundamental studies on chiral recognition of Ent by cytoplasmic esterases, we synthesized the enantiomer D-EP, which displays enhanced antibacterial activity against *E. coli*. Lastly, we demonstrated that Ent conjugation facilitates Pt uptake in bacteria and reduces Pt uptake in HEK293T cells. We propose the following mechanism for L/D-EP (**Figure 2.23**): upon Ent-mediated delivery into the *E. coli* cytoplasm, L/D-EP undergoes intracellular reduction and thereby releases one equivalent of cisplatin, acetate and the L/D-Ent-containing ligand. Cisplatin further undergoes aquation, and the resulting electrophilic complexes ($[Pt(NH_3)_2Cl(H_2O)]^+$ and $[Pt(NH_3)_2(H_2O)_2]^{2+}$) readily bind to the purine bases of DNA, resulting in cross-links which distort and bend the DNA structure.[68-70] In response, bacteria initiate the SOS response, which mediates the inhibition of cell division while damaged DNA is repaired.[51] With L-EP treatment, esterase-mediated L-Ent cleavage releases bound Fe, which increases bacterial fitness and leads to the formation of extreme filaments. Such extreme filaments are not observed for D-EP because the D-Ent scaffold is not a substrate for Ent esterases. Moreover, D-EP exhibits significantly enhanced antibacterial activity compared to L-EP. This outcome provides a foundation for further leveraging D-Ent in siderophore-based delivery. More broadly, the current work also provides a modular synthetic approach for repurposing other Pt-based anticancer agents and metallopharmaceuticals as targeted antibiotics against bacterial pathogens using siderophores.

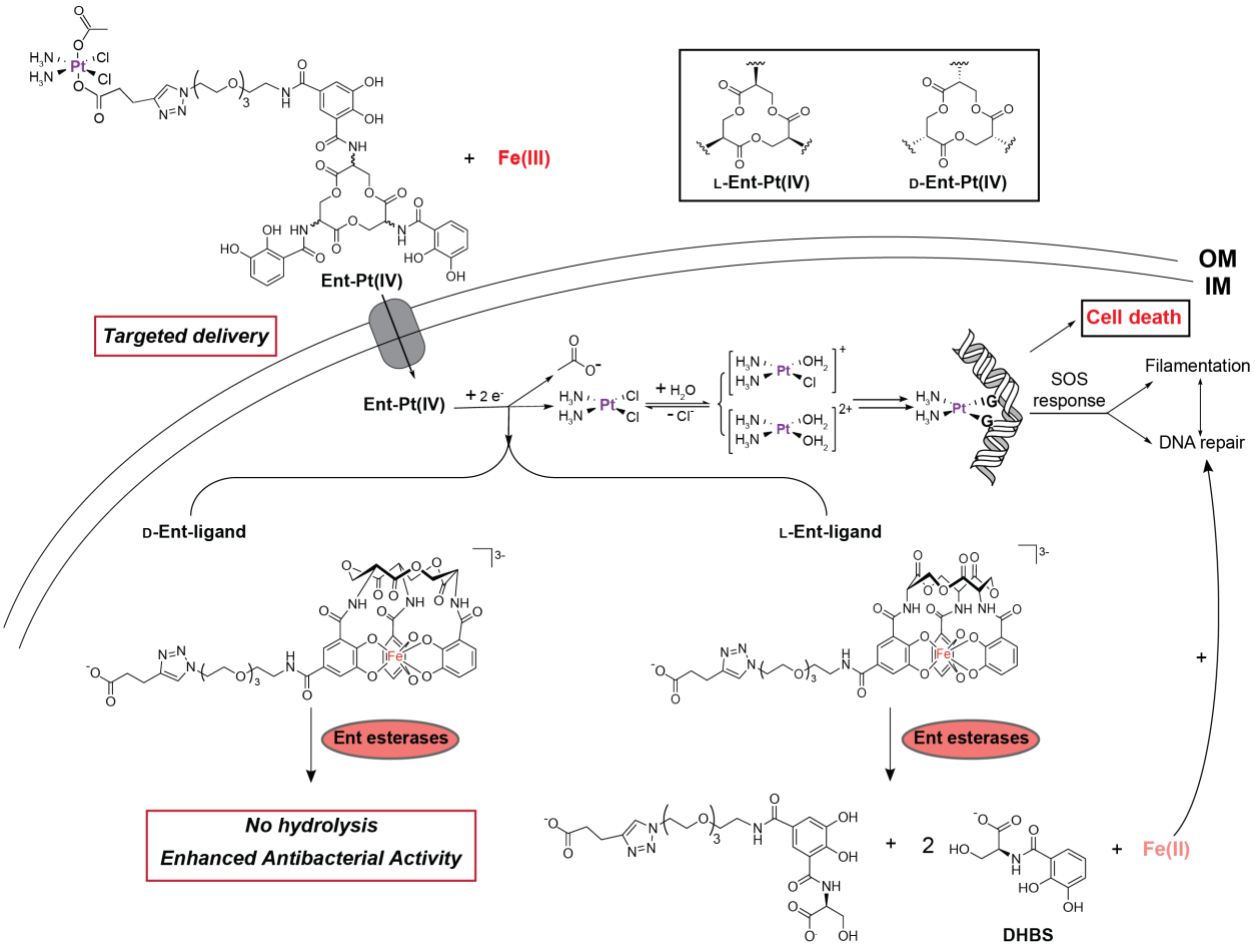

Figure 2.23. Proposed model for the activity for L- and D-EP against *E. coli*. DHBS, 2,3-dihydroxybenzoyl serine; G, a guanine base. Reduction of Fe(III) to Fe(II) that occurs during release of the metal ion is not catalyzed by the Ent esterases.

Along with our prior work on the Ent-Cipro conjugate,[20] the present work also deepens our appreciation of the role of esterase-catalyzed Ent hydrolysis in the activity of Ent conjugates with cytoplasmic targets. In the case of Ent-Cipro, the pathogen-associated esterase IroD was required for antibacterial activity, indicating that hydrolysis of the Fe-Ent moiety by IroD was an essential processing step for Ent-Cipro activation. By contrast, Fes and IroD compromised the potency of L-EP, indicating that hydrolysis of the Fe-Ent moiety by these enzymes provides *E. coli* with a fitness advantage. The different outcomes for Ent-Cipro and L-EP may result, at least in part, to the relatively potencies of the two cargos. Ciprofloxacin is approximately 10^3-fold more potent

than cisplatin. Thus, for Ent-Cipro, less conjugate and therefore less Fe needs to be delivered to the cell for cell death. Regardless, the current results highlight that it is necessary to think about the delivery of nutrient Fe bound to the siderophore moiety, especially for cargos with cytoplasmic targets. In addition to our current examination of D-Ent as a strategy to avoid Fe(III) release, Ga(III)-loaded SACs have been studied to avoid Fe co-delivery and thereby afford enhanced antibacterial activity compared to the corresponding Fe(III)-loaded SACs.[71-73] In a preliminary investigation, we observed negligible antibacterial activity when treating *E. coli* K12 and CFT073 with Ga(III)-bound L-EP. This observation is consistent with a prior report that Ga(III)-Ent is a poor transport substrate for the Ent uptake machinery.[74]

In closing, despite advances in drug repurposing, no drugs have been repurposed as antibiotics to date.[75] Studies of SACs have mainly focused on modifying classic antibiotics.[18] To our knowledge, only one example of a SAC designed for drug repurposing has been reported, a compound containing a mycobacterial siderophore linked to the anti-malarial drug artemisinin that targets *Mycobacterium tuberculosis*.[76] We anticipate that the current exploration of Ent-directed cisplatin delivery will motivate further efforts towards leveraging the siderophore-based "Trojan-horse" strategy for repurposing a broad scope of non-antibiotic toxic drugs into targeted antibacterials.

2.6 Experimental Section

Instrumentation

High-performance liquid chromatography (HPLC). Semi-preparative and analytical HPLC were performed by using an Agilent 1200 series HPLC system outfitted with an Agilent Zorbax reverse-phase C18 column (5 μm, 9.4 × 250 mm) at a flow rate of 4 mL/min and a Clipeus

reverse-phase C18 column (5 μm, 4.6 × 250 mm; Higgins Analytical, Inc.) at a flow rate of 1 mL/min, respectively. Preparative HPLC was performed by using an Agilent PrepStar system outfitted with a Phenomenex Luna reverse-phase C18 column (10 μm, 21.2 × 250 mm) at a flow rate of 10 mL/min. The multiwavelength detectors were set to read the absorbance at 220, 280, and 316 (catecholate absorption) nm.

Solvent A was Milli-Q water (18.2 MΩ·cm) with trifluoroacetic acid (TFA, purchased from Millipore Sigma) that was filtered through a 0.2-μm bottle-top filter before use. Solvent B was HPLC grade acetonitrile (MeCN, purchased from Millipore Sigma) with TFA. The amount of TFA in each eluent is indicated in the synthetic procedures. Each HPLC method began with a four-minute equilibration at 0% B followed by a gradient of increasing %B. For analytical HPLC performed to evaluate conjugate purity, the entire portion of each HPLC-purified compound was dissolved in a mixture of 1:1 H_2O/MeCN and an aliquot was taken for HPLC analysis, and the remaining solution was subsequently frozen and lyophilized to dryness.

Liquid chromatography/mass spectrometry (LC/MS). LC/MS was performed using a nominal mass Agilent 6125B mass spectrometer attached to an Agilent 1260 Infinity LC with an electrospray (ESI) source. High-resolution mass spectrometry was performed using a high-resolution Agilent 6545 mass spectrometer coupled to an Agilent Infinity 1260 LC system with a Jet Stream ESI source. For all LC/MS analyses, solvent A was 0.1% formic acid/H_2O and solvent B was 0.1% formic acid/MeCN (LC/MS grade MeCN, Millipore Sigma). The samples were analyzed using a solvent gradient of 5–95% B over 6 min with a flow rate of 0.4 mL/min. All LC/MS instruments are housed in the MIT Department of Chemistry Instrumentation Facility (DCIF).

Inductively coupled plasma-mass spectrometry (ICP-MS). Metal analysis was conducted using an Agilent 7900 ICP-MS system in helium mode outfitted with an integrated autosampler housed in the Center for Environmental Health Sciences (CEHS) Bioanalytical Core Facility at MIT. To quantify Fe concentration, the instrument was calibrated using standards prepared by serial dilution of an environmental calibration standard solution (1000 ppm each of Ca, Fe, K, Mg, Na; 10 ppm each of Ag, Al, As, Ba, Be, Cd, Co, Cr, Cu, Mn, Mo, Ni, Pb, Sb, Se, Th, Tl, U, V, Zn; Agilent, part number 5183-4688). To quantify Pt concentration, the instrument was calibrated using standards prepared by serial dilution of a Pt standard solution (1 ppm Pt; Millipore Sigma). Terbium (1 ppb Tb; Agilent) was used as an internal standard. All samples were prepared as 2 mL solutions in 5% HNO_3 (Honeywell, TraceSELECT; 69.0%) in 15 mL Falcon tubes, transferred to ICP-MS polypropylene vials (Agilent) and analyzed.

For whole-cell metal analyses of bacterial cells or HEK293T cells, cell pellets diluted into solutions of 3% HNO_3 were liquefied using a Milestone UltraWAVE digestion system housed in the CEHS Core Facility at MIT. A standard microwave protocol (15 min ramp to 200 °C at 1,500 W power; 10 min ramp to 220 °C at 1,500 W power) was used for the acid digestion.

NMR spectroscopy. ^{1}H NMR spectra were collected on a two-channel Bruker Avance-III HD Nanobay 400 MHz spectrometer or a three-channel Bruker Avance Neo 500 MHz spectrometer (both are equipped with a 5-mm liquid-nitrogen cooled Prodigy broad band observe cryoprobe). ^{195}Pt NMR and 2-dimentional (2-D) NMR spectra were collected on a three-channel Bruker Avance Neo 500 MHz spectrometer (equipped with a 5-mm BBFO SmartProbe) at ambient probe temperature (293 K). All NMR spectrometers are housed in the MIT DCIF.

Optical absorption spectroscopy. Optical absorption spectra were recorded on a Beckman Coulter DU800 spectrophotometer (1-cm quartz cuvettes, Starna).

Microscopy. Phase-contrast and fluorescence microscopy imaging were carried out using a Zeiss Axioplan2 upright microscope equipped with a 100× oil-immersion objective lens. Phase-contrast images were acquired using the trans phase channel. For LIVE/DEAD cell viability assays, the Texas Red (λ_{ex} = 532–587 nm; λ_{em} = 608–683 nm) and GFP (λ_{ex} = 457–487 nm; λ_{em} = 502–538 nm) channels were used to acquire images of the DEAD (red) and LIVE (green) cells, respectively.

Synthesis

General synthetic methods. Anhydrous *N*,*N*-dimethylformamide (DMF) and dichloromethane (DCM) were purchased from VWR. Anhydrous dimethyl sulfoxide (DMSO) was purchased from Millipore Sigma and used as received. All other chemicals were purchased from Millipore Sigma, VWR or Alfa Aesar in the highest available purity and used as received.

EMD TLC silica gel 60 F_{254} plates were used for analytical thin layer chromatography. EMD PLC silica gel 60 F_{254} plates of 2-mm thickness were used for preparative TLC. Sigma-Aldrich silica gel (70–230 mesh, 60 Å) was used for flash column chromatography.

Syntheses of Ent **1**, L-Ent-N_3 **7**, D-Ent-N_3 and *cis, cis, trans*-[$Pt(NH_3)_2Cl_2(OOCCH_3)(OH)$] were based on published procedures.[19, 40, 77-78]

Scheme 2.3. Synthesis of Pt(IV)-alkyne **6**.

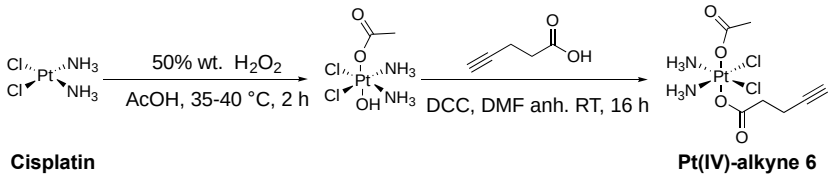

***cis, cis, trans*-[Pt(NH_3)$_2$$Cl_2$($OOCCH_3$)($OOCCH_2CH_2C{\equiv}CH$)] (denoted hereafter as Pt(IV)-alkyne 6).** The synthesis of Pt(IV)-alkyne was performed using a literature procedure with modifications.[39] *cis, cis, trans*-[Pt(NH_3)$_2$(Cl)$_2$($OOCCH_3$)(OH)] (50 mg, 0.13 mmol) was suspended in anhydrous DMF (6 mL). 4-Pentynoic acid (53 mg, 0.053 mmol) was dissolved in anhydrous DMF (1.3 mL) and combined with *N,N'*-dicyclohexylcarbodiimide (DCC, 115 mg, 0.56 mmol). The mixture was placed in an ultrasonic bath for 15 min, during which time a white precipitate formed. The mixture was centrifuged (4,500 rpm, 15 min, room temperature), and the supernatant was added slowly to the above suspension. The reaction was purged with N_2 and stirred in the dark at room temperature for 16 h, resulting in a clear yellow solution. The reaction mixture was concentrated by air stream to yield a yellow oil, to which water (12 mL) was added. The mixture was sonicated for 5 min, which resulted in precipitation of the dicyclohexylurea byproduct, which was removed by vacuum filtration. The filtrate was washed with Et_2O and the combined solution was lyophilized, affording a yellow powder. The crude product was dissolved in 1:1 H_2O/MeCN, filtered through a 0.45-μm PTFE filter (purchased from VWR), and purified by preparative HPLC (0–100% B over 30 min, 10 mL/min, 0.1% TFA in solvents A and B). The eluate at 15.4 min was collected and lyophilized to give the pure product as a white powder (33 mg, 56% yield). MS (ESI+): $[M+H]^+$ *m/z* calcd, 457.0038; found, 457.0016. $[M+Na]^+$ *m/z* calcd, 478.9857; found, 478.9843. ^{1}H NMR (500 MHz, D_2O): δ 2.04 (3H, s), 2.30 (1H, t, J = 2.6 Hz), 2.36–2.39 (2H, m), 2.57–2.60 (2H, t, J = 7.0 Hz). ^{195}Pt NMR (500 MHz, D_2O): δ 1073.82.

L-Ent-Pt(IV) (L-EP, 4). L-Ent-N_3 **7** (38.3 mg, 0.042 mmol) was dissolved in DMF (600 μL) to give a 70 mM solution. The solution was divided into aliquots (9.5 μL, 0.7 mg in each aliquot). Pt(IV)-alkyne **6** (48 mg, 0.10 mmol) was dissolved in DMF (179 μL) to give a 586 mM solution. To each aliquot of the L-Ent-N_3 **7** solution (70 mM)**,** 2.8 μL of the Pt(IV)-alkyne **6**

solution (586 mM) was added, followed by 8 μL of Milli-Q water. A DMF solution containing 50 mM *tris*[(1-benzyl-1*H*-1,2,3-triazol-4-yl)methyl]amine (TBTA) and 50 mM $Cu(MeCN)_4PF_6$ was freshly prepared and 19.7 μL of the solution was added to each aliquot. The resulting solutions were briefly mixed by using a vortex mixer and incubated on a benchtop rotator at room temperature in the dark. After 3 h, each aliquot was diluted with 160 μL of 1:1 H_2O/MeCN, centrifuged (13,000 rpm, 10 min, 4 °C), and purified by preparative HPLC (0–100% B over 30 min, 10 mL/min, 0.005% TFA was used in solvent A and B; this low TFA % was used to prevent decomposition). The product eluted at 20.9 min, and the collected fractions were combined and lyophilized, which afforded a pale-green powder. Further purification was performed by semi-preparative HPLC (0–100% B over 30 min, 4 mL/min, 0.005% TFA). The product eluted at 13.8 min and was collected and lyophilized, which afforded L-EP as a white powder (3.7 mg, 6%). The product purity was evaluated by analytical HPLC (0–100% B over 30 min, 1 mL/min, 0.005% TFA; retention time 17.3 min). HRMS (ESI+): $[M+H]^+$ *m/z* calcd, 1370.2569; found, 1370.2650. $[M+Na]^+$ *m/z* calcd, 1391.2407; found, 1391.2474. ^{1}H NMR (500 MHz, DMSO_d_6): δ 1.92 (3H, s), 2.53 (2H, t, J = 7.6 Hz), 2.81 (2H, t, J = 7.3 Hz), 3.52 (12H, m), 3.80 (2H, t, J = 5.4), 4.3–4.45 (5H, m), 4.63–4.69 (3H, m), 4.89–4.96 (3H, m), 6.56 (6H, br), 6.75 (2H, t, J = 8.0 Hz), 6.98 (2H, d, J = 7.8 Hz), 7.36 (2H, d, J = 8.2 Hz), 7.46 (1H, m), 7.86 (1H, s), 7.93 (1H, m), 8.32 (1H, t, J = 5.5 Hz), 9.12 (2H, d, J = 6.8 Hz), 9.29 (1H, d, J = 7.0 Hz), 9.41 (2H, s), 9.72 (1H, s), 11.62 (2H, s), 11.92 (1H, s). ^{195}Pt signal was detected by ^{1}H-^{195}Pt HMQC NMR (500 MHz, DMSO_d_6): δ 1226.95. The product structure was also characterized by 2-dimensinal (2-D) NMR including ^{1}H-^{1}H COSY, ^{1}H-^{13}C HSQC and ^{1}H-^{13}C HMBC.

D-Ent-Pt(IV) (D-EP, 5). D-Ent-Pt(IV) was synthesized as described for L-Ent-Pt(IV) (L-EP, **4**) except that D-Ent-N_3 was employed instead of L-Ent-N_3. HRMS (ESI+): $[M+H]^+$ *m/z* calcd,

1370.2569; found, 1370.2669. $[M+Na]^+$ *m/z* calcd, 1391.2407; found, 1391.2459. ^{1}H NMR (500 MHz, DMSO_d_6): δ 1.92 (3H, s), 2.53 (2H, t, J = 7.6 Hz), 2.81 (2H, t, J = 7.3 Hz), 3.52 (12H, m), 3.80 (2H, t, J = 5.4), 4.38–4.45 (5H, m), 4.63–4.69 (3H, m), 4.89–4.96 (3H, m), 6.56 (6H, br), 6.75 (2H, t, J = 8.0 Hz), 6.98 (2H, d, J = 7.8 Hz), 7.36 (2H, d, J = 8.2 Hz), 7.46 (1H, s), 7.86 (1H, s), 7.93 (1H, s), 8.33 (1H, t, J = 5.5 Hz), 9.12 (2H, d, J = 6.8 Hz), 9.29 (1H, d, J = 7.0 Hz), 9.41 (2H, s), 9.73 (1H, s), 11.62 (2H, s), 11.92 (1H, s). ^{195}Pt signal was detected by ^{1}H-^{195}Pt HMQC NMR (500 MHz, DMSO_d_6): δ 1226.95. The product structure was also characterized by 2-dimensinal (2-D) NMR including ^{1}H-^{1}H COSY, ^{1}H-^{13}C HSQC and ^{1}H-^{13}C HMBC.

Storage and handling of Ent and Ent-Pt(IV) conjugates

All precursors, Ent and Ent-Pt(IV) conjugates were stored as either powders or DMSO stock solutions at -20 °C. The concentration of Ent stock solutions (~10 mM) were determined by using Beer's law and the reported extinction coefficient for enterobactin in MeOH (ε_{316} = 9500 M^{-1} cm^{-1}).[79] An aliquot of the DMSO stock solution was diluted into MeOH for this analysis. Concentrations of L-EP and D-EP stock solutions were determined by quantifying Pt concentration using ICP-MS. The stock solution concentrations were 5–12 mM. To minimize multiple freeze–thaw cycles, the stock solutions were divided into 10 μL aliquots and stored at -20 °C. Aliquots were routinely analyzed by analytical HPLC to confirm the integrity of the samples.

Stability evaluation of L-Ent-Pt(IV)

A 0.5-μL aliquot of a DMSO stock solution of L-EP (5.2 mM determined by ICP-MS) was diluted in 250 μL of water, phosphate buffered saline (PBS), or modified M9 medium with varying thiamine concentrations. The resulting mixtures were divided into five 50-μL aliquots. The

aliquots were incubated at 30 °C with shaking at 150 rpm in the dark for 0, 2, 5, 10 and 20 h, respectively. Aliquots were flash frozen in liquid N_2 at each time point and stored at -80°C before HPLC analysis. HPLC samples were prepared by thawing each sample and centrifuging at 13,000 rpm for 10 min, and the resulting supernatants were analyzed by analytical HPLC (0–100 B% in 30 min, 1 mL/min, 0.005%TFA in solvents A and B). The percent of remaining L-EP at each time point was determined by integrating the peak area of L-EP (17.3 min) in each sample. The peak areas were normalized to that of the sample at t = 0 min. The correlation of peak area versus time was plotted, and the half-life ($t_{1/2}$) was estimated from each curve. Decomposition products were analyzed by LC/MS. This experiment was performed once for optimizing growth medium conditions.

Microbiology, microscopy, and cell culture methods

General materials. Lysogeny broth (LB; tryptone 10 g/L, yeast extract 5 g/L, NaCl 10 g/L), M9 minimal salts 5×, casamino acids, and agar were purchased from Becton Dickinson (BD). LB medium and Milli-Q water (18.2 MΩ·cm, 0.22-μm filter) used for bacterial cultures or for preparing working solutions of the tested compounds were sterilized in an autoclave. Modified M9 medium was sterilized by passage through a sterile 0.22-μm filter. Sterile polypropylene culture tubes and adhesive PCR film seals were purchased from VWR. Sterile polystyrene 96-well plates and 6-well plates used for culturing were purchased from Corning Incorporated. LIVE/DEAD BacLight Bacterial Viability Kits were purchased from Thermo Fisher (Invitrogen Molecular Probes). Agarose (PCR grade) for microscopy was purchased from Bio-Rad. Microscope slides and microscope cover glasses were purchased from VWR. Cisplatin (≥99.9% trace metals basis) and $Fe(acac)_3$ (≥99.9% trace metals basis) were purchased from Sigma-Aldrich.

Bacterial strains. Bacterial strains employed in this study are summarized in **Table 2.2.** Freezer stocks were prepared from single colonies in 25% glycerol/ LB medium.

Table 2.2. Bacterial strains employed in this study.[20, 57]

Strain	Relevant characteristics or genotype	Source / reference
E. coli K12 BW25113	Common lab strain, non-pathogenic	[57]
E. coli JW5086	*E. coli* K12 BW25113 Δ*fepA*	[57]
E. coli CFT073	Clinical isolate, UPEC	ATCC 700928
E. coli MSC 206	CFT073 Δ*fepA*::kan (KanR)	[20]
E. coli MSC 219	CFT073 Δ*iroN*::tetRA (TetR)	[20]
E. coli MSC 228	CFT073 Δ*fepC*::kan (KanR)	[20]
E. coli MSC 230	CFT073 Δ*fepDG*::kan (KanR)	[20]
E. coli MSC 216	CFT073 Δ*fepA*::kan Δ*iroN*::tetRA (KanR TetR)	[20]
E. coli W3104	Lysogenic for bacteriophage λ	Carolina Biological

General procedures for bacterial growth assays and microscopy. Growth of *E. coli* under Fe-deficient conditions was performed in a modified M9 medium (Na_2HPO_4 6.8 g/L, KH_2PO_4 3 g/L, NaCl 0.5 g/L, NH_4Cl 1 g/L, 0.4% glucose, 0.2% casein amino acids, 2 mM $MgSO_4$, 0.1 mM $CaCl_2$, 0.6 μg/mL thiamine). The Fe content of modified M9 medium was determined by ICP-MS to be 0.6–0.7 μM Fe. These Fe-deficient conditions cause *E. coli* to express siderophore biosynthesis and transport machinery, including genes for enterobactin biosynthesis and transport encoded by the enterobactin gene cluster as well as the *iroA* cluster for salmochelin biosynthesis and transport.

Working solutions of Ent-Pt(IV) and Pt(IV)-alkyne were prepared via dilutions in 10% DMSO/H_2O. Working solutions of cisplatin were freshly prepared by dissolving cisplatin in modified M9 medium before treatment. The Fe(III)-bound L-EP and D-EP complexes were prepared prior to all microbiology and imaging assays because the modified M9 medium contains insufficient Fe to fully complex the siderophore following addition to the culture. $Fe(acac)_3$ (25 mM stock in DMSO, concentration determined by ICP-MS) was used to prepare the Fe(III) complexes, which were formed by incubating 10 μL of L-EP and D-EP working solution with 0.9 μL of a 10× $Fe(acac)_3$ solution in 10% DMSO/H_2O for 5 min prior to addition to the culture. We note that L-EP and D-EP refer to the corresponding ferric complexes in the discussion of the biological assays. For all microbiology assays, the final cultures contained 1% v/v DMSO, except for cultures with cisplatin treatment which do not contain DMSO.

Overnight cultures of *E. coli* were prepared in 15 mL polypropylene tubes by inoculating 5 mL of medium with the appropriate freezer stock. The overnight cultures were incubated at 37 °C for 16–18 h in a tabletop incubator set at 150 rpm. Each overnight culture was diluted 1:100 into 5 mL of fresh medium at 37 °C with shaking at 150 rpm until OD_{600} reached 0.6 ± 0.1 (measured on a Beckmann Coulter DU800 spectrophotometer). Each culture was subsequently diluted in fresh medium to achieve an OD_{600} value of 0.005 (~5×10^6 CFU/mL). A 90 μL aliquot of the diluted culture was combined with a 10 μL aliquot of a 10× working solution of in a 96-well plate. The plate was sealed with an adhesive film (purchased from VWR) and incubated at 30 °C with shaking at 500 rpm for 20 h in the BioTek LogPhase 600 (LP600) microbiology reader (96-well plate format). Growth curves were recorded as OD_{600} values that were collected every hour in the LP600 microbiology reader. Growth assays of L-EP were performed using a two-fold dilution series spanning 0–60 μM, and assays of D-EP were performed using a ten-fold dilution

series spanning 0–10 μM. Each well condition was prepared in duplicate and at least five independent replicates using two synthetic batches of each conjugate and were performed on different days. The resulting mean OD_{600} values are reported, and the error bars are the standard deviation from the independent replicates. Statistical differences compared to untreated controls were calculated using two-tailed student *t* test assuming unequal variances.

Samples for microscopy were prepared by taking aliquots of *E. coli* culture at t = 11 h (mid-log phase). For samples that require only phase-contrast imaging, a 5 μL aliquot of each culture was pipetted on an agarose pad (1% w/w agarose/Milli-Q water) which was placed on a microscope slide. The sample was then covered with a glass coverslip. For LIVE/DEAD viability assays, a 90 μL aliquot of each bacterial culture was centrifuged at 3,000 rpm at 4 °C for 15 min. The resulting cell pellet was resuspended in 0.85% NaCl and the OD_{600} was adjusted to 0.2 using 0.85% NaCl. A 25 μL aliquot of each bacterial suspension was incubated with 25 μL of LIVE/DEAD dye mixture (48 μM SYTO9 and 240 μM propidium iodide) at 30 °C for 15 min in the dark, and 5 μL of the suspension was pipetted on an agarose pad which was placed on a microscope slide. The sample was then covered with a glass coverslip. For each type of microscopy experiment, each condition was repeated in at least three biological replicates using two different synthetic batches. Representative micrographs for each condition are shown in figures.

We selected 11 h as the time point to determine inhibitory effects and morphological changes because of the following considerations: (i) the 11 h time point is in the mid-log phase of bacterial growth as determined by growth curves; (ii) there is sufficient cell density to determine growth inhibitory effects and have sufficient cells to image; (iii) initial microbiology studies indicated that the stability of L-EP under these conditions was sufficient for our studies (*vide infra*).

We note that the OD_{600} values may be affected by bacterial filamentation with filamentation causing enhanced OD_{600} relative to a culture of the same cell density exhibiting normal morphology. Consequently, we believe the microscopy studies are more revealing in terms of L/D-EP activity.

Image analysis. The microscopy images were processed using the FIJI software (8-bit image type). For phase-contrast images, contrast enhancement was performed by setting saturated pixels as 0.1%. For fluorescence images, fluorescence background subtraction was performed using a rolling ball method with a radius of 150 pixels.

For cell counting, samples were prepared and imaged from at least three biological replicates. Images were acquired at three channels (trans-phase, Texas Red and GFP). 500–1000 cells were counted for each condition. Cell size was measured based on phase-contrast images. By adjusting threshold using available algorithms in FIJI, cells were identified as particles in the resulting binary images. The perimeter of each particle was measured by the software. We note that most of normal and elongated cells could be well-identified by algorithms, but the selection of many filamentous cells needed to be adjusted manually using the polygon tool. Cell viability was determined by counting red and green cells manually based on the corresponding fluorescence images.

Induction of lysogenic bacteria. The induction of lysogenic bacteria was performed based on a published procedure.[50] *E. coli* W3104 was inoculated in 5 mL of modified M9 medium and grown for 18 h at 37 °C. A 50 μL aliquot of the overnight culture was diluted in 5 mL of modified M9 medium, which was then incubated at 37 °C until the OD_{600} reached 0.5 (~7 h). Then, 0.5 μL aliquots of bacterial culture were added to 100 μL portions of modified M9 medium containing 0 (untreated), 7.5, 15 and 30 μM cisplatin in a 96-well plate. After incubation at 30 °C for 10 h, each

culture was diluted 1:10, 1:100, and 1:1000, and 10 μL of each diluted culture was spotted onto an LB agar plate on which a lawn of *E. coli* CFT073 had been freshly plated. After spotting, the plate was incubated at 37 °C for 12 h to allow plaque formation. To test the effect of L-EP, 0.5 μL aliquot of exponentially growing *E. coli* W3104 culture was then incubated in 100 μL of the modified M9 medium which contained 15 μM L-EP, 15 μM Ent and 1% DMSO, respectively.

The *E. coli* CFT073 lawn was prepared by inoculating 4 mL of molten top agar (0.5% LB agar) with 100 μL of an overnight culture of *E. coli* CFT073 grown in LB medium. Following gentle mixing, 3 mL of the inoculated molten top agar was layered atop a preheated (37 °C) LB agar plate and allowed to solidify.

Pt uptake by *E. coli*. *E. coli* CFT073 was inoculated in 5 mL of modified M9 medium and grown for 18 h at 37 °C. A 50 mL aliquot of the overnight culture was diluted in 5 mL of modified M9 medium, which was then incubated at 37 °C until the OD_{600} reached 0.6. A 4 mL portion of the culture was centrifuged at 3,500 rpm and 4°C for 10 min, and the resulting cell pellet was resuspended in 1 mL of fresh modified M9 medium. Then, to a 90 μL aliquot of the diluted culture, a 10 μL aliquot working solution of 150 μM L-EP, D-EP, or Pt(IV)-alkyne (in 10% DMSO/H_2O) was added. After incubation at 30 °C with shaking at 150 rpm for 30 min, cell pellets were harvested by centrifuging each culture at 3,500 rpm for 10 min. To measure the Pt content in the supernatant, 90 μL of each supernatant was diluted into 1.91 mL of 5% HNO_3 for ICP-MS analysis. To measure the cell-associated Pt content, the cell pellets were first washed with fresh modified M9 medium, and then washed with fresh modified M9 containing 2% w/w aqueous EDTA. The resulting cell pellets were suspended in 2 mL of 5% HNO_3 and digested for ICP-MS analysis. Mass of cell-associated Pt and mass of Pt in the supernatant of each sample were

calculated using Pt contents determined by ICP-MS. Cell-associated Pt% was determined according to equation 1.

$$\text{Cell-associated Pt\%} = \frac{\text{mass of cell-associated Pt (μg)}}{\text{mass of cell-associated Pt (μg) + mass of Pt in the supernatant (μg)}} \quad \text{(eq 1)}$$

Pt uptake by HEK293T cells. Materials for tissue culture were kindly provided by the Shoulders lab at MIT. HEK293T cells were purchased from ATCC. The DMEM medium was purchased from Corning Incorporated. Penicillin and streptomycin were purchased from Corning Incorporated.

HEK293T cells (passages 12–18) were plated at a density of 750,000 cells per well in a 6-well plate (2.5 mL/well) in DMEM supplemented with 1% penicillin/streptomycin and incubated at 37 °C and 5% CO_2 for 24 h. Working solutions of L-EP and D-EP (6 μM) were prepared in 10% DMSO/PBS (PBS purchased from Millipore Sigma). Working solutions of cisplatin were freshly prepared by dissolving cisplatin in PBS (6 μM) before treatment. Each working solution (0.5 mL) was added to each well of cell culture to give the final treatment concentration as 1 μM. Cells were treated for 6 h at 37°C and 5% CO_2, transferred to a 15 mL conical tube and centrifuged at 500 rcf for 5 min. To measure the Pt content in the supernatant, 200 μL of each supernatant was diluted into 1.8 mL of 5% HNO_3 for ICP-MS analysis. To measure the cell-associated Pt content, cell pellets were washed with 2 mL of PBS three times, and the resulting cell pellets were suspended in 2 mL of 5%HNO_3 and digested for ICP-MS analysis. Mass of cell-associated Pt and mass of Pt in the supernatant of each sample were calculated using Pt contents determined by ICP-MS. Cell-associated Pt% were determined by ICP-MS as described above (eq 1).

2.7 Supporting Discussion

We examined the stability of L-EP in a modified M9 growth medium supplemented with 16.5 μg/mL of thiamine that we employed in prior studies of Ent–antibiotic conjugates.[20, 29, 44] Analytical HPLC revealed that apo L-EP decomposed in this modified M9 medium with a $t_{1/2} < 2$ h at 30 °C (**Figures 2.24A** and **2.25A**). The HPLC chromatograms showed loss of the L-EP peak at 17.3 min and formation of a new peak at 17.6 min. LC/MS analysis of the new peak afforded a *m/z* of 1012.3 for the major ion species, which corresponds to the Ent-containing axial ligand (theoretical $[M+H]^+ = 1012.3$, **Figure 2.25C** compound **d**). This result indicated that L-EP readily decomposed with the release of its two carboxylate axial ligands in the modified M9 medium. Other decomposition peaks included hydrolysis products of the Ent-containing axial ligand where (i) the Ent trilactone moiety was linearized by one ester hydrolysis event (compound **b**) and (ii) further degraded to the linear dimer form by a second ester hydrolysis event (compound **a**). This analysis prompted us to further examine the stability of L-EP. Previous studies of Pt(IV) complexes demonstrated that release of the axial ligand of a Pt(IV) center can result from hydrolysis or reduction.[27, 30, 33] Moreover, the Ent trilactone is prone to hydrolysis.[80] Consequently, we considered these three degradation pathways in our subsequent experiments.

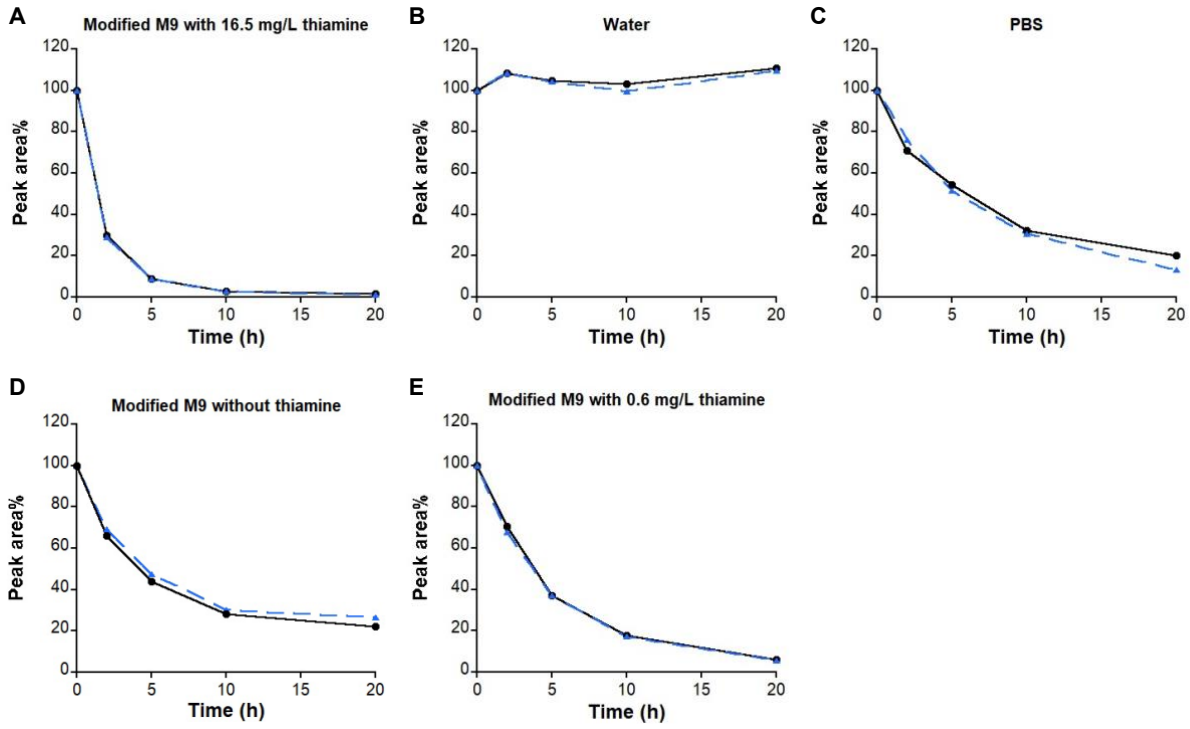

Figure 2.24. Stability of L-EP in **(A)** modified M9 medium with 16.5 μg/mL thiamine, **(B)** water, **(C)** PBS, modified M9 medium **(D)** without thiamine and **(E)** with 0.6 μg/mL thiamine at 30 °C. Stability was determined by integrating the peak area of L-EP in each sample and normalizing it to that of the sample at t = 0 h. Decomposition products were analyzed by LC/MS; black line: 220 nm; blue dash line: 316 nm.

Stability in water and PBS. We first tested the stability of L-EP towards hydrolysis by incubating it in water and found that the molecule is stable in water with negligible decomposition observed during the 20-h incubation at 30 °C (**Figure 2.24B**). We then evaluated the stability of L-EP in the presence of phosphate salts (Na_2HPO_4 and KH_2PO_4), which are components of the modified M9 medium, by incubating it in PBS and found a $t_{1/2}$ ~ 5 h (**Figure 2.24C**). Unlike the decomposition pattern we observed for L-EP incubated in the modified M9 medium (**Figure 2.25**), HPLC and LC/MS revealed that in PBS the Pt(IV) moiety retained its axial ligands over the 20-h incubation, and that the predominant decomposition pathway was the hydrolysis of the Ent moiety (**Figure 2.26A**). We also evaluated the stability of Ent in PBS, which showed a similar hydrolysis pattern (**Figures 2.26B** and **2.26C**).

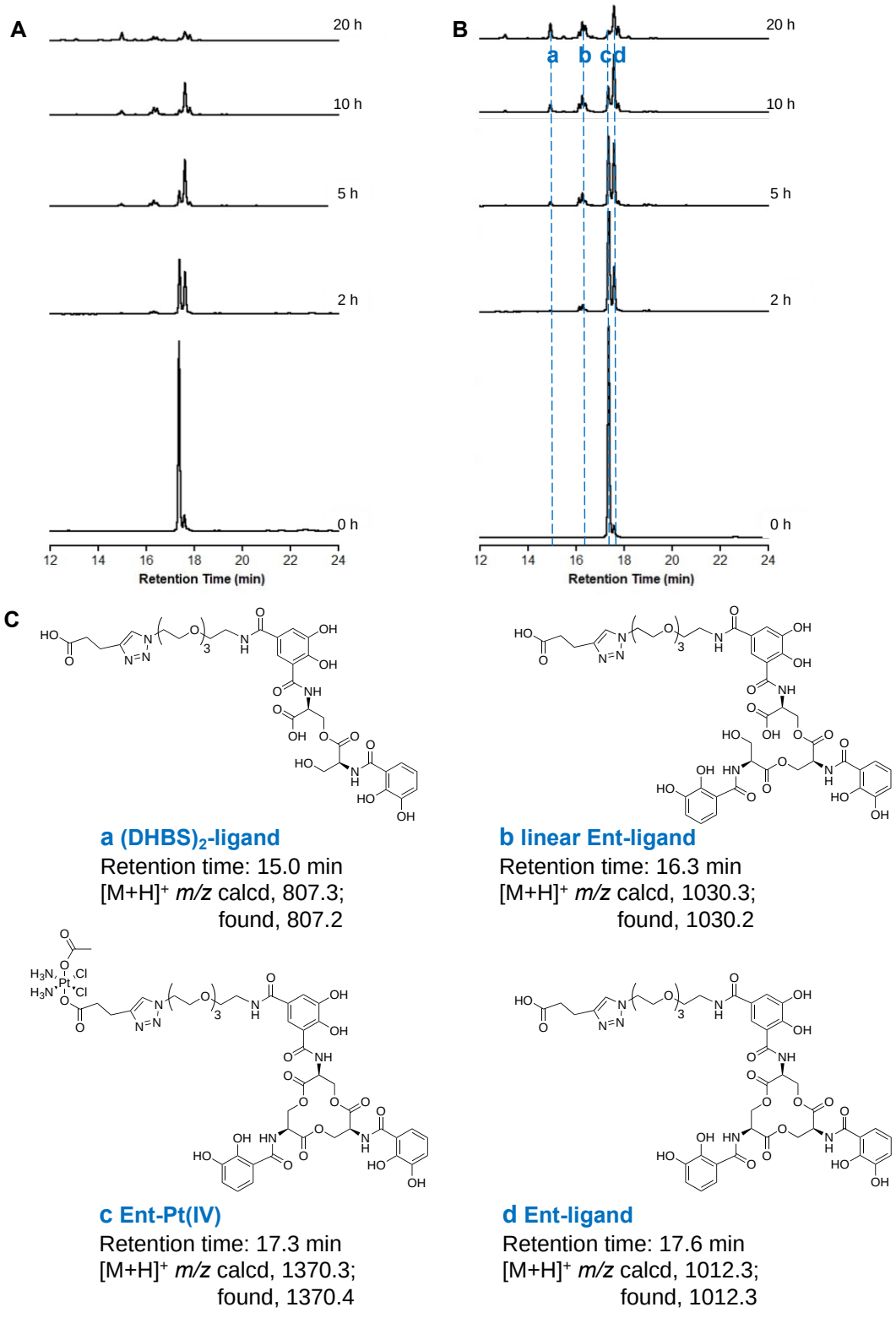

Figure 2.25. Analytical HPLC traces (220 nm absorption) of L-EP decomposition in the modified M9 medium with **(A)** 16.5 μg/mL thiamine and **(B)** 0.6 μg/mL thiamine at 30 °C. **(C)** Compounds detected by LC/MS. DHBS, 2,3-dihydroxybenzoyl serine.

Further analysis of L-EP stability in the modified M9 medium. We then investigated the effect of glucose and casamino acids (medium components) by incubating L-EP in modified M9 medium without added thiamine and found a $t_{1/2} \sim 5$ h (**Figure 2.24D**). Under these conditions, the decomposition pathway was similar to that in PBS; the Pt(IV) moiety retained its axial ligands and Ent hydrolysis occurred (HPLC not shown). Consequently, we speculated that thiamine content of the medium could be problematic for L-EP stability. Thiamine is a cofactor involved in redox chemistry, and we further speculated that the instability of L-EP in the modified M9 medium resulted from redox chemistry and reduction of the Pt(IV) center, which causes release of the two axial ligands.[81]

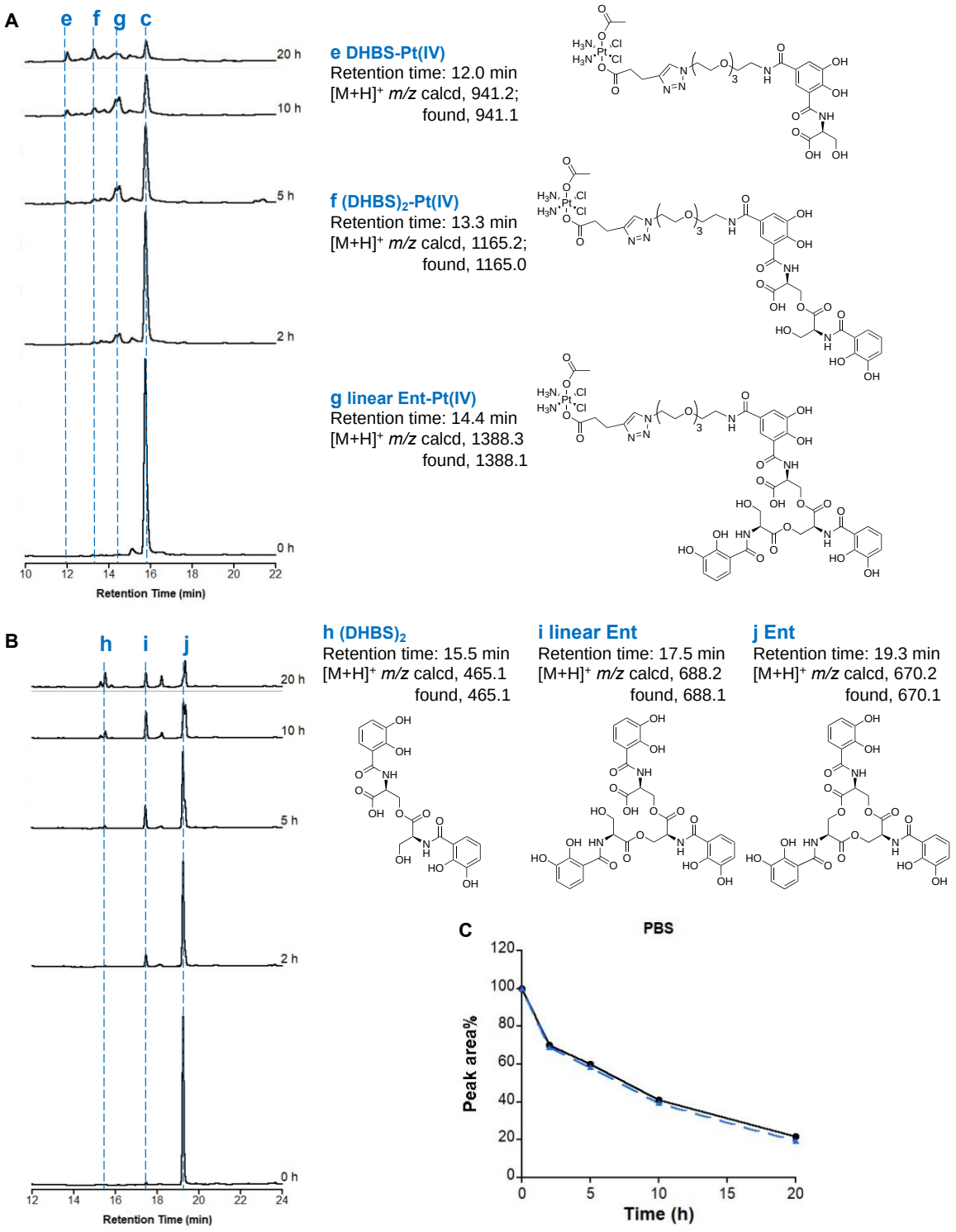

Figure 2.26. Analytical HPLC traces (220 nm absorption) and LC/MS analysis of **(A)** L-EP and **(B)** Ent decomposition in PBS at 30 °C. **(C)** Stability of Ent in PBS at 30 °C. Stability was determined by integrating the peak area of Ent in each sample and normalizing it to that of the sample at t = 0 h; black line: 220 nm; blue dash line: 316 nm. DHBS, 2,3-dihydroxybenzoyl serine. Note: the retention time of L-EP **c** was shifted to 15.8 min.

Because thiamine is required for the growth of *E. coli* CFT073 mutants employed in this study, we decreased the thiamine concentration in the modified M9 medium to 0.6 μg/mL and found that L-EP showed enhanced stability with a $t_{1/2}$ ~ 5 h at 30 °C (**Figure 2.24D**). Although *E. coli* growth was generally slower with this reduced thiamine level, the majority of strains grew well and reached mid-log phase after ~11 h of growth at 30 °C (**Appendix A.3**). Initial microbiology studies indicated that the stability of L-EP under these conditions was sufficient in this medium for our studies. In particular, following 11-h treatment with L-EP, siderophore receptor/transporter-dependent growth inhibitory effects and morphological changes were observed among the *E. coli* strains used in this study. Therefore, we moved forward using modified M9 medium with 0.6 μg/mL of thiamine and determining bacterial growth and morphology after 11-h treatment for all microbiology assays presented in this work.

Potential uptake of L-EP decomposition products. We note that bacterial uptake of L-EP decomposition products identified in the stability study may occur during the assays presented in this work. In particular, uptake of the released axial Ent ligand (**d** in **Figure 2.25C**) and its hydrolysis products (**a** and **b** in **Figure 2.25C**) would result in Fe(III) uptake in the absence of Pt uptake and potentially contribute to enhanced bacterial fitness. Uptake of L-EP hydrolysis products that contain the Pt(IV) cargo and a hydrolyzed Ent moiety (**e**, **f**, **g** in **Figure 2.26A**) may also occur.

Although we did not perform the stability test on D-EP, we expect similar results for its stability in PBS and modified media containing different levels of thiamine.

2.8 Acknowledgments

This work was supported by the 2018 Professor Amar G. Bose Research Grant. NMR and MS instrumentation is housed by the MIT DCIF. The ICP-MS instrument at MIT is maintained by

the MIT CEHS (NIH P30-ES002109). Instrumentation for phase-contrast and fluorescence microscopy instrumentation is housed by the W. M. Keck Microscopy Facility at Whitehead Institute. We thank Phoom Chairatana, Timothy Johnstone and Artur Sargun for technical assistance during the early stage of this project. We thank Jessica Patrick in the Shoulders lab at MIT for assistance with tissue culture.

2.9 References

1. Brown, E. D.; Wright, G. D., Antibacterial drug discovery in the resistance era. *Nature* **2016,** *529*, 336-343.

2. Blaser, M., Stop the killing of beneficial bacteria. *Nature* **2011,** *476*, 393-394.

3. Cho, I.; Blaser, M. J., The human microbiome: at the interface of health and disease. *Nat. Rev. Genet.* **2012,** *13*, 260-270.

4. Farha, M. A.; Brown, E. D., Drug repurposing for antimicrobial discovery. *Nat. Microbiol.* **2019,** *4*, 565-577.

5. Czech, T.; Lalani, R.; Oyewumi, M. O., Delivery systems as vital tools in drug repurposing. *AAPS PharmSciTech.* **2019,** *20*, 116.

6. Hider, R. C.; Kong, X., Chemistry and biology of siderophores. *Nat. Prod. Rep.* **2010,** *27*, 637-657.

7. Pantopoulos, K.; Porwal, S. K.; Tartakoff, A.; Devireddy, L., Mechanisms of mammalian iron homeostasis. *Biochemistry* **2012,** *51*, 5705-5724.

8. Braun, V.; Hantke, K., Recent insights into iron import by bacteria. *Curr. Opin. Chem. Biol.* **2011,** *15*, 328-334.

9. Hood, M. I.; Skaar, E. P., Nutritional immunity: transition metals at the pathogen-host interface. *Nat. Rev. Microbiol.* **2012,** *10*, 525-537.

10. Weinberg, E. D., Nutritional immunity. Host's attempt to withold iron from microbial invaders. *J. Am. Med. Assoc.* **1975,** *231*, 39-41.

11. McPherson, C. J.; Aschenbrenner, L. M.; Lacey, B. M.; Fahnoe, K. C.; Lemmon, M. M.; Finegan, S. M.; Tadakamalla, B.; O'Donnell, J. P.; Mueller, J. P.; Tomaras, A. P., Clinically relevant Gram-negative resistance mechanisms have no effect on the efficacy of MC-1, a novel siderophore-conjugated monocarbam. *Antimicrob. Agents Chemother* **2012,** *56*, 6334-6342.

12. Braun, V.; Pramanik, A.; Gwinner, T.; Köberle, M.; Bohn, E., Sideromycins: tools and antibiotics. *Biometals* **2009,** *22*, 3-13.

13. Nolan, E. M.; Fischbach, M. A.; Koglin, A.; Walsh, C. T., Biosynthetic tailoring of microcin E492m: post-translational modification affords an antibacterial siderophore–peptide conjugate. *J. Am. Chem. Soc.* **2007,** *129*, 14336-14347.

14. Sassone-Corsi, M.; Nuccio, S.-P.; Liu, H.; Hernandez, D.; Vu, C. T.; Takahashi, A. A.; Edwards, R. A.; Raffatellu, M., Microcins mediate competition among Enterobacteriaceae in the inflamed gut. *Nature* **2016,** *540*, 280-283.

15. Vassiliadis, G.; Destoumieux-Garzón, D.; Lombard, C.; Rebuffat, S.; Peduzzi, J., Isolation and characterization of two members of the siderophore-microcin family, microcins M and H47. *Antimicrob. Agents Chemother.* **2010,** *54*, 288-297.

16. Palmer, J. D.; Mortzfeld, B. M.; Piattelli, E.; Silby, M. W.; McCormick, B. A.; Bucci, V., Microcin H47: a class IIb microcin with potent activity against multidrug resistant *Enterobacteriaceae*. *ACS Infect. Dis.* **2020,** *6*, 672-679.

17. Roosenberg II, J. M.; Lin, Y.-M.; Lu, Y.; Miller, M. J., Studies and syntheses of siderophores, microbial iron chelators, and analogs as potential drug delivery agents. *Curr. Med. Chem.* **2000,** *7*, 159-197.

18. Lin, Y. M.; Ghosh, M.; Miller, P. A.; Möllmann, U.; Miller, M. J., Synthetic sideromycins (skepticism and optimism): selective generation of either broad or narrow spectrum Gram-negative antibiotics. *Biometals* **2019,** *32*, 425-451.

19. Zheng, T.; Nolan, E. M., Enterobactin-mediated delivery of *β*-lactam antibiotics enhances antibacterial activity against pathogenic *Escherichia coli*. *J. Am. Chem. Soc.* **2014,** *136*, 9677-9691.

20. Neumann, W.; Sassone-Corsi, M.; Raffatellu, M.; Nolan, E. M., Esterase-catalyzed siderophore hydrolysis activates an enterobactin-ciprofloxacin conjugate and confers targeted antibacterial activity. *J. Am. Chem. Soc.* **2018,** *140*, 5193-5201.

21. Sargun, A.; Johnstone, T. C.; Zhi, H.; Raffatellu, M.; Nolan, E. M., Enterobactin- and salmochelin-β-lactam conjugates induce cell morphologies consistent with inhibition of penicillin-binding proteins in uropathogenic *Escherichia coli* CFT073. *Chem. Sci.* **2021,** *12*, 4041-4056.

22. Sargun, A.; Sassone-Corsi, M.; Zheng, T.; Raffatellu, M.; Nolan, E. M., Conjugation to enterobactin and salmochelin S4 enhances the antimicrobial activity and selectivity of *β*-lactam antibiotics against nontyphoidal *Salmonella*. *ACS Infect. Dis.* **2021,** *7*, 1248-1259.

23. Raymond, K. N.; Dertz, E. A.; Kim, S. S., Enterobactin: an archetype for microbial iron transport. *Proc. Natl. Acad. Sci. U. S. A.* **2003,** *100*, 3584-3588.

24. Lewis, K., Platforms for antibiotic discovery. *Nat. Rev. Drug Discov.* **2013,** *12*, 371-387.

25. Rosenberg, B.; Van Camp, L.; Krigas, T., Inhibition of cell division in *Escherichia coli* by electrolysis products from a platinum electrode. *Nature* **1965,** *205*, 698-699.

26. Rosenberg, B.; Van Camp, L.; Grimley, E. B.; Thomson, A. J., The inhibition of growth or cell division in *Escherichia coli* by different ionic species of platinum(IV) complexes. *J. Biol. Chem.* **1967,** *242*, 1347-1352.

27. Johnstone, T. C.; Suntharalingam, K.; Lippard, S. J., The next generation of platinum drugs: targeted Pt(II) agents, nanoparticle delivery, and Pt(IV) prodrugs. *Chem. Rev.* **2016,** *116*, 3436-3486.

28. Dhar, S.; Kolishetti, N.; Lippard, S. J.; Farokhzad, O. C., Targeted delivery of a cisplatin prodrug for safer and more effective prostate cancer therapy in vivo. *Proc. Natl. Acad. Sci. U.S.A.* **2011,** *108*, 1850-1855.

29. Chairatana, P.; Zheng, T.; Nolan, E. M., Targeting virulence: salmochelin modification tunes the antibacterial activity spectrum of β-lactams for pathogen-selective killing of *Escherichia coli*. *Chem. Sci.* **2015,** *6*, 4458-4471.

30. Wilson, J. J.; Lippard, S. J., Synthetic methods for the preparation of platinum anticancer complexes. *Chem. Rev.* **2014,** *114*, 4470-4495.

31. Hambley, T. W.; Battle, A. R.; Deacon, G. B.; Lawrenz, E. T.; Fallon, G. D.; Gatehouse, B. M.; Webster, L. K.; Rainone, S., Modifying the properties of platinum(IV) complexes in order to increase biological effectiveness. *J. Inorg. Biochem.* **1999,** *77*, 3-12.

32. Reithofer, M. R.; Bytzek, A. K.; Valiahdi, S. M.; Kowol, C. R.; Groessl, M.; Hartinger, C. G.; Jakupec, M. A.; Galanski, M.; Keppler, B. K., Tuning of lipophilicity and cytotoxic potency by structural variation of anticancer platinum (IV) complexes. *J. Inorg. Biochem.* **2011,** *105*, 46-51.

33. Wexselblatt, E.; Yavin, E.; Gibson, D., Platinum(IV) prodrugs with haloacetato ligands in the axial positions can undergo hydrolysis under biologically relevant conditions. *Angew. Chem. Int. Ed.* **2013,** *52*, 6059-6062.

34. Chin, C. F.; Tian, Q.; Setyawati, M. I.; Fang, W.; Tan, E. S. Q.; Leong, D. T.; Ang, W. H., Tuning the activity of platinum(IV) anticancer complexes through asymmetric acylation. *J. Med. Chem.* **2012,** *55*, 7571-7582.

35. Wexselblatt, E.; Gibson, D., What do we know about the reduction of Pt(IV) pro-drugs? *J. Inorg. Biochem.* **2012,** *117*, 220-229.

36. Ong, J. X.; Yap, S. Q.; Wong, D. Y. Q.; Chin, C. F.; Ang, W. H., Platinum(IV) carboxylate prodrug complexes as versatile platforms for targeted chemotherapy. *Chimia* **2015,** *69*, 100-103.

37. Chen, S.; Yao, H.; Zhou, Q.; Tse, M. K.; Gunawan, Y. F.; Zhu, G., Stability, reduction, and cytotoxicity of platinum(IV) anticancer prodrugs bearing carbamate axial ligands: comparison with their carboxylate analogues. *Inorg. Chem.* **2020,** *59*, 11676-11687.

38. Hall, M. D.; Hambley, T. W., Platinum(IV) antitumour compounds: their bioinorganic chemistry. *Coord. Chem. Rev.* **2002,** *232*, 49-67.

39. Zhang, J. Z.; Bonnitcha, P.; Wexselblatt, E.; Klein, A. V.; Najajreh, Y.; Gibson, D.; Hambley, T. W., Facile preparation of mono-, di- and mixed-carboxylato platinum(IV) complexes for versatile anticancer prodrug design. *Chemistry* **2013,** *19*, 1672-1676.

40. Zheng, T.; Bullock, J. L.; Nolan, E. M., Siderophore-mediated cargo delivery to the cytoplasm of *Escherichia coli* and *Pseudomonas aeruginosa*: syntheses of monofunctionalized

enterobactin scaffolds and evaluation of enterobactin–cargo conjugate uptake. *J. Am. Chem. Soc.* **2012,** *134*, 18388-18400.

41. Kubas, G.; Monzyk, B.; Crumbliss, A., Tetrakis(acetonitrile) copper(I) hexafluorophosphate. In *Inorganic Syntheses*; John Wiley & Sons, Inc., **1979**, Vol. *19*. 90-92.

42. Hall, M. D.; Telma, K. A.; Chang, K.-E.; Lee, T. D.; Madigan, J. P.; Lloyd, J. R.; Goldlust, I. S.; Hoeschele, J. D.; Gottesman, M. M., Say no to DMSO: dimethylsulfoxide inactivates cisplatin, carboplatin, and other platinum complexes. *Cancer Res.* **2014,** *74*, 3913-3922.

43. Chan, T. R.; Hilgraf, R.; Sharpless, K. B.; Fokin, V. V., Polytriazoles as copper(I)-stabilizing ligands in catalysis. *Org. Lett.* **2004,** *6*, 2853-2855.

44. Blango, M. G.; Ott, E. M.; Erman, A.; Veranic, P.; Mulvey, M. A., Forced resurgence and targeting of intracellular uropathogenic *Escherichia coli* reservoirs. *PLoS One* **2014,** *9*, e93327.

45. Fischbach, M. A.; Lin, H.; Liu, D. R.; Walsh, C. T., *In vitro* characterization of IroB, a pathogen-associated *C*-glycosyltransferase. *Proc. Natl. Acad. Sci. U.S.A.* **2005,** *102*, 571-576.

46. Fischbach, M. A.; Lin, H.; Liu, D. R.; Walsh, C. T., How pathogenic bacteria evade mammalian sabotage in the battle for iron. *Nat. Chem. Biol.* **2006,** *2*, 132-138.

47. Hantke, K.; Nicholson, G.; Rabsch, W.; Winkelmann, G., Salmochelins, siderophores of *Salmonella enterica* and uropathogenic *Escherichia coli* strains, are recognized by the outer membrane receptor IroN. *Proc. Natl. Acad. Sci. U.S.A.* **2003,** *100*, 3677-3682.

48. Lin, H.; Fischbach, M. A.; Liu, D. R.; Walsh, C. T., In vitro characterization of salmochelin and enterobactin trilactone hydrolases IroD, IroE, and Fes. *J. Am. Chem. Soc.* **2005,** *127*, 11075-11084.

49. Léveillé, S.; Caza, M.; Johnson, J. R.; Clabots, C.; Sabri, M.; Dozois, C. M., Iha from an *Escherichia coli* urinary tract infection outbreak clonal group A strain is expressed in vivo in the mouse urinary tract and functions as a catecholate siderophore receptor. *Infect. Immun.* **2006,** *74*, 3427-3436.

50. Johnstone, T. C.; Alexander, S. M.; Lin, W.; Lippard, S. J., Effects of monofunctional platinum agents on bacterial growth: a retrospective study. *J. Am. Chem. Soc.* **2014,** *136*, 116-118.

51. Jamieson, E. R.; Lippard, S. J., Structure, recognition, and processing of cisplatin−DNA adducts. *Chem. Rev.* **1999,** *99*, 2467-2498.

52. Witkin, E. M., The radiation sensitivity of *Escherichia coli* B: a hypothesis relating filament formation and prophage induction. *Proc. Natl. Acad. Sci. U. S. A.* **1967,** *57*, 1275-1279.

53. Adler, H. I.; Hardigree, A. A., Postirradiation growth, division, and recovery in bacteria. *Radiat. Res.* **1965,** *25*, 92-102.

54. Rosenkranz, H. S.; Garro, A. J.; Levy, J. A.; Carr, H. S., Studies with hydroxyurea I. The reversible inhibition of bacterial DNA synthesis and the effect of hydroxyurea on the bactericidal action of streptomycin. *Biochim. Biophys. Acta* **1966,** *114*, 501-515.

55. Lippert, B., *Cisplatin: chemistry and biochemistry of a leading anticancer drug*. John Wiley & Sons, 1999. DOI:10.1002/9783906390420.

56. Reslova, S., The induction of lysogenic strains of *Escherichia coli* by *cis*-dichlorodiammineplatinum (II). *Chem.-Biol. Interact.* **1971,** *4*, 66-70.

57. Baba, T.; Ara, T.; Hasegawa, M.; Takai, Y.; Okumura, Y.; Baba, M.; Datsenko, K. A.; Tomita, M.; Wanner, B. L.; Mori, H., Construction of *Escherichia coli* K-12 in-frame, single-gene knockout mutants: the Keio collection. *Mol. Syst. Biol.* **2006,** *2*, 2006.0008.

58. Zobell, C. E.; Cobet, A. B., Filament formation by *Escherichia coli* at increased hydrostatic pressures. *J. Bacteriol.* **1964,** *87*, 710-719.

59. *LIVE/DEAD BacLight Bacterial Viability Kit Protocol*. https://www.thermofisher.com/us/en/home/references/protocols/cell-and-tissue-analysis/protocols/live-dead-baclight-bacterial-viability-protocol.html.

60. Hagan, E. C.; Mobley, H. L. T., Uropathogenic *Escherichia coli* outer membrane antigens expressed during urinary tract infection. *Infect. Immun.* **2007,** *75*, 3941-3949.

61. Puig, S.; Ramos-Alonso, L.; Romero, A. M.; Martínez-Pastor, M. T., The elemental role of iron in DNA synthesis and repair. *Metallomics* **2017,** *9*, 1483-1500.

62. Abergel, R. J.; Zawadzka, A. M.; Hoette, T. M.; Raymond, K. N., Enzymatic hydrolysis of trilactone siderophores: where chiral recognition occurs in enterobactin and bacillibactin iron transport. *J. Am. Chem. Soc.* **2009,** *131*, 12682-12692.

63. Fadzen, C. M.; Wolfe, J. M.; Zhou, W.; Cho, C.-F.; von Spreckelsen, N.; Hutchinson, K. T.; Lee, Y.-C.; Chiocca, E. A.; Lawler, S. E.; Yilmaz, O. H.; Lippard, S. J.; Pentelute, B. L., A platinum(IV) prodrug—perfluoroaryl macrocyclic peptide conjugate enhances platinum uptake in the brain. *J. Med. Chem.* **2020,** *63*, 6741-6747.

64. Gabano, E.; Ravera, M.; Colangelo, D.; Osella, D., Bioinorganic chemistry: the study of the fate of platinum-based antitumour drugs. *Curr. Chem. Biol.* **2007,** *1*, 278-289.

65. Alessio, M.; Zanellato, I.; Bonarrigo, I.; Gabano, E.; Ravera, M.; Osella, D., Antiproliferative activity of Pt(IV)-bis(carboxylato) conjugates on malignant pleural mesothelioma cells. *J. Inorg. Biochem.* **2013,** *129*, 52-57.

66. Ravera, M.; Gabano, E.; Zanellato, I.; Bonarrigo, I.; Alessio, M.; Arnesano, F.; Galliani, A.; Natile, G.; Osella, D., Cellular trafficking, accumulation and DNA platination of a series of cisplatin-based dicarboxylato Pt(IV) prodrugs. *J. Inorg. Biochem.* **2015,** *150*, 1-8.

67. Raveendran, R.; Braude, J. P.; Wexselblatt, E.; Novohradsky, V.; Stuchlikova, O.; Brabec, V.; Gandin, V.; Gibson, D., Pt(IV) derivatives of cisplatin and oxaliplatin with phenylbutyrate axial ligands are potent cytotoxic agents that act by several mechanisms of action. *Chem. Sci.* **2016,** *7*, 2381-2391.

68. Lippard, S. J., New chemistry of an old molecule: *cis*-[$Pt(NH_3)_2Cl_2$]. *Science* **1982,** *218*, 1075-1082.

69. Takahara, P. M.; Rosenzweig, A. C.; Frederick, C. A.; Lippard, S. J., Crystal structure of double-stranded DNA containing the major adduct of the anticancer drug cisplatin. *Nature* **1995,** *377*, 649-652.

70. Takahara, P. M.; Frederick, C. A.; Lippard, S. J., Crystal structure of the anticancer drug cisplatin bound to duplex DNA. *J. Am. Chem. Soc.* **1996,** *118*, 12309-12321.

71. Tsionou, M. I.; Knapp, C. E.; Foley, C. A.; Munteanu, C. R.; Cakebread, A.; Imberti, C.; Eykyn, T. R.; Young, J. D.; Paterson, B. M.; Blower, P. J.; Ma, M. T., Comparison of macrocyclic and acyclic chelators for gallium-68 radiolabelling. *RSC Adv.* **2017,** *7*, 49586-49599.

72. Emery, T.; Hoffer, P. B., Siderophore-mediated mechanism of gallium uptake demonstrated in the microorganism *Ustilago sphaerogena*. *J. Nucl. Med.* **1980,** *21*, 935-939.

73. Pandey, A.; Savino, C.; Ahn, S. H.; Yang, Z.; Van Lanen, S. G.; Boros, E., Theranostic gallium siderophore ciprofloxacin conjugate with broad spectrum antibiotic potency. *J. Med. Chem.* **2019,** *62*, 9947-9960.

74. Ecker, D. J.; Matzanke, B. F.; Raymond, K. N., Recognition and transport of ferric enterobactin in *Escherichia coli*. *J. Bacteriol.* **1986,** *167*, 666-673.

75. Boyd, N. K.; Teng, C.; Frei, C. R., Brief overview of approaches and challenges in new antibiotic development: a focus on drug repurposing. *Front. Cell. Infect. Microbiol.* **2021,** *11*, 684515.

76. Miller, M. J.; Walz, A. J.; Zhu, H.; Wu, C.; Moraski, G.; Möllmann, U.; Tristani, E. M.; Crumbliss, A. L.; Ferdig, M. T.; Checkley, L.; Edwards, R. L.; Boshoff, H. I., Design, synthesis, and study of a mycobactin−artemisinin conjugate that has selective and potent activity against tuberculosis and malaria. *J. Am. Chem. Soc.* **2011,** *133*, 2076-2079.

77. Ramirez, R. J.; Karamanukyan, L.; Ortiz, S.; Gutierrez, C. G., A much improved synthesis of the siderophore enterobactin. *Tetrahedron lett.* **1997,** *38*, 749-752.

78. Ravera, M.; Gabano, E.; Tinello, S.; Zanellato, I.; Osella, D., May glutamine addiction drive the delivery of antitumor cisplatin-based Pt(IV) prodrugs? *J. Inorg. Biochem.* **2017,** *167*, 27-35.

79. Scarrow, R. C.; Ecker, D. J.; Ng, C.; Liu, S.; Raymond, K. N., Iron(III) coordination chemistry of linear dihydroxyserine compounds derived from enterobactin. *Inorg. Chem.* **1991,** *30*, 900-906.

80. Zheng, T.; Nolan, E. M., Evaluation of (acyloxy)alkyl ester linkers for antibiotic release from siderophore-antibiotic conjugates. *Bioorg. Med. Chem. Lett.* **2015,** *25*, 4987-4991.

81. Frank, R. A. W.; Leeper, F. J.; Luisi, B. F., Structure, mechanism and catalytic duality of thiamine-dependent enzymes. *Cell. Mol. Life Sci.* **2007,** *64*, 892-905.

Chapter 3.

Investigation of Siderophore–Platinum(IV) Conjugates Reveals Differing Antibacterial Activity and DNA Damage Depending on the Platinum Cargo

This chapter is based on submitted work under the same title (Guo, C., Wang, K.A., Nolan, E. M. *submitted for publication*, May 31st, 2023).

3.1 Contributions: E.M.N. and C.G. conceived of the presented idea. C.G. conducted the experiments and performed data analysis. K.A.W. constructed the reporter strain *E. coli* JW0334 *pSulAp_lacZ*. C.G. wrote the manuscript with the support from E.M.N. and K.A.W.

3.2 Abstract

The growing threat of bacterial infections coupled with the dwindling arsenal of effective antibiotics has heightened the urgency for innovative strategies to combat bacterial pathogens, particularly Gram-negative strains, which pose a significant challenge due to their outer membrane permeability barrier. In this study, we repurpose clinically approved anticancer agents as targeted antibacterials. We report two new siderophore–platinum(IV) conjugates, both of which consist of an oxaliplatin-based Pt(IV) prodrug (oxPt(IV)) conjugated to enterobactin (Ent), a triscatecholate siderophore employed by Enterobacteriaceae for iron acquisition. We demonstrate that the Ent transport machinery delivers L/D-Ent-oxPt(IV) (L/D-EOP) into the *Escherichia coli* cytoplasm, where the Pt(IV) prodrug is presumably activated by reductive elimination, releasing the oxaliplatin warhead. Both L/D-EOP induce filamentation in *E. coli*, except for mutants defective in Ent transport machinery. D-EOP exhibits enhanced potency, attributed to the inability of Ent esterases to hydrolyze D-Ent. L/D-EOP treatment leads to enhanced Pt uptake by bacterial cells but reduced Pt uptake by human cells compared to oxaliplatin. To further elucidate the antibacterial activity of Ent–Pt(IV) conjugates, we probed DNA damage caused by L/D-EOP and the previously reported cisplatin-based conjugates L/D-EP. A comparative analysis of these four conjugates reveals a correlation between antibacterial activity and the ability to induce DNA damage. This work expands the scope of Pt cargos targeted to the cytoplasm of Gram-negative bacteria via Ent

conjugation, provides insight into the cellular consequences of Ent–Pt(IV) in *E. coli*, and furthers our understanding of the potential of Pt-based therapeutics for antibacterial applications.

3.3 Introduction

Infectious diseases are among the top ten causes of death globally.[1] Recently, increased attention has been given to developing new antibiotics against bacterial pathogens, especially Gram-negative species, which are intrinsically difficult to treat due to the presence of an outer membrane (OM).[2] To overcome the permeability barrier of the OM, research efforts focused on understanding OM structure and function have revealed innovative strategies for drug delivery.[3] For example, characterization and exploitation of uptake systems that are critical for the establishment and progression of infection have provided new approaches to antibiotic development.[3]

The siderophore-based "Trojan-horse" strategy involves leveraging bacterial acquisition pathways for the essential nutrient iron (Fe) to deliver drugs into bacterial cells. Bacteria utilize siderophores, small molecules that chelate Fe(III), to obtain this essential transition metal nutrient under Fe-limiting conditions, such as during infection.[4-6] The molecular recognition of siderophores by their cognate membrane-associated uptake machinery can be hijacked for efficient and targeted drug delivery, which has been demonstrated by the natural occurrence of sideromycins and class IIb microcins, as well as synthetic siderophore–antibiotic conjugates (SACs).[7-14] We have designed SACs using enterobactin (Ent), one of the best-studied bacterial siderophores with a remarkably high affinity for Fe ($K_a \sim 10^{49}$ M^{-1}),[15] as the delivery vector.[16] Previously, we conjugated Ent with β-lactam antibiotics (Ent-β-lactams) and a fluoroquinolone

(Ent-ciprofloxacin) and demonstrated that Ent can efficiently deliver drug cargos into the periplasm and cytoplasm of Gram-negative bacteria expressing the Ent transport machinery.[17-20]

Beyond traditional antibiotics, we recently evaluated the Ent-based SAC approach for drug repurposing.[21] We focused on the FDA-approved Pt-based anticancer agent cisplatin because studies of Pt therapeutics originated from the antibacterial activity and mode of action of cisplatin in bacterial cells.[22-25] In recent years, there has been a renewed interest regarding the antibacterial effects of Pt agents.[26-30] We took inspiration from the strategy of Pt(IV) prodrugs, which have been widely studied for the development of safe and targeted Pt anticancer therapy.[31-33] Pt(IV) complexes are known for their kinetic inertness compared to Pt(II) compounds, making them good candidates for masking Pt(II) toxicity prior to cell entry.[31] In a proof-of-concept study, we designed and evaluated a pair of conjugates consisting of a cisplatin-based Pt(IV) prodrug attached to either the natural siderophore L-Ent or to its enantiomer D-Ent (L/D-EP **1,2, Figure 3.1A**). L/D-EP are delivered via Ent transport machinery into the *E. coli* cytoplasm, where the Pt(IV) prodrug is presumably activated by the reducing environment, leading to the release of cisplatin that causes growth inhibition and cell filamentation (**Figure 3.1B**).[21] We found that D-EP showed greater antibacterial activity than L-EP. We attributed this increased potency to the D-Ent moiety directing conjugate delivery through the Ent transport machinery at levels similar to L-EP while preventing Fe release for bacterial metabolic use, as D-Ent is not a substrate for the cytoplasmic L-Ent esterases (**Figure 3.1B**).[34] Lastly, we showed that Ent conjugation results in markedly reduced Pt uptake by human cells and markedly enhanced Pt uptake by bacterial cells as compared to cisplatin. Overall, Ent modification repurposed the generally toxic anticancer agent cisplatin as a targeted antibiotic and set the stage for further investigations into Ent-based Pt antibacterials.[21]

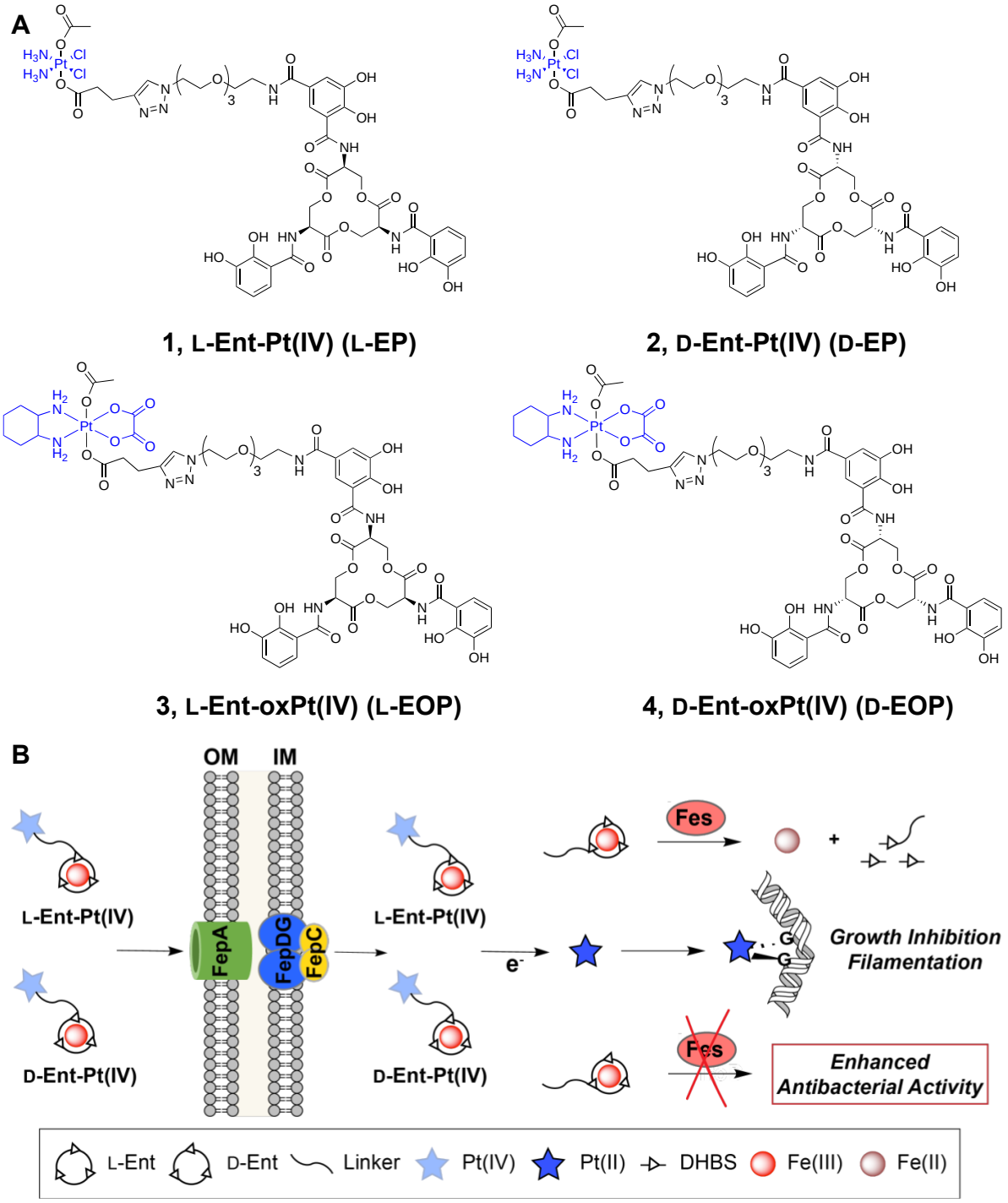

Figure 3.1. (A) Chemical structures of previously reported cisplatin-based L/D-Ent-Pt(IV) conjugates (L/D-EP) **1**,**2**[21] and oxaliplatin-based L/D-Ent-oxPt(IV) conjugates (L/D-EOP) **3,4** described in this work. Chemical structures of cisplatin and oxaliplatin are highlighted in blue. **(B)** Cartoon depiction of the working model for repurposing Pt-based anticancer agents as antibiotics that selectively target Gram-negative bacteria via Ent transport machinery, based on prior work of L/D-EP.[21] Ent transport and processing machinery is shown for *E. coli* K12. The Fe reductase that facilitates Fe release is not shown. DHBS, 2,3-dihydroxybenzoyl serine; G, a guanine base.

Moreover, others recently reported siderophore-based conjugates that repurposed the anticancer agent methotrexate as an antibiotic against Gram-positive and Gram-negative bacteria.[35] These independent reports on siderophore-modified anticancer agents as antibacterials illustrate that siderophore-based drug repurposing is gaining attention. Along these lines, we are motivated to expand the application of Ent-based drug repurposing to other metal-based anticancer agents, including the globally approved Pt agents carboplatin and oxaliplatin.[36] Carboplatin shares a similar spectrum of activity with cisplatin but has overall lower toxicity,[37-38] and oxaliplatin is used for treating cancers where cisplatin has minimal efficacy due to its distinct spectrum of antitumor activity and no reported cross-resistance with cisplatin and carboplatin.[39-40] Intrigued by the unique features of oxaliplatin, we selected to evaluate oxaliplatin as a new cargo for Ent–Pt(IV) conjugates.

In this study, we report two new Ent–Pt(IV) conjugates harboring an oxaliplatin(IV) prodrug cargo (L/D-EOP **3,4**, **Figure 3.1A**) and investigate their effects on the growth and morphology of *E. coli.* Our work demonstrates that L/D-EOP are selectively imported into the *E. coli* cytoplasm via the Ent transport machinery, enhancing Pt uptake by bacterial cells relative to oxaliplatin and inducing cell filamentation. The D-Ent congener affords the most potent antibacterial activity in this study, which highlights the importance of limiting Fe release from the siderophore. To further understand the antibacterial activity of Ent–Pt(IV) conjugates, we performed a comparative analysis of the DNA damage caused by L/D-EOP and L/D-EP and found that the antibacterial activity of Ent-Pt(IV) conjugates largely depends on the intrinsic potency of the Pt cargo and correlates with the extent of DNA damage. Taken together, this work expands the scope of the SAC approach for repurposing anticancer agents as antibiotics and demonstrates different cellular consequences depending on the molecular identity of the Pt cargo. These findings

offer valuable insights for guiding the future design of Ent–Pt(IV) conjugates for the purpose of antibacterial therapeutics.

3.4 Results

Design and synthesis of L/D-EOP. Based on our prior studies of Ent–antibiotic conjugates and L/D-EP **1,2**, the oxaliplatin-based conjugates L/D-EOP **3,4** were designed with an oxaliplatin-based Pt(IV) prodrug attached to the Ent scaffold through a poly(ethylene glycol) $(PEG)_3$ linker at the C5 position of one catechol moiety (**Figure 3.1A** and **Scheme 3.1**).[16-21] The syntheses were carried out via copper-catalyzed azide-alkyne cycloaddition (CuAAC) from L/D-Ent-PEG_3-N_3 **6,7**[16-17] and the alkyne-functionalized oxaliplatin(IV) precursor oxPt(IV)-alkyne **5**. The CuAAC reaction was first performed based on the procedure for L/D-EP.[21] Specifically, the Cu(I) salt $Cu(MeCN)_4PF_6$ was used as the catalyst, *tris*[(1-benzyl-1*H*-1,2,3-triazol-4-yl)methyl]amine (TBTA) was used as the Cu-binding ligand to accelerate the reaction, and a mixture of water and DMF instead of DMSO (used in syntheses of Ent-β-lactam conjugates[17]) was used to avoid potential ligand exchange of Pt center with the nucleophilic sulfur atom of DMSO. Following HPLC purification, L/D-EOP **3,4** were obtained with a yield of ~16%, which was slightly higher than that of L/D-EP.[21]

We routinely synthesize Ent-β-lactams from L-Ent-PEG_3-N_3 **6** and alkyne-modified β-lactams using Cu(II) and sodium ascorbate (NaAsc) to generate Cu(I) in situ.[17, 19-20, 41] Although this approach affords Ent-β-lactams in moderate to high yields (40–80%),[17, 19-20] we did not employ it in the synthesis of L/D-EP due to the concern of potential Pt(IV) reduction caused by NaAsc.[38, 42-45] During attempts to optimize the CuAAC reaction described above that afforded L/D-EOP **3,4**, we reconsidered in situ reduction of Cu(II) and evaluated the stability of oxPt(IV)-alkyne **5** in the

presence of NaAsc in water and DMF. We found that oxPt(IV)-alkyne **5** remained stable throughout the 8 h incubation with NaAsc. Consequently, we coupled oxPt(IV)-alkyne **5** to L/D-Ent-PEG_3-N_3 **6,7** using NaAsc and $CuSO_4$ in a mixture of water and DMF with the addition of TBTA. We detected negligible quantities of the dissociated Ent-containing axial ligand during HPLC purification, suggesting that a small portion of L/D-EOP **3,4** was reduced under these reaction conditions. Nevertheless, the reaction reached completion within 20 min, affording L/D-EOP **3,4** with an improved yield of 41% and high purity following HPLC purification (**Figure 3.2**).

Scheme 3.1. Synthesis of L/D-EOP via click chemistry.

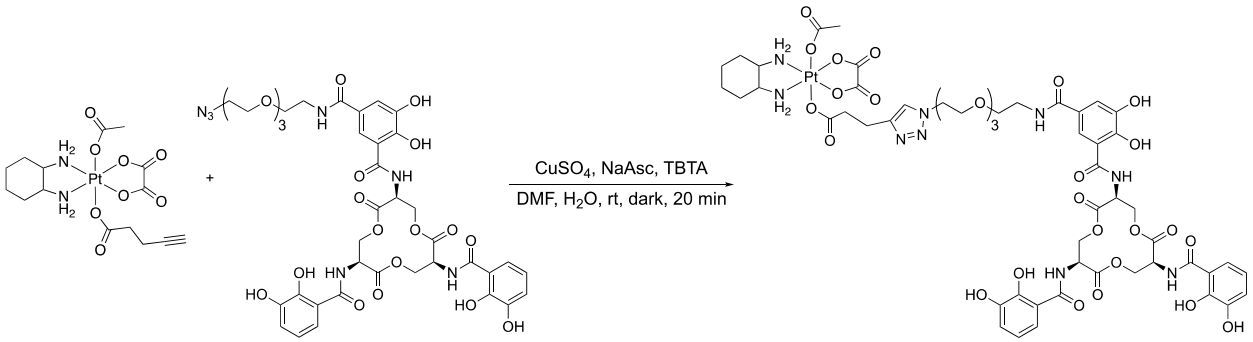

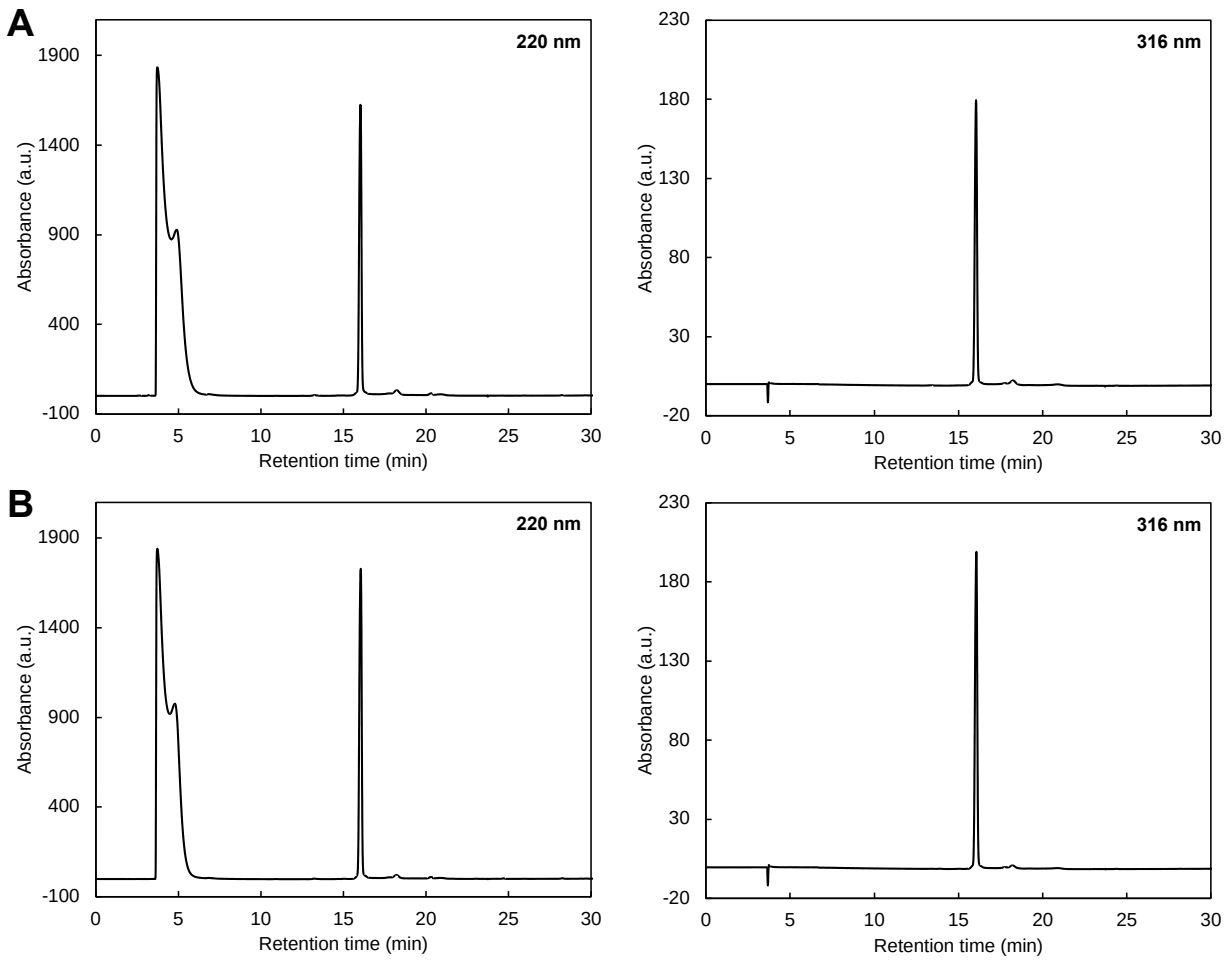

Figure 3.2. Analytical HPLC traces of purified **(A)** L-EOP and **(B)** D-EOP (retention time: 16.0 min). The peak at ca. 5 min in the 220 nm traces is DMSO.

D-EOP exhibits enhanced antibacterial activity against *E. coli* compared to oxaliplatin and L-EOP. We first evaluated the stability of D-EOP in a modified M9 growth medium supplemented with thiamine, which was employed in prior studies of Ent-based SACs including L/D-EP.[18-21, 41] The low Fe content of this medium (600–700 nM Fe by ICP-MS) induces bacterial siderophore biosynthesis and transport machineries, and thiamine is added to support the growth of *E. coli* CFT073 mutants.[21] We found that D-EOP was adequately stable in this medium for microbiology experiments, showing stability similar to what we previously observed for L-EP (see Section **3.8**, **Supporting Discussion**). Given the low Fe content of the medium and

micromolar concentration range of L/D-EOP used throughout the biological studies, L/D-EOP were preloaded with 0.9 equivalents of Fe(III) prior to each experiment.

In contrast to cisplatin, which was discovered for its ability to inhibit cell division and induce filamentation in *E. coli*,[22-23] there is limited information about how oxaliplatin impacts bacterial growth. One recent report published during the course of this investigation showed that oxaliplatin has lower antibacterial activity than cisplatin against *E. coli* MG1655, a close K12 derivative.[46] To our knowledge, the effects of oxaliplatin treatment on bacterial morphology have not been described. We first evaluated the antibacterial activity of oxaliplatin against two *E. coli* strains by monitoring culture turbidity, including the laboratory strain BW25113 (hereafter K12)[47] and the uropathogenic clinical isolate CFT073.[48] Consistent with the prior report, we found that oxaliplatin displays lower antibacterial activity against *E. coli* than cisplatin. Oxaliplatin exhibited negligible growth inhibition against both *E. coli* K12 and CFT073 at concentrations up to 60 μM (**Figure 3.3**). By contrast, cisplatin significantly reduced the turbidity of K12 and CFT073 cultures at ≥30 μM.[21]

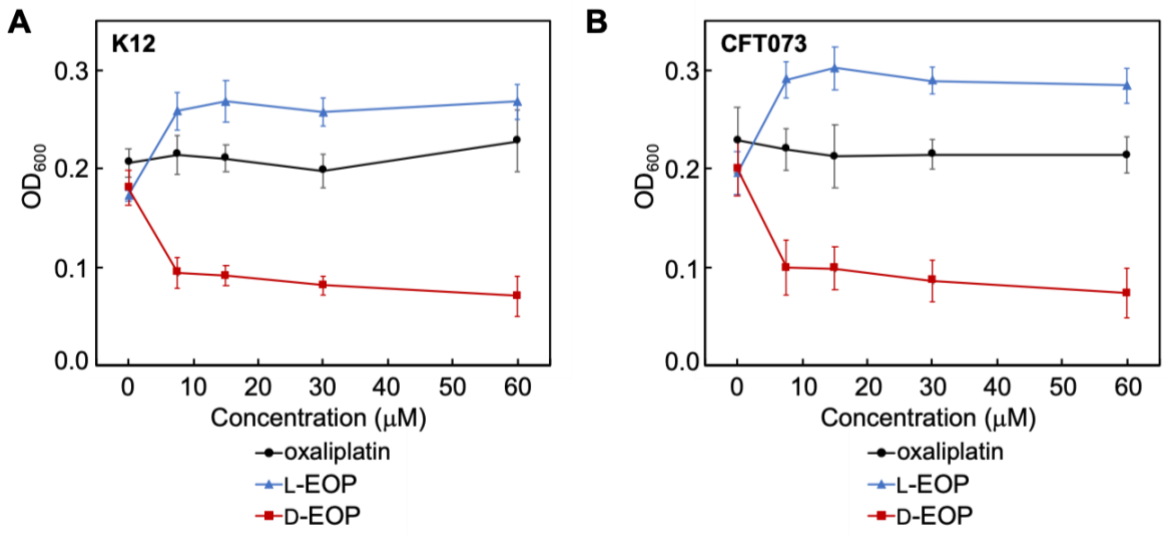

Figure 3.3. Antibacterial activity of oxaliplatin and L/D-EOP against **(A)** *E. coli* K12 and **(B)** *E. coli* CFT073 (mean ± standard deviation, n = 8). All assays were performed in modified M9 medium (11 h, 30 °C with shaking).

Next, we assayed the antibacterial activity of L/D-EOP against K12 and CFT073. We found that L-EOP was less effective than oxaliplatin, resulting in a slight growth promotion in both strains (**Figure 3.3**). This observation could be attributed to the combined effects resulting from co-delivery of a Pt payload with limited potency and nutrient Fe from the L-Ent moiety, consistent with our prior study where L-EP was less effective at inhibiting *E. coli* growth than cisplatin.[21] By contrast, the enantiomer D-EOP inhibited bacterial growth (**Figure 3.3**). Treatment of *E. coli* K12 and CFT073 with 7.5 μM and 60 μM D-EOP resulted in a turbidity reduction by 50% and >60%, respectively relative to the untreated control. A direct comparison showed that D-EOP is less potent than D-EP against these two *E. coli* strains (**Figure 3.4**). Growth curves revealed that D-EOP exhibits bacteriostatic activity against both strains, as evidenced by the delay in the onset of growth followed by the growth resumption after 12 h treatment (**Appendix B.3**). Overall, both L/D-EOP conjugates are less growth inhibitory against *E. coli* compared to L/D-EP,[21] which correlates with the relative antibacterial activities of the oxaliplatin and cisplatin cargos. The correlation between the relative efficacy of Ent–Pt(IV) conjugates and the potencies of the attached Pt cargos is attributed to reductive elimination during cytoplasmic activation. This process releases the corresponding Pt(II) warheads cisplatin and oxaliplatin, which are responsible for growth inhibition. The released L-Ent provides Fe to bacteria, increasing bacterial fitness and compromising antibacterial activity, whereas D-Ent renders the bound Fe unavailable, thereby conferring increased antibacterial activity.

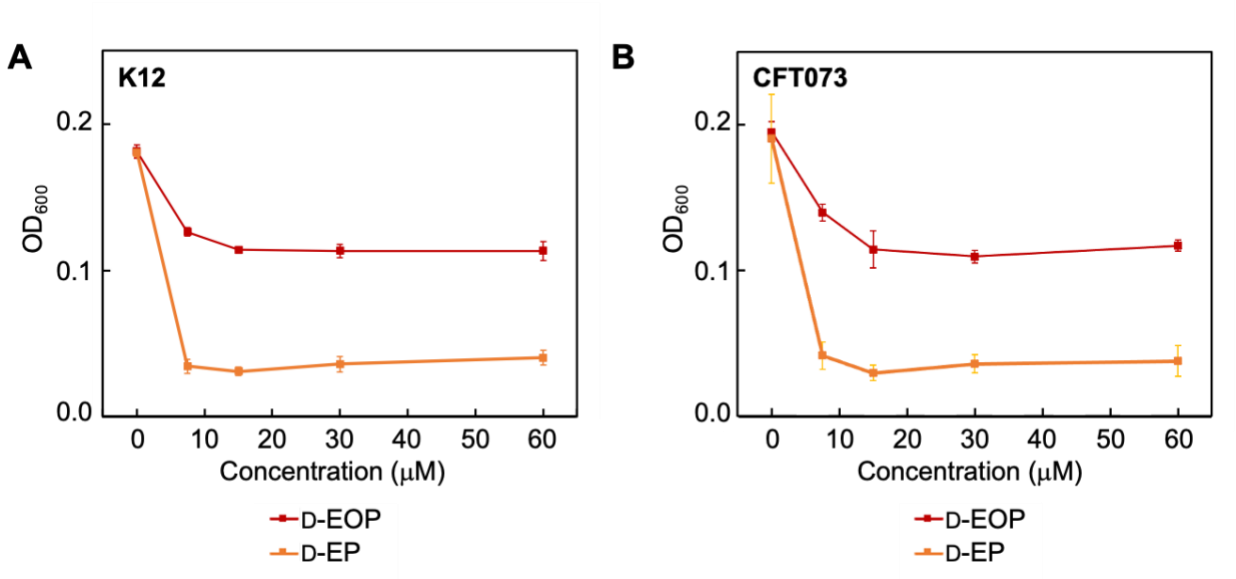

Figure 3.4. Antibacterial activity of D-EOP and D-EP against **(A)** *E. coli* K12 and **(B)** CFT073. All assays were performed in modified M9 medium (11 h, 30 °C, 500 rpm; mean ± standard deviation; n = 3).

Ent transport machinery is required for the antibacterial activity of D-EOP. We reasoned that L/D-EOP are actively imported into the *E. coli* cytoplasm by the Ent transport machinery expressed by all *E. coli* strains, including the OM receptor FepA, the periplasmic binding protein FepB, and the inner membrane (IM) ATP-binding cassette transporter FepCDG.[18, 21] *E. coli* CFT073 harbors the pathogen-associated *iroA* gene cluster which encodes an OM receptor named IroN that also transports Ent.[49] To examine the uptake pathway, we evaluated whether key components of the Ent transport machinery are required for D-EOP antibacterial activity against *E. coli*.

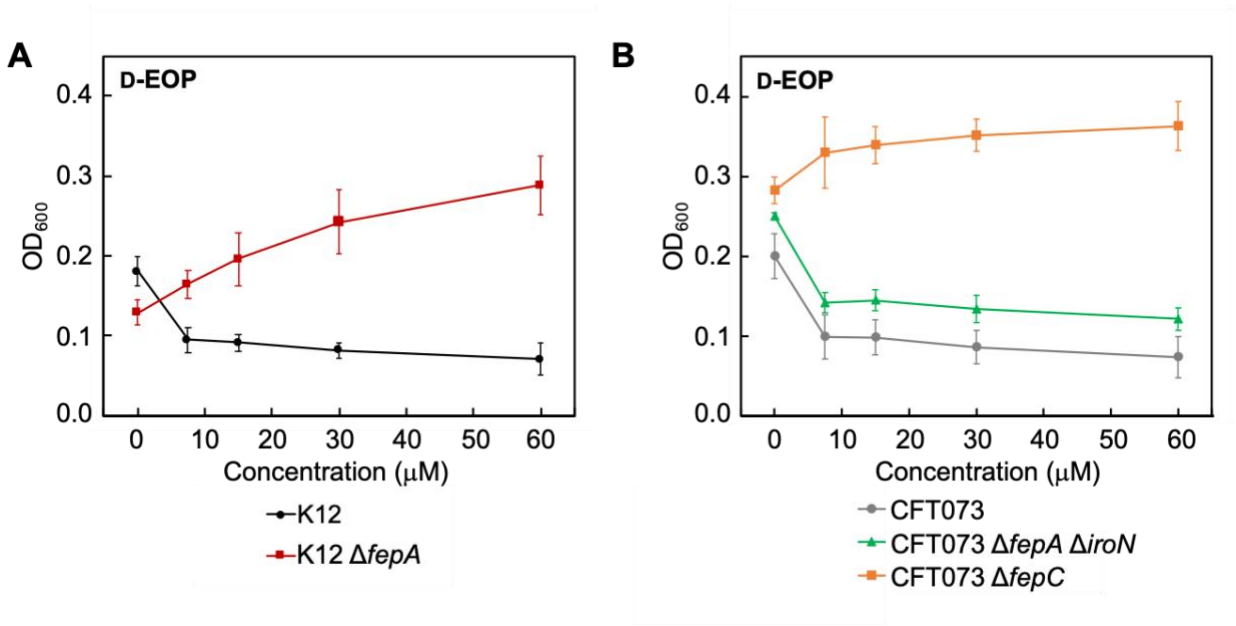

Figure 3.5. Antibacterial activity of D-EOP against **(A)** *E. coli* K12 and its Δ*fepA* mutant; **(B)** *E. coli* CFT073 and its Δ*fepA* Δ*iroN* and Δ*fepC* mutants (mean ± standard deviation, n ≥ 5). All assays were performed in modified M9 medium (11 h, 30 °C with shaking).

We first investigated the role of the OM receptor FepA by treating K12 and its Δ*fepA* mutant (JW5086 from the Keio Collection)[47] with 0–60 μM D-EOP. In contrast to the growth inhibition of D-EOP against the parent strain, the Δ*fepA* mutant was not inhibited by D-EOP at all tested concentrations (**Figure 3.5A**), indicating that FepA is required for the uptake of D-EOP into *E. coli* K12. We note that the K12 Δ*fepA* mutant exhibits a growth defect in the modified M9 medium and appears to be very sensitive to any slight change in Fe content. Consequently, we speculate that the growth promotion observed for K12 Δ*fepA* treated with D-EOP results from partial decomposition of D-EOP which releases Fe into the growth medium providing this nutrient to the bacteria. We also evaluated the antibacterial activity of D-EOP against the CFT073 Δ*fepA* Δ*iroN* mutant. D-EOP inhibited the growth of this mutant (**Figure 3.5B**), which was expected based on prior studies with Ent-β-lactams and L/D-EP.[19, 21] This result likely reflects the fact that CFT073 has additional receptors for Fe(III)-Ent as well as unknown OM receptors for Ent and its

hydrolysis products.[19-21, 50-51] We speculate that one or more of these OM receptors also transports D-EOP and other Ent-based conjugates.

We then studied whether the IM transporter FepCDG is necessary for the antibacterial activity of D-EOP. We focused these studies on the CFT073 Δ*fepC* mutant because the K12 Δ*fepC*, Δ*fepD*, and Δ*fepG* mutants showed severe growth defects in the modified M9 medium. In contrast to the parent strain, no growth inhibition was observed for the CFT073 Δ*fepC* mutant after treatment with up to 60 μM D-EOP (**Figure 3.5B**), indicating that the Ent IM transporter is required for the antibacterial activity of D-EOP.

Bacterial morphologies indicate that the Ent transport machinery transports L/D-EOP into the *E. coli* cytoplasm. Many Pt compounds slow bacterial cell division and produce a filamentous phenotype.[27] We observed this phenomenon during studies of L/D-EP and concluded that turbidity measurements are insufficient to describe Pt-induced growth defects.[21] In alignment with these observations, we investigated bacterial morphological changes following treatment with oxaliplatin and L/D-EOP by bright-field microscopy. We also examined cell viability by fluorescence microscopy after LIVE/DEAD staining, which distinguishes cells with intact or compromised OM using the fluorescent dyes SYTO 9 (green) and propidium iodide (red), respectively.[52]

We first treated *E. coli* with 0–60 μM oxaliplatin and observed that oxaliplatin induced filamentation (cell perimeter 20–50 μm) in both K12 and CFT073 cells. Filamentation occurred starting at 15 μM oxaliplatin and LIVE/DEAD staining showed that most elongated cells were live at this concentration **(Figure 3.6)**. At higher concentrations of oxaliplatin (30 and 60 μM), long filaments (cell perimeter >50 μm) formed and LIVE-DEAD staining revealed a mixture of live and dead filamentous cells (**Figures 3.6**, **3.7A** and **3.7C)**. We previously reported that cisplatin

induced filamentation in both K12 and CFT073 starting at a lower concentration of 7.5 μM. Within the range of 7.5–60 μM, we observed that the filaments induced by cisplatin were generally longer than those induced by an equivalent concentration of oxaliplatin (**Figure 3.6**).[21] Overall, oxaliplatin induces filamentous morphologies like cisplatin and other Pt compounds,[21, 27] but appears to be less potent than cisplatin. We note that the prodrug precursor oxPt(IV)-alkyne **5** did not induce filamentation in any strains evaluated in this study (**Figure 3.8**).

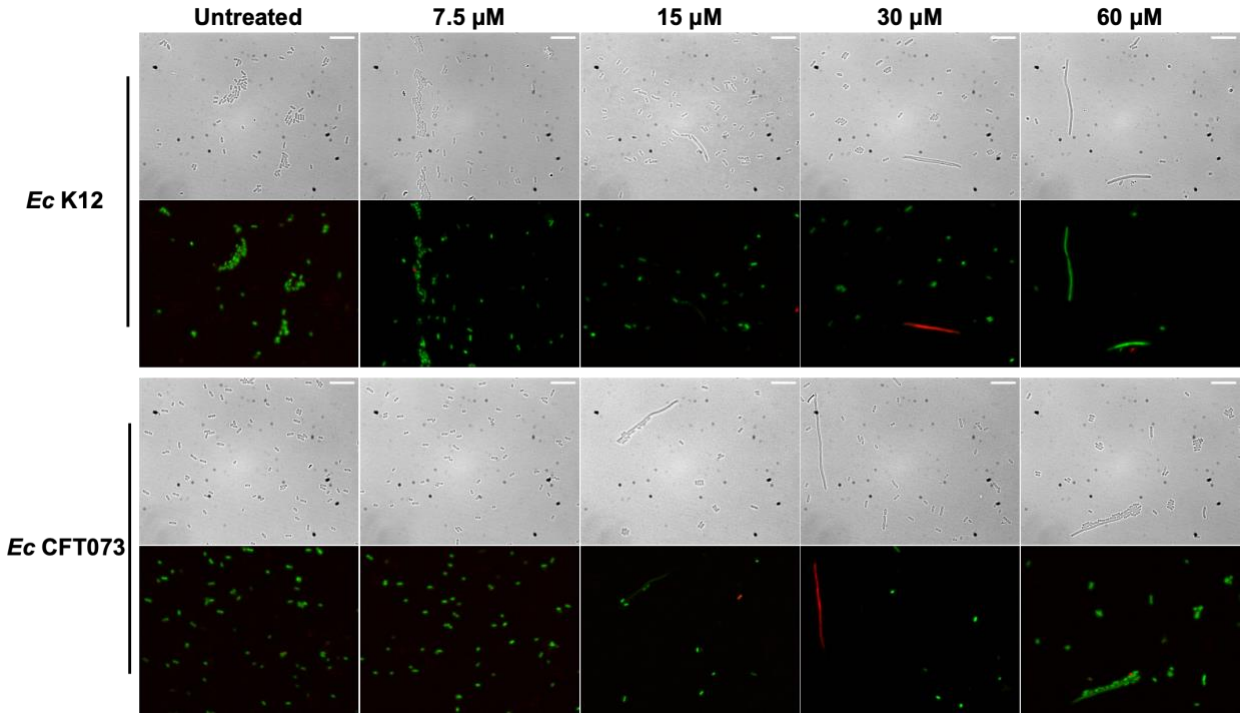

Figure 3.6. Representative bright-field and fluorescence micrographs of *E. coli* K12 and CFT073 treated with oxaliplatin (scale bar = 10 μm).

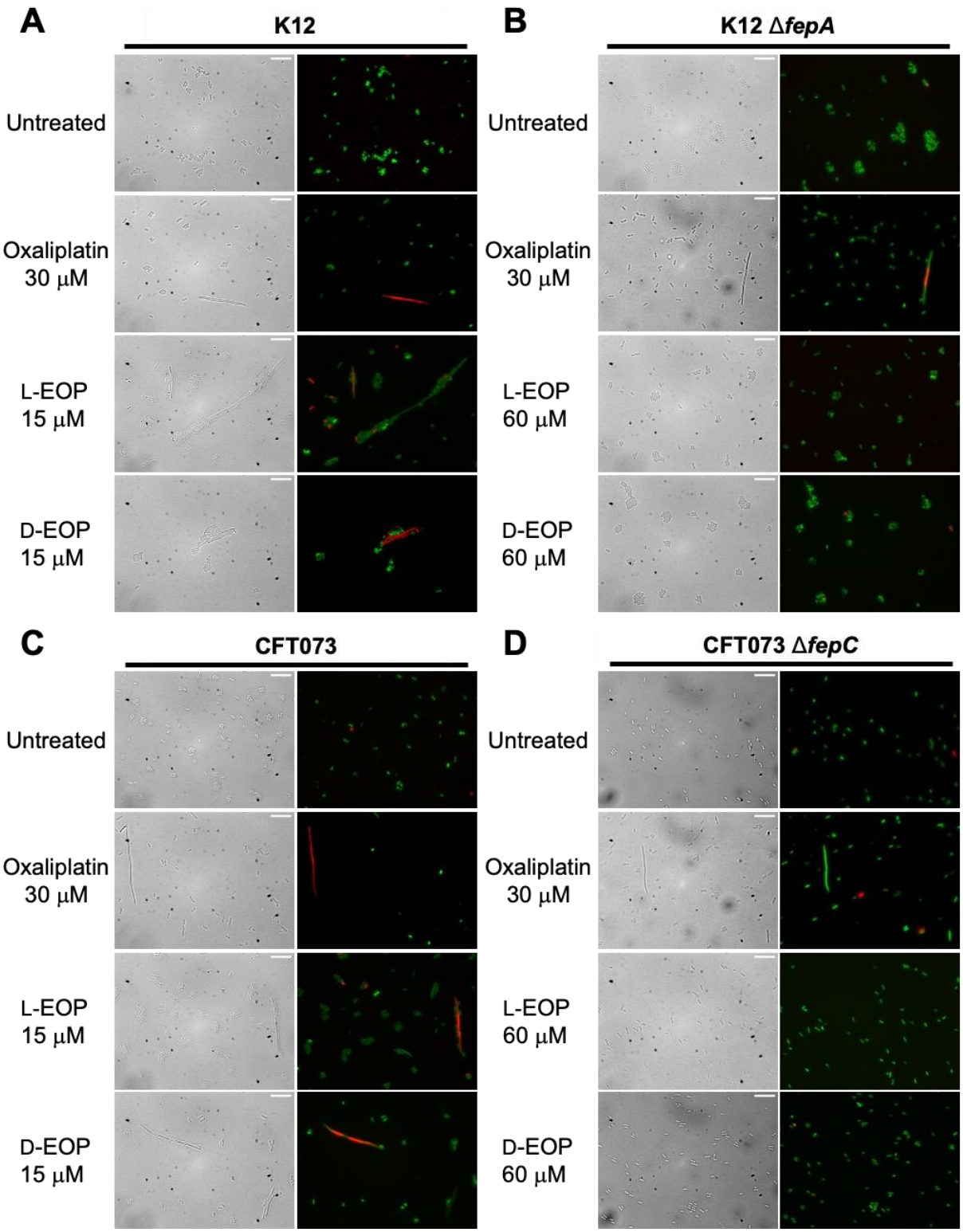

Figure 3.7. Comparison of bacterial morphologies and viability of *E. coli* **(A)** K12, **(B)** K12 Δ*fepA*, **(C)** CFT073, and **(D)** CFT073 Δ*fepC* treated with oxaliplatin and L/D-EOP (scale bar = 10 μm). All assays were performed in modified M9 medium (11 h, 30 °C with shaking).

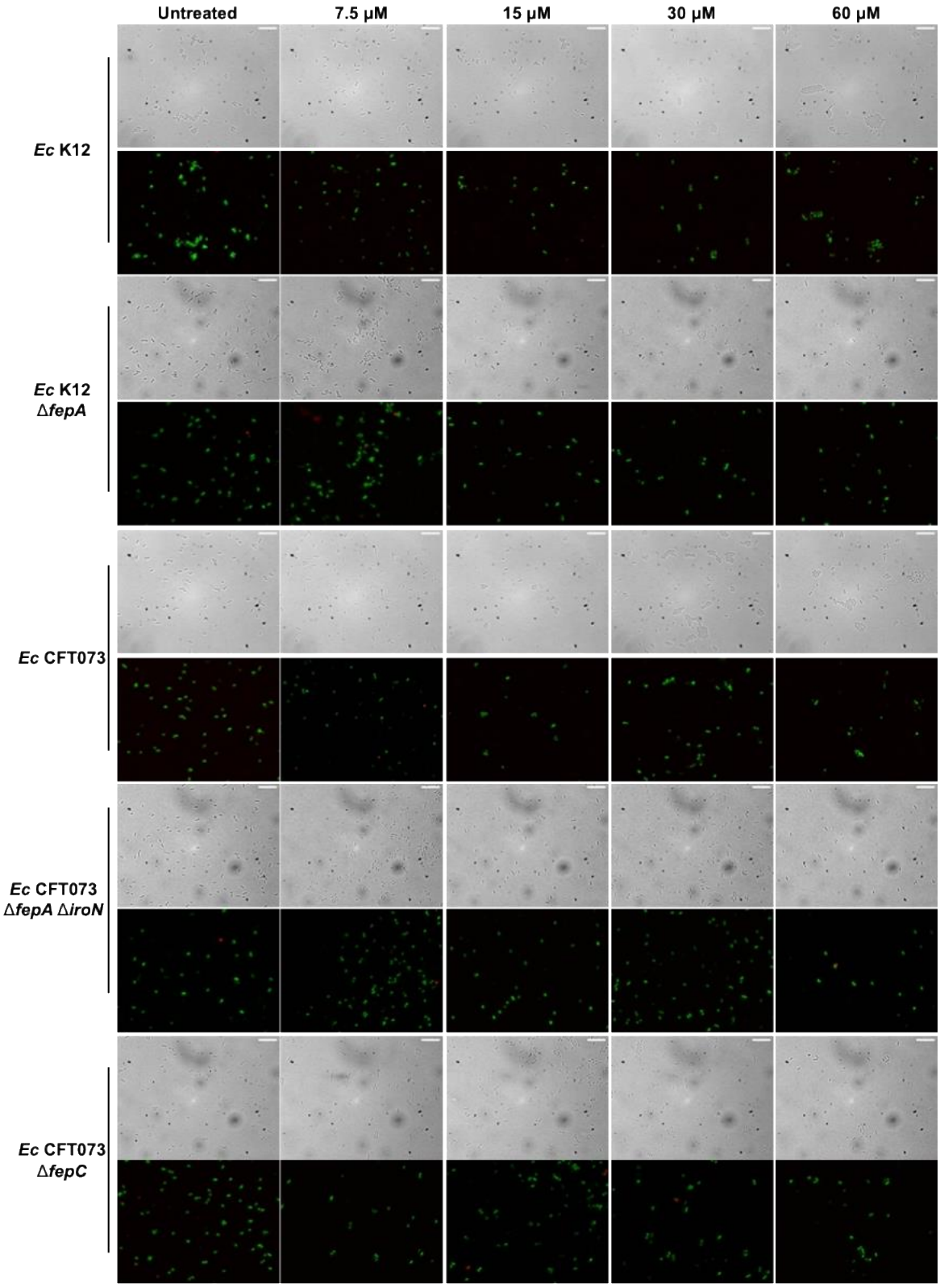

Figure 3.8. Representative bright-field and fluorescence micrographs of *E. coli* K12, CFT073 and their mutants treated with oxPt(IV)-alkyne (scale bar = 10 µm).

We then investigated the effects of L/D-EOP on bacterial morphology. We found that L-EOP was more potent than oxaliplatin in inducing filamentation in both K12 and CFT073. Long filaments were observed at all tested concentrations (7.5–60 μM, **Figure 3.9**), which were longer than those induced by oxaliplatin (**Figures 3.7A, 3.7C,** and **3.9)**. D-EOP also induced long filamentation in both K12 and CFT073 at all tested concentrations (**Figures 3.7A, 3.7C,** and **3.10)**. Consistent with the enhanced antibacterial activity of D-EOP, the filaments induced by D-EOP were relatively short compared to those induced by the same concentration of L-EOP, and most filamentous cells were dead as confirmed by LIVE/DEAD staining (**Figure 3.10**).

We also examined bacterial mutants defective in the Ent transport machinery. Elongation or filamentation was induced by oxaliplatin in K12 Δ*fepA*, CFT073 Δ*fepA* Δ*iroN*, and CFT073 Δ*fepC* (**Figure 3.11**). By contrast, L/D-EOP induced filamentation in the parent strains but not the K12 Δ*fepA* or CFT073 Δ*fepC* mutants. Most of K12 Δ*fepA* and CFT073 Δ*fepC* cells were normal-sized and viable after treatment with L/D-EOP (**Figures 3.7B, 3.7D, 3.9,** and **3.10)**, consistent with the abolished antibacterial activity of D-EOP against these mutants (**Figure 3.5**). We note that CFT073 Δ*fepA* Δ*iroN* also exhibited filamentous morphology after L/D-EOP treatment (**Figures 3.9** and **3.10**), as expected from the growth experiment (**Figure 3.5B**). Taken together, we conclude that the OM receptor FepA and the IM transporter FepCDG are responsible for the uptake of L/D-EOP into *E. coli* cytoplasm, indicating that L/D-EOP target Gram-negative bacteria expressing the Ent uptake machinery.

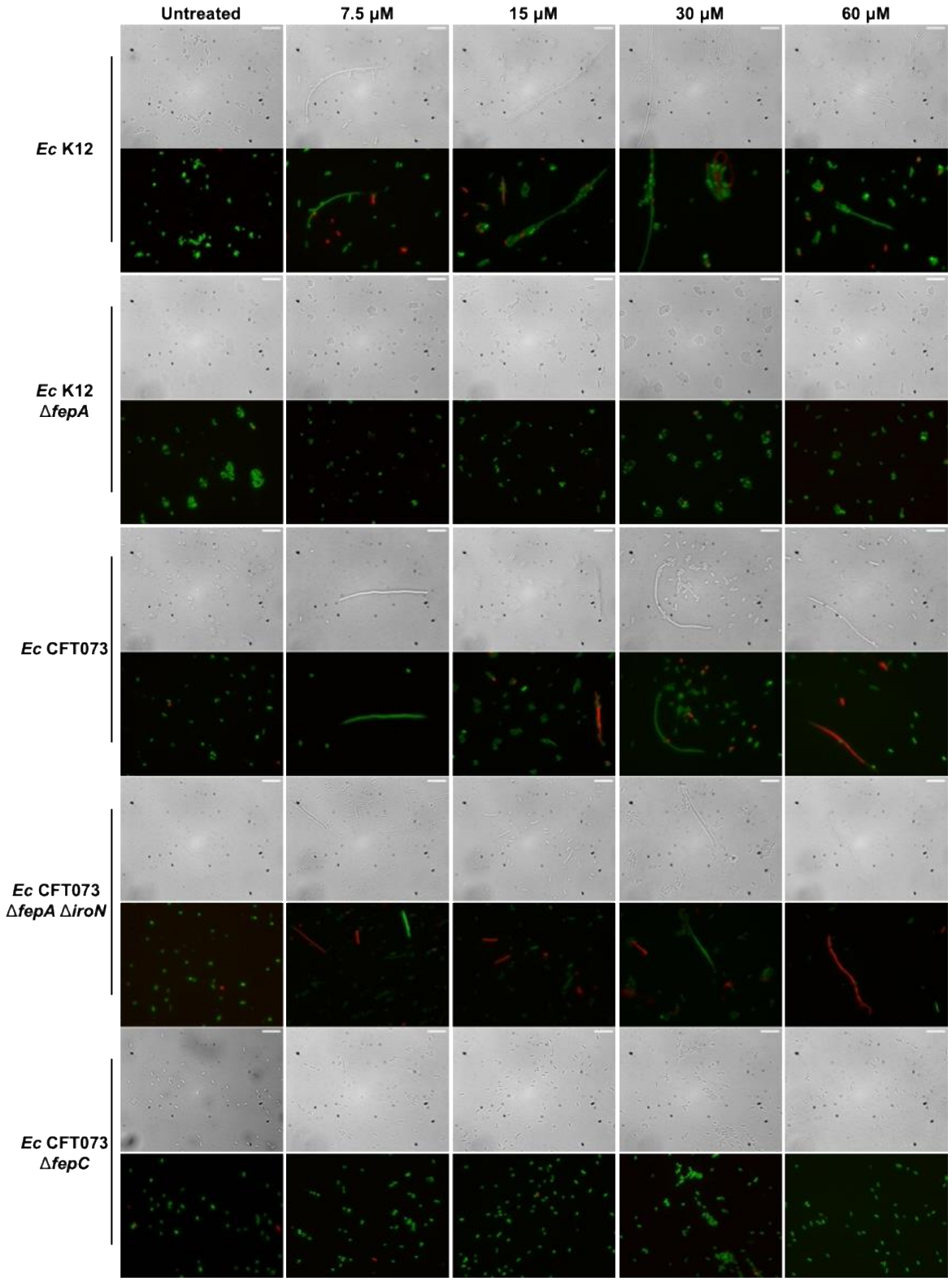

Figure 3.9. Representative bright-field and fluorescence micrographs of *E. coli* K12, CFT073 and their mutants treated with L-EOP (scale bar = 10 µm).

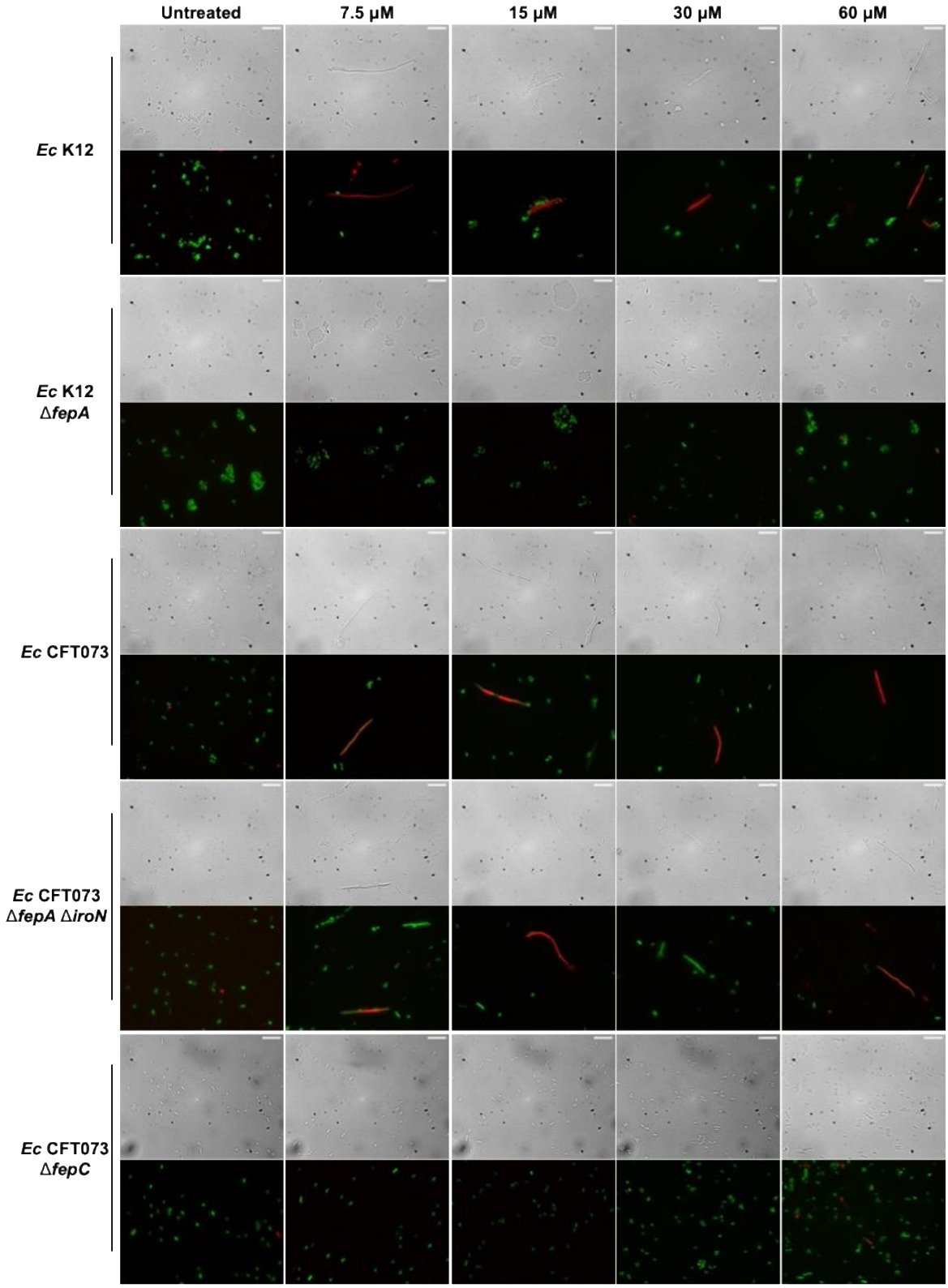

Figure 3.10. Representative bright-field and fluorescence micrographs of *E. coli* K12, CFT073 and their mutants treated with D-EOP (scale bar = 10 µm).

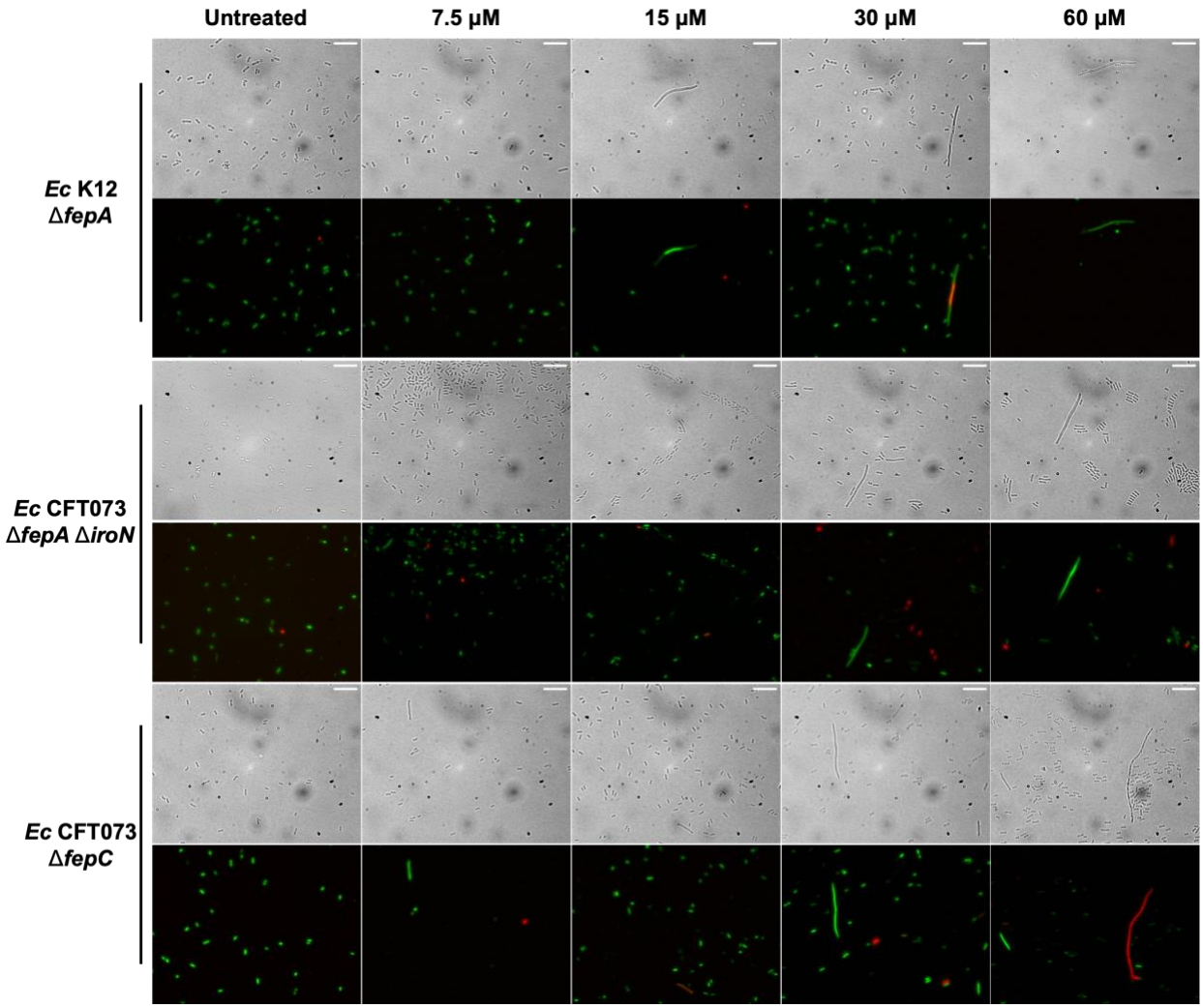

Figure 3.11. Representative bright-field and fluorescence micrographs of K12 Δ*fepA*, CFT073 Δ*fepA* Δ*iroN*, and CFT073 Δ*fepC* treated with oxaliplatin (scale bar = 10 μm).

Ent conjugation enhances Pt uptake by bacterial cells while reducing that by human cells. It is generally believed that Pt(II) anticancer agents like cisplatin and oxaliplatin primarily enter mammalian cells through passive diffusion, with active transport (*e.g.*, the organic cation transporter and copper transporter 1) as a secondary pathway.[53-54] Ent conjugation is proposed to decrease Pt uptake by human cells, as L/D-EOP are too large for passive diffusion, and human cells lack machinery for Ent active transport and facilitate Pt uptake by *E. coli* cells through active transport.[21] In support of this notion, studies of Pt uptake by *E. coli* CFT073 revealed a significant

enhancement in Pt uptake for L/D-EOP compared to oxaliplatin and the prodrug precursor oxPt(IV)-alkyne **5**. Specifically, Pt uptake was 37-fold and 28-fold greater for *E. coli* CFT073 when treated with L-EOP (15.7%) or D-EOP (11.6%), respectively, compared to oxaliplatin (0.4 %) (**Figure 3.12A**). L-EOP facilitates Pt uptake to a slightly greater extent than D-EOP, but the overall levels are similar, which is consistent with our prior study of L/D-EP.[21] By contrast, HEK293T cells showed negligible Pt uptake for L/D-EOP and oxPt(IV)-alkyne **5** (0.02–0.03%), which is ~7-fold lower compared to oxaliplatin treatment (0.14%) (**Figure 3.12B**). Collectively, L/D-EOP facilitated targeted Pt uptake by *E. coli* but lead to negligible Pt uptake by human cells.

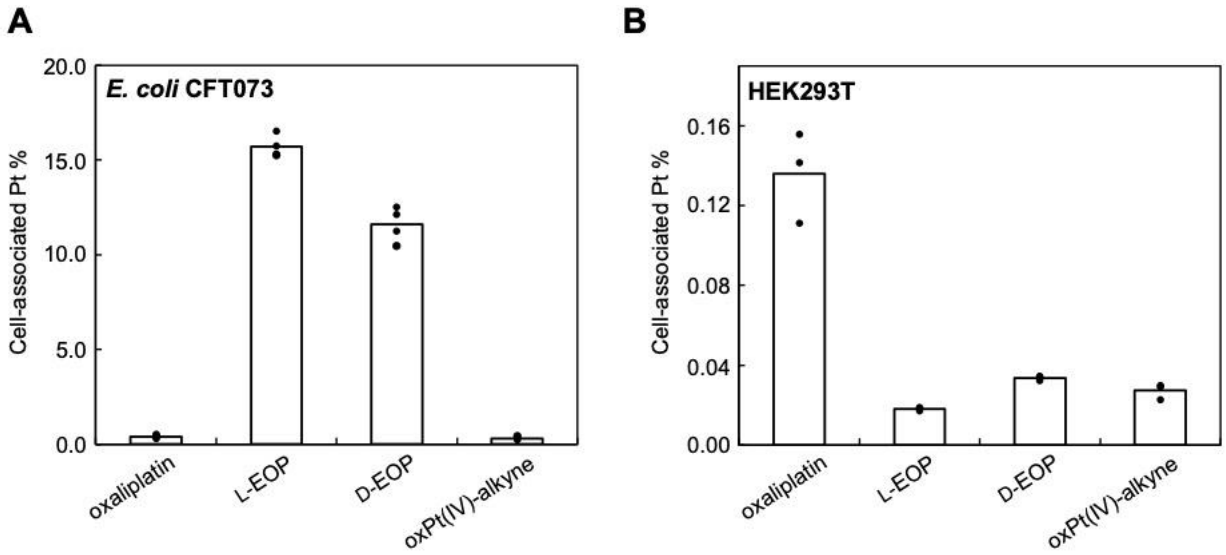

Figure 3.12. Pt uptake in **(A)** *E. coli* CFT073 and **(B)** HEK293T cells treated with 1 μM oxaliplatin, L/D-EOP, and oxaliplatin-alkyne **5**. *E. coli* CFT073 cells were treated for 30 min in modified M9 medium at 30 °C (n = 4), and HEK293T cells were treated for 6 h in DMEM+1% penicillin/streptomycin at 37 °C, 5% CO_2 (n = 3).

L/D-EOP induce lysis in lysogenic bacteria. Given that cell filamentation is an indicator of Pt-induced DNA damage,[55] we sought to further investigate the cellular fates of oxaliplatin and L/D-EOP in *E. coli* by probing DNA damage. We started by examining the abilities of oxaliplatin and L/D-EOP to induce lysis in lysogenic bacteria, which is an experimental approach utilized in

early and recent studies of Pt compounds.[21, 27, 56-57] Briefly, lysogenic bacteria are bacteria harboring a prophage, the genetic information of a bacterial virus (bacteriophage λ).[56] The expression of viral genes is repressed under normal conditions but is induced in response to DNA damage, leading to the production of viral particles and ultimately cell lysis. We treated the lysogenic bacterial strain *E. coli* W3104 with the three Pt compounds and spotted the resulting cell suspensions on a lawn of nonlysogenic *E. coli* CFT073. Pt-induced DNA damage triggers the production of viral particles, which are released from lysed *E. coli* W3104, preventing the growth of *E. coli* CFT073 and resulting in plaque formation on the lawn.[27]

We observed plaques on a lawn of CFT073 when spotted with a 100-fold diluted suspension of *E. coli* W3104 that was treated with ≥15 μM oxaliplatin (**Figure 3.13A**). When we treated *E. coli* W3104 with 15 μM L/D-EOP, 15 μM L-Ent, or 1% DMSO (control), we observed plaque formation on CFT073 only when W3104 was treated with 15 μM L/D-EOP at 100-fold dilution (**Figure 3.13B** and **Table 3.1**). No plaques formed in the areas where the compound solutions were spotted, indicating that the plaque formation was due to the release of viral particles from lysed W3104 cells. Overall, the ability of L/D-EOP to induce bacterial filamentation (**Figure 3.7**) and initiate lysis in lysogenic bacteria suggests that oxaliplatin and L/D-EOP cause DNA damage in *E. coli*.

Table 3.1. Effects of L/D-EOP on lysogenic *E. coli*[a]

	oxaliplatin	L-EOP	D-EOP	L-Ent	1% DMSO	Untreated
***Ec* W3104 suspension**	+	+	+	–	–	–
Compound solution	–	–	–	–	–	–

[a] The development of plaques in a lawn of non-lysogenic *E. coli* CFT073 following spotting 100-fold diluted suspensions of *E. coli* W3104 treated with 15 μM of each compound or solutions containing only the corresponding compound. +, plaque formation; –, no plaque observed. Representative images of agar plates are shown in **Figure 3.13**. L-Ent and L/D-EOP were preloaded with 0.9 equivalents of Fe(III).

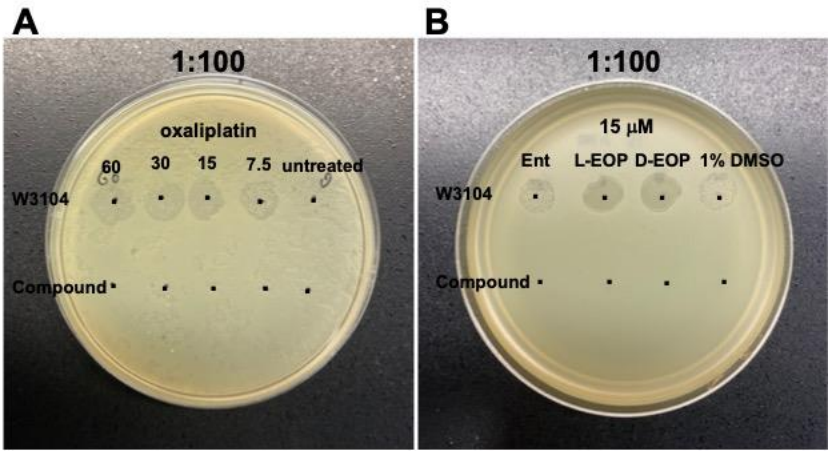

Figure 3.13. Effects of **(A)** oxaliplatin and **(B)** L/D-EOP on lysogenic *E. coli.* Representative images of the development of plaques in a lawn of non-lysogenic *E. coli* CFT073 following application of 10 μL drops of 100-fold diluted suspensions of treated *E. coli* W3104 and solutions containing only the corresponding compound. *E. coli* W3104 was treated with 7.5–60 μM oxaliplatin, 15 μM ferric Ent, 15 μM ferric L/D-EOP, and 1% DMSO.

A comparison of conditions for plaque formation resulting from L-EP[21] and L/D-EOP treatment of W3104 revealed two noteworthy differences. First, plaque formation occurred with a higher-fold dilution of W3104 treated with 15 μM L-EP compared to 15 μM L/D-EOP (1000-fold and 100-fold, respectively). Second, plaque formation occurred after W3104 was treated with apo L-EP, whereas L/D-EOP treatment afforded plaque formation only when the conjugate was preloaded with Fe(III). The Ent OM receptors recognize and transport ferric Ent and consequently

ferric Ent–Pt(IV),[18] and we reason that treatment with 15 μM apo conjugate results in <1 μM conjugate available for efficient transport into W3014 cells in the Fe-deficient M9 medium (<1 μM Fe). This quantity of ferric L-EP led to the production of sufficient viral particles for plaque formation; however, the same quantity of L/D-EOP could not yield enough viral particles. Overall, the results from lysogenic bacteria assays indicate that Ent–Pt(IV) conjugates harboring both cisplatin and oxaliplatin induce DNA damage in *E. coli*. However, the data also suggest that L/D-EOP induce less DNA damage to bacterial cells compared to L/D-EP.

L/D-EOP cause less DNA damage in *E. coli* compared to L/D-EP. To further investigate the ability of L/D-EOP and L/D-EP to cause DNA damage in *E. coli*, we constructed a reporter strain by transforming *E. coli* JW0334, a Δ*lacY* mutant from the Keio Collection,[47] with a reporter plasmid *pSulAp_lacZ*. This reporter plasmid places control of the expression of *lacZ* under the SOS-inducible promoter for *sulA*. In the SOS regulon, *sulA* encodes the cell division inhibitor SulA, which is closely associated with the inhibition of cell division and the consequent filamentation when DNA is damaged.[58-59] The *sulA* promoter has been employed in reporter systems for the SOS response and has been shown to be induced efficiently upon DNA damage.[60-61] The reporter strain *E. coli* JW0334 *pSulAp_lacZ* allowed us to compare the extent of DNA damage based on levels of the SOS response induced by each Pt compound, which was determined by measuring the reporter activity using a β-galactosidase activity assay.

We first validated that *E. coli* JW0334 *pSulAp_lacZ* was a selective reporter for the SOS response by treating the strain with a sub-MIC concentration of ciprofloxacin, an SOS-inducing agent, or tetracycline, a non-SOS-inducing agent. Following ciprofloxacin treatment, the reporter activity increased in a time- and concentration-dependent manner (**Figure 3.14A**). By contrast, tetracycline did not affect the reporter activity (**Figure 3.14A**). We also found that the low-Fe

condition of the modified M9 medium did not affect the reporter activity compared to growing *E. coli* JW0334 *pSulAp_lacZ* in modified M9 with the addition of 5 μM Fe (**Figure 3.14A**).

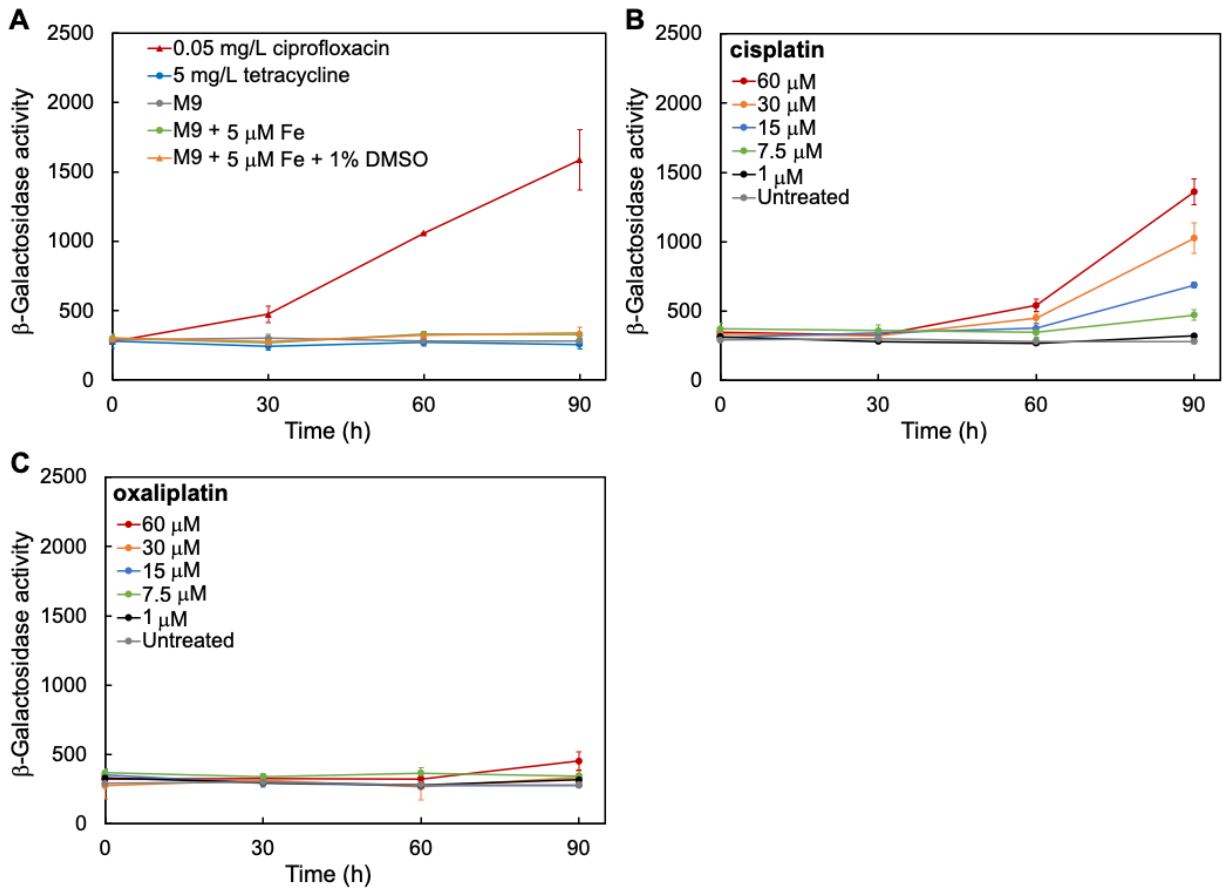

Figure 3.14. β-Galactosidase activity of *E. coli* JW0334 *pSulAp_lacZ* after treatment with **(A)** ciprofloxacin or tetracycline, **(B)** cisplatin, and **(C)** oxaliplatin for 90 min (mean ± standard deviation, n ≥ 3). All assays were performed in modified M9 medium (30 °C with shaking).

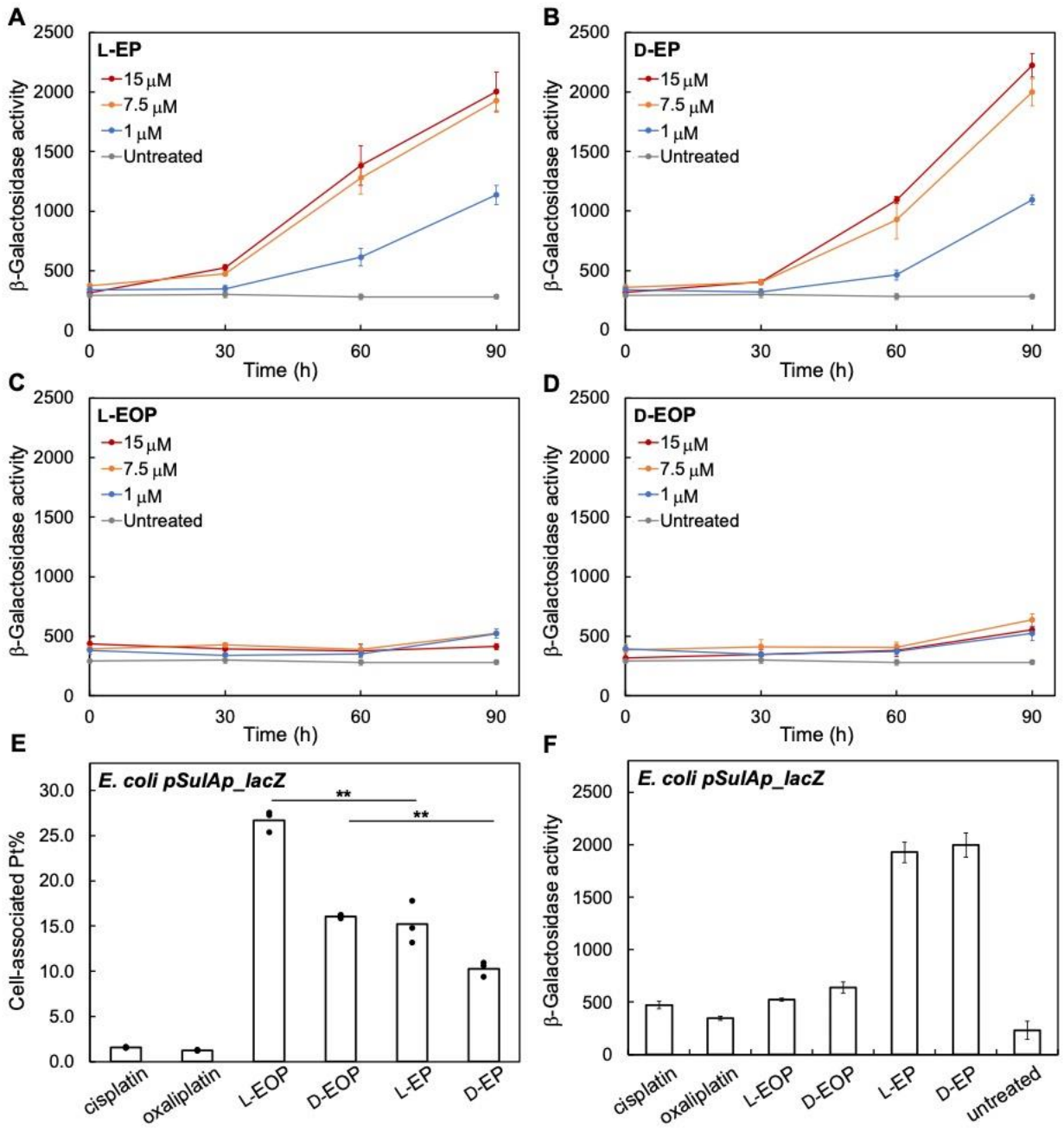

Figure 3.15. β-Galactosidase activity of *E. coli* JW0334 *pSulAp_lacZ* after treatment with **(A)** L-EP, **(B)** D-EP, **(C)** L-EOP, **(D)** D-EOP, and **(E)** Pt uptake in *E. coli pSulAp_lacZ* after treatment with 1 μM Pt compounds for 30 min (n = 3). Statistical differences were calculated using two-tailed Student's *t* test assuming unequal variances; $^{**}P < 0.01$. **(F)** β-Galactosidase activity of *E. coli pSulAp_lacZ* after treatment with 7.5 μM Pt compounds for 90 min (mean ± standard deviation, n = 3). All assays were performed in modified M9 medium (30 °C with shaking).

We then measured the levels of SOS response in the reporter strain induced by different Pt compounds. First, we treated the reporter strain with 0–60 μM cisplatin or oxaliplatin. Whereas cisplatin treatment increased the reporter activity in a time- and concentration-dependent manner (**Figure 3.14B**), negligible induction of the reporter activity occurred following oxaliplatin treatment (**Figure 3.14C**). Likewise, treatment with L/D-EP led to a time- and concentration-dependent increase in the reporter (**Figures 3.15A** and **3.15B**) and treatment with L/D-EOP had negligible impact on reporter activity for the first 60 min and a slight increase in reporter activity occurred after 90 min treatment (**Figures 3.15C** and **3.15D)**. Comparison of the reporter responses to cisplatin and L/D-EP revealed that L/D-EP induced higher levels of SOS response (**Figure 3.15F**).

To determine whether the observed β-galactosidase activities from the reporter strain are influenced by cellular Pt concentration, we conducted a Pt uptake assay using the reporter strain and the six Pt compounds. The results were consistent with what was observed for Pt uptake with *E. coli* CFT073 (**Figure 3.12A** and ref[21]) where treatment with the L-enantiomers results in somewhat greater Pt uptake than treatment with the D-enantiomers. For each enantiomer pair (e.g., L-EP and L-EOP, D-EP and D-EOP), Pt uptake indicated somewhat greater uptake of the oxaliplatin conjugates than the cisplatin conjugates (**Figure 3.15E**). Overall, our results from the reporter assay and Pt uptake assay show that while L/D-EP treatment leads to slightly lower Pt uptake in *E. coli*, L/D-EP induce markedly higher levels of SOS response compared to L/D-EOP (**Figure 3.15F**). This finding supports the notion that the higher potency of L/D-EP results from the cisplatin cargo inducing more DNA damage in *E. coli* than the oxaliplatin cargo in L/D-EOP.

Recombination-deficient *E. coli* exhibits enhanced susceptibility to L/D-EP and L/D-EOP. As a complementary approach to probing DNA damage, we evaluated the susceptibility of a bacterial DNA repair mutant to the Ent–Pt(IV) conjugates. A prior report showed that major

recombination pathways are critical to protect *E. coli* against cisplatin toxicity, demonstrated by the increased susceptibility of recombination-deficient *E. coli* mutants to cisplatin relative to the parent strain *E. coli* AB1157 (a K12 derivative).[62] We employed *E. coli* AB1157 and its mutant defective in RecG and RuvC, two enzymes involved in the late steps of the recombination pathway. We chose the Δ*recG* Δ*ruvC* mutant due to its hypersensitivity to cisplatin and its ability to grow in the modified M9 medium.

We first evaluated the susceptibility of *E. coli* AB1157 and Δ*recG* Δ*ruvC* to cisplatin. Consistent with the prior report,[62] growth of the parent strain was partially inhibited by cisplatin, and the hypersensitive Δ*recG* Δ*ruvC* mutant was fully killed when treated with ≥7.5 μM cisplatin (**Figures 3.16A** and **3.16C**). Oxaliplatin showed negligible growth inhibition against AB1157 (**Figure 3.16B**), and concentration-dependent growth inhibition of the Δ*recG* Δ*ruvC* mutant with the turbidity almost reduced to the baseline value at 60 μM oxaliplatin (**Figure 3.16D**). These data align with the higher potency of cisplatin than oxaliplatin against *E. coli*. Moreover, the enhanced susceptibility of the Δ*recG* Δ*ruvC* mutant to oxaliplatin compared to the parent strain suggested that the recombination pathway is also important for bacterial survival after oxaliplatin treatment, presumably through repairing the DNA damage caused by oxaliplatin.

The results for L/D-EP and L/D-EOP followed similar trends. For the cisplatin conjugates, *E. coil* AB1157 was not inhibited by L-EP and was partially inhibited by D-EP (**Figure 3.16A**). Conversely, the Δ*recG* Δ*ruvC* mutant was fully killed after treatment with ≥7.5 μM L/D-EP (**Figure 3.16C**). The oxaliplatin conjugates L/D-EOP showed negligible inhibition against *E. coli* AB1157; however, the Δ*recG* Δ*ruvC* mutant was inhibited slightly by L-EOP and to a much greater extent by D-EOP (turbidity reduction by 8% or >90% after treatment with 15 μM L- or D-EOP, respectively) (**Figures 3.16B** and **3.16D**). These results show that the antibacterial activities of

L/D-EP and L/D-EOP can be countered by recombination. Since recombination is one of the DNA repair pathways responsible for managing the DNA damage, our data indicate that all four conjugates cause DNA damage. The increased susceptibility of *E. coil* AB1157 and its recombinant-deficient mutant to L/D-EP compared to L/D-EOP suggest that L/D-EP-induced DNA damage is more severe compared to L/D-EOP-induced DNA damage, which is consistent with our analyses above using lysogenic *E. coli* and a plasmid-borne reporter.

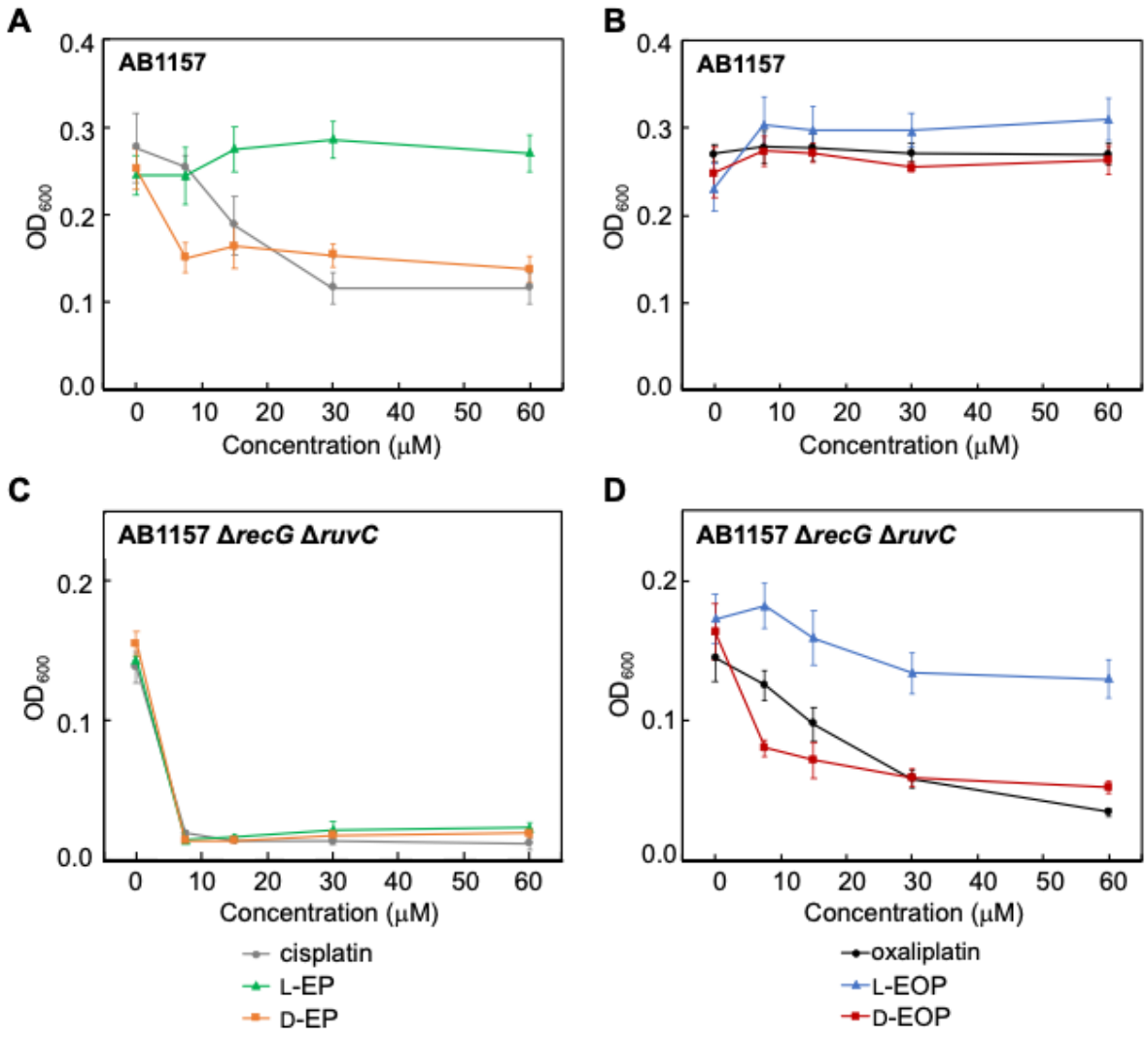

Figure 3.16. Susceptibility of *E. coli* AB1157 to **(A)** cisplatin and L/D-EP and **(B)** oxaliplatin and L/D-EOP; *E. coli* AB1157 Δ*recG* Δ*ruvC* to **(C)** cisplatin and L/D-EP and **(D)** oxaliplatin and L/D-EOP. All assays were performed in modified M9 medium (11 h, 30 °C, 500 rpm; mean ± standard deviation; n ≥ 4).

3.5 Discussion

In this study, we report two novel Ent–Pt(IV) conjugates harboring an oxaliplatin-based Pt(IV) prodrug, further expanding the scope of SAC-based drug repurposing and Pt cargos that can be selectively delivered into the *E. coli* cytoplasm by the Ent uptake machinery. Notably, D-EOP showed enhanced antibacterial activity compared to oxaliplatin and L-EOP, which we attribute to enhanced uptake due to the siderophore combined with the blocked release of Fe by cytoplasmic Ent esterases. Compared to the cisplatin conjugates L/D-EP, L/D-EOP exhibit lower antibacterial activity, which we largely attribute to the lower potency of oxaliplatin compared to cisplatin.

Motivated to gain further insight into the antibacterial activity and cellular fates of Pt agents in *E. coli*, we investigated the consequences of cisplatin, oxaliplatin, L/D-EOP, and L/D-EP treatment on indicators of DNA damage. We analyzed the abilities of these compounds to induce the lytic cycle in a lysogenic bacterial strain, determined DNA damage levels by measuring the SOS response using an in-cell reporter system and evaluated the susceptibility of an *E. coli* DNA repair mutant to these Pt complexes. Our data present compelling evidence that cisplatin and L/D-EP cause more DNA damage compared to oxaliplatin and L/D-EOP, which correlates with the higher antibacterial activities of cisplatin and L/D-EP.

The lesser degree of DNA damage in *E. coli* induced by oxaliplatin and L/D-EOP in our studies is consistent with analyses by others focused on oxaliplatin as an anticancer agent in eukaryotic cells. A study showed that oxaliplatin exhibits slower DNA binding kinetics and less Pt–DNA adduct formation on a model oligonucleotide compared to cisplatin,[63] a result that could be rationalized based on the slow dissociation of the oxalate ligand in oxaliplatin, which presumably delays aquation of the Pt center and therefore biomolecular cross-linking.[64-65]

Moreover, these observations were recapitulated in human A549 cells where oxaliplatin treatment resulted in significantly less binding to cellular DNA than cisplatin.[63] It was also reported that eukaryotic DNA polymerases bypass oxaliplatin-GG adducts more efficiently than cisplatin-GG adducts.[66] Recent investigations probing the distinct spectrum of antitumor activity of oxaliplatin provided evidence for an alternative mode of cytotoxicity against human cells, involving the disruption of ribosome biogenesis and induction of the nucleolar stress response.[40, 63, 65] Moving forward, we expect that studies of the current and future Ent–Pt(IV) conjugates will provide design principles for new repurposed antibiotic warheads and rekindle interest in the physiological consequences of Pt on bacteria. Indeed, the antibacterial activity of various Pt-based anticancer agents and the Ent–Pt(IV) conjugates described in this work against other bacterial pathogens warrant further investigation.

3.6 Conclusion

The successful targeting of Ent–Pt(IV) conjugates harboring cisplatin and oxaliplatin to *E. coli* illustrates the potential of siderophore-based drug repurposing and deepens our understanding of the antibacterial activity of these conjugates. Specifically, this work demonstrates a link between the antibacterial activity of Ent–Pt(IV) and the intrinsic potency of the Pt warhead. Moreover, by probing DNA damage, this work indicates that at least some observations from studies in human cells are recapitulated in bacteria cells and reveals a correlation between the antibacterial activity of Ent–Pt(IV) conjugates and their ability to cause DNA damage in *E. coli*. Collectively, these findings provide motivation for the future design and investigation of other siderophore-based Pt antibacterials. Such investigations are essential for exploring the therapeutic potential of Pt compounds in combating bacterial infections.

3.7 Experimental section

Instrumentation

High-performance liquid chromatography (HPLC). Semi-preparative and analytical HPLC were performed by using an Agilent 1200 series HPLC system outfitted with an Agilent Zorbax C18 column (5 μm, 9.4 × 250 mm) at a flow rate of 4 mL/min and a Clipeus C18 column (5 μm, 4.6 × 250 mm; Higgins Analytical, Inc.) at a flow rate of 1 mL/min, respectively. Preparative HPLC was performed by using an Agilent PrepStar system outfitted with a Phenomenex Luna C18 column (10 μm, 21.2 × 250 mm) at a flow rate of 10 mL/min. The multiwavelength detectors were set to read the absorbance at 220, 280, and 316 (catecholate absorption) nm.

Solvent A was Milli-Q water (18.2 MΩ·cm, (18.2 MΩ·cm, 0.22-μm filter) with trifluoroacetic acid (TFA, purchased from Millipore Sigma) that was filtered through a 0.2-μm bottle-top filter before use. Solvent B was HPLC grade acetonitrile (MeCN, purchased from Millipore Sigma) with TFA. The amount of TFA in each eluent is indicated in the synthetic procedures. Each HPLC method began with a four-minute equilibration at 0% B followed by a gradient of increasing %B. For analytical HPLC performed to evaluate conjugate purity, the entire portion of each HPLC-purified compound was dissolved in a mixture of 1:1 H_2O/MeCN, an aliquot was taken for HPLC analysis, and the remaining solution was subsequently frozen and lyophilized to dryness.

Liquid chromatography/mass spectrometry (LC/MS). LC/MS was performed using a nominal mass Agilent 6125B mass spectrometer with an electrospray (ESI) source attached to an Agilent 1260 Infinity LC. High-resolution mass spectrometry was performed using a high-resolution Agilent 6545 mass spectrometer with a Jet Stream ESI source coupled to an Agilent

Infinity 1260 LC system. For all LC/MS analyses, solvent A was 0.1% formic acid/H_2O and solvent B was 0.1% formic acid/MeCN (LC/MS grade MeCN, Millipore Sigma). The samples were analyzed using a solvent gradient of 5–95% B over 6 min with a flow rate of 0.4 mL/min. All LC/MS instruments are housed in the MIT Department of Chemistry Instrumentation Facility (DCIF).

Inductively coupled plasma-mass spectrometry (ICP-MS). Metal analysis was conducted using an Agilent 7900 ICP-MS system in helium mode outfitted with an integrated autosampler housed in the Center for Environmental Health Sciences (CEHS) Bioanalytical Core Facility at MIT. To quantify Fe concentration, the instrument was calibrated using standards prepared by serial dilution of an environmental calibration standard solution (1000 ppm each of Ca, Fe, K, Mg, Na; 10 ppm each of Ag, Al, As, Ba, Be, Cd, Co, Cr, Cu, Mn, Mo, Ni, Pb, Sb, Se, Th, Tl, U, V, Zn; Agilent, part number 5183-4688). To quantify Pt concentration, the instrument was calibrated using standards prepared by serial dilution of a Pt standard solution (1 ppm Pt; Millipore Sigma). Terbium (1 ppb Tb; Agilent) was used as an internal standard. All samples were prepared as 2 mL solutions in 5% HNO_3 (Honeywell, TraceSELECT; 69.0%) in 5 mL centrifuge tubes, transferred to ICP-MS polypropylene vials (Agilent) and analyzed.

For whole-cell metal analyses of *Escherichia coli* cells or HEK293T cells, cell pellets diluted into solutions of 3% HNO_3 were liquefied using a Milestone UltraWAVE digestion system housed in the CEHS Core Facility at MIT. A standard microwave protocol (15 min ramp to 200 °C at 1,500 W power; 10 min ramp to 220 °C at 1,500 W power) was used for the acid digestion.

NMR spectroscopy. ^1H NMR spectra were collected on a two-channel Bruker Avance-III HD Nanobay 400 MHz spectrometer, a three-channel Bruker Avance Neo 500 MHz spectrometer, or a four-channel Bruker Avance Neo 600 MHz spectrometer (both 400 MHz and 500 MHz

spectrometers are equipped with a 5 mm liquid-nitrogen cooled Prodigy broad band observe cryoprobe; the 600 MHz spectrometer is equipped with a 5 mm helium-cooled QCI-F cryoprobe). ^{195}Pt NMR and 2-dimentional (2D) NMR spectra were collected on a three-channel Bruker Avance Neo 500 MHz spectrometer (equipped with a 5 mm BBFO SmartProbe) at ambient probe temperature (293 K). All NMR spectrometers are housed in the MIT DCIF.

Optical absorption spectroscopy. Optical absorption spectra were recorded on a Beckman Coulter DU800 spectrophotometer (1 cm quartz cuvettes, Starna) and used to determine concentrations of Ent stock solutions (*vide infra*).

Microscopy. Bright-field and fluorescence microscopy imaging were carried out using a Zeiss Axioplan2 upright microscope equipped with a 100× oil-immersion objective lens. Bright-field images were acquired using the Trans_DIC channel. All microscopy equipment is housed in the W. M. Keck Microscopy Facility at Whitehead Institute. For LIVE/DEAD cell viability assays, the Texas Red (λ_{ex} = 532–587 nm; λ_{em} = 608–683 nm) and GFP (λ_{ex} = 457–487 nm; λ_{em} = 502–538 nm) channels were used to acquire images of the DEAD (red) and LIVE (green) cells, respectively.

Synthesis

General synthetic methods. Anhydrous *N*,*N*-dimethylformamide (DMF), dichloromethane (DCM), and dimethyl sulfoxide (DMSO) were purchased from Millipore Sigma and used as received. All other chemicals were purchased from Millipore Sigma, VWR, TCI chemicals, or Alfa Aesar in the highest available purity and used as received.

Supelco TLC silica gel 60 matrix plates with fluorescent indicator were used for analytical thin layer chromatography. Supelco PLC silica gel 60 matrix plates with fluorescent indicator of

2-mm thickness were used for preparative TLC. Sigma-Aldrich silica gel (70–230 mesh, 60 Å) was used for flash column chromatography.

Ent and L/D-Ent-PEG$_3$-N$_3$ **6,7**, and L/D-EP **1,2** were synthesized following published procedures.[16-17, 21, 67] *t*-[Pt(DACH)(ox)(OAc)(OH)] (DACH = *trans*-(1*R*,2*R*)-1,2,diaminocyclohexane, ox = oxalato) was synthesized following based on the reported procedure for *c, c, t*-[Pt(NH$_3$)$_2$Cl$_2$(OAc)(OH)].[21]

Synthesis of *t*-[Pt(DACH)(ox)(OAc)(OOCCH$_2$CH$_2$C≡CH)] (denoted hereafter as oxPt(IV)-alkyne 5). The synthesis of oxPt(IV)-alkyne **5** was performed based on reported procedures.[21] *t*-[Pt(DACH)(ox)(OAc)(OH)] (41 mg, 0.087 mmol) was suspended in anhydrous DMF (4 mL). 4-Pentynoic acid (34 mg, 0.35 mmol) was dissolved in anhydrous DMF (800 μL) and combined with *N*,*N*′-dicyclohexylcarbodiimide (DCC, 75 mg, 0.36 mmol). The mixture was placed in an ultrasonic bath for 15 min, during which time a white precipitate formed. The mixture was centrifuged (4,500 rpm, 15 min, room temperature), and the supernatant was added slowly to the above suspension. The reaction was purged with N$_2$ and stirred in the dark at room temperature for 16 h, resulting in a clear yellow solution. The reaction mixture was concentrated by air stream to yield a yellow oil, which was diluted with 1:1 H$_2$O/MeCN, filtered through a 0.45 μm PTFE filter (purchased from VWR), and purified by preparative HPLC (0–100% B over 30 min, 10 mL/min, 0.1% TFA in solvents A and B). The eluate from 15.6–16.6 min was collected and lyophilized to give the pure product as a white powder (29 mg, 61% yield). MS (ESI+): $[M+H]^+$ calcd. 554.1097, exptl. 554.1096. $[M+Na]^+$ calcd. 576.0917, exptl. 576.0915. ^{1}H NMR (500 MHz, D$_2$O): δ 2.82 (m, 2H), 2.50 (m, 2H), 2.36 (m, 2H), 2.21–2.23 (m, 3H), 1.99 (s, 3H), 1.46–1.58 (d, *J* = 9.7 Hz, 4H), 1.18 (m, 2H). ^{13}C NMR (500 MHz, D$_2$O): δ 181.7, 181.3, 166.4, 83.9, 69.9, 62.0, 61.3, 34.6, 30.8, 23.4, 22.1, 14.6. ^{195}Pt NMR (500 MHz, D$_2$O): *δ* 1577.15.

Synthesis of L-Ent-oxPt(IV) (L-EOP 3). L-EOP was first synthesized based on the report procedure for L-EP,[21] affording a yield of ~5% following HPLC purification. To optimize the conjugation reaction, another two CuAAC methods were tested but did not yield the conjugates as expected, including $CuBr(PPh_3)_3$ and in situ generation of Cu(I) by incubating $Cu(OAc)_2$ in *tert*-BuOH.[68-69] Multiple reaction conditions were tested, and two most effective methods are described below. The second method using $CuSO_4$+NaAsc afforded the highest yield at 41%.

Method 1. $Cu(MeCN)_4PF_6$. L-Ent-PEG_3-N_3 **6** (32 μL of a 17 mM solution in DMF, 0.55 μmol) and oxPt(IV)-alkyne **5** (121 μL of a 9.0 mM solution in DMF, 1.1 μmol) were combined, to which 63.5 μL of DMF was added. TBTA (11 μL of a 50 mM solution in DMF, 0.55 μmol) was added to the azide/alkyne mixture, followed by the addition of $Cu(MeCN)_4PF_6$ (11 μL of a 50 mM solution in DMF, 0.55 μmol). The resulting solution was briefly mixed by a vortex mixer and incubated on a benchtop rotator at room temperature in the dark. After 6 h, the reaction mixture was diluted with 1:1 MeCN:water and purified by preparative HPLC (0–100% B over 30 min, 10 mL/min, 0.005% TFA was used in solvents A and B; this low percent TFA was used to prevent decomposition). The eluant at 21.3 min was collected, flash frozen in liquid N_2, and lyophilized, which afforded L-EOP as a white powder (~4.9 mg, 16%).

Method 2. $CuSO_4$+NaAsc.[17, 19-20] L-Ent-PEG_3-N_3 **6** (73 μL of an 11.3 mM solution in DMF, 0.83 μmol) and oxPt(IV)-alkyne **5** (50 μL of a 50 mM solution in DMF, 2.5 μmol) were combined, to which 100 μL of DMF was added. An aliquot of $CuSO_4$ (50 μL of a 90 mM solution in water, 4.5 μmol) and TBTA (100 μL of a 50 mM solution in DMF, 5.0 μmol) were combined to give a blue solution, to which sodium ascorbate (NaAsc, 100 μL of a 90 mM solution in water, 9.0 μmol) was added. The color of the solution immediately changed from blue to pale yellow indicating reduction of Cu(II) to Cu(I) and the mixture was added to the alkyne/azide mixture. The

reaction was incubated on a benchtop rotator for 20 min in the dark at room temperature. Then, the reaction mixture was diluted with 1:1 MeCN:water and purified by preparative HPLC (0–100% B over 40 min, 10 mL/min; 0.005% TFA was used in solvents A and B to prevent decomposition). The eluate at 24.9 min was collected, flash frozen in liquid N_2, and lyophilized, affording L-EOP as a white powder (0.5 mg, 41%).

HRMS (ESI+): $[M+H]^+$ calcd, 1468.3729; found, 1468.3726. ^{1}H NMR (500 MHz, DMSO_d$_6$): δ 11.91 (s, 1H), 11.62 (s, 2H), 9.73 (s, 1H), 9.42 (s, 2H), 9.29 (d, 1H, *J* = 6.9 Hz), 9.10 (d, 2H, *J* = 7.1 Hz), 8.18–8.43 (m, 5H), 7.93 (d, 1H, *J* = 2.2 Hz), 7.76 (s, 1H), 7.45 (d, 1H, *J* = 2.2 Hz), 7.35 (d, 2H, *J* = 8.1 Hz), 6.97 (d, 2H, *J* = 9.0 Hz), 6.75 (t, 2H, *J* = 8.1 Hz), 4.92 (m, 3H), 4.66 (m, 3H), 4.44 (t, 2H, *J* = 5.4 Hz), 4.41 (m, 3H), 3.78 (t, 2H, *J* = z, 3H), 1.49 (d, 2H, *J* = 10.0 Hz), 1.37–1.43 (m, 2H), 1.13–1.19 (m, 2H). ^{195}Pt signal was detected by ^{1}H-^{195}Pt HMQC NMR (500 MHz, DMSO_d$_6$): δ 1111.71 (s).

D-Ent-oxPt(IV) (D-EOP, 4). D-EOP **4** was synthesized as described for L-EOP **3** (Method 2. $CuSO_4$+NaAsc), except that D-Ent-PEG$_3$-N$_3$ **7** was employed instead of L-Ent-PEG$_3$-N$_3$ **6**, affording a yield of 31%.

HRMS (ESI+): $[M+H]^+$ calcd, 1468.3729; found, 1468.3727. ^{1}H NMR (500 MHz, DMSO_d$_6$): δ 11.91 (s, 1H), 11.62 (s, 2H), 9.73 (s, 1H), 9.42 (s, 2H), 9.29 (d, 1H, *J* = 6.9 Hz), 9.10 (d, 2H, *J* = 7.1 Hz), 8.18–8.43 (m, 5H), 7.93 (d, 1H, *J* = 2.2 Hz), 7.76 (s, 1H), 7.45 (d, 1H, *J* = 2.2 Hz), 7.35 (d, 2H, *J* = 8.1 Hz), 6.97 (d, 2H, *J* = 9.0 Hz), 6.75 (t, 2H, *J* = 8.1 Hz), 4.92 (m, 3H), 4.66 (m, 3H), 4.44 (t, 2H, *J* = 5.4 Hz), 4.41 (m, 3H), 3.78 (t, 2H, *J* = z, 3H), 1.49 (d, 2H, *J* = 10.0 Hz), 1.37–1.43 (m, 2H), 1.13–1.19 (m, 2H). ^{195}Pt signal was detected by ^{1}H-^{195}Pt HMQC NMR (500 MHz, DMSO_d$_6$): δ 1111.71 (s).

Storage and handling of Ent and Ent-oxPt(IV) conjugates

All synthetic precursors, Ent and L/D-EOP were stored as either powders or DMSO stock solutions at -20 °C. Concentrations of Ent stock solutions (~10 mM) were determined using Beer's law and the reported extinction coefficient for apo Ent in MeOH (ε_{316} = 9500 M^{-1} cm^{-1}).[70] An aliquot of the DMSO stock solution was diluted into MeOH for this analysis. Concentrations of L/D-EOP stock solutions were determined by quantifying Pt concentration using ICP-MS. The stock solution concentrations were 5–12 mM. To minimize multiple freeze–thaw cycles, all stock solutions were divided into 10 μL aliquots and stored at -80 °C. Aliquots were routinely analyzed by analytical HPLC to confirm the integrity of the samples. Multiple synthetic batches of L/D-EOP were employed throughout this work.

Stability evaluation of D-EOP

The DMSO stock solution of D-EOP was diluted in 260 μL of modified M9 medium (Na_2HPO_4 6.8 g/L, KH_2PO_4 3 g/L, NaCl 0.5 g/L, NH_4Cl 1 g/L, 0.4% glucose, 0.2% casein amino acids, 2 mM $MgSO_4$, 0.1 mM $CaCl_2$, 0.6 μg/mL thiamine) to afford a 30 μM D-EOP solution. The resulting mixture was divided into five 50 μL aliquots. The aliquots were incubated at 30 °C with shaking at 150 rpm in the dark for 0, 2, 5, 10, and 20 h, respectively. At each time point, an aliquot was flash frozen in liquid N_2 and then stored at -80°C. Analytical HPLC samples were prepared by thawing each sample and centrifuging the sample (13,000 rpm and 4 °C for 10 min). The resulting supernatants were analyzed by analytical HPLC (0–100 B% in 30 min, 1 mL/min, 0.005%TFA in solvents A and B). The percent of remaining D-EOP at each time point was determined by integrating the peak area of D-EOP in each sample. Decomposition products were

analyzed by LC/MS. The results from this study are described in Section **3.8, Supporting Discussion.**

Molecular biology methods

Construction of *E. coli pSulAp_lacZ*. To make the plasmid *pSulAp_lacZ*, a plasmid backbone derived from *pBAD-HisA* (purchased from Invitrogen) was first prepared. *pBAD-HisA* (50 ng/μL) was double digested by incubation with NdeI (1 U/μL) and HindIII-HF (1 U/μL) in 20 μL 1X Cutsmart buffer for 2.5 h before the enzymes were heat inactivated by incubation at 80 °C for 1 h on a heating block. The linearized plasmid was then amplified with overhangs (containing part of the *sulA* promoter) with primers pBAD_HindIII-f and pBAD_sulAp-r using Q5 polymerase following the manufacturer's instructions (**Table 3.2**). The amplicon was purified using the PCR Cleanup Kit from Qiagen following the manufacturer's instructions. To prepare the *lacZ* fragment, *lacZ* with overhangs was amplified from *E. coli* MG1655 gDNA (purified using the Wizard Genomic DNA Purification Kit from Invitrogen) with the primers sulAp-lacZ-f and pBAD_lacZ-r (**Table 3.2**) using Q5 polymerase. The amplicon was then purified using the Qiagen PCR Cleanup Kit. The two purified fragments were then ligated together in 1:1 molar ratio (50 ng of the *pBAD* fragment) using the NEB HiFi DNA Assembly Mix in a 10 μL reaction volume. The isothermal reaction proceeded at 50 °C for 2.5 h in a thermocycler. All 10 μL of the reaction mixture was then used to transform a 200 μL aliquot of chemically competent *E. coli* TOP10 cells. The isothermal reaction mixture was incubated with the cells on ice for 30 minutes before the cells were heat shocked at 42 °C for 30 s. The cells were then incubated on ice for 5 minutes before 700 μL LB was added, and the cells were rescued for 40 minutes at 37 °C with shaking on an orbital shaker (250 rpm). Cells were then pelleted via centrifugation, resuspended in ~150 μL LB, and

plated onto LB-agar supplemented with 100 μg/mL ampicillin. The plates were incubated at 37 °C for ~15 h. Colonies were picked and screened for ligated plasmid by colony PCR using the sulAp-lacZ-f/pBAD_lacZ-r primer pair and analysis via 1% agarose gel electrophoresis. Hits were cultivated in LB supplemented with 100 μg/mL ampicillin for 12 h at 37 °C on an orbital shaker (250 rpm), the plasmid was purified using the Qiagen Miniprep Kit, and the fidelity of the promoter region was verified by Sanger sequencing (Quintara Biosciences). *E. coli* JW0334 *pSulAp_lacZ* was constructed by transforming chemically competent *E. coli* JW0334 (the Δ*lacY* mutant from the Keio Collection)[47] with *pSulAp_lacZ* via heat shock at 42 °C for 30 s.

Table 3.2. Synthetic oligonucleotides used for molecular cloning.[a]

Name	Sequence (5′ to 3′)
sulAp-lacZ-f	ggatgtactgtacatccatacagtaactcaccaggaggaattaaccATGACCATGATTACGGATTCAC
pBAD_lacZ-r	ttctctcatccgccaaaacagccaagcttTTATTTCTGACACCAGACCAAC
pBAD_HindIII-f	AAGCTTGGCTGTTTTGG
pBAD_sulAp-r	tgagttactgtatggatgtacagtacatccagtgacaacaaagatcaacccAGACGGTCACAGCTTG

[a] The sequences are shown from the 5′ to 3′. Overhangs for isothermal assembly are shown in lowercase letters.

Microbiology, microscopy, and cell culture methods

General materials. Lysogeny broth (LB; tryptone 10 g/L, yeast extract 5 g/L, NaCl 10 g/L), M9 minimal salts 5×, casamino acids, and agar were purchased from Becton Dickinson (BD). LB medium and Milli-Q water (18.2 MΩ·cm, 0.22-μm filter) used for bacterial cultures or for preparing working solutions of the tested compounds were sterilized in an autoclave. Modified M9 medium was sterilized by passage through a sterile 0.22-μm filter. Sterile polypropylene culture

tubes and adhesive PCR film seals were purchased from VWR. Sterile polystyrene 96-well plates and 6-well plates used for culturing were purchased from Corning Incorporated. LIVE/DEAD BacLight Bacterial Viability Kits were purchased from Thermo Fisher (Invitrogen Molecular Probes). Agarose (PCR grade) for microscopy was purchased from Bio-Rad. Microscope slides and microscope cover glasses were purchased from VWR. Cisplatin (≥99.9% trace metals basis) and $Fe(acac)_3$ (≥99.9% trace metals basis) were purchased from Sigma-Aldrich. Oxaliplatin (98%) was purchased from AmBeed. Synthetic oligonucleotides were purchased from IDT. Enzymes and buffers used for molecular cloning were purchased from NEB.

Bacterial strains. Bacterial strains employed in this study are summarized in **Table 3.3**. Freezer stocks were prepared from single colonies in 25% glycerol/LB medium.

Table 3.3. Bacterial strains employed in this study.[18, 47]

Strain	Relevant characteristics or genotype	Source
E. coli K12 BW25113	Common lab strain, non-pathogenic, derivative of K12	[47]
E. coli JW5086	*E. coli* K12 BW25113 Δ*fepA*	[47]
E. coli CFT073	Clinical isolate, UPEC	ATCC 700928
E. coli MSC 216	CFT073 Δ*fepA*::kan Δ*iroN*::*tetRA* (Kan^R Tet^R)	[18]
E. coli MSC 228	CFT073 Δ*fepC*::kan (Kan^R)	[18]
E. coli W3104	Lysogenic for bacteriophage λ	Carolina Biological
E. coli JW0334 *pSulAp_lacZ*	*E. coli* strain used for reporter assay: *E. coli* JW0334 carrying *pSulAp_lacZ*	This study
E. coli AB1157	K12 derivative; *thr-1 ara-14 leuB6–(gpt-proA)62 lacY1 tsx-33 glnV44(AS) galK2(Oc) hisG4(Oc)rfbD1 mgl-51 rpoS396(Am) rpsL31(StrR)kdgK51 xylA5 mtl-1 argE3(Oc) thi-1*	[62]
E. coli N3398	As AB1157 but Δ*recG258*::Kan Δ*ruvC53 eda51*::Tn*10*	[62]

General procedures for bacterial growth assays and microscopy. Growth of *E. coli* under Fe-deficient conditions was performed in a modified M9 medium. The Fe content of the modified M9 medium was determined by ICP-MS to be 0.6–0.7 μM Fe. These Fe-deficient conditions cause *E. coli* to express siderophore biosynthesis and transport machinery, including genes for enterobactin biosynthesis and transport encoded by the enterobactin gene cluster as well as the *iroA* cluster for salmochelin biosynthesis and transport.[21]

Working solutions of L/D-EOP were prepared via dilutions in 10% DMSO/H_2O. Working solutions of oxaliplatin were freshly prepared by dissolving oxaliplatin in modified M9 medium

before treatment. The Fe(III)-bound L/D-EOP complexes were prepared before all microbiology and imaging assays because the modified M9 medium contains insufficient Fe to fully complex the siderophore following addition to the culture. $Fe(acac)_3$ (13 mM stock in DMSO, concentration determined by ICP-MS) was used to prepare the Fe(III) complexes, which were formed by incubating 10 μL of L/D-EOP working solution with 0.9 μL of a 10× $Fe(acac)_3$ solution in 10% DMSO/H_2O for 5 min prior to addition to the culture. We note that L/D-EOP refer to the corresponding ferric complexes in the discussion of the biological assays. For all microbiology assays, the final cultures contained 1% v/v DMSO, except for cultures with oxaliplatin treatment which do not contain DMSO.

Overnight cultures of *E. coli* were prepared in 15 mL polypropylene tubes by inoculating 5 mL of medium with the appropriate freezer stock. The overnight cultures were incubated at 37 °C for 16–18 h in a tabletop incubator set at 150 rpm. Each overnight culture was diluted 1:100 into 5 mL of fresh medium at 37 °C with shaking at 250 rpm A30 °C with shaking at 500 rpm for 20 h in the BioTek LogPhase 600 (LP600) microbiology reader (96-well plate format). Growth curves were recorded as OD_{600} values collected every hour in the LP600 microbiology reader. Growth assays of L/D-EOP were performed using a two-fold dilution series spanning 0–60 μM. Each well condition was prepared in duplicate and at least four independent replicates using two synthetic batches of each conjugate and were performed on different days. The resulting mean OD_{600} values are reported, and the error bars are the standard deviation from the independent replicates. Statistical differences compared to untreated controls were calculated using two-tailed student *t* test assuming unequal variances.

Samples for microscopy were prepared by taking aliquots of *E. coli* culture at t = 11 h (mid-log phase). For samples that require only bright-field imaging, a 5 μL aliquot of each culture was

pipetted on an agarose pad (1% w/w agarose/Milli-Q water) which was placed on a microscope slide. The sample was then covered with a glass coverslip. Representative micrographs for each condition are shown in the figures. For LIVE/DEAD viability assays, a 90 μL aliquot of each bacterial culture was centrifuged at 3,000 rpm at 4 °C for 15 min. The resulting cell pellet was resuspended in 0.85% NaCl and the OD_{600} was adjusted to 0.2 using 0.85% NaCl. A 25 μL aliquot of each bacterial suspension was incubated with 25 μL of LIVE/DEAD dye mixture (48 μM SYTO9 and 240 μM propidium iodide) at 30 °C for 15 min in the dark, and 5 μL of the suspension was pipetted on an agarose pad which was placed on a microscope slide. The sample was then covered with a glass coverslip. For each type of microscopy experiment, each condition was repeated in at least three biological replicates using two different synthetic batches. Representative micrographs for each condition are shown in figures.

We selected 11 h as the time point to determine inhibitory effects and morphological changes because of the following considerations described previously:[21] (i) the 11 h time point is in the mid-log phase of bacterial growth as determined by growth curves; (ii) there is sufficient cell density to determine growth inhibitory effects and have sufficient cells to image; (iii) initial microbiology studies indicated that the stability of L/D-EOP under these conditions was sufficient for our studies.

Image analysis. The microscopy images were processed using the FIJI software (8-bit image type). For bright-field images, contrast enhancement was performed by setting saturated pixels as 0.1%. For fluorescence images, fluorescence background subtraction was performed using a rolling ball method with a radius of 150 pixels.

Induction of lysogenic bacteria. The induction of lysogenic bacteria was performed based on a published procedure.[27] *E. coli* W3104 was inoculated in 5 mL of modified M9 medium and

grown for 18 h at 37 °C with shaking. A 50 μL aliquot of the overnight culture was diluted in 5 mL of modified M9 medium, which was then incubated at 37 °C until the OD_{600} reached 0.6 (~7 h). Then, 0.5 μL aliquots of bacterial culture were added to 100 μL portions of modified M9 medium containing 0 (untreated), 7.5, 15 and 30 μM oxaliplatin in a 96-well plate. After incubation at 30 °C for 10 h, each culture was diluted 1:10, 1:100, and 1:1000, and 10 μL of each diluted culture was spotted onto an LB agar plate on which a lawn of *E. coli* CFT073 had been freshly plated. After spotting, the plate was incubated at 37 °C for 12 h to allow plaque formation. To test the effect of L/D-EOP, 0.5 μL aliquot of exponentially growing *E. coli* W3104 culture was then incubated in 100 μL of the modified M9 medium which contained 15 μM L/D-EP, 15 μM L-Ent, or 1% DMSO, respectively.

The *E. coli* CFT073 lawn was prepared by inoculating 4 mL of molten top agar (0.5% LB agar) with 100 μL of an overnight culture of *E. coli* CFT073 grown in LB medium. Following gentle mixing, 3 mL of the inoculated molten top agar was layered atop a preheated (37 °C) LB agar plate and allowed to solidify.

Pt uptake by *E. coli*. *E. coli* CFT073 or *E. coli* JW0334 *pSulAp_lacZ* was inoculated in 5 mL of modified M9 medium and grown for 18 h at 37 °C. A 50 μL aliquot of the overnight culture was diluted in 5 mL of modified M9 medium, which was then incubated at 37 °C until the OD_{600} reached 0.6. A 4 mL portion of the culture was centrifuged at 3,500 rpm and 4°C for 10 min, and the resulting cell pellet was resuspended in 1 mL of fresh modified M9 medium. Then, to a 90 μL aliquot of the diluted culture, a 10 μL aliquot working solution of 10 μM L-EOP, D-EOP, or oxPt(IV)-alkyne **5** (in 10% DMSO/H_2O) was added. After incubation at 30 °C with shaking at 150 rpm for 30 min, cell pellets were harvested by centrifuging each culture at 3,500 rpm and 4°C for 10 min. To measure the Pt content in the supernatant, 90 μL of each supernatant was diluted into

1.91 mL of 5% HNO_3 for ICP-MS analysis. To measure the cell-associated Pt content, the cell pellets were first washed with fresh modified M9 medium, and then washed with fresh modified M9 containing 2% w/w aqueous EDTA. The resulting cell pellets were suspended in 2 mL of 5% HNO_3 and digested for ICP-MS analysis. Mass of cell-associated Pt and mass of Pt in the supernatant of each sample were calculated using Pt concentrations determined by ICP-MS. Cell-associated Pt% was determined according to equation 3.1.

$$\text{Cell-associated Pt\%} = \frac{\text{mass of cell-associated Pt (μg)}}{\text{mass of cell-associated Pt (μg) + mass of Pt in the supernatant (μg)}} \qquad \text{(eq 3.1)}$$

Pt uptake by HEK293T cells. Materials for tissue culture were kindly provided by the Shoulders lab at MIT. HEK293T cells were purchased from ATCC. DMEM was purchased from Corning Incorporated. Penicillin and streptomycin were purchased from Corning Incorporated.

HEK293T cells (passages 10–20) were plated at a density of 750,000 cells per well in a 6-well plate (2.5 mL/well) in DMEM supplemented with 1% penicillin/streptomycin and incubated at 37 °C and 5% CO_2 for 24 h. Working solutions of L-EOP and D-EOP (6 μM) were prepared in 10% DMSO/PBS (PBS purchased from Millipore Sigma). Working solutions of oxaliplatin were freshly prepared by dissolving oxaliplatin in PBS (6 μM) before treatment. Each working solution (0.5 mL) was added to each well of cell culture to give the final treatment concentration as 1 μM. Cells were treated for 6 h at 37°C and 5% CO_2, transferred to a 15 mL conical tube and centrifuged at 500 rcf and 4°C for 5 min. To measure the Pt content in the supernatant, 200 μL of each supernatant was diluted into 1.8 mL of 5% HNO_3 for ICP-MS analysis. To measure the cell-associated Pt content, cell pellets were washed with 2 mL of PBS three times, and the resulting cell pellets were suspended in 2 mL of 5%HNO_3 and digested for ICP-MS analysis. Mass of cell-

associated Pt and mass of Pt in the supernatant of each sample were calculated using Pt concentrations determined by ICP-MS. Cell-associated Pt% were determined by ICP-MS as described above (eq 1).

***E. coli* JW0334 *pSulAp_lacZ* reporter assay.**[71-73] *E. coli* JW0334 *pSulAp_lacZ* was grown to mid-log phase ($OD_{600} \approx 0.6$) in modified M9 medium at 37 °C. Culture aliquots (90 μL) were inoculated into the wells of sterile 96-well plates, and 10 μL of appropriately diluted compound stock was added to give the indicated final concentration. Plates were incubated at 30 °C with shaking for 30, 60, and 90 min, respectively. During growth, aliquots of 80 μL of permeabilization solution (25mM Na_2HPO_4, 50 mM KCl, 2 mM $MgSO_4$, 0.8 mg/mL hexadecyltrimethylammonium bromide (CTAB), 0.4 mg/mL sodium deoxycholate, 50 mM dithiothreitol) were added into another 96-well plates. Aliquots of 85.7 μL of substrate solution (60 mM Na_2HPO_4, 40 mM NaH_2PO_4, 1 mg/mL o-nitrophenyl-β-D-galactoside (ONPG, purchased from VWR), 0.8 mg/mL CTAB, 50 mM dithiothreitol) were added into another 96-well plates. The OD_{600} was measured using a BioTek Synergy HT plate reader, and a 20 μL of the culture was rapidly added to the 80 μL of permeabilization solution to give the sample solution. After the last sample solution was prepared, aliquots of 14.3 μL of sample solution were added to wells containing substrate solution and incubated at 30 °C with shaking. After 30-min incubation, aliquots of 100 μL of stop solution (1 M Na_2CO_3) were added. The plate was agitated and the A_{420} and A_{550} were recorded. β-Galactosidase activity was calculated using equation 3.2 as Miller units.

$$\text{β-Galactosidase activity} = \frac{1000 \times (A_{420} - 1.75 \times A_{550})}{OD_{600} \times \text{time (in min)} \times \text{volume (in mL)}} \qquad \text{(eq 3.2)}$$

3.8 Supporting Discussion

We selected D-EOP to perform the stability evaluation, and we expect similar results for the stability of L-EOP. Analytical HPLC revealed that apo D-EOP decomposed in the modified M9 medium with a $t_{1/2}$ ~ 5 h at 30 °C, which is in the same range as L-EP.[21] LC/MS analysis afforded *m/z* values of 1485.1 and 1262.1 for the major decomposition products after 5 h incubation, which correspond to the hydrolysis products of D-EOP where the Ent trilactone moiety was linearized by one or two or ester hydrolysis events, yielding linear D-EOP and $(DHBS)_2$-oxPt(IV) (*m/z* calcd. 1485.4 and 1262.3, respectively; DHBS, 2,3-dihydroxybenzoyl serine). Therefore, we moved forward using modified M9 medium with 0.6 μg/mL of thiamine and determining bacterial growth and morphology after 11 h treatment for all microbiology assays presented in this work. These are the same conditions that were used in prior studies of L/D-EP.[21]

We note that bacterial uptake of L/D-EOP hydrolysis products that contain the oxPt(IV) cargo and a hydrolyzed Ent moiety may also occur during the microbiology assays.

3.9 Acknowledgements

This work was supported by the 2018 Professor Amar G. Bose Research Grant. C.G received graduate student fellowship support from the Stephen J. Lippard Fellowship. NMR and MS instrumentation is housed by the MIT DCIF. The ICP-MS instrument is maintained by the MIT CEHS (NIH P30-ES002109). Instrumentation for bright-field and fluorescence microscopy instrumentation is housed by the W. M. Keck Microscopy Facility at Whitehead Institute. We thank Jessica E. Patrick for assistance with tissue culture. We thank Professor John Essigmann and Dr. Bogdan I. Fedeles for kindly providing the *E. coli* AB1157 and AB1157 Δ*recG* Δ*ruvC* strains.

We thank Professor Fang Wang for helpful discussions. We thank Wei Hao Lee for assistance with image analysis.

3.10 References

1. Prioritization of pathogens to guide discovery, research and development of new antibiotics for drug-resistant bacterial infections, including tuberculosis. World Health Organization: 2017.

2. Walsh, C.; Wencewicz, T., *Antibiotics: challenges, mechanisms, opportunities*. John Wiley & Sons: 2020.

3. Zgurskaya, H. I.; Löpez, C. A.; Gnanakaran, S., Permeability barrier of Gram-negative cell envelopes and approaches to bypass it. *ACS Infect. Dis.* **2015,** *1*, 512-522.

4. Hider, R. C.; Kong, X., Chemistry and biology of siderophores. *Nat. Prod. Rep.* **2010,** *27*, 637-657.

5. Weinberg, E. D., Nutritional immunity. Host's attempt to withold iron from microbial invaders. *J. Am. Med. Assoc.* **1975,** *231*, 39-41.

6. Weinberg, E. D., Iron availability and infection. *Biochim. Biophys. Acta.* **2009,** *1790*, 600-605.

7. Braun, V.; Pramanik, A.; Gwinner, T.; Köberle, M.; Bohn, E., Sideromycins: tools and antibiotics. *Biometals* **2009,** *22*, 3-13.

8. Thomas, X.; Destoumieux-Garzón, D.; Peduzzi, J.; Afonso, C.; Blond, A.; Birlirakis, N.; Goulard, C.; Dubost, L.; Thai, R.; Tabet, J.-C., Siderophore peptide, a new type of post-translationally modified antibacterial peptide with potent activity. *J. Biol. Chem.* **2004,** *279*, 28233-28242.

9. Nolan, E. M.; Fischbach, M. A.; Koglin, A.; Walsh, C. T., Biosynthetic tailoring of microcin E492m: post-translational modification affords an antibacterial siderophore–peptide conjugate. *J. Am. Chem. Soc.* **2007,** *129*, 14336-14347.

10. Vassiliadis, G.; Destoumieux-Garzón, D.; Lombard, C.; Rebuffat, S.; Peduzzi, J., Isolation and characterization of two members of the siderophore-microcin family, microcins M and H47. *Antimicrob. Agents Chemother.* **2010,** *54*, 288-297.

11. Palmer, J. D.; Mortzfeld, B. M.; Piattelli, E.; Silby, M. W.; McCormick, B. A.; Bucci, V., Microcin H47: a class IIb microcin with potent activity against multidrug resistant *Enterobacteriaceae*. *ACS Infect. Dis.* **2020,** *6*, 672-679.

12. Sassone-Corsi, M.; Nuccio, S.-P.; Liu, H.; Hernandez, D.; Vu, C. T.; Takahashi, A. A.; Edwards, R. A.; Raffatellu, M., Microcins mediate competition among Enterobacteriaceae in the inflamed gut. *Nature* **2016,** *540*, 280-283.

13. Vassiliadis, G.; Destoumieux-Garzón, D.; Peduzzi, J., Class II microcins. In *Prokaryotic antimicrobial peptides: from genes to applications*, Drider, D.; Rebuffat, S., Eds. Springer New York: New York, NY, 2011; pp 309-332.

14. Rayner, B.; Verderosa, A. D.; Ferro, V.; Blaskovich, M. A. T., Siderophore conjugates to combat antibiotic-resistant bacteria. *RSC Med. Chem.* **2023,** *14*, 800-822.

15. Loomis, L. D.; Raymond, K. N., Solution equilibria of enterobactin and metal-enterobactin complexes. *Inorg. Chem.* **1991,** *30*, 906-911.

16. Zheng, T.; Bullock, J. L.; Nolan, E. M., Siderophore-mediated cargo delivery to the cytoplasm of *Escherichia coli* and *Pseudomonas aeruginosa*: syntheses of monofunctionalized enterobactin scaffolds and evaluation of enterobactin–cargo conjugate uptake. *J. Am. Chem. Soc.* **2012,** *134*, 18388-18400.

17. Zheng, T.; Nolan, E. M., Enterobactin-mediated delivery of *β*-lactam antibiotics enhances antibacterial activity against pathogenic *Escherichia coli*. *J. Am. Chem. Soc.* **2014,** *136*, 9677-9691.

18. Neumann, W.; Sassone-Corsi, M.; Raffatellu, M.; Nolan, E. M., Esterase-catalyzed siderophore hydrolysis activates an enterobactin-ciprofloxacin conjugate and confers targeted antibacterial activity. *J. Am. Chem. Soc.* **2018,** *140*, 5193-5201.

19. Sargun, A.; Johnstone, T. C.; Zhi, H.; Raffatellu, M.; Nolan, E. M., Enterobactin- and salmochelin-β-lactam conjugates induce cell morphologies consistent with inhibition of penicillin-binding proteins in uropathogenic *Escherichia coli* CFT073. *Chem. Sci.* **2021,** *12*, 4041-4056.

20. Sargun, A.; Sassone-Corsi, M.; Zheng, T.; Raffatellu, M.; Nolan, E. M., Conjugation to enterobactin and salmochelin S4 enhances the antimicrobial activity and selectivity of *β*-lactam antibiotics against nontyphoidal *Salmonella*. *ACS Infect. Dis.* **2021,** *7*, 1248-1259.

21. Guo, C.; Nolan, E. M., Heavy-metal Trojan horse: enterobactin-directed delivery of platinum(IV) prodrugs to *Escherichia coli*. *J. Am. Chem. Soc.* **2022,** *144*, 12756-12768.

22. Rosenberg, B.; Van Camp, L.; Krigas, T., Inhibition of cell division in *Escherichia coli* by electrolysis products from a platinum electrode. *Nature* **1965,** *205*, 698-699.

23. Rosenberg, B.; Van Camp, L.; Grimley, E. B.; Thomson, A. J., The inhibition of growth or cell division in *Escherichia coli* by different ionic species of platinum(IV) complexes. *J. Biol. Chem.* **1967,** *242*, 1347-1352.

24. Monti-Bragadin, C.; Ramani, L.; Samer, L.; Mestroni, G.; Zassinovich, G., Effects of cis-dichlorodiammineplatinum(II) and related transition metal complexes on *Escherichia coli*. *Antimicrob. Agents Chemother.* **1975,** *7*, 825-827.

25. Rosenberg, B., Some biological effects of platinum compounds. *Platin. Met. Rev.* **1971,** *15*, 42-51.

26. Joyce, K.; Saxena, S.; Williams, A.; Damurjian, C.; Auricchio, N.; Aluotto, S.; Tynan, H.; Demain, A. L., Antimicrobial spectrum of the antitumor agent, cisplatin. *J. Antibiot.* **2010,** *63*, 530-532.

27. Johnstone, T. C.; Alexander, S. M.; Lin, W.; Lippard, S. J., Effects of monofunctional platinum agents on bacterial growth: a retrospective study. *J. Am. Chem. Soc.* **2014,** *136*, 116-118.

28. Chowdhury, N.; Wood, T. L.; Martínez-Vázquez, M.; García-Contreras, R.; Wood, T. K., DNA-crosslinker cisplatin eradicates bacterial persister cells. *Biotechnol. Bioeng.* **2016,** *113*, 1984-1992.

29. Yuan, M.; Chua, S. L.; Liu, Y.; Drautz-Moses, D. I.; Yam, J. K. H.; Aung, T. T.; Beuerman, R. W.; Salido, M. M. S.; Schuster, S. C.; Tan, C.-H., Repurposing the anticancer drug cisplatin with the aim of developing novel *Pseudomonas aeruginosa* infection control agents. *Beilstein. J. Org. Chem.* **2018,** *14*, 3059-3069.

30. Hummell, N. A.; Kirienko, N. V., Repurposing bioactive compounds for treating multidrug-resistant pathogens. *J. Med. Microbiol.* **2020,** *69*, 881-894.

31. Johnstone, T. C.; Suntharalingam, K.; Lippard, S. J., The next generation of platinum drugs: targeted Pt(II) agents, nanoparticle delivery, and Pt(IV) prodrugs. *Chem. Rev.* **2016,** *116*, 3436-3486.

32. Dhar, S.; Kolishetti, N.; Lippard, S. J.; Farokhzad, O. C., Targeted delivery of a cisplatin prodrug for safer and more effective prostate cancer therapy in vivo. *Proc. Natl. Acad. Sci. U.S.A.* **2011,** *108*, 1850-1855.

33. Wilson, J. J.; Lippard, S. J., Synthetic methods for the preparation of platinum anticancer complexes. *Chem. Rev.* **2014,** *114*, 4470-4495.

34. Abergel, R. J.; Zawadzka, A. M.; Hoette, T. M.; Raymond, K. N., Enzymatic hydrolysis of trilactone siderophores: where chiral recognition occurs in enterobactin and bacillibactin iron transport. *J. Am. Chem. Soc.* **2009,** *131*, 12682-12692.

35. Zhao, S.; Wang, Z. P.; Lin, Z.; Wei, G.; Wen, X.; Li, S.; Yang, X.; Zhang, Q.; Jing, C.; Dai, Y.; Guo, J.; He, Y., Drug repurposing by siderophore conjugation: synthesis and biological evaluation of siderophore-methotrexate conjugates as antibiotics. *Angew. Chem. Int. Ed.* **2022,** *61*, e202204139.

36. Sazonova, E. V.; Kopeina, G. S.; Imyanitov, E. N.; Zhivotovsky, B., Platinum drugs and taxanes: can we overcome resistance? *Cell Death Discov.* **2021,** *7*, 155.

37. Kelland, L., The resurgence of platinum-based cancer chemotherapy. *Nat. Rev. Cancer.* **2007,** *7*, 573-584.

38. Wexselblatt, E.; Gibson, D., What do we know about the reduction of Pt(IV) pro-drugs? *J. Inorg. Biochem.* **2012,** *117*, 220-229.

39. Alcindor, T.; Beauger, N., Oxaliplatin: a review in the era of molecularly targeted therapy. *Curr. Oncol.* **2011,** *18*, 18-25.

40. Bruno, P. M.; Liu, Y.; Park, G. Y.; Murai, J.; Koch, C. E.; Eisen, T. J.; Pritchard, J. R.; Pommier, Y.; Lippard, S. J.; Hemann, M. T., A subset of platinum-containing chemotherapeutic agents kills cells by inducing ribosome biogenesis stress. *Nat. Med.* **2017,** *23*, 461-471.

41. Chairatana, P.; Zheng, T.; Nolan, E. M., Targeting virulence: salmochelin modification tunes the antibacterial activity spectrum of β-lactams for pathogen-selective killing of *Escherichia coli*. *Chem. Sci.* **2015,** *6*, 4458-4471.

42. Mayr, J.; Heffeter, P.; Groza, D.; Galvez, L.; Koellensperger, G.; Roller, A.; Alte, B.; Haider, M.; Berger, W.; Kowol, C. R.; Keppler, B. K., An albumin-based tumor-targeted oxaliplatin prodrug with distinctly improved anticancer activity in vivo. *Chem. Sci.* **2017,** *8*, 2241-2250.

43. Corinti, D.; Crestoni, M. E.; Fornarini, S.; Dabbish, E.; Sicilia, E.; Gabano, E.; Perin, E.; Osella, D., A multi-methodological inquiry of the behavior of cisplatin-based Pt(IV) derivatives in the presence of bioreductants with a focus on the isolated encounter complexes. *J. Biol. Inorg. Chem.* **2020,** *25*, 655-670.

44. Liu, X.; Wenisch, D.; Barth, M. C.; Cseh, K.; Kowol, C. R.; Jakupec, M. A.; Gibson, D.; Keppler, B. K.; Weigand, W., Novel oxaliplatin(IV) complexes conjugated with ligands bearing pendant 1,2-dithiolane/1,2-diselenolane/cyclopentyl motifs. *Dalton Trans.* **2022,** *51*, 16824-16835.

45. Thiabaud, G.; He, G.; Sen, S.; Shelton, K. A.; Baze, W. B.; Segura, L.; Alaniz, J.; Munoz Macias, R.; Lyness, G.; Watts, A. B.; Kim, H. M.; Lee, H.; Cho, M. Y.; Hong, K. S.; Finch, R.; Siddik, Z. H.; Arambula, J. F.; Sessler, J. L., Oxaliplatin Pt(IV) prodrugs conjugated to gadolinium-texaphyrin as potential antitumor agents. *Proc. Natl. Acad. Sci. U.S.A.* **2020,** *117*, 7021-7029.

46. Gupta, A.; Bernacchia, L.; Kad, N. M., Culture media, DMSO and efflux affect the antibacterial activity of cisplatin and oxaliplatin. *Lett. Appl. Microbiol.* **2022,** *75*, 951-956.

47. Baba, T.; Ara, T.; Hasegawa, M.; Takai, Y.; Okumura, Y.; Baba, M.; Datsenko, K. A.; Tomita, M.; Wanner, B. L.; Mori, H., Construction of *Escherichia coli* K-12 in-frame, single-gene knockout mutants: the Keio collection. *Mol. Syst. Biol.* **2006,** *2*, 2006.0008.

48. Mobley, H.; Green, D. M.; Trifillis, A. L.; Johnson, D. E.; Chippendale, G. R.; Lockatell, C. V.; Jones, B. D.; Warren, J. W., Pyelonephritogenic *Escherichia coli* and killing of cultured human renal proximal tubular epithelial cells: role of hemolysin in some strains. *Infect. Immun.* **1990,** *58*, 1281-1289.

49. Hantke, K.; Nicholson, G.; Rabsch, W.; Winkelmann, G., Salmochelins, siderophores of *Salmonella enterica* and uropathogenic *Escherichia coli* strains, are recognized by the outer membrane receptor IroN. *Proc. Natl. Acad. Sci. U.S.A.* **2003,** *100*, 3677-3682.

50. Léveillé, S.; Caza, M.; Johnson, J. R.; Clabots, C.; Sabri, M.; Dozois, C. M., Iha from an *Escherichia coli* urinary tract infection outbreak clonal group A strain is expressed in vivo in the mouse urinary tract and functions as a catecholate siderophore receptor. *Infect. Immun.* **2006,** *74*, 3427-3436.

51. Hagan, E. C.; Mobley, H. L. T., Uropathogenic *Escherichia coli* outer membrane antigens expressed during urinary tract infection. *Infect. Immun.* **2007,** *75*, 3941-3949.

52. ThermoFischer Scientific LIVE/DEAD BacLight bacterial viability kits. https://www.thermofisher.com/document-connect/document-connect.html?url=https://assets.thermofisher.com/TFS-Assets/LSG/manuals/mp07007.pdf&title=TElWRSYjNDc7REVBRCAmbHQ7aSZndDtCYWMmbHQ7L2kmZ3Q7TGlnaHQgQmFjdGVyaWFsIFZpYWJpbGl0eSBLaXRz (accessed June 19, 2020).

53. Hall, M. D.; Okabe, M.; Shen, D.-W.; Liang, X.-J.; Gottesman, M. M., The role of cellular accumulation in determining sensitivity to platinum-based chemotherapy. *Annu. Rev. Pharmacol. Toxicol.* **2008,** *48*, 495-535.

54. Buß, I.; Hamacher, A.; Sarin, N.; Kassack, M.; Kalayda, G., Relevance of copper transporter 1 and organic cation transporters 1–3 for oxaliplatin uptake and drug resistance in colorectal cancer cells. *Metallomics* **2018,** *10*, 414-425.

55. Jamieson, E. R.; Lippard, S. J., Structure, recognition, and processing of cisplatin−DNA adducts. *Chem. Rev.* **1999,** *99*, 2467-2498.

56. Lippert, B., *Cisplatin: chemistry and biochemistry of a leading anticancer drug*. John Wiley & Sons: 1999.

57. Reslova, S., The induction of lysogenic strains of *Escherichia coli* by *cis*-dichlorodiammineplatinum (II). *Chem.-Biol. Interact.* **1971,** *4*, 66-70.

58. Justice, S. S.; Hunstad, D. A.; Seed, P. C.; Hultgren, S. J., Filamentation by *Escherichia coli* subverts innate defenses during urinary tract infection. *Proc. Natl. Acad. Sci. U. S. A.* **2006,** *103*, 19884-19889.

59. Huisman, O.; D'Ari, R.; George, J., Further characterization of *sfiA* and *sfiB* mutations in *Escherichia coli*. *J. Bacteriol.* **1980,** *144*, 185-191.

60. Friedberg, E. C.; Walker, G. C.; Siede, W.; Wood, R. D., *DNA repair and mutagenesis*. American Society for Microbiology Press: 2005.

61. McCool, J. D.; Long, E.; Petrosino, J. F.; Sandler, H. A.; Rosenberg, S. M.; Sandler, S. J., Measurement of SOS expression in individual *Escherichia coli* K-12 cells using fluorescence microscopy. *Mol. Microbiol.* **2004,** *53*, 1343-1357.

62. Zdraveski, Z. Z.; Mello, J. A.; Marinus, M. G.; Essigmann, J. M., Multiple pathways of recombination define cellular responses to cisplatin. *Chem. Biol.* **2000,** *7*, 39-50.

63. Pigg, H. C.; Yglesias, M. V.; Sutton, E. C.; McDevitt, C. E.; Shaw, M.; DeRose, V. J., Time-dependent studies of oxaliplatin and other nucleolar stress-inducing Pt(II) derivatives. *ACS Chem. Biol.* **2022,** *17*, 2262-2271.

64. Kozelka, J., Molecular origin of the sequence-dependent kinetics of reactions between cisplatin derivatives and DNA. *Inorg. Chim. Acta.* **2009,** *362*, 651-668.

65. Sutton, E. C.; McDevitt, C. E.; Prochnau, J. Y.; Yglesias, M. V.; Mroz, A. M.; Yang, M. C.; Cunningham, R. M.; Hendon, C. H.; DeRose, V. J., Nucleolar stress induction by oxaliplatin and derivatives. *J. Am. Chem. Soc.* **2019,** *141*, 18411-18415.

66. Vaisman, A.; Masutani, C.; Hanaoka, F.; Chaney, S. G., Efficient translesion replication past oxaliplatin and cisplatin GpG adducts by human DNA polymerase *η*. *Biochemistry* **2000,** *39*, 4575-4580.

67. Ramirez, R. J. A.; Karamanukyan, L.; Ortiz, S.; Gutierrez, C. G., A much improved synthesis of the siderophore enterobactin. *Tetrahedron Lett.* **1997,** *38*, 749-752.

68. Lal, S.; Díez-González, S., [$CuBr(PPh_3)_3$] for azide-alkyne cycloaddition reactions under strict Click conditions. *J. Org. Chem.* **2011,** *76*, 2367-2373.

69. Michaels, H. A.; Zhu, L., Ligand-assisted, copper(II) acetate-accelerated azide-alkyne cycloaddition. *Chem. Asian. J.* **2011,** *6*, 2825-2834.

70. Scarrow, R. C.; Ecker, D. J.; Ng, C.; Liu, S.; Raymond, K. N., Iron(III) coordination chemistry of linear dihydroxyserine compounds derived from enterobactin. *Inorg. Chem.* **1991,** *30*, 900-906.

71. Shapiro, E.; Baneyx, F., Stress-based identification and classification of antibacterial agents: second-generation *Escherichia coli* reporter strains and optimization of detection. *Antimicrob. Agents Chemother.* **2002,** *46*, 2490-2497.

72. Miller, J. H., *Experiments in molecular genetics*. Cold Spring Harbor Laboratory Press: 1972.

73. Miller, J. H., *A short course in bacterial genetics: a laboratory manual and handbook for Escherichia coli and related bacteria*. Cold Spring Harbor Laboratory Press: 1993.

Appendix A.

Supplemental Data for Chapter 2

A.1 NMR spectroscopic data

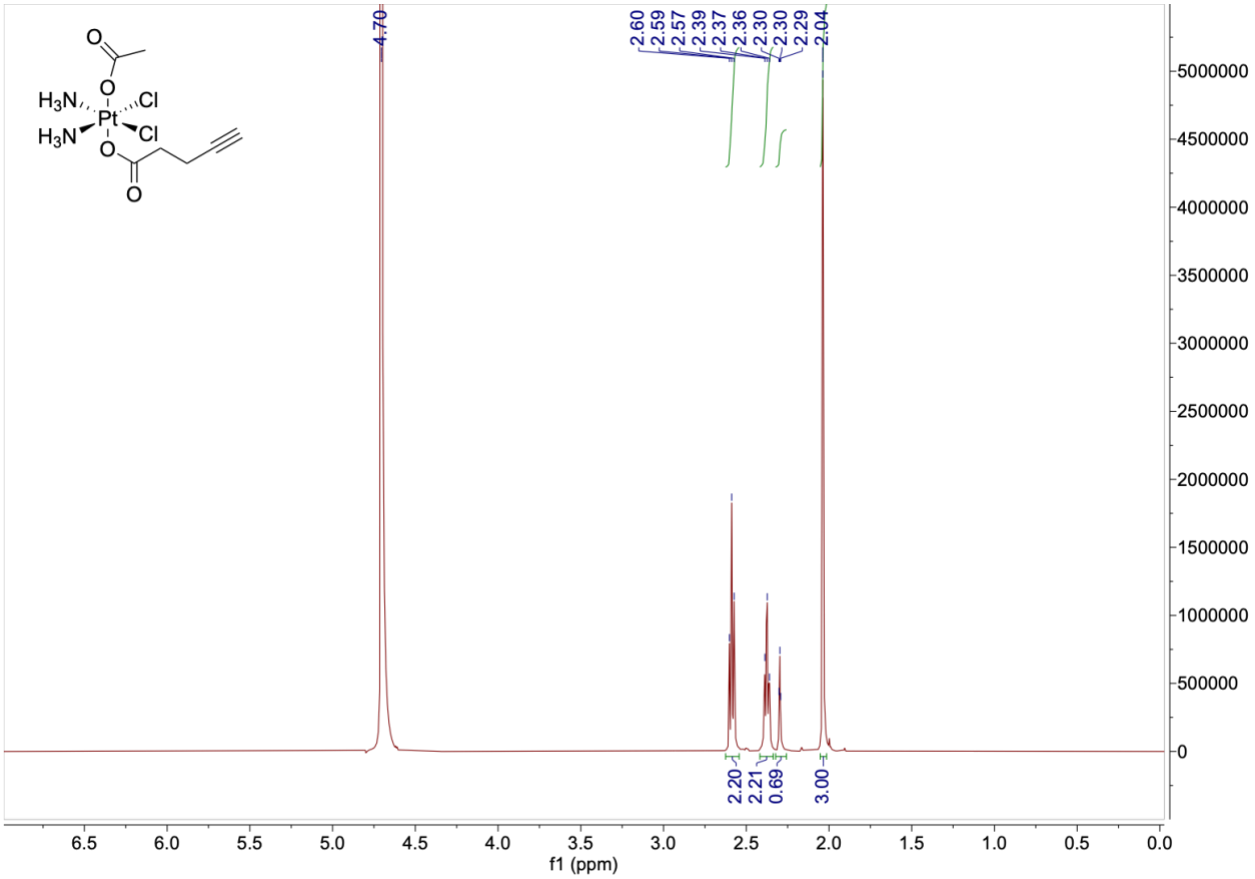

Figure A.1. ^{1}H NMR spectrum of *cis, cis, trans*-[Pt(NH_3)$_2$$Cl_2$($OOCCH_3$)($OOCCH_2CH_2C{\equiv}CH$)] (Pt(IV)-alkyne **6**) in D_2O.

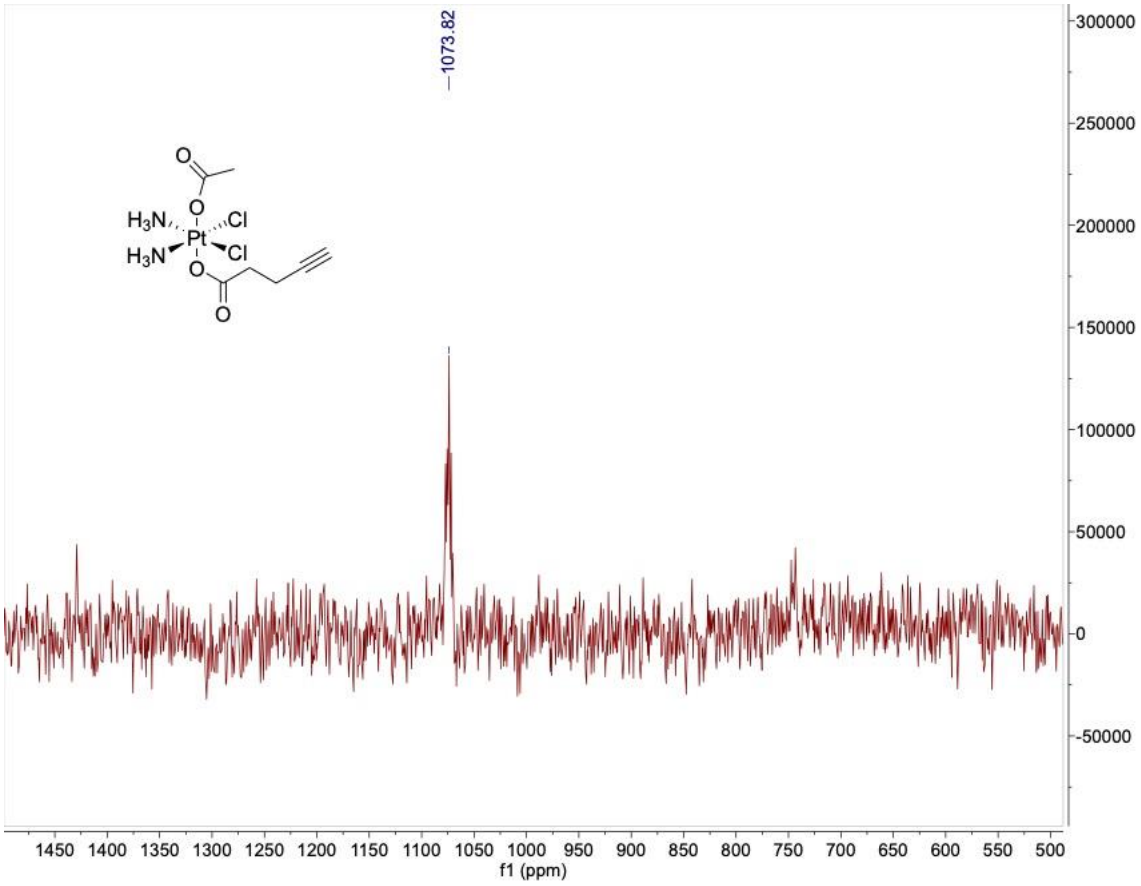

Figure A.2. ^{195}Pt NMR spectrum of *cis*, *cis*, *trans*-[Pt(NH_3)$_2$$Cl_2$($OOCCH_3$)($OOCCH_2CH_2C{\equiv}CH$)] (Pt(IV)-alkyne **6**) in D_2O.

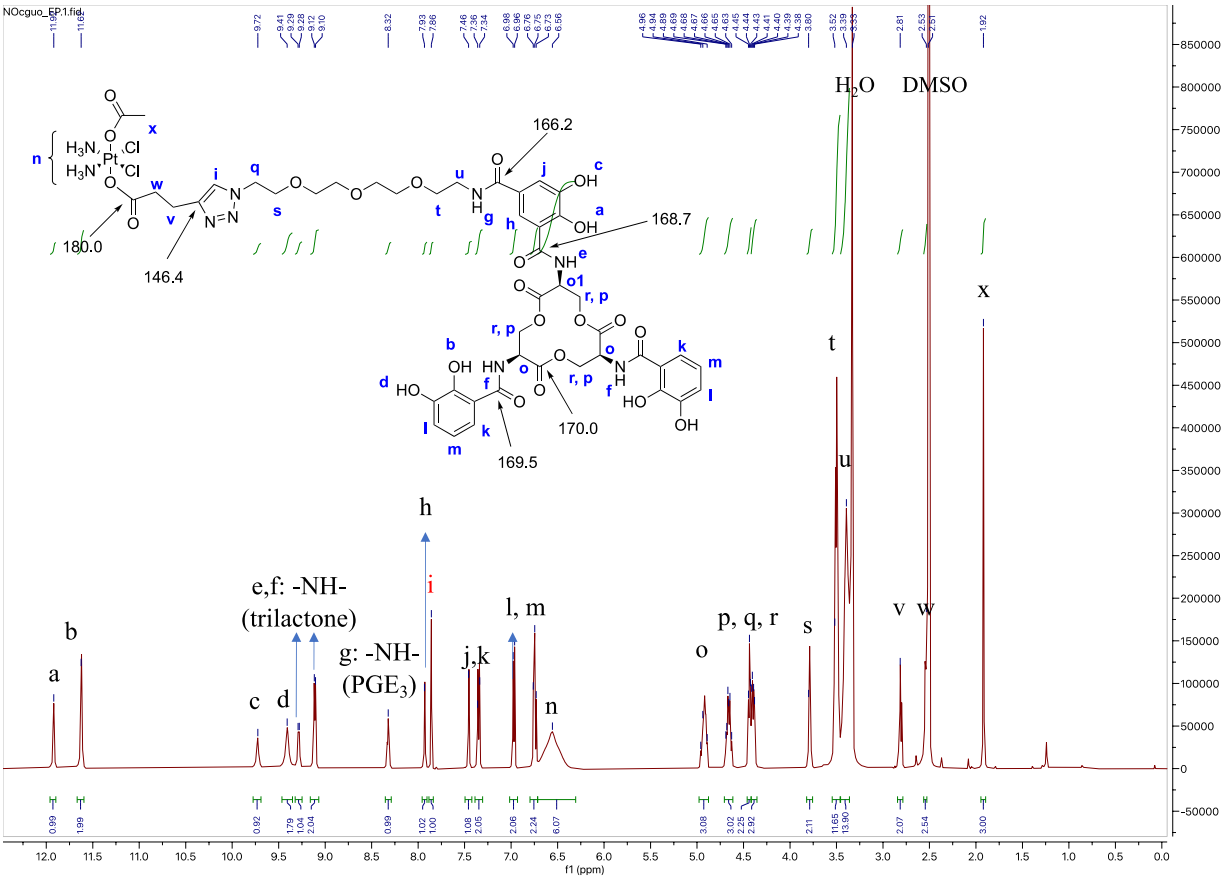

Figure A.3. ^{1}H NMR spectrum of L-Ent-Pt(IV) **4** in DMSO-d$_6$.

Table A.1. Peak assignment of NMR spectroscopic data of L-Ent-Pt(IV) **4** in DMSO-d_6.

Label	H1	COSY	C13	HMBC	Comments
a	11.92, s			151.1, 146.2, 115.6	
b	11.62, 2H, s			148.9, 146.7, 115.6	
c	9.72, s				
d	9.41, 2H, s				
e	9.29, d	o1		168.8	
f1	9.12, d	o2, o3		169.5, 63.8, 51.5	
f2	9.12, d				
g	8.32, t	u		166.3	
h	7.93, m	j	119.0	168.7, 166.2, 151.1, 118.0	
i	7.86, s		122.9	146.4	
j	7.46, m	h	118.1	166.2, 151.0, 146.1, 118.9	
k1	7.36, d	m; l	118.7	169.5, 149.0, 119.8	
k2	7.36, d				
l1	6.98, d	m; k	119.7	149.0, 146.7, 118.8	
l2	6.98, d				
m1	6.75, t	k, l	118.9	146.7, 115.5; 119.4	
m2	6.75, t				
n	6.56, 6H, br				
o1	4.92, m	e, p, r	51.7	169.9, 63.8	63.8: r,p
o2	4.92, m	f, p, r			
o3	4.92, m				
p1	4.65, m	o, r	63.8	170.0, 51.6	51.5: o
p2	4.65, m				
p3	4.65, m				
q	4.43, 2H, t	s	49.6	122.9, 69.0	122.9: i
r1	4.39, m	o, p	63.8	170.0, 51.6	
r2	4.39, m				
r3	4.39, m				
s	3.80, 2H, t	q	69.2	69.9, 49.6	49.6: q
t	3.52, nH, m	u	69.8, 70.1	70.0, 39.6	overlapping with water peak; integration is off
u	3.39, nH, m	g, t	39.5	166.2, 69.4	
v	2.81, 2H, t	w	22.1	180.2, 146.4, 123.0, 35.7	123.0: i
w	2.53, 2H, t	v	35.8	180.2, 146.4, 21.9	
x	1.92, 3H, s		23.2	178.7	

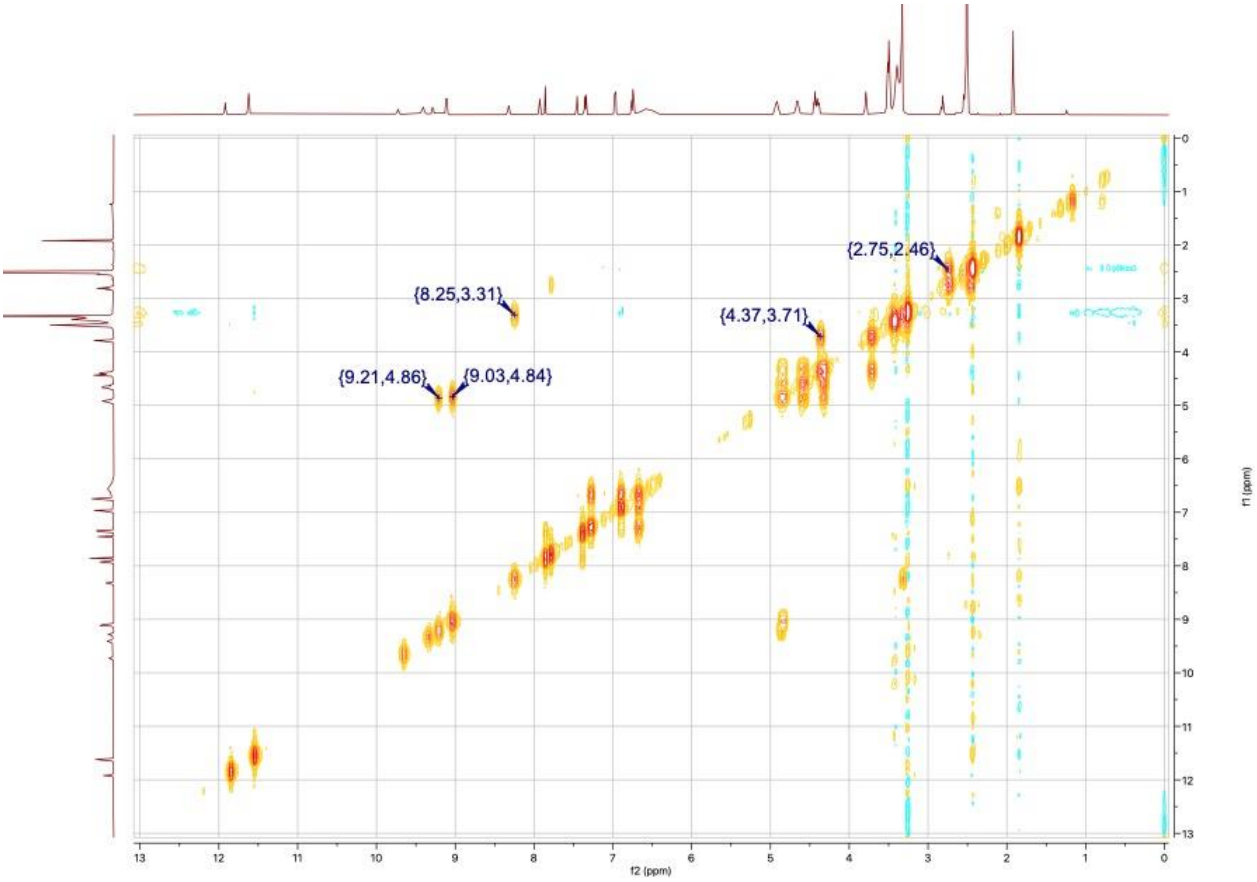

Figure A.4. ^{1}H COSY spectrum of L-Ent-Pt(IV) **4** in DMSO-d_6.

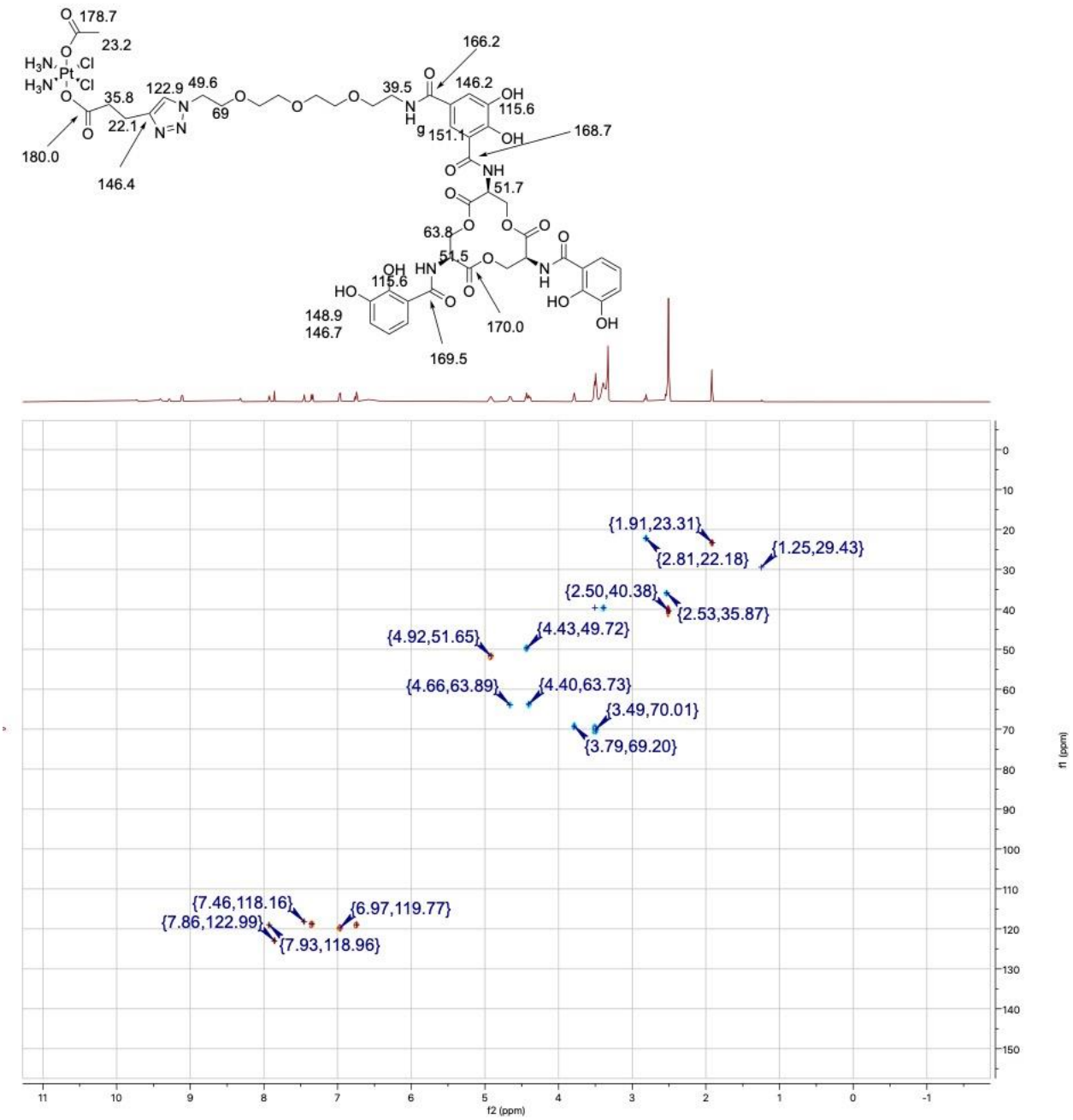

Figure A.5. ^{1}H-^{13}C HSQC spectrum of L-Ent-Pt(IV) **4** in DMSO-d_6.

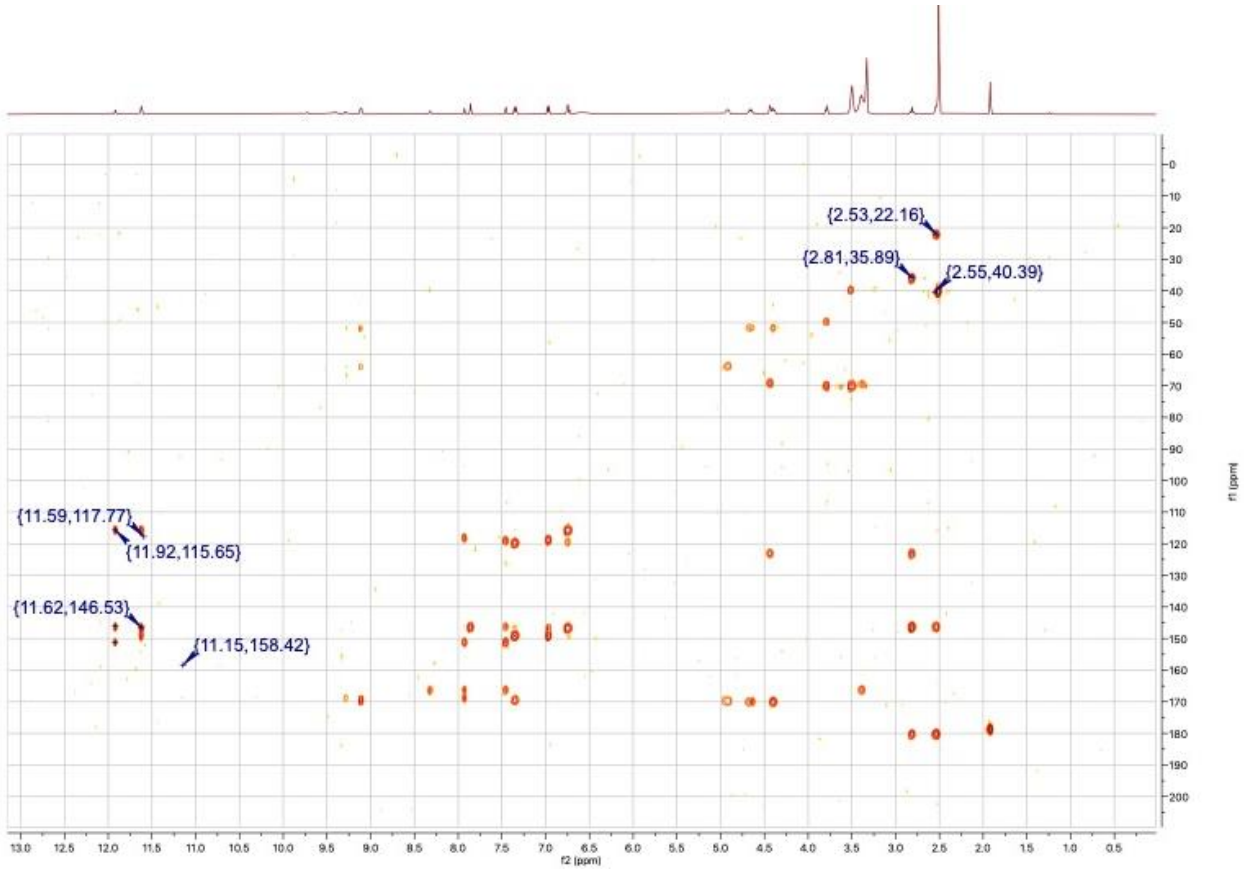

Figure A.6. ^{1}H-^{13}C HMBC spectrum of L-Ent-Pt(IV) **4** in DMSO-d_6.

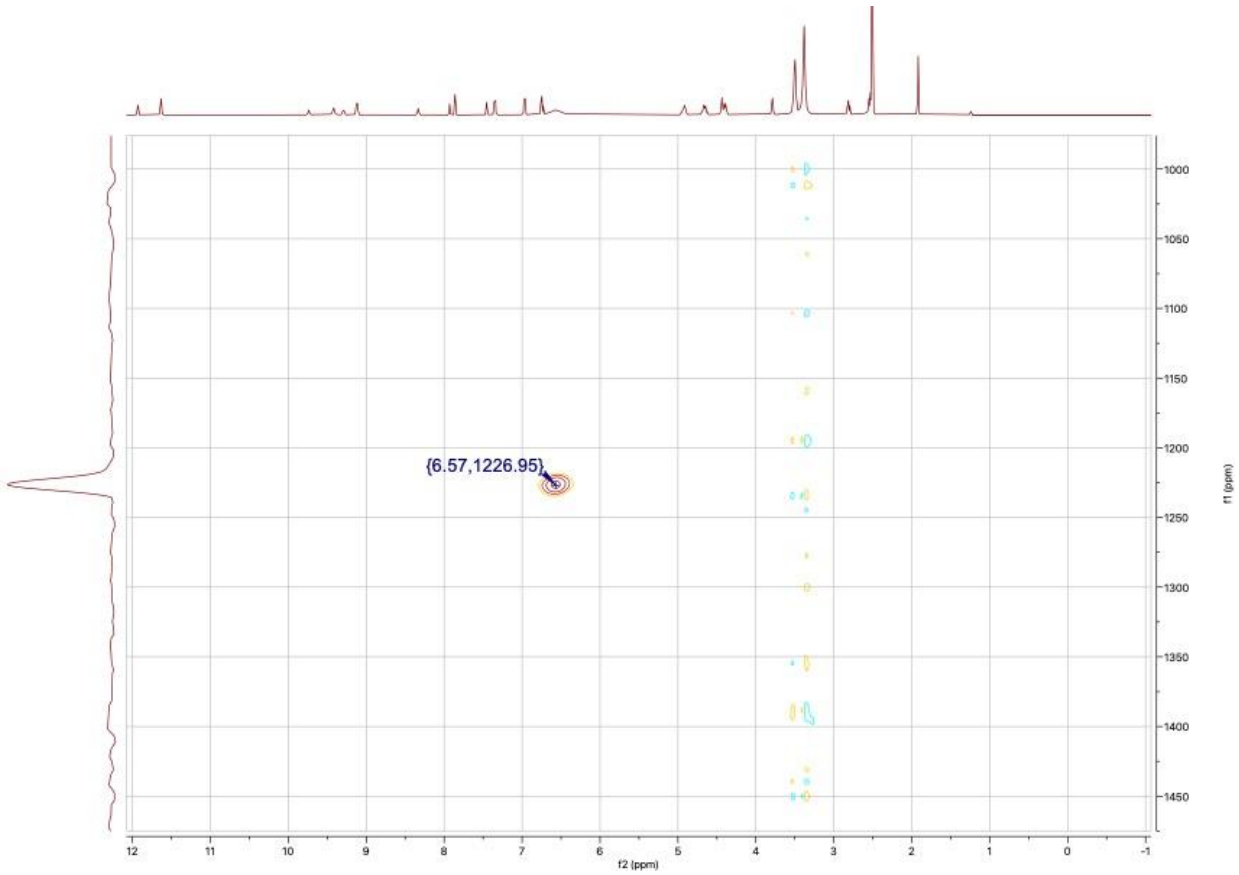

Figure A.7. ^{1}H-^{195}Pt HMQC spectrum of L-Ent-Pt(IV) **4** in DMSO-d_6.

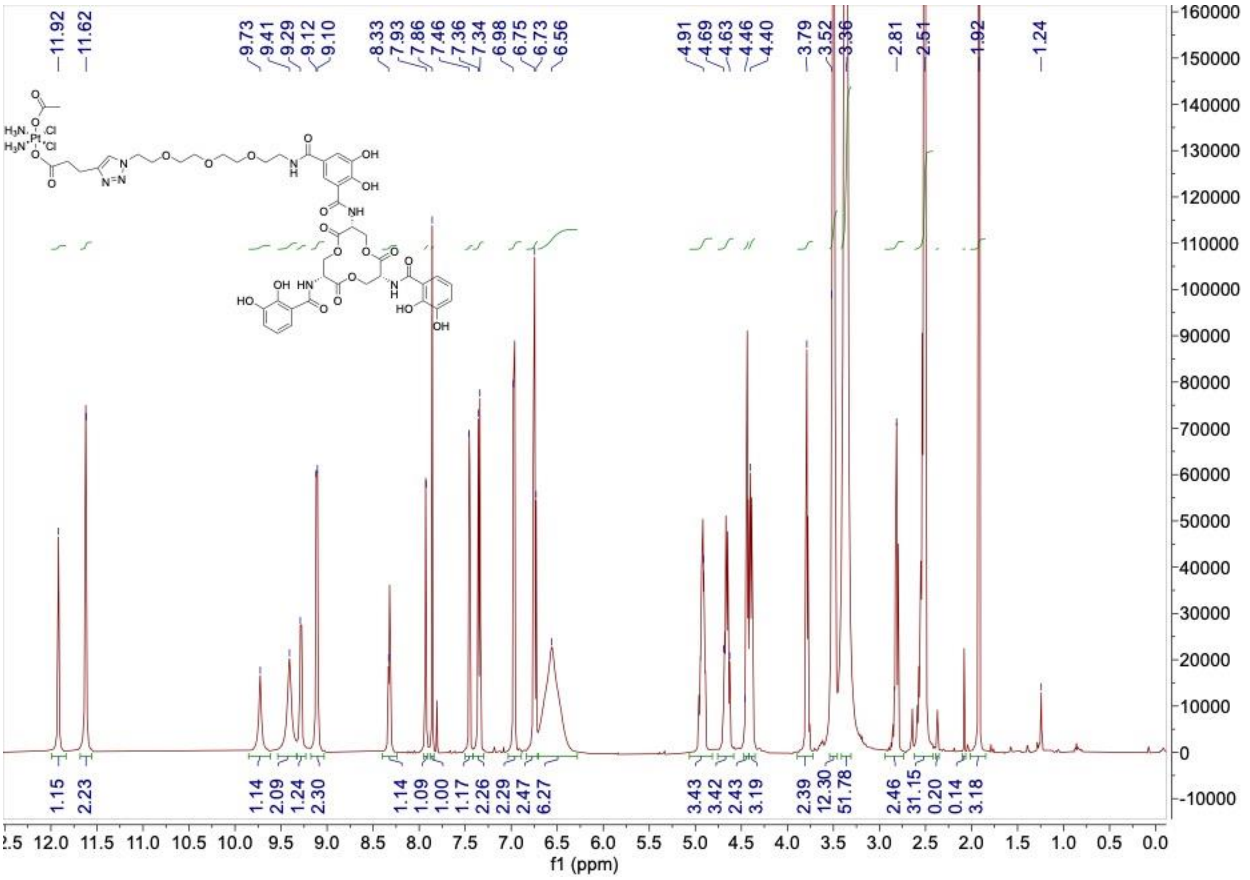

Figure A.8. ^{1}H NMR spectrum of D-Ent-Pt(IV) **5** in DMSO-d_6.

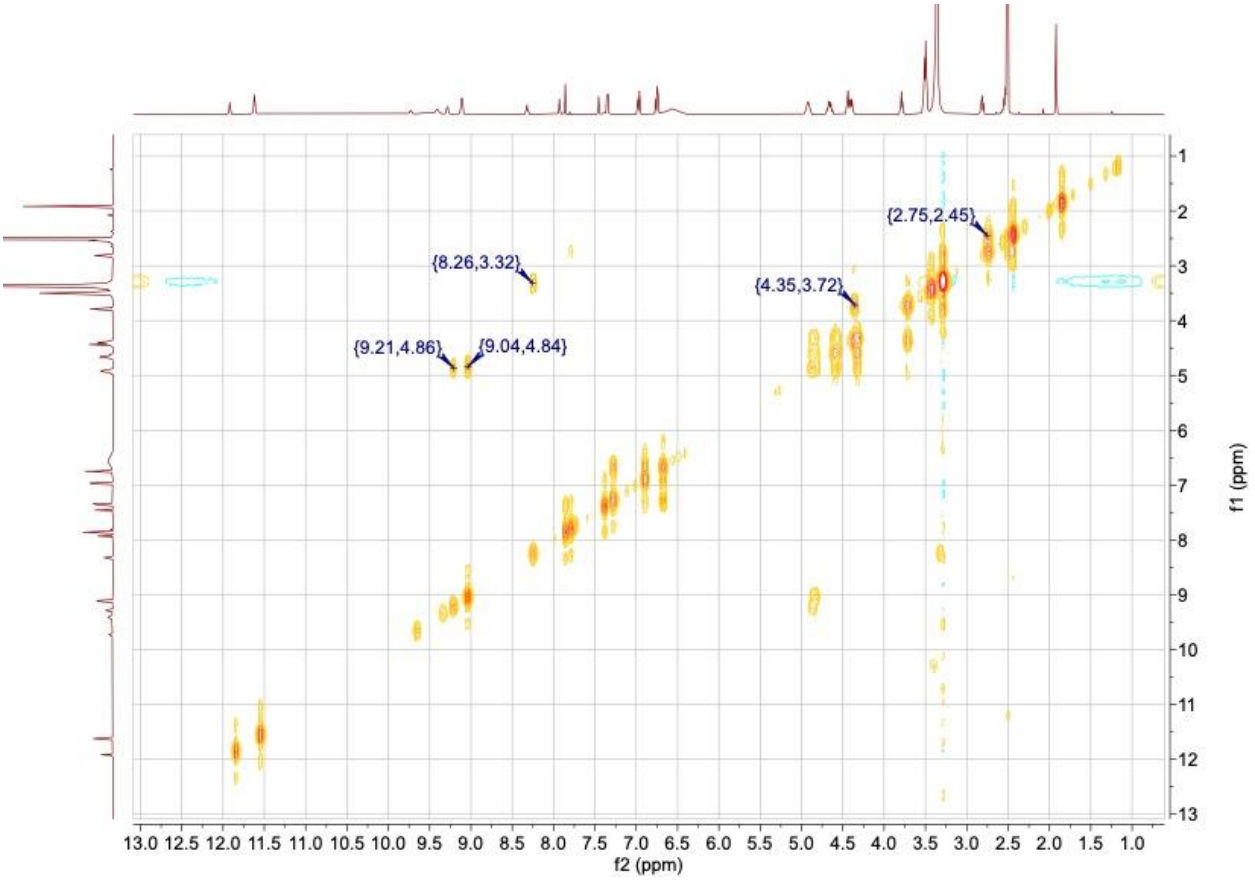

Figure A.9. ^{1}H COSY spectrum of D-Ent-Pt(IV) **5** in DMSO-d_6.

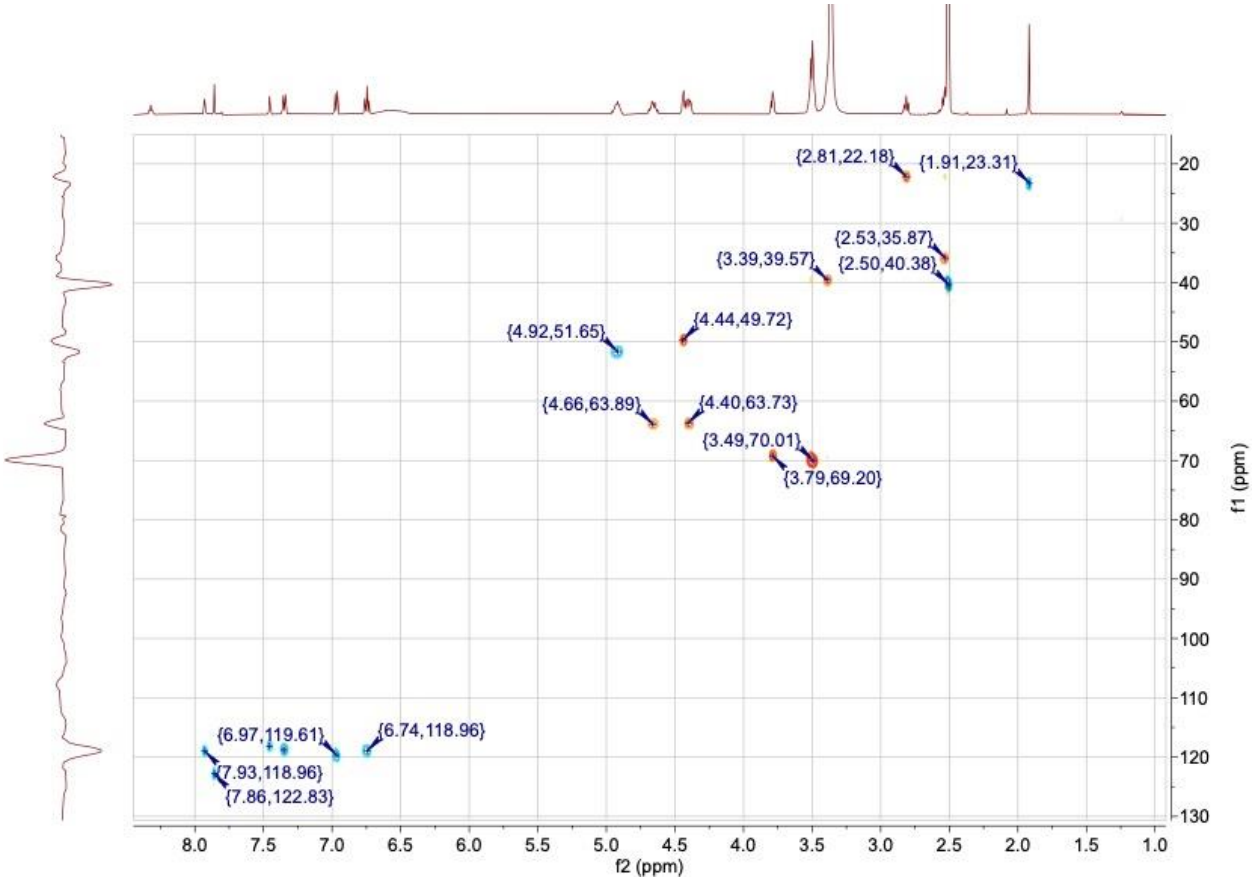

Figure A.10. ^{1}H-^{13}C HSQC spectrum of D-Ent-Pt(IV) **5** in DMSO-d_6.

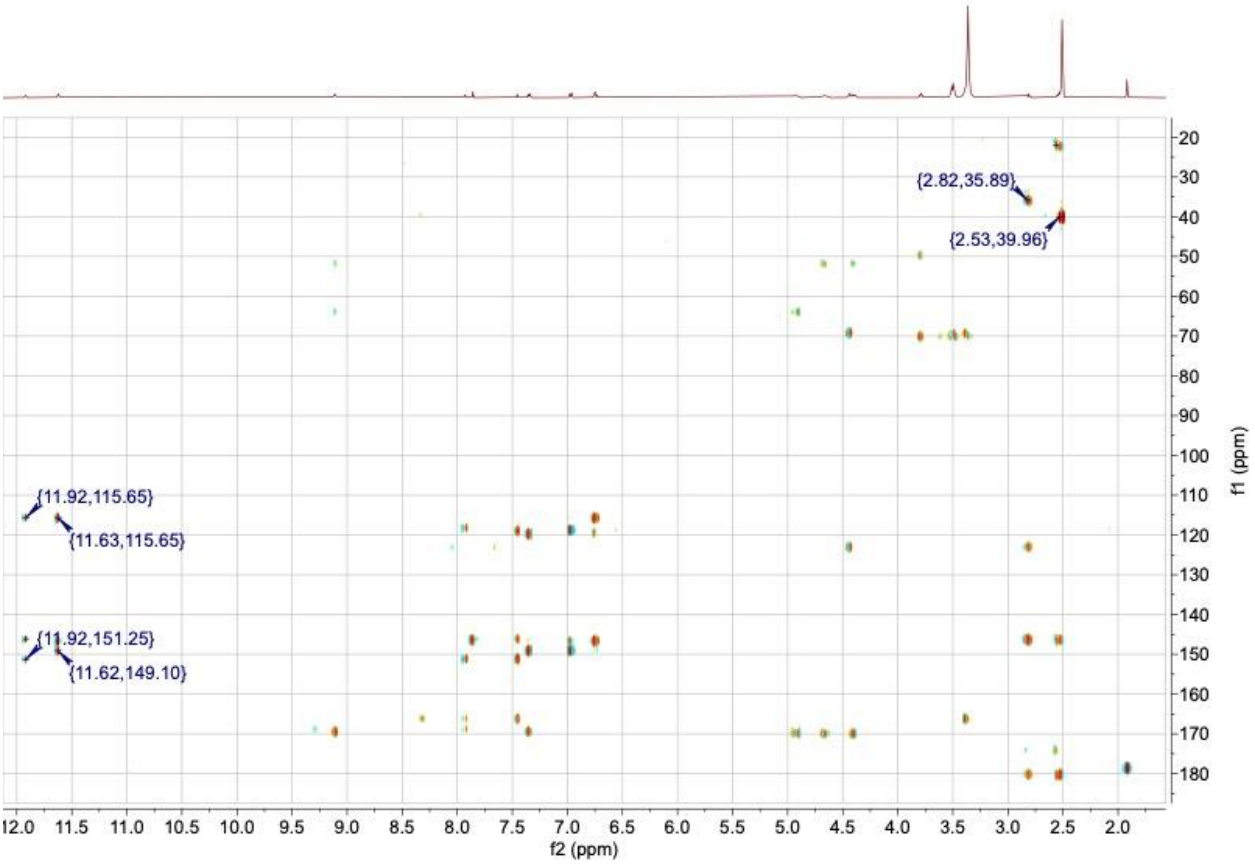

Figure A.11. ^{1}H-^{13}C HMBC spectrum of D-Ent-Pt(IV) **5** in DMSO-d_6.

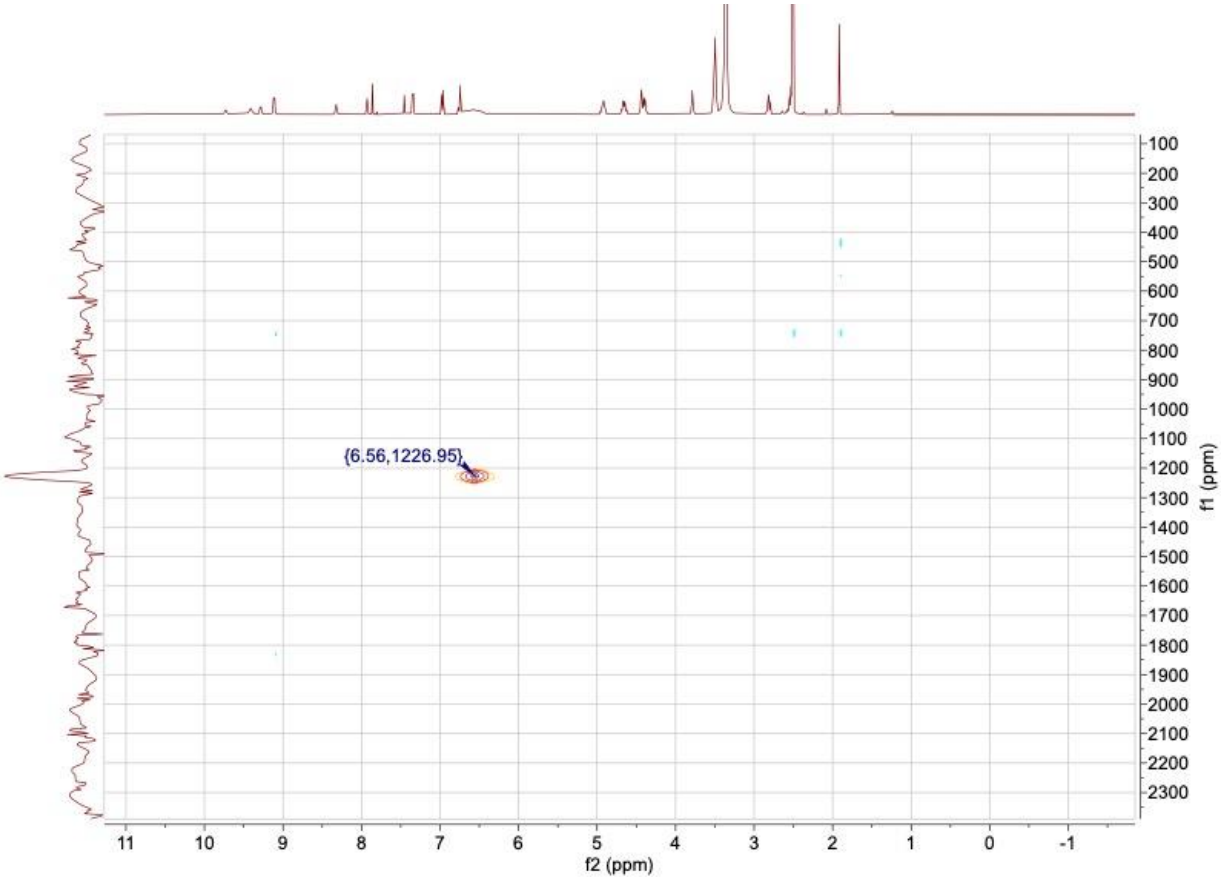

Figure A.12. ^{1}H-^{195}Pt HMQC spectrum of D-Ent-Pt(IV) **5** in DMSO-d_6.

A.2 Supplementary results of antibacterial activity and microscopy.

Table A.2. Quantitative analysis of L-EP-induced bacterial morphologies and viability.

Strain	[L-EP] (μM)	Normal size (%)	Elongation (%)	Filamentation (%)	Extreme filamentation (%)	Viability (%)
E. coli CFT073	0	99.7	0.3	0.0	0.0	96.7
	7.5	77.7	18.2	3.9	0.2	88.1
	15	73.2	18.8	7.0	1.1	80.1
	30	60.5	22.4	13.0	4.1	75.7
	60	31.4	29.3	21.1	18.2	52.9
E. coli CFT073 Δ*fepC*	0	100.0	0.0	0.0	0.0	98.7
	7.5	99.3	0.7	0.0	0.0	99.3
	15	96.6	3.4	0.0	0.0	99.6
	30	93.7	6.3	0.0	0.0	97.1
	60	78.7	18.4	2.8	0.0	97.0
E. coli CFT073 Δ*fepDG*	0	99.7	0.3	0.0	0.0	99.4
	7.5	97.7	2.1	0.2	0.0	98.8
	15	97.2	2.8	0.0	0.0	97.5
	30	91.9	8.1	0.0	0.0	98.5
	60	82.8	15.2	1.9	0.1	95.4
E. coli CFT073 Δ*fes*	0	100.0	0.0	0.0	0.0	98.8
	7.5	69.1	21.2	8.7	1.0	42.2
	15	48.6	18.7	15.8	16.9	66.2
	30	63.1	12.2	9.9	14.8	66.2
	60	39.3	16.4	18.0	26.3	41.2
E. coli CFT073 Δ*iroD*	0	100.0	0.0	0.0	0.0	97.7
	7.5	60.6	30.8	7.9	0.7	77.2
	15	55.0	27.4	15.3	2.3	70.6
	30	42.8	27.2	19.0	11.0	60.7
	60	48.1	17.8	14.8	19.3	59.0
E. coli K12	0	100.0	0.0	0.0	0.0	96.0
	7.5	54.4	20.4	14.8	10.3	68.2
	15	30.5	24.9	13.8	30.8	57.6
	30	38.1	10.1	14.4	37.4	51.3
	60	19.8	4.7	9.1	66.4	54.7
E. coli K12 Δ*fepA*	0	100.0	0.0	0.0	0.0	100
	7.5	99.7	0.1	0.1	0.0	97.5
	15	99.1	0.3	0.7	0.0	94.7
	30	85.1	12.5	2.0	0.4	93.2
	60	51.2	37.6	10.4	0.7	87.3

Table A.3. Antibacterial activity of cisplatin, L-EP and D-EP based on OD_{600} (mean ± standard deviation).

Strain	[cisplatin] (μM)	OD_{600}	[L-EP] (μM)	OD_{600}	[D-EP] (μM)	OD_{600}
E. coli CFT073	0	0.25±0.008	0	0.21±0.02	0	0.20±0.02
	7.5	0.23±0.02	7.5	0.16±0.02	0.01	0.20±0.01
	15	0.19±0.01	15	0.16±0.02	0.1	0.15±0.02
	30	0.12±0.02	30	0.14±0.03	1	0.086±0.02
	60	0.10±0.02	60	0.13±0.01	10	0.052±0.01
E. coli CFT073 Δ*fepC*	0	0.29±0.03	0	0.28±0.008	0	0.31±0.05
	7.5	0.29±0.02	7.5	0.32±0.03	0.01	0.30±0.02
	15	0.27±0.04	15	0.32±0.02	0.1	0.33±0.02
	30	0.15±0.05	30	0.29±0.02	1	0.30±0.04
	60	0.026±0.02	60	0.25±0.03	10	0.29±0.05
E. coli CFT073 Δ*fepDG*	0	0.32±0.03	0	0.28±0.007	0	0.30±0.03
	7.5	0.30±0.02	7.5	0.33±0.05	0.01	0.31±0.03
	15	0.22±0.04	15	0.30±0.03	0.1	0.32±0.02
	30	0.058±0.04	30	0.28±0.03	1	0.29±0.07
	60	0.015±0.008	60	0.23±0.03	10	0.28±0.05
E. coli CFT073 Δ*fes*	0	0.30±0.02	0	0.30±0.05	0	0.30±0.03
	7.5	0.29±0.01	7.5	0.20±0.04	0.01	0.30±0.05
	15	0.32±0.07	15	0.13±0.05	0.1	0.28±0.01
	30	0.23±0.06	30	0.088±0.04	1	0.25±0.05
	60	0.040±0.02	60	0.069±0.02	10	0.085±0.04
E. coli CFT073 Δ*iroD*	0	0.30±0.004	0	0.28±0.05	0	0.28±0.03
	7.5	0.30±0.01	7.5	0.26±0.04	0.01	0.28±0.02
	15	0.30±0.02	15	0.20±0.01	0.1	0.25±0.01
	30	0.35±0.06	30	0.15±0.01	1	0.14±0.04
	60	0.022±0.007	60	0.09±0.01	10	0.043±0.02
E. coli K12	0	0.25±0.04	0	0.19±0.02	0	0.22±0.03
	7.5	0.25±0.07	7.5	0.16±0.02	0.01	0.21±0.02
	15	0.21±0.06	15	0.15±0.01	0.1	0.065±0.01
	30	0.15±0.004	30	0.13±0.007	1	0.040±0.005
	60	0.075±0.02	60	0.14±0.006	10	0.034±0.01
E. coli K12 Δ*fepA*	0	0.18±0.03	0	0.13±0.02	0	0.15±0.01
	7.5	0.15±0.04	7.5	0.28±0.1	0.01	0.15±0.02
	15	0.13±0.04	15	0.21±0.1	0.1	0.14±0.03
	30	0.10±0.03	30	0.17±0.1	1	0.11±0.007
	60	0.060±0.02	60	0.16±0.1	10	0.12±0.02

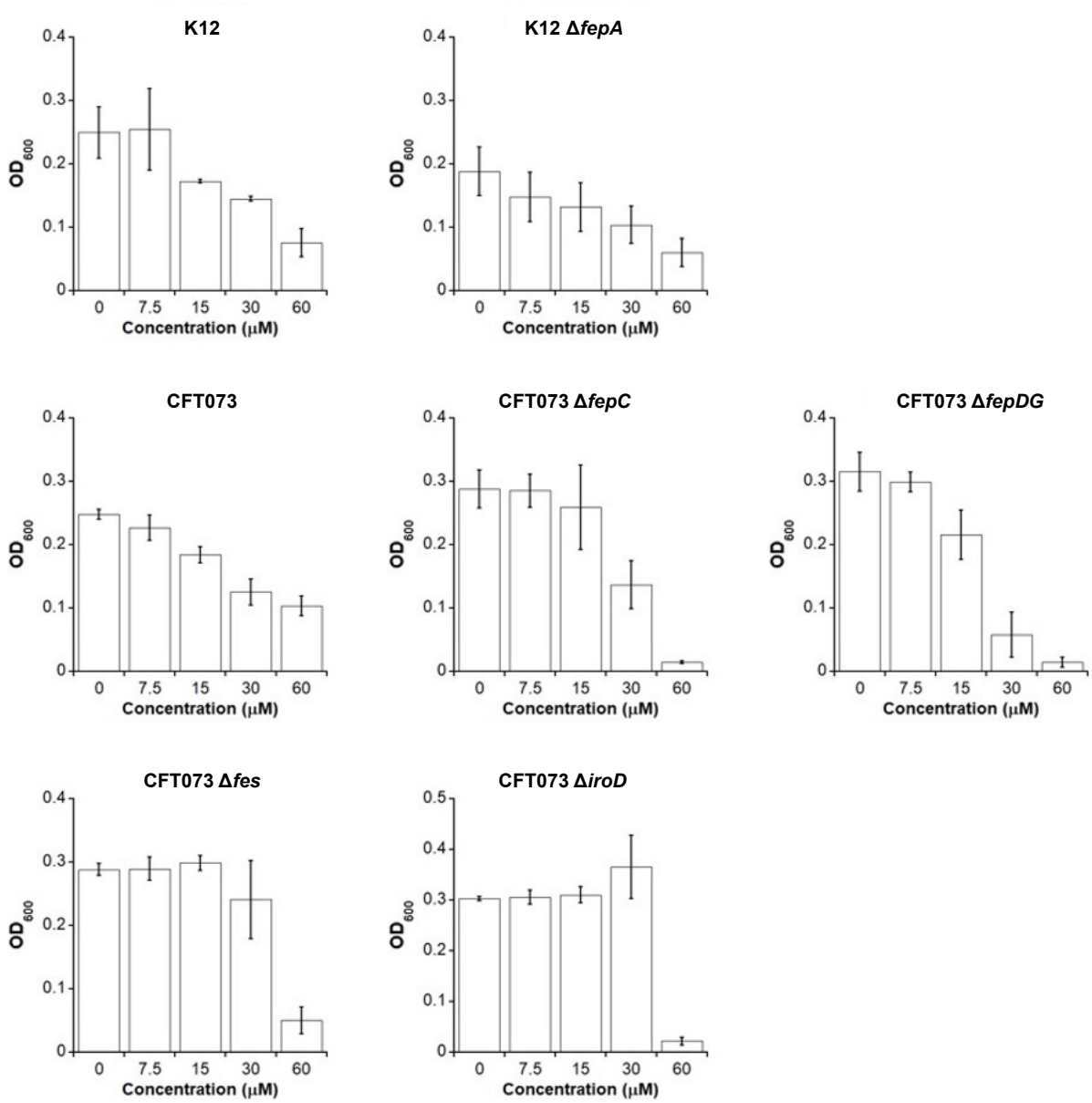

Figure A.13. Antibacterial activity of cisplatin against *E. coli* K12 and its Δ*fepA* mutant; *E. coli* CFT073 and its Δ*fepC*, Δ*fepDG*, Δ*fes* and Δ*iroD* mutants based on OD_{600} (data shown in **Table A.3**). All assays were performed in modified M9 medium (11 h, 30 °C, 500 rpm; mean ± standard deviation, $n \geq 4$).

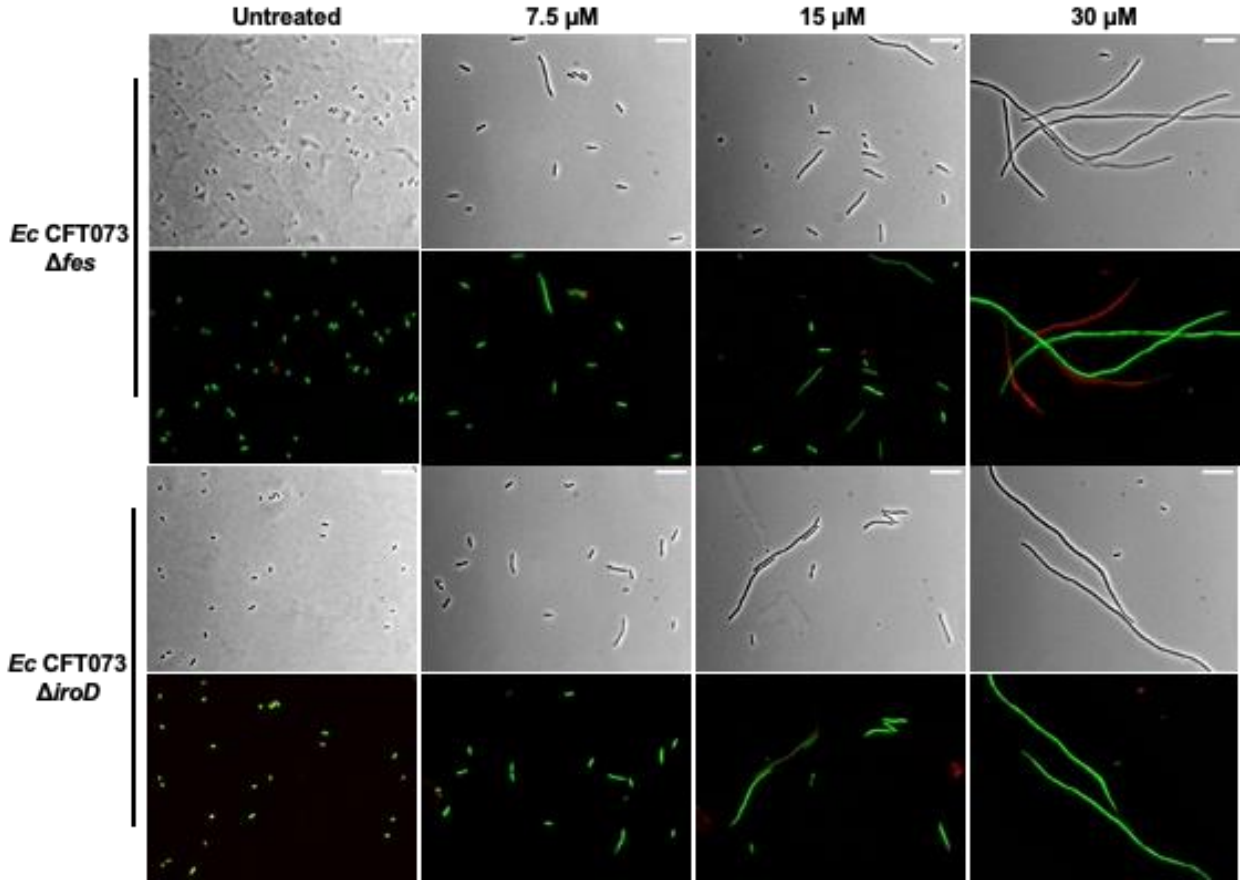

Figure A.14. Representative phase-contrast and fluorescence micrographs of *E. coli* CFT073 and its Δ*fes* and Δ*iroD* mutants treated with cisplatin (scale bar = 10 µm).

A.3 Growth curves

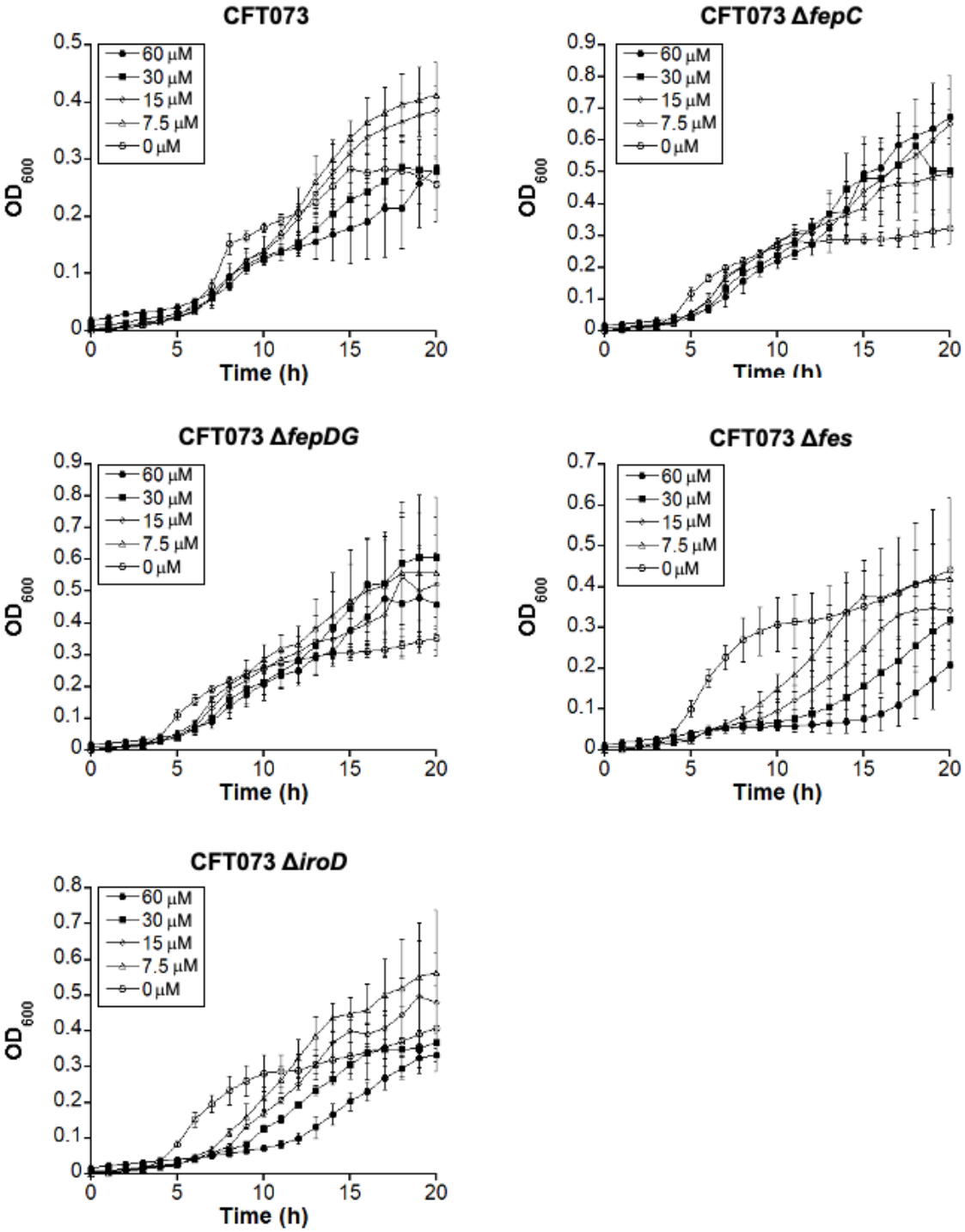

Figure A.15. Growth curves of *E. coli* CFT073 and its Δ*fepC*, Δ*fepDG*, Δ*fes* and Δ*iroD* mutants treated with L-EP in modified M9 at 30 °C (mean ± standard deviation, n ≥ 3). We note that the large error bars after ~14 h are presumably due to decomposition of L-EP in the modified M9 medium.

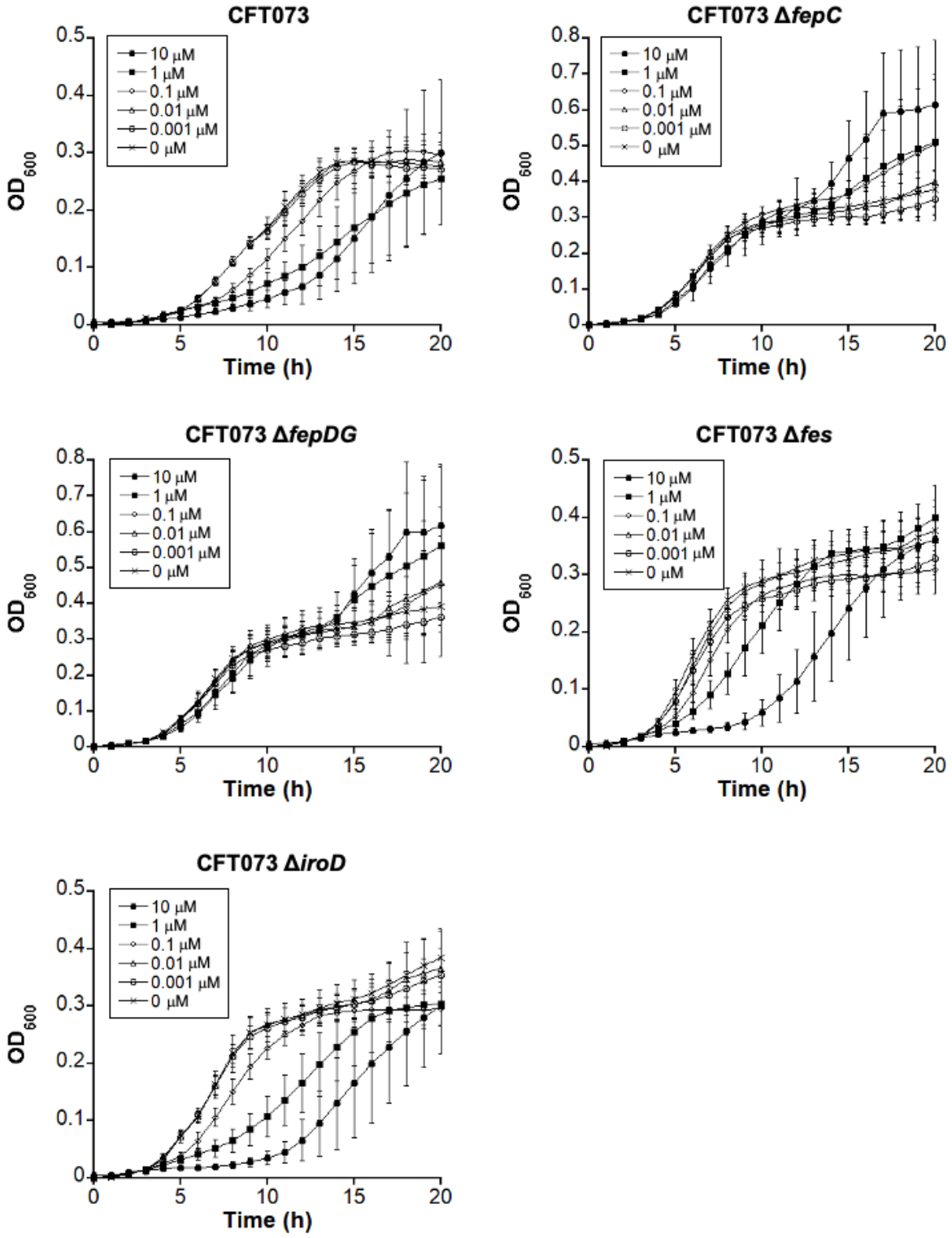

Figure A.16. Growth curves of *E. coli* CFT073 and its Δ*fepC*, Δ*fepDG*, Δ*fes* and Δ*iroD* mutants treated with D-EP in modified M9 at 30 °C (mean ± standard deviation, n ≥ 3). We note that the large error bars after ~14 h are presumably due to decomposition of D-EP in the modified M9 medium.

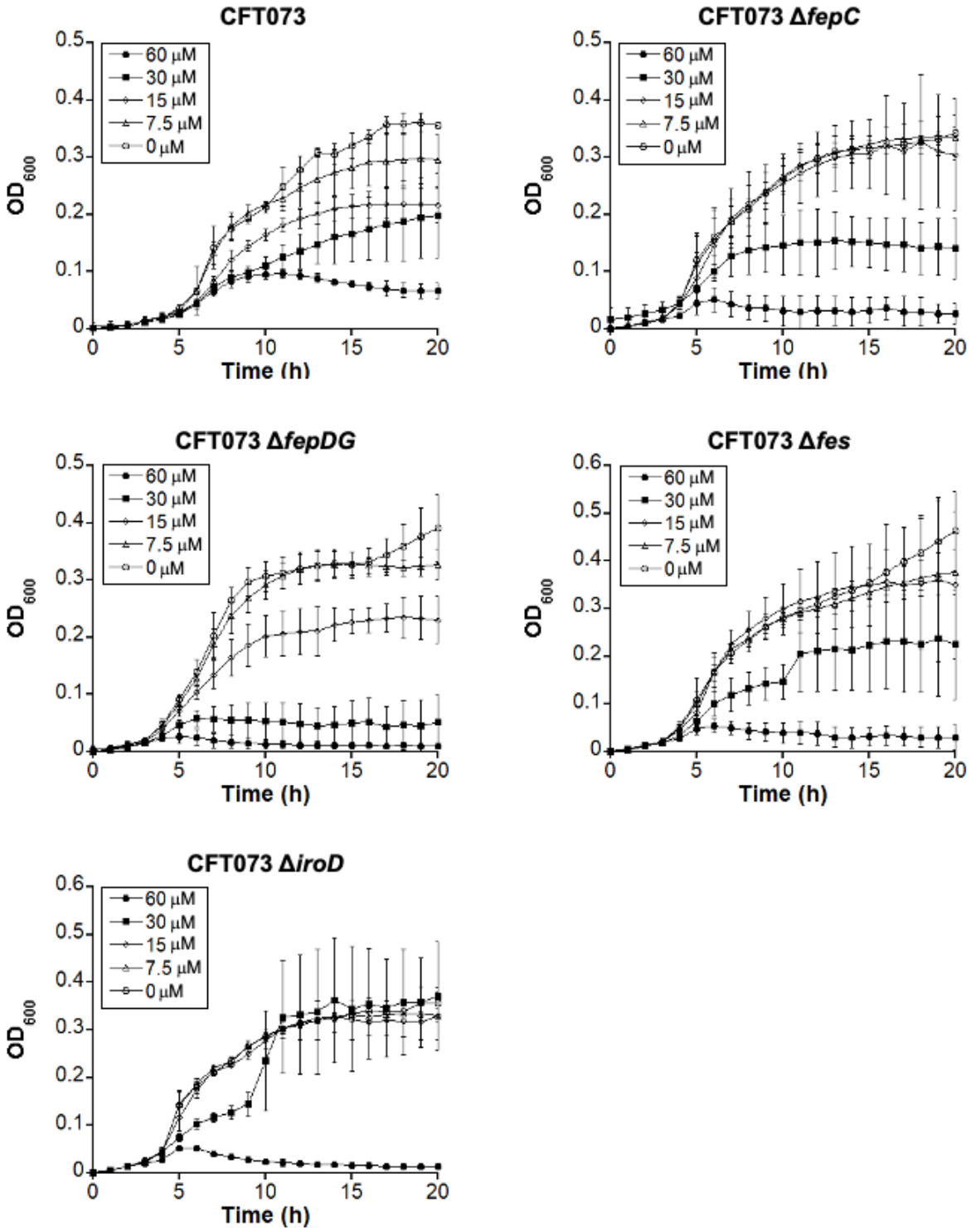

Figure A.17. Growth curves of *E. coli* CFT073 and its Δ*fepC*, Δ*fepDG*, Δ*fes* and Δ*iroD* mutants treated with cisplatin in modified M9 at 30 °C (mean ± standard deviation, n ≥ 3).

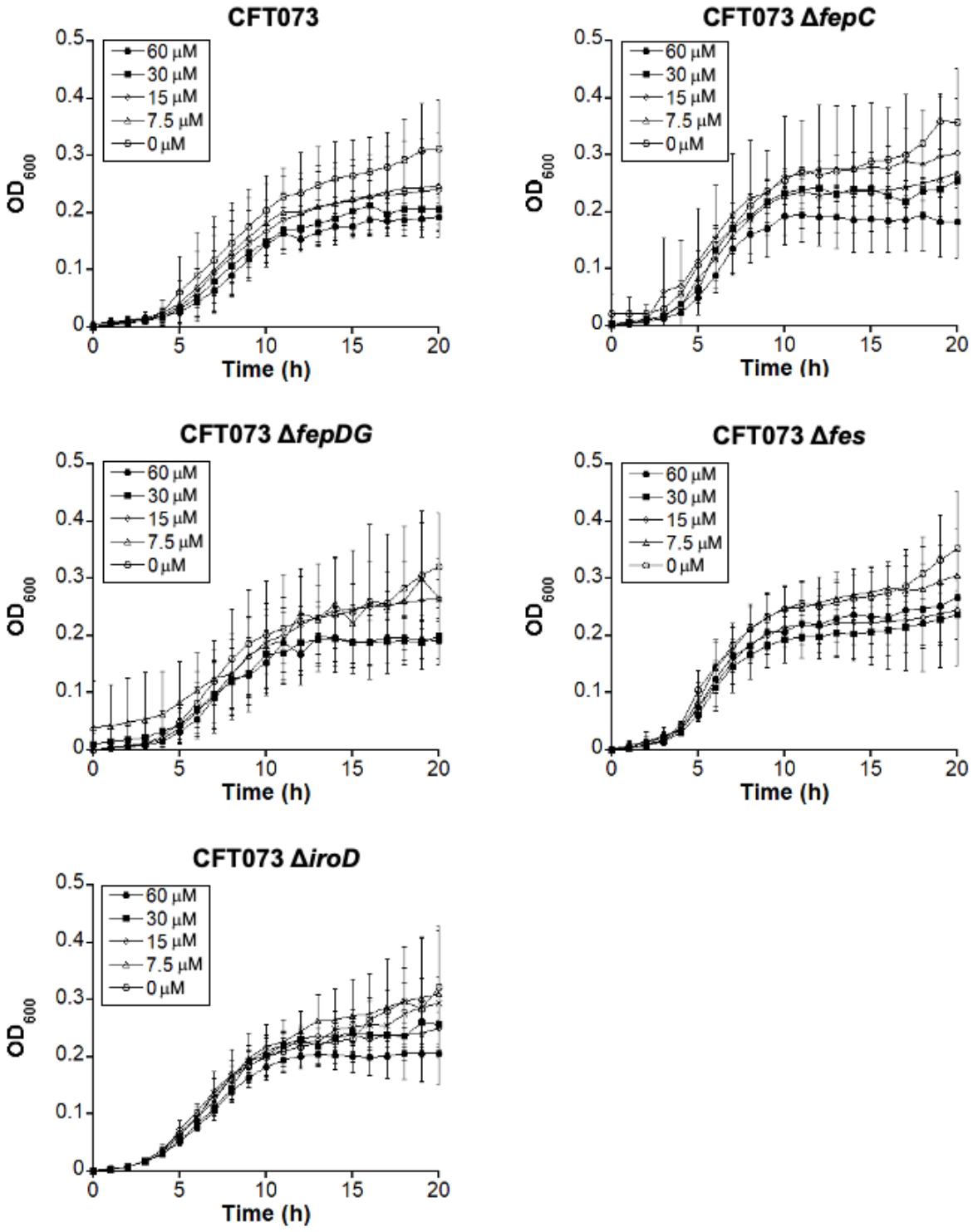

Figure A.18. Growth curves of *E. coli* CFT073 and its Δ*fepC*, Δ*fepDG*, Δ*fes* and Δ*iroD* mutants treated with Pt(IV)-alkyne in modified M9 at 30 °C (mean ± standard deviation, n ≥ 3).

Appendix B.

Supplemental Data for Chapter 3

B.1 NMR spectroscopic data

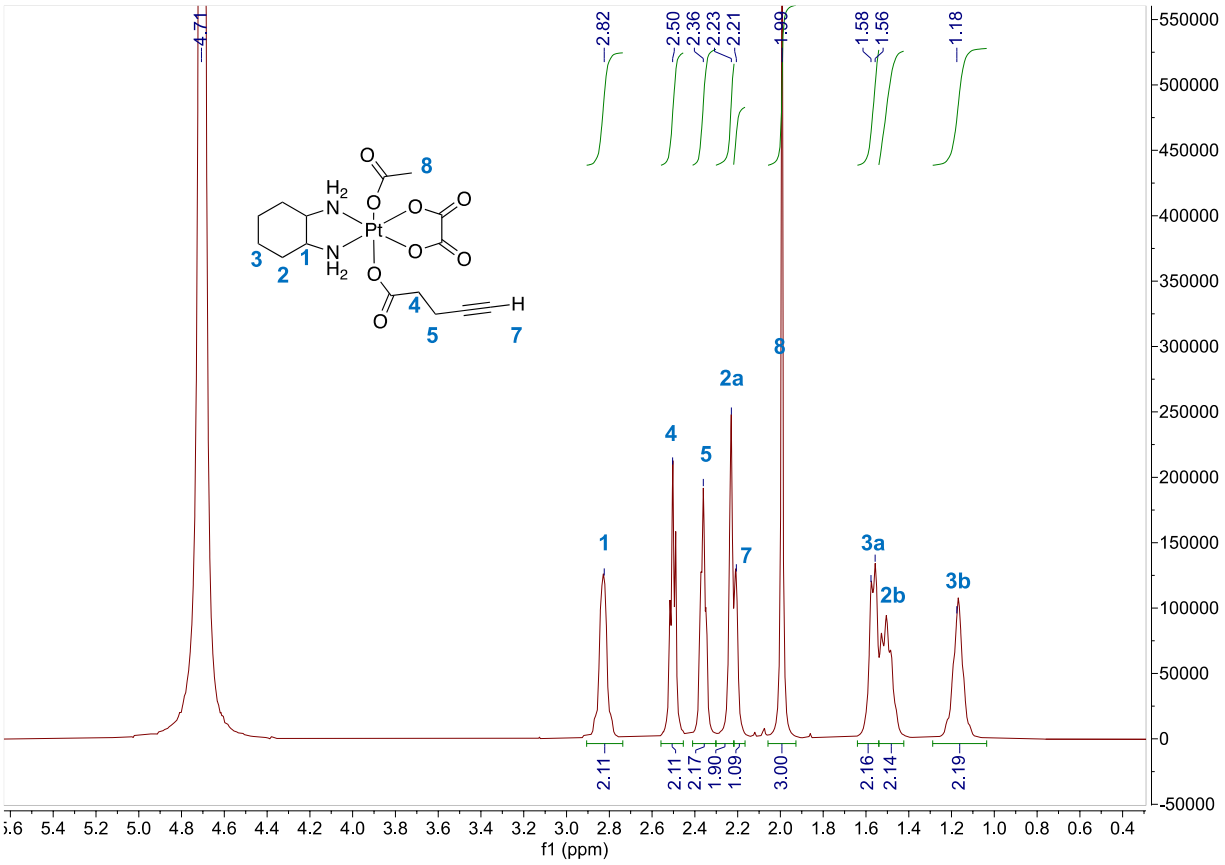

Figure B.1. ^{1}H NMR spectrum of oxPt(IV)-alkyne **5** in D_2O.

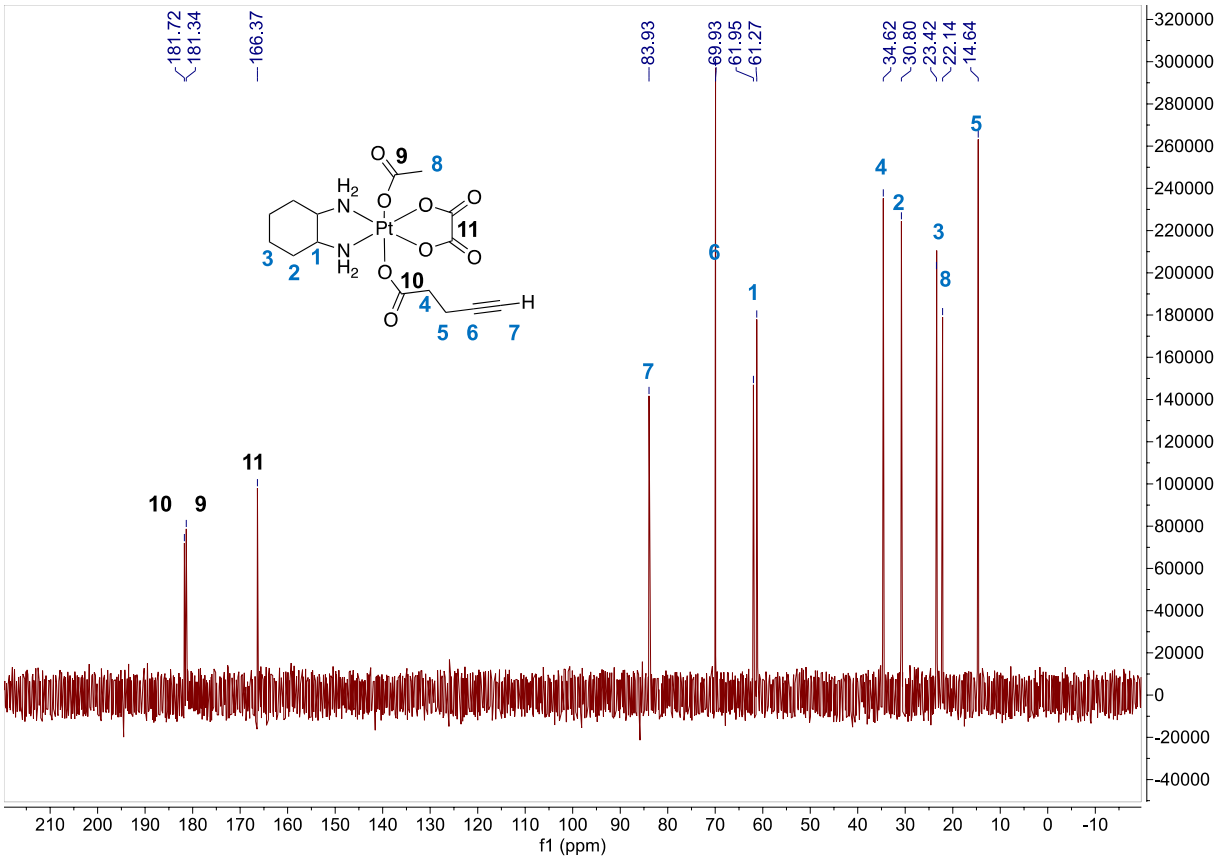

Figure B.2. ^{13}C NMR spectrum of oxPt(IV)-alkyne **5** in D_2O.

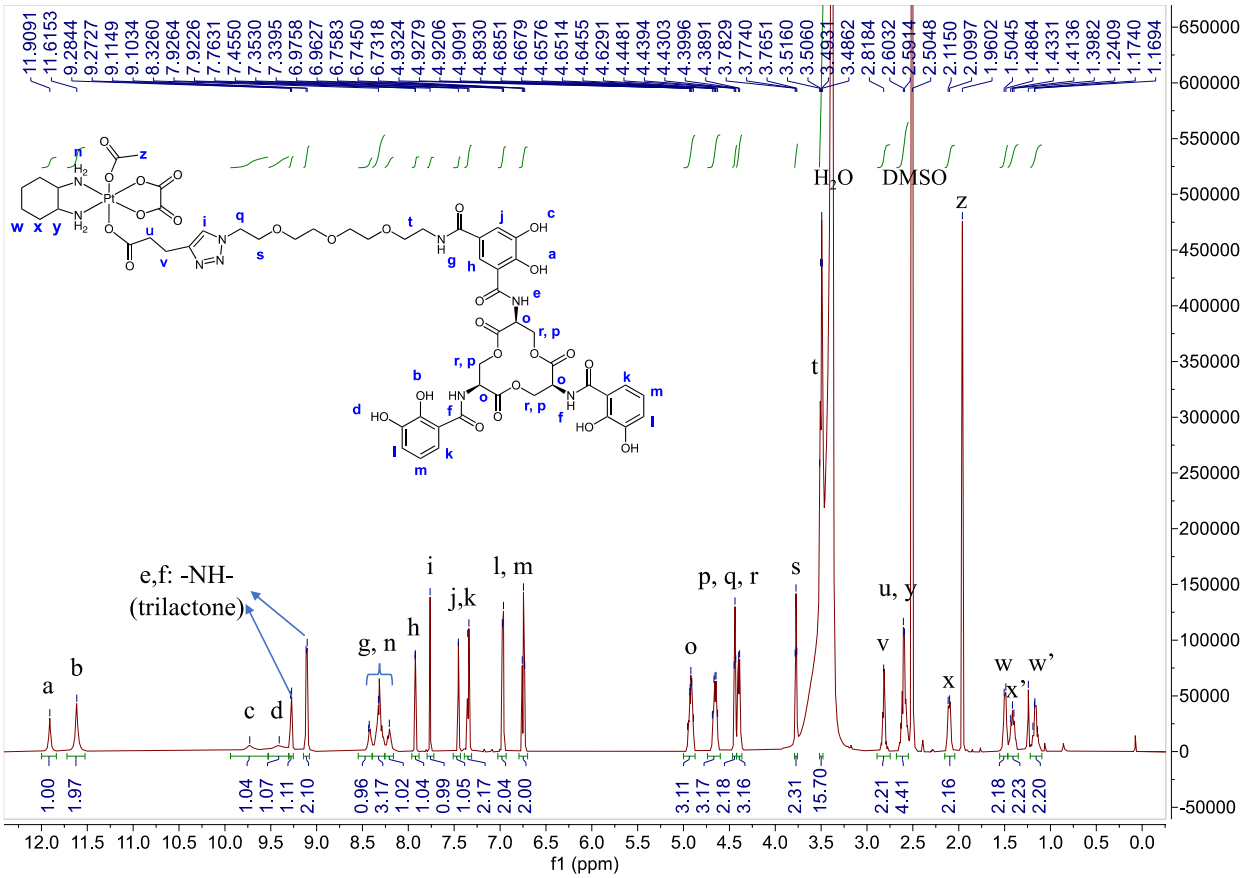

Figure B.3. ^{1}H NMR spectrum of L-Ent-oxPt(IV) **3** in DMSO_d6.

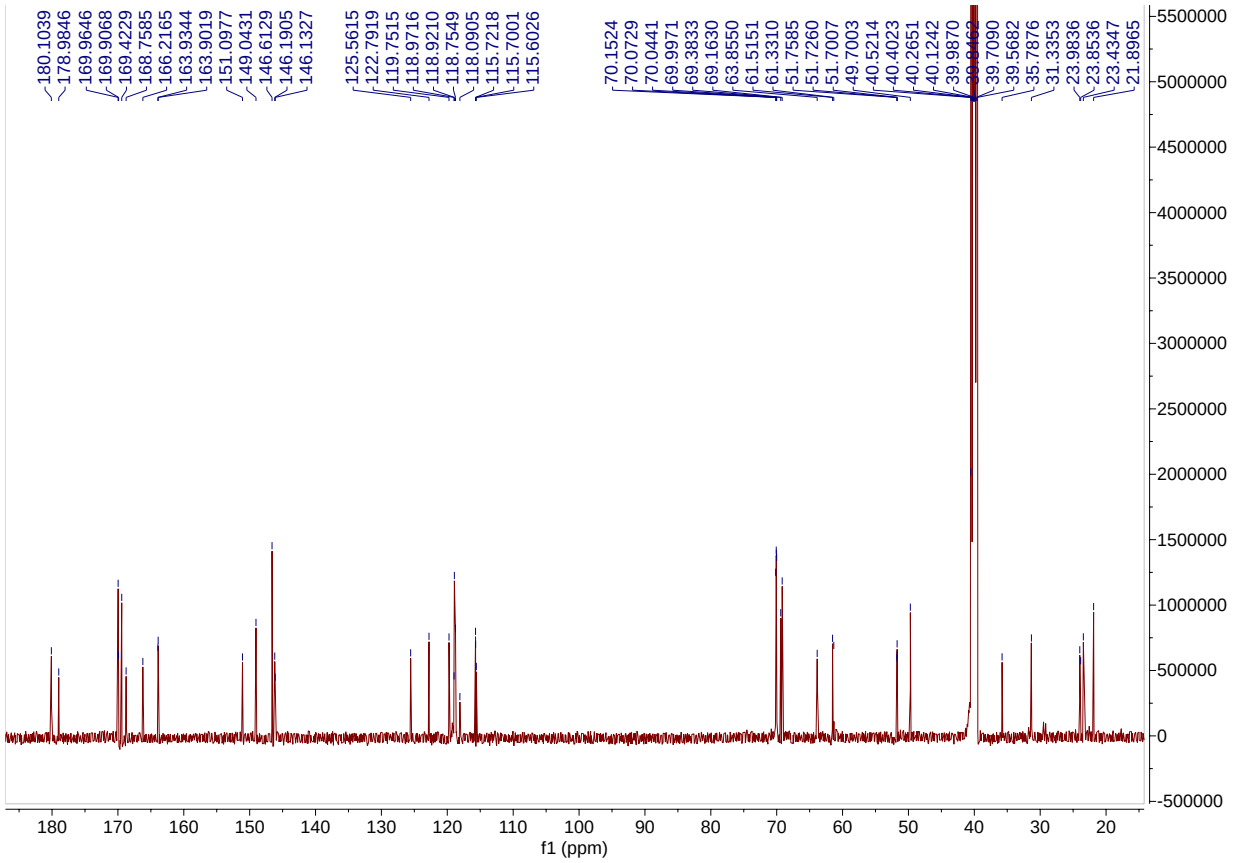

Figure B.4. ^{13}C NMR spectrum of L-Ent-oxPt(IV) **3** in DMSO_d6.

Table B.1. Peak assignment of L-Ent-oxPt(IV) **3**.

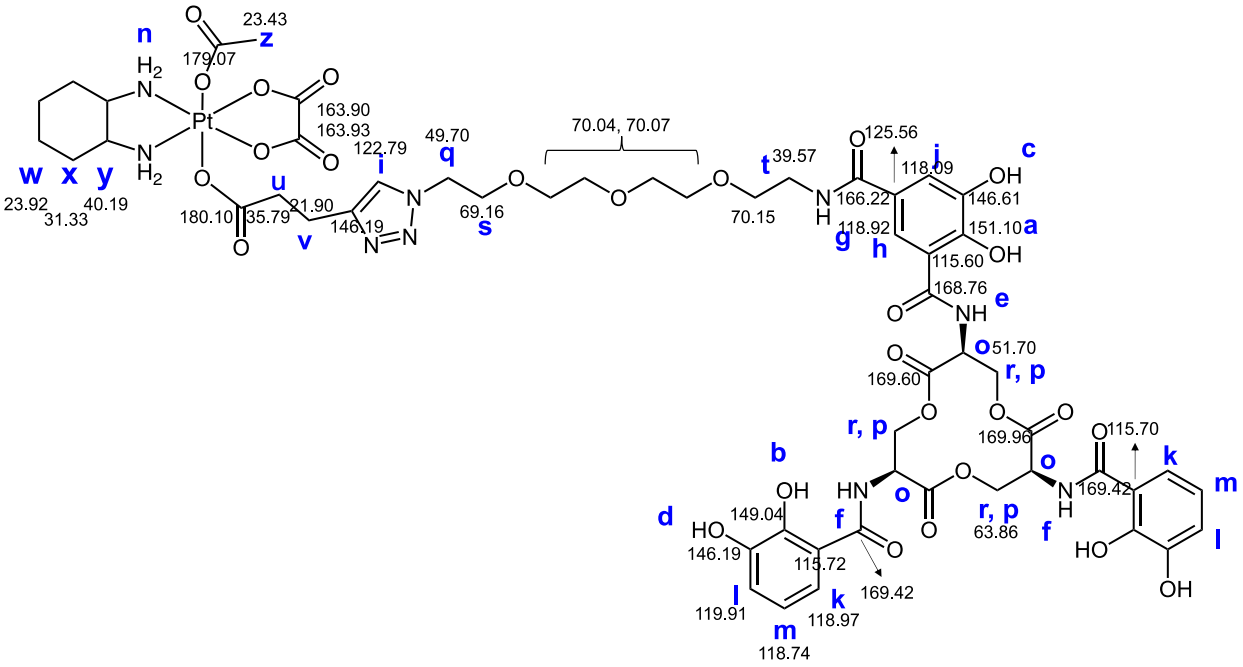

Label	H1	C13	C13 (HSQC)	C13 (HMBC)	Comments
a	11.91 (s, 1H)			146.57	
b	11.62 (s, 2H)			149.44	
c	9.73 (s, 1H)				
d	9.42 (s, 2H)				
e	9.29 (d, 1H)			51.66, 63.75, 168.8	*J* = 6.9 Hz
f	9.10 (d, 2H)			63.94, 51.66, 169.38,	*J* = 7.1 Hz
g,n	8.18–8.43 (m, 5H)			39.58, 166.27,	
h	7.93 (d, 1H)	118.92	118.99	118.13, 151.06, 168.80, 166,27, 125.53	*J* = 2.2 Hz
i	7.76 (s, 1H)	122.79	122.64	146.19	
j	7.45 (d, 1H)	118.09	118.16	118.91, 151.06, 166.27	*J* = 2.2 Hz
k	7.35 (d, 2H)	118.97	118.83	149.12, 169.38	*J* = 8.1 Hz
l	6.97 (d, 2H)	119.75	119.70	149.12, 118.71	*J* = 9.0 Hz
m	6.75 (t, 2H)	118.74	118.99	115.79	*J* = 8.1 Hz
o	4.92 (m, 3H)	51.7	51.79	169.77, 63.94	
p,r	4.66 (m, 3H)	63.86	63.90	169.97, 51.86	
q	4.44 (t, 2H)	49.7	48.24	69.21, 122.80	*J* = 5.4 Hz
p,r	4.41 (m, 3H)		67.74	51.66, 169.95	
s	3.78 (t, 2H)	69.16	69.21	49.72, 69.99	*J* = 5.3 Hz
t	3.51 (m, 12H)	70.15, 39.57	39.52, 67.89	39.58, 70.18,	
v	2.80 (m, 2H)	21.9	21.98	122.80, 146.19, 180.10, 35.68	
u,y	2.65–2.57 (m, 5H) 2.65–2.57 (m, 5H)	40.12, 61.33	40.18, 61.4175	21.84, 40.17, 61.41, 61.21	
x	2.12–2.08 (m, 2H)	31.33	31.39	23.79, 61.41	
z	1.96 (s, 3H)	23.43	23.42	178.93	
w	1.49 (d, 2H)	23.98	24.09	31.39, 61.41	*J* = 10.0 Hz
x	1.37–1.43 (m, 2H)	31.33	31.39		
w'	1.13–1.19 (m, 2H)	23.85	23.92		

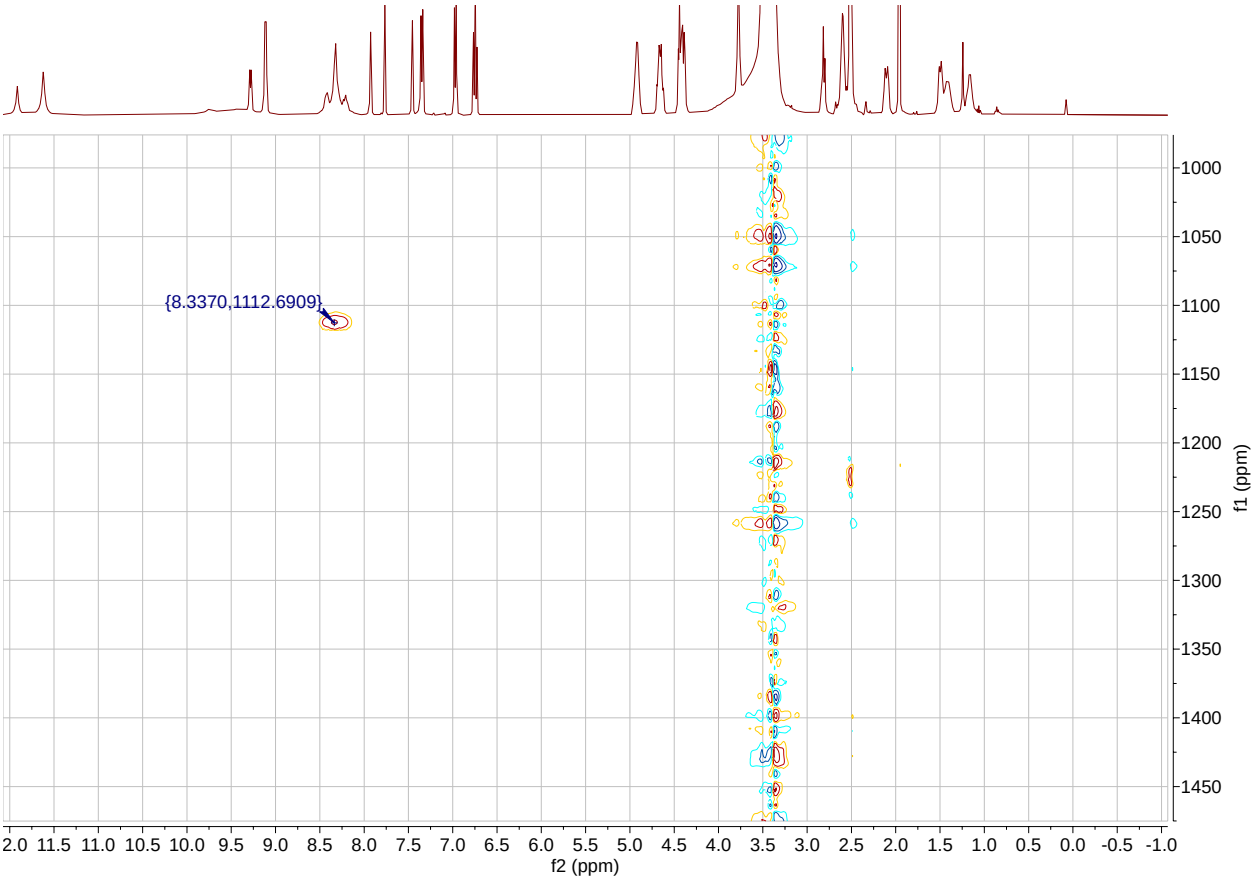

Figure B.5. ^{1}H-^{195}Pt HMQC spectrum of L-Ent-oxPt(IV) **3** in DMSO_d6.

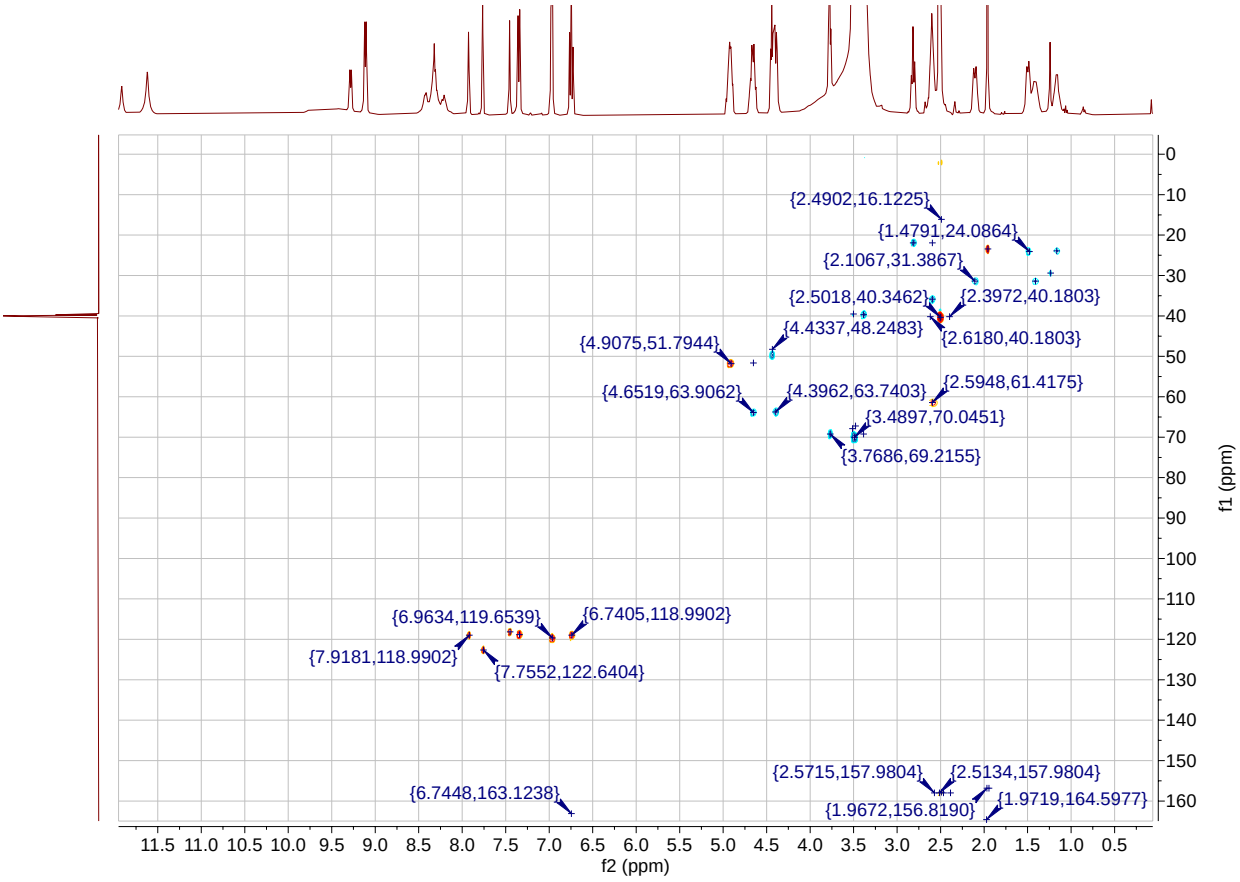

Figure B.6. ^{1}H-^{13}C HSQC spectrum of L-Ent-oxPt(IV) **3** in DMSO_d6.

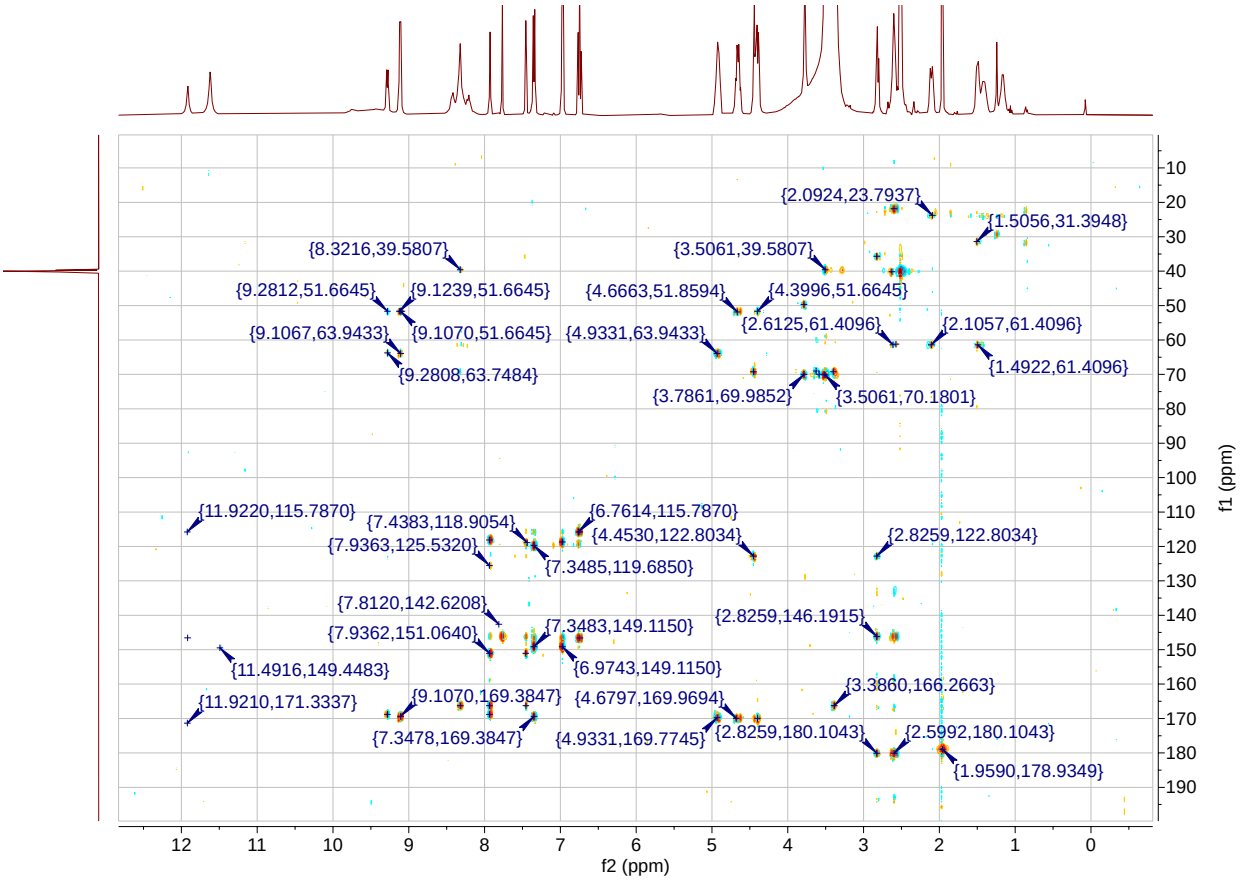

Figure B.7. ^{1}H-^{13}C HMBC spectrum of L-Ent-oxPt(IV) **3** in DMSO_d6.

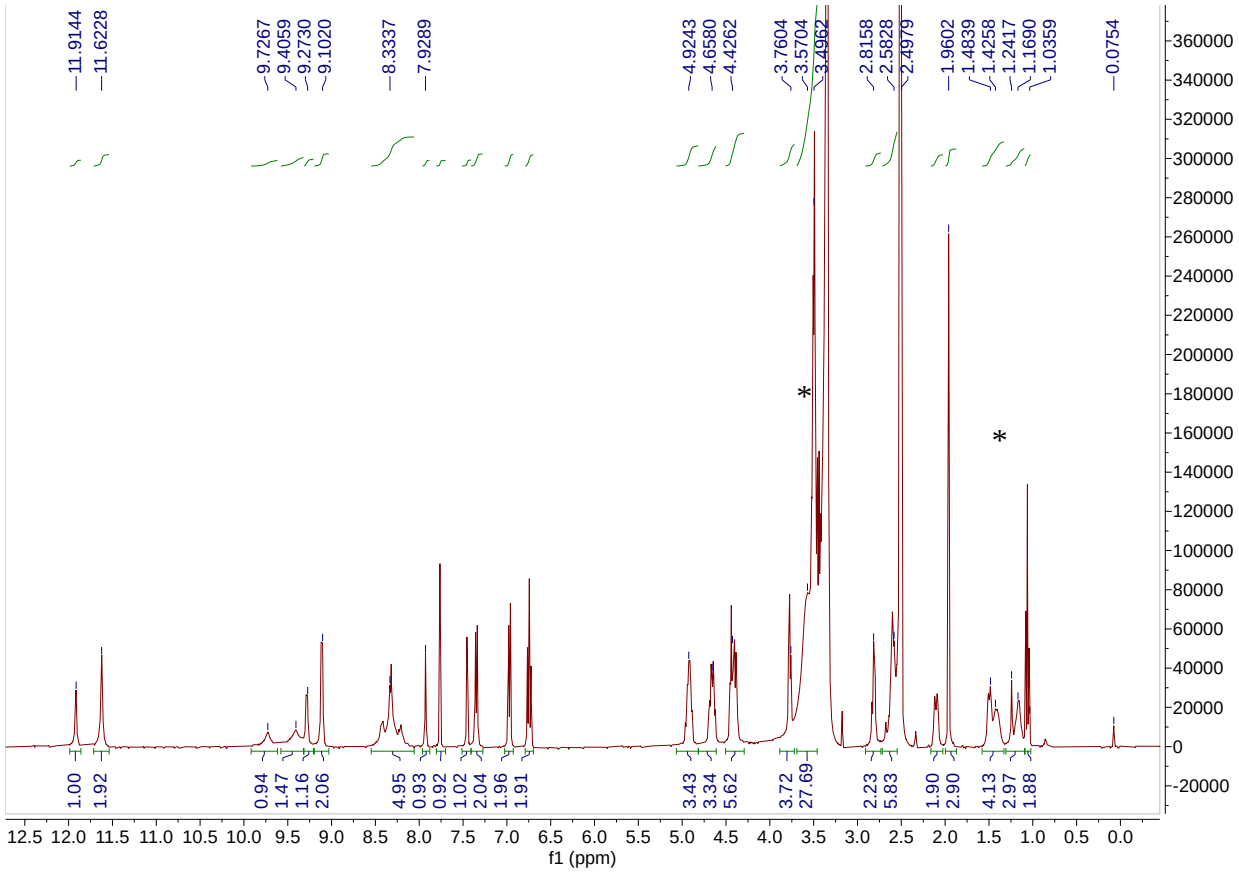

Figure B.8. ^{1}H NMR spectrum of D-Ent-oxPt(IV) **4** in DMSO_d6.

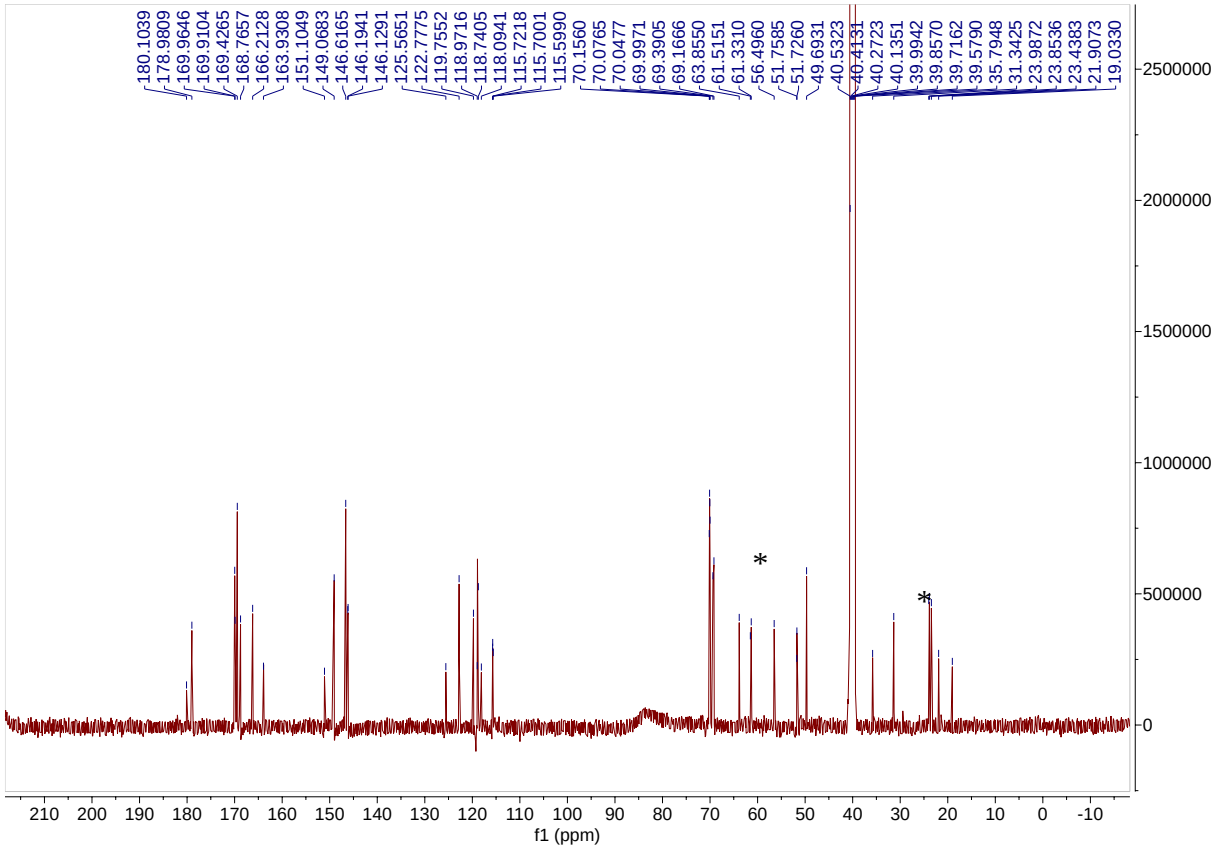

Figure B.9. ^{13}C NMR spectrum of D-Ent-oxPt(IV) **4** in DMSO_d6.

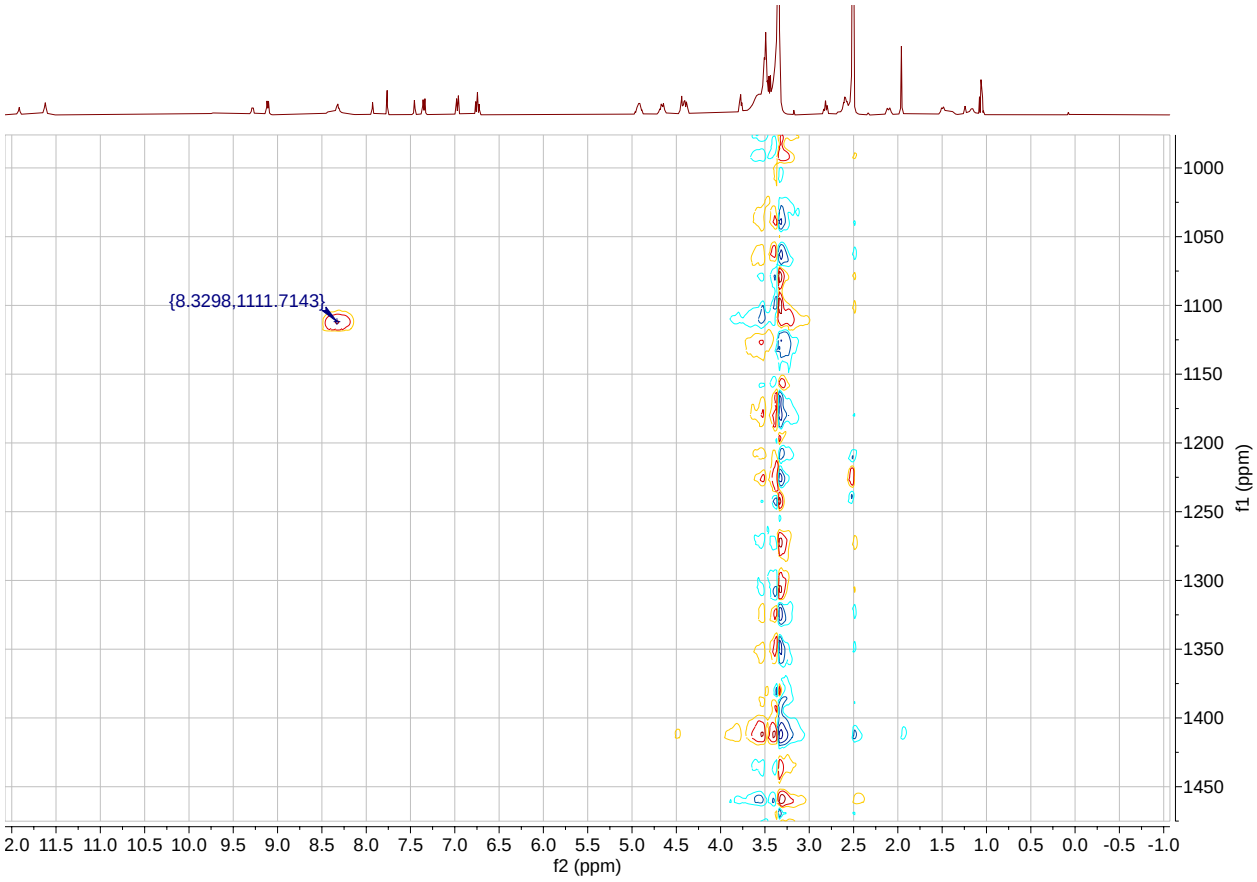

Figure B.10. ^{1}H-^{195}Pt HMQC spectrum of D-Ent-oxPt(IV) **4** in DMSO_d6.

B.2 Supplementary results of antibacterial activity and microscopy.

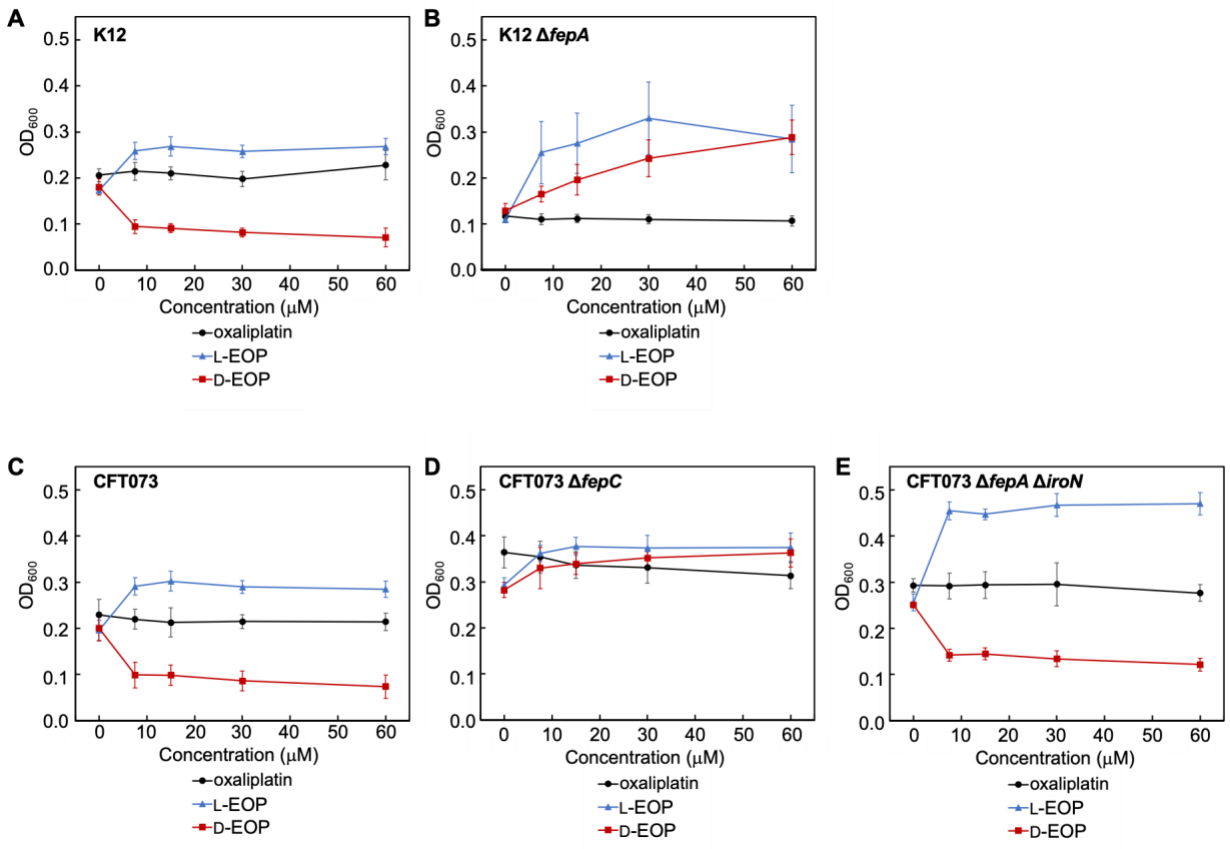

Figure B.11. Antibacterial activity of oxaliplatin and L/D-EOP against *E. coli* K12, CFT073 and their mutants. All assays were performed in modified M9 medium (11 h, 30 °C, 500 rpm; mean ± standard deviation; $n \geq 4$).

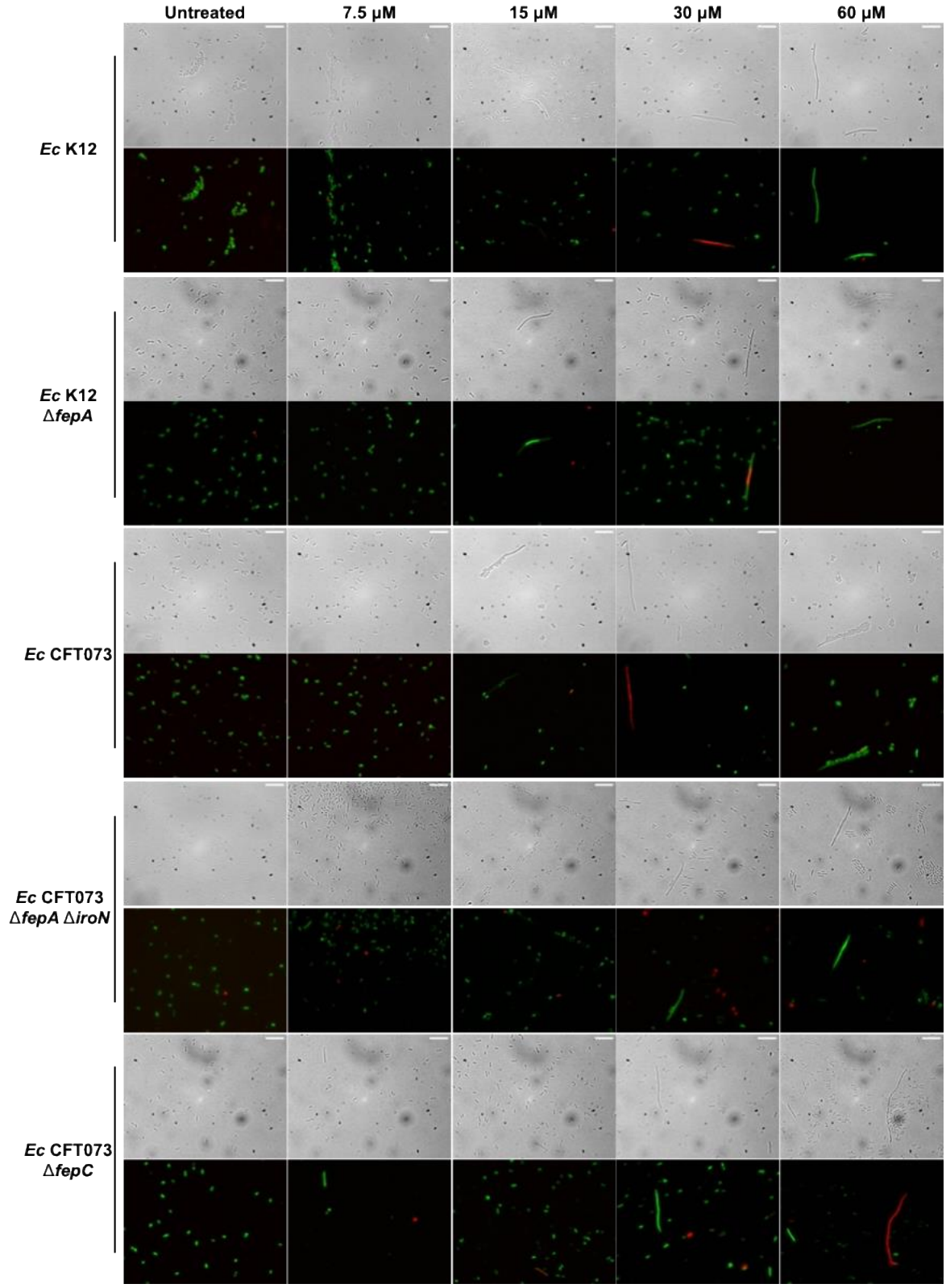

Figure B.12. Representative bright-field and fluorescence micrographs of *E. coli* K12, CFT073 and their mutants treated with oxaliplatin (scale bar = 10 µm).

B.3 Growth curves

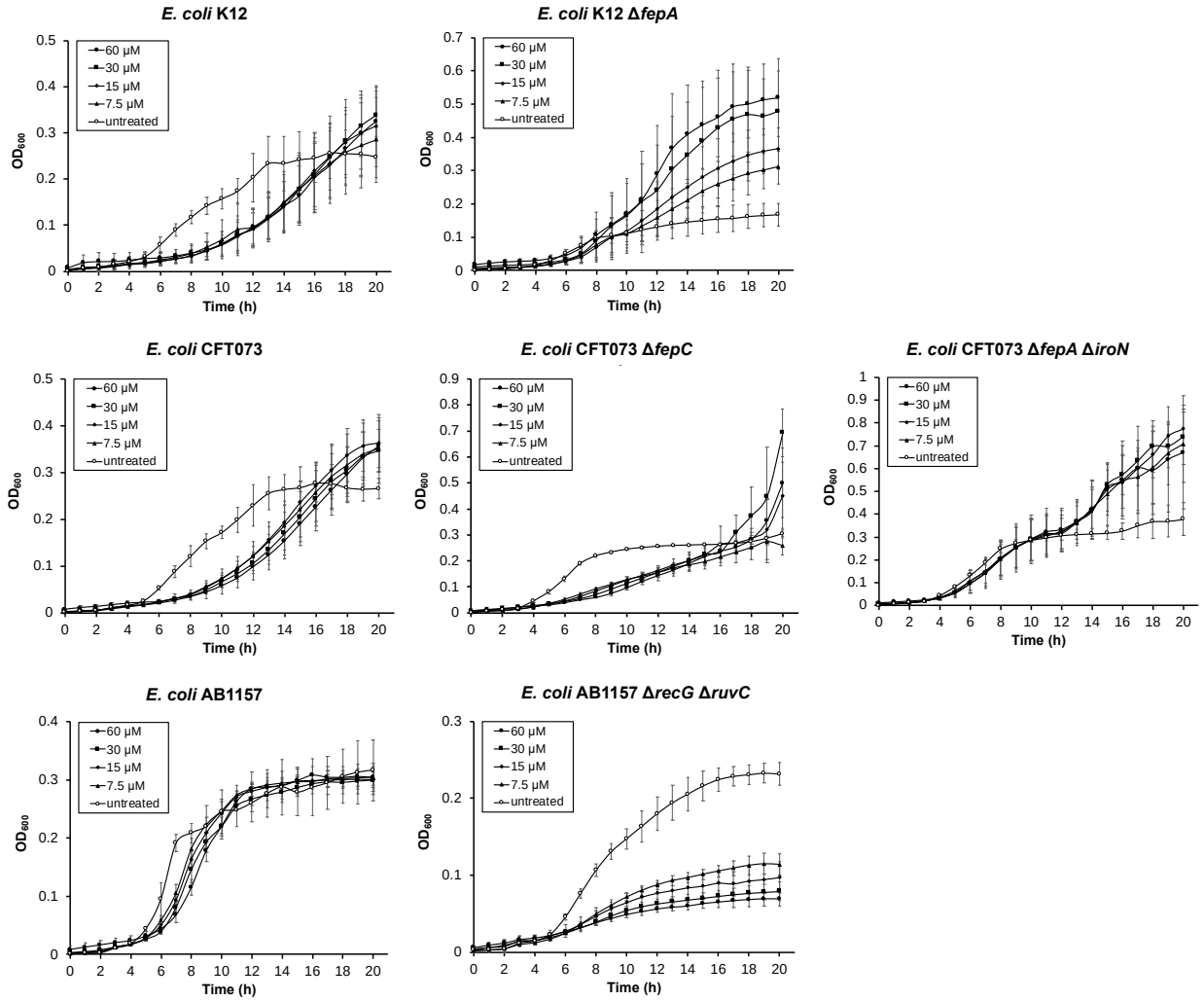

Figure B.13. Growth curves of *E. coli* K12, CFT073, AB1157 and their mutants treated with D-EOP in modified M9 at 30 °C (mean ± standard deviation, n ≥ 5). The MIC of D-EOP is not determined in this study.

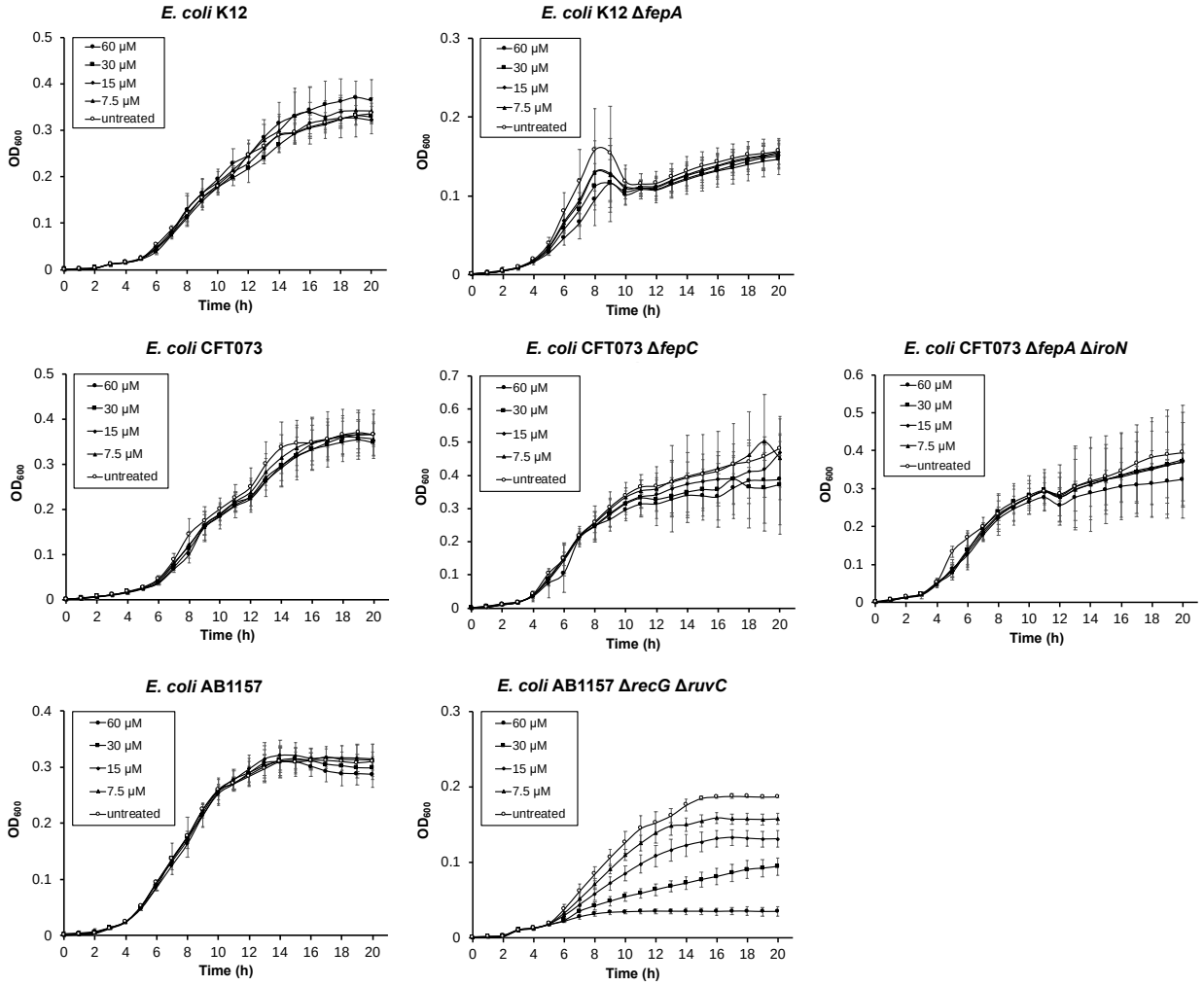

Figure B.14. Growth curves of *E. coli* K12, CFT073, AB1157 and their mutants treated with oxaliplatin in modified M9 at 30 °C (mean ± standard deviation, n ≥ 4).

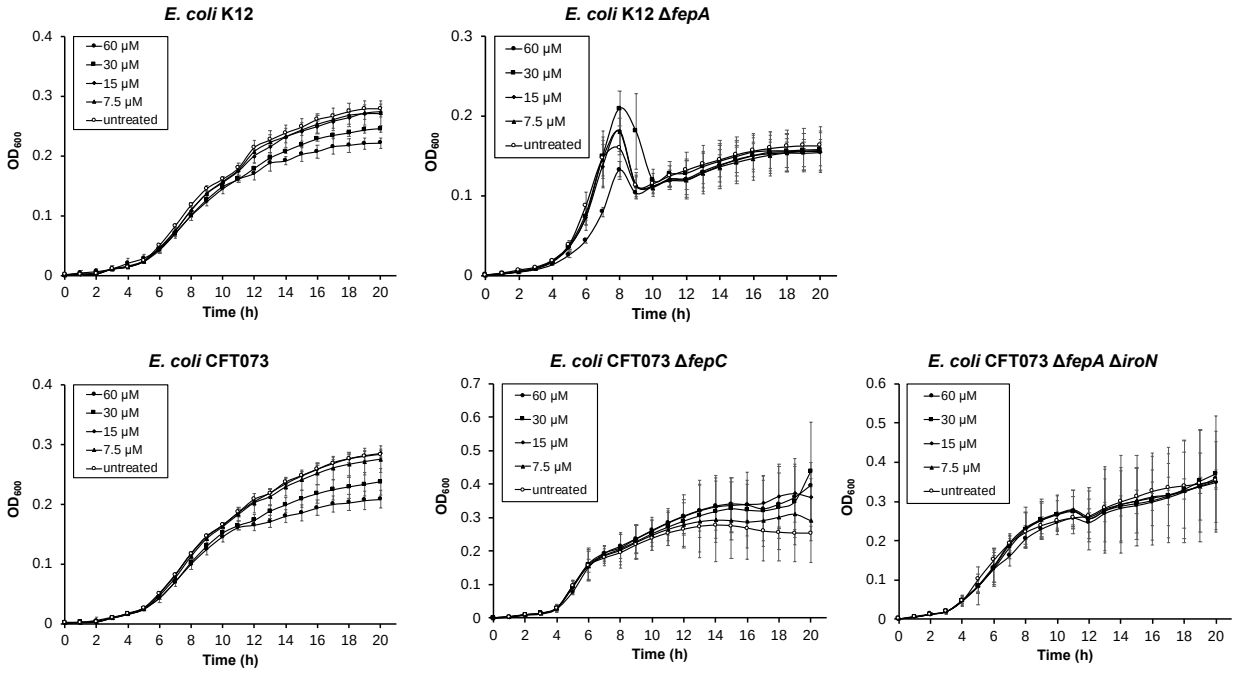

Figure B.15. Growth curves of *E. coli* K12, CFT073 and their mutants treated with oxPt(IV)-alkyne in modified M9 at 30 °C (mean ± standard deviation, n ≥ 3).

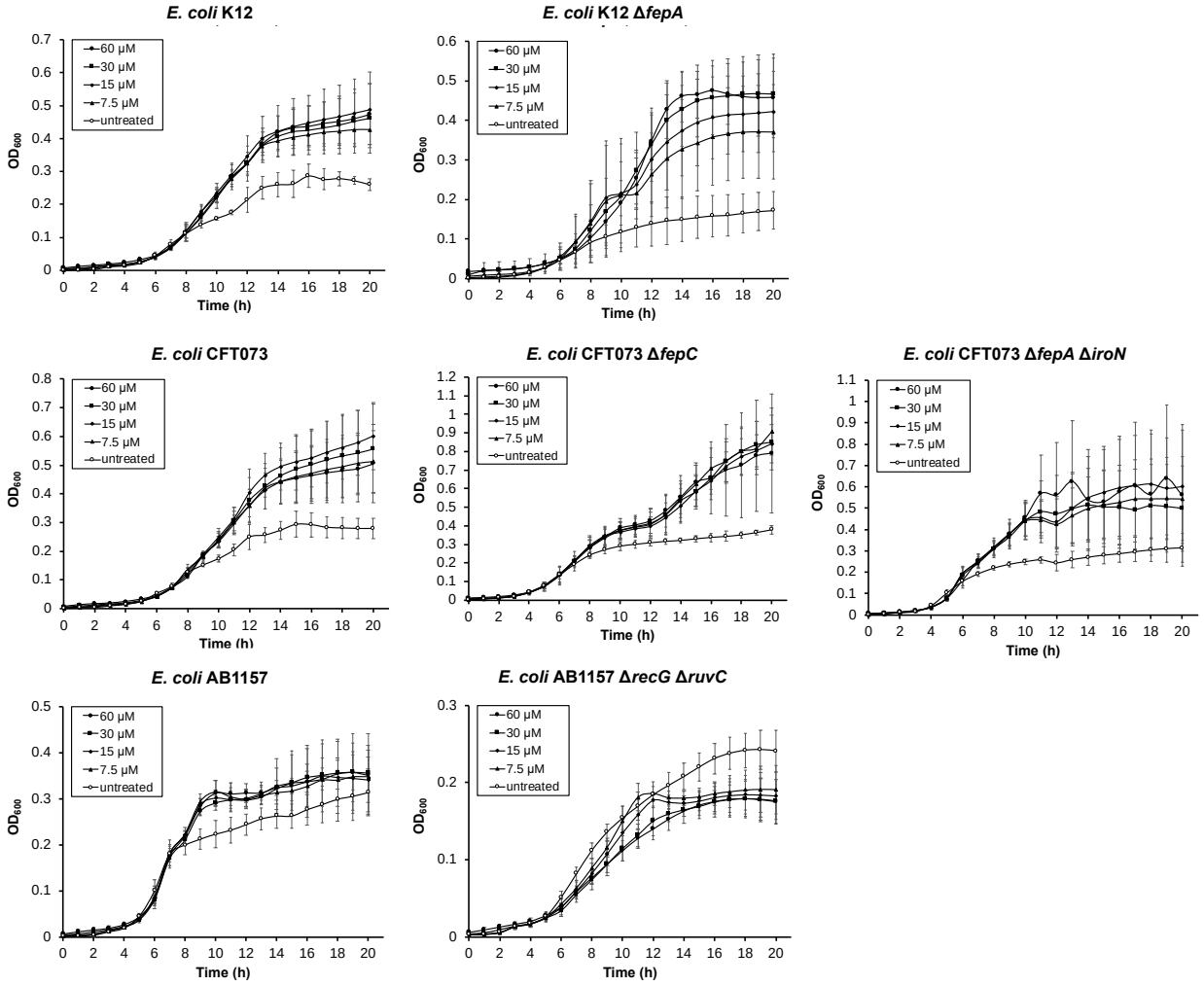

Figure B.16. Growth curves of *E. coli* K12, CFT073, AB1157 and their mutants treated with L-EOP in modified M9 at 30 °C (mean ± standard deviation, n ≥ 5).